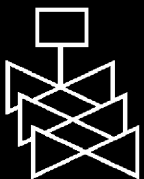
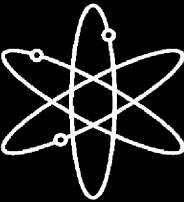


Thermal Hydraulic Uncertainty Analysis in Pressurized Thermal Shock Risk Assessment

Methodology and Implementation on Oconee-1,
Beaver Valley, and Palisades Nuclear Power Plants



**U.S. Nuclear Regulatory Commission
Office of Nuclear Regulatory Research
Washington, DC 20555-0001**



**AVAILABILITY OF REFERENCE MATERIALS
IN NRC PUBLICATIONS**

NRC Reference Material

As of November 1999, you may electronically access NUREG-series publications and other NRC records at NRC's Public Electronic Reading Room at <http://www.nrc.gov/reading-rm.html>. Publicly released records include, to name a few, NUREG-series publications; *Federal Register* notices; applicant, licensee, and vendor documents and correspondence; NRC correspondence and internal memoranda; bulletins and information notices; inspection and investigative reports; licensee event reports; and Commission papers and their attachments.

NRC publications in the NUREG series, NRC regulations, and *Title 10, Energy*, in the Code of *Federal Regulations* may also be purchased from one of these two sources.

1. The Superintendent of Documents
U.S. Government Printing Office
Mail Stop SSOP
Washington, DC 20402-0001
Internet: bookstore.gpo.gov
Telephone: 202-512-1800
Fax: 202-512-2250
2. The National Technical Information Service
Springfield, VA 22161-0002
www.ntis.gov
1-800-553-6847 or, locally, 703-605-6000

A single copy of each NRC draft report for comment is available free, to the extent of supply, upon written request as follows:

Address: Office of the Chief Information Officer,
Reproduction and Distribution
Services Section
U.S. Nuclear Regulatory Commission
Washington, DC 20555-0001
E-mail: DISTRIBUTION@nrc.gov
Facsimile: 301-415-2289

Some publications in the NUREG series that are posted at NRC's Web site address <http://www.nrc.gov/reading-rm/doc-collections/nuregs> are updated periodically and may differ from the last printed version. Although references to material found on a Web site bear the date the material was accessed, the material available on the date cited may subsequently be removed from the site.

Non-NRC Reference Material

Documents available from public and special technical libraries include all open literature items, such as books, journal articles, and transactions, *Federal Register* notices, Federal and State legislation, and congressional reports. Such documents as theses, dissertations, foreign reports and translations, and non-NRC conference proceedings may be purchased from their sponsoring organization.

Copies of industry codes and standards used in a substantive manner in the NRC regulatory process are maintained at—

The NRC Technical Library
Two White Flint North
11545 Rockville Pike
Rockville, MD 20852-2738

These standards are available in the library for reference use by the public. Codes and standards are usually copyrighted and may be purchased from the originating organization or, if they are American National Standards, from—

American National Standards Institute
11 West 42nd Street
New York, NY 10036-8002
www.ansi.org
212-642-4900

Legally binding regulatory requirements are stated only in laws; NRC regulations; licenses, including technical specifications; or orders, not in NUREG-series publications. The views expressed in contractor-prepared publications in this series are not necessarily those of the NRC.

The NUREG series comprises (1) technical and administrative reports and books prepared by the staff (NUREG-XXXX) or agency contractors (NUREG/CR-XXXX), (2) proceedings of conferences (NUREG/CP-XXXX), (3) reports resulting from international agreements (NUREG/IA-XXXX), (4) brochures (NUREG/BR-XXXX), and (5) compilations of legal decisions and orders of the Commission and Atomic and Safety Licensing Boards and of Directors' decisions under Section 2.206 of NRC's regulations (NUREG-0750).

DISCLAIMER: This report was prepared as an account of work sponsored by an agency of the U.S. Government. Neither the U.S. Government nor any agency thereof, nor any employee, makes any warranty, expressed or implied, or assumes any legal liability or responsibility for any third party's use, or the results of such use, of any information, apparatus, product, or process disclosed in this publication, or represents that its use by such third party would not infringe privately owned rights.

Thermal-Hydraulic Uncertainty Analysis in Pressurized Thermal Shock Risk Assessment

Methodology and Implementation on Oconee-1, Beaver Valley, and
Palisades Nuclear Power Plants

Manuscript Completed: November 2004
Date Published:

Prepared by:

Y.H. J. Chang, A. Mosleh, K. Almenas

Center for Risk and Reliability
University of Maryland
College Park, MD 20742

NRC Project Manager
David Bessette

Prepared for:

U.S. Nuclear Regulatory Commission
Office of Nuclear Regulatory Research
Division of Systems Analysis and Regulatory Effectiveness
Washington, DC 20555-0001



ABSTRACT

A method was developed to evaluate thermal hydraulic uncertainty for the analysis of pressurized thermal shock. This was part of a joint program with probabilistic risk assessment (PRA) and probabilistic fracture mechanics (PFM). The objective was to perform a comprehensive, best-estimate analysis of PTS, with uncertainty quantification for three representative pressurized water reactors, Oconee-1, Beaver Valley-1, and Palisades. A top-down approach was used that has some similarities to the Code Scaling, Applicability, and uncertainty (CSAU) method. The thermal hydraulic analysis was based on the application of the RELAP5/MOD3 code. The uncertainty method developed addressed both boundary conditions and physical models in the RELAP5 code. The method utilized the nominal range sensitivity analysis (NRSA) method to determine the relative affects of the various key influencing parameters that contributed to uncertainty.

FOREWORD

The reactor pressure vessel is exposed to neutron radiation during normal operation. Over time, the vessel steel becomes progressively more brittle in the region adjacent to the core. If a vessel had a preexisting flaw of critical size *and* certain severe system transients occurred, this flaw could propagate rapidly through the vessel, resulting in a through-wall crack. The severe transients of concern, known as pressurized thermal shock (PTS), are characterized by rapid cooling (i.e., thermal shock) of the internal reactor pressure vessel surface that may be combined with repressurization. The simultaneous occurrence of critical-size flaws, embrittled vessel, and a severe PTS transient is a very low probability event. The current study shows that U.S. pressurized-water reactors do not approach the levels of embrittlement to make them susceptible to PTS failure, even during extended operation well beyond the original 40-year design life.

Advancements in our understanding and knowledge of materials behavior, our ability to realistically model plant systems and operational characteristics, and our ability to better evaluate PTS transients to estimate loads on vessel walls have shown that earlier analyses, performed some 20 years ago as part of the development of the PTS rule, were overly conservative, based on the tools available at the time. Consistent with the NRC's Strategic Plan to use best-estimate analyses combined with uncertainty assessments to resolve safety-related issues, the NRC's Office of Nuclear Regulatory Research undertook a project in 1999 to develop a technical basis to support a risk-informed revision of the existing PTS Rule, set forth in Title 10, Section 50.61, of the *Code of Federal Regulations* (10 CFR 50.61).

Two central features of the current research approach were a focus on the use of realistic input values and models and an *explicit* treatment of uncertainties (using currently available uncertainty analysis tools and techniques). This approach improved significantly upon that employed in the past to establish the existing 10 CFR 50.61 embrittlement limits. The previous approach included unquantified conservatisms in many aspects of the analysis, and uncertainties were treated *implicitly* by incorporating them into the models.

This report is one of a series of 21 reports that provide the technical basis that the staff will consider in a potential revision of 10 CFR 50.61. The risk from PTS was determined from the integrated results of the Fifth Version of the Reactor Excursion and Leak Analysis Program (RELAP5) thermal-hydraulic analyses, fracture mechanics analyses, and probabilistic risk assessment. This report documents the thermal hydraulic uncertainty analyses performed. The uncertainty analyses were used to establish a range of boundary conditions to be used in determining the overall PTS uncertainty. A Phenomena Identification and Ranking Technique was used to identify the most important parameters affecting the three thermal hydraulic boundary conditions of downcomer temperature, pressure and heat transfer coefficient.



Brian W. Sheron, Director
Office of Nuclear Regulatory Research
U.S. Nuclear Regulatory Commission

CONTENTS

ABSTRACT	iii
FOREWORD.....	v
EXECUTIVE SUMMARY	xvii
ACKNOWLEDGMENTS.....	xxi
ABBREVIATIONS	xxiii
NOMENCLATURE	xxv
1. INTRODUCTION.....	1-1
1.1 Background	1-1
1.2 Achievements and Observations.....	1-2
1.3 Limitations	1-3
1.4 Tasks and Process.....	1-4
2. LITERATURE REVIEW AND STUDY RESTRICTIONS.....	2-2
3. THERMAL HYDRAULIC UNCERTAINTY ASSESSMENT PROCESS	3-1
4. IMPORTANT SYSTEM CHARACTERISTICS AND PTS CLASSIFICATION MATRIX	4-1
4.1 PTS Driving Forces from a Thermal Hydraulic Perspective	4-1
4.2 Simple Nuclear Power Plant System Model.....	4-3
4.3 Downcomer Temperature Influencing Factors	4-5
4.3.1 Heat Capacities	4-6
4.3.2 Heat Sources.....	4-7
4.3.3 Heat Sinks	4-7
4.3.4 RCS Coolant Flow Rate	4-14
4.3.5 Vessel Energy Distribution	4-15
4.4 Pressure Influencing Factors.....	4-19
4.4.1 Change in RCS Coolant Inventory	4-20
4.4.2 Change in RCS Energy	4-20
4.4.3 Short Term Rapid RCS Steam Condensation	4-20
4.5 PTS Event Classification Matrix	4-21
5. MODEL UNCERTAINTY CHARACTERISTICS	5-1
5.1 Important Phenomena Contributing to Uncertainty of RELAP5 Calculations	5-1
5.2 Uncertainties Associated with Critical Flow.....	5-3
5.3 Flow Oscillations and Numerical Flows.....	5-9
5.3.1 Oscillation With A Physical Basis	5-10
5.3.2 Numerically Induced Flow	5-13
5.4 Treatment of Model Uncertainty	5-14

6.	PARAMETER UNCERTAINTY	6-1
6.1	Identification of Tdc Influencing Parameters	6-1
6.2	Finite Discrete Uncertainty Representation	6-3
6.3	Sensitivity Indicator	6-4
6.4	Uncertainty Assessment and Identification of Representative Scenarios	6-6
6.5	Parameters Rankings	6-10
7.	RESULTS OF THERMAL HYDRAULIC UNCERTAINTY ASSESSMENT	7-1
7.1	Oconee-1 Representative Scenarios for Thermal Hydraulic Uncertainty	7-1
7.1.1	1.5-inch to 4-inch LOCA	7-4
7.1.2	4-inch to 8-inch LOCA	7-6
7.1.3	Greater than 8-inch LOCA	7-10
7.1.4	Pressurizer SRV Stuck Open Without Valve Reclosure	7-11
7.1.5	Pressurizer SRV Stuck Open and Later Reclosed	7-14
7.2	Beaver Valley Representative Scenarios for Thermal Hydraulic Uncertainty	7-18
7.2.1	1.4-to 4-inch LOCA	7-18
7.2.2	4-inch to 8-inch LOCA	7-22
7.2.3	Greater Than 8-inch LOCA	7-25
7.2.4	Pressurizer Valve(s) Stuck Open and Remaining Open	7-25
7.2.5	One and Two Pressurizer SRVs Stuck Open and Reclosed	7-32
7.3	Palisades Thermal Hydraulic Uncertainty Representative Scenarios	7-38
7.3.1	1.4-inch to 4-inch LOCA	7-39
7.3.2	4-inch to 8-inch LOCA	7-41
7.3.3	Greater than 8 inch LOCA	7-44
8.	DISCUSSION	8-1
8.1	Sensitivity Assessment Matrix	8-1
8.2	Sensitivity Trends and Comparisons	8-3
8.2.1	Break Size	8-3
8.2.2	HPI State and HPI Flow Rate	8-5
8.2.3	Decay Heat	8-7
8.2.4	Season	8-9
8.2.5	Break Location	8-12
8.2.6	Reactor Vessel Vent Valve State	8-12
8.2.7	Convective Heat Transfer Coefficient	8-15
8.2.8	Recirculation Flow	8-16
8.2.9	Pressurizer SRV Reclose Timing and HPI Throttling Timing	8-17
8.3	Parameter Ranking	8-19
9.	SUMMARY AND CONCLUSIONS	9-1
10.	REFERENCES	10-1

Appendices

A.	Uncertainty Characteristics and Classification.....	A-1
A.1	Characteristics of Uncertainty Propagation.....	A-1
A.2	Damped Uncertainty.....	A-2
A.3	Proportional Uncertainty.....	A-4
A.4	Augmented Uncertainty.....	A-8
A.5	Classification of RCS Circulation Modes.....	A-9
A.6	Characteristics of Inventory Based Two-Phase Flow States in OTSG PWRs.....	A-12
B.	Effect of Convective Heat Transfer on Vessel Wall Temperature.....	B-1
C.	Steam Generator Heat Transfer	C-1
D.	Program to Calculate Temperature Distributions	D-1
E.	Sensitivity Assessment of Parameters	E-1
F.	Description Thermal Hydraulic Runs for Oconee-1.....	F-1

Figures

Figure 1-1	Conceptual model of the PTS uncertainty analysis process	1-5
Figure 1-2	Implemented model of PTS uncertainty analysis process	1-6
Figure 2-1	Code Scaling, Applicability, and Uncertainty (CSAU) methodology	2-4
Figure 2-2	Process of the H.B. Robinson Unit-2 PTS uncertainty methodology	2-5
Figure 3-1	Probability density and cumulative distribution function diagrams for identifying representative scenarios	3-5
Figure 4-1	Schematic of PWR heat capacities and mass/energy sink/source terms	4-4
Figure 4-2	Decay heat for infinite operating time, 10 hours, and power ascension	4-8
Figure 4-3	Energy flows for different size surge line breaks	4-9
Figure 4-4	Energy flows for different size surge line breaks and SRVs stuck open	4-9
Figure 4-5	Energy flows for single steam generator tube rupture	4-10
Figure 4-6	Types and locations of boundary conditions for OTSG	4-12
Figure 4-7	Heat transfer rate from the primary to the secondary system of a steam generator for different secondary system breaks	4-13
Figure 4-8	Heat transfer rate from the primary system to the secondary system of a steam generator when the steam generator is overfed by MFW and AFW.	4-13
Figure 4-9	Downcomer temperatures for feed-and-bleed scenarios where decay heat and RCP state are varied (pressurizer PORV opens and stays open for the first 400 seconds)	4-16
Figure 4-10	$T_{dc}(t)$ for different combination of RCP and HPI states for overfeeding of both steam generators	4-16
Figure 4-11	Side view the B&W reactor coolant system geometry (OTSG)	4-17
Figure 4-12	Interfaces between cold water, hot water, and steam in reactor pressure vessel and cold leg	4-18
Figure 4-13	Energy flow through RVVVs to the downcomer region for different sizes of LOCA based on RELAP5 calculations	4-19
Figure 4-14	RCS pressures for different sizes of surge line LOCA	4-20
Figure 4-15	RCS temperature trends for two secondary side breaks compared to heatup from decay heat (RCS heat capacity 1690 MJ/K)	4-22
Figure 4-16	RCS temperature trends for two LOCA break sizes (2-inch, 8-inch) compared to heatup from decay heat (RCS heat capacity 1690 MJ/K)	4-22
Figure 4-17	Energy transfer from the primary to secondary for two scenarios where both steam generators are broken	4-24
Figure 4-18	Overview of the PRA event tree approach in modeling PTS scenarios	4-29
Figure 5-1	Critical mass flow rate vs. pressure (saturated liquid 2-inch break)	5-6
Figure 5-2	Critical flow energy discharge rate vs. pressure (saturated liquid 2-inch break) Region between two dashed lines is where flow stagnation could occur	5-6
Figure 5-3	Critical mass flow rate as function of break area $P = 7$ MPa (1028 psia), $TSAT = 559K$ (546F)	5-7
Figure 5-4	Critical flow energy discharge rate as function of break area $P = 7$ MPa (1028 psia), $TSAT = 559K$ (546F)	5-7
Figure 5-5	Critical flow mass flow rate as function of break area $P = 2$ MPa (290 psia), $TSAT = 486K$ (414F)	5-8
Figure 5-6	Critical flow energy discharge rate as function of break area $P = 2$ MPa (290 psia), $TSAT = 486K$ (414F)	5-8
Figure 5-7	Critical mass flow rate as function of void fraction (saturated liquid 2 inch break) $P = 7$ MPa (290 psia)	5-9
Figure 5-8	T_{dc} oscillation during feed-and-bleed transient with loss of heat sink	5-12
Figure 5-9	Cold leg flow velocities (feed and bleed transient with loss of heat sink)	5-12

Figure 5-10 T_{dc} and cold leg velocities (feed and bleed transient with loss of heat sink).....	5-13
Figure 5-11 Flow rates in cold legs A1 and A2 for a 1.71-inch break	5-15
Figure 5-12 Flow rates in hot leg A for two LOCAs with different break sizes	5-15
Figure 5-13 Effect of numerical parallel channel flow on T_{dc}	5-16
Figure 6-1 Probability density and cumulative density functions for a category of LOCAs	6-8
Figure 6-2 Linearly additive assumption compared with RELAP5 calculations for a 2.8-inch surge line LOCA.....	6-9
Figure 6-3 Parameter rankings for 2.8-inch LOCA (base case location is surge line)	6-11
Figure 6-4 Parameter rankings for 5.7-inch LOCA (base case location is surge line)	6-11
Figure 6-5 Parameter rankings for 8-inch LOCA (base case location is surge line)	6-12
Figure 7-1 Probability distribution for T_{sen} for LOCAs 1.5-inch to 4-inch (7128 combinations in total).....	7-5
Figure 7-2 Cumulative density function and identification of representative scenarios for LOCAs 1.5-inch to 4-inch.....	7-6
Figure 7-3 The five T_{dc} traces of representative scenarios of LOCAs 1.5-inch to 4-inch	7-7
Figure 7-4 The five P traces of representative scenarios of LOCAs 1.5-inch to 4-inch	7-8
Figure 7-5 Probability distribution of T_{sen} of LOCAs 4-inch to 8-inch (336 combinations in total).....	7-8
Figure 7-6 Cumulative distribution function and identification of representative scenarios of LOCAs 4-inch to 8-inch	7-9
Figure 7-7 The three T_{dc} traces of the representative scenarios of LOCAs 4-inch to 8-inch....	7-9
Figure 7-8 The three P traces of the representative scenarios of LOCAs 4-inch to 8-inch....	7-10
Figure 7-9 $T_{dc}(t)$ and P(t) plots for 16-inch LOCA	7-11
Figure 7-10 $T_{dc}(t)$ for the six representative scenarios for pressurizer SRV stuck open and remaining open	7-13
Figure 7-11 P(t) for the six representative scenarios for pressurizer SRV stuck open and remaining open	7-13
Figure 7-12 $T_{dc}(t)$ for representative scenarios for pressurizer SRV stuck open and later reclosed (full power).....	7-16
Figure 7-13 P(t) for representative scenarios for pressurizer SRV stuck open and later reclosed (full power).....	7-16
Figure 7-14 $T_{dc}(t)$ for pressurizer SRV stuck open and later reclosed (hot zero power)	7-17
Figure 7-15 P(t) for pressurizer SRV stuck open and later reclosed (hot zero power)	7-17
Figure 7-16 Probability distribution of representative scenarios of LOCAs 1.4-inch to 4-inch	7-19
Figure 7-17 Cumulative distribution function and the five representative scenarios of LOCAs 1.4-inch to 4-inch.....	7-20
Figure 7-18 $T_{dc}(t)$ of the five representatives scenarios for LOCAs 1.4-inch to 4-inch	7-21
Figure 7-19 P(t) of the five thermal hydraulic uncertainty representatives for LOCAs 1.4-inch to 4-inch.....	7-21
Figure 7-20 Probability distribution of the representative scenarios of LOCAs 4-inch to 8-inch.....	7-23
Figure 7-21 Cumulative distribution function and the three representative scenarios for LOCAs 4-inch to 8-inch.....	7-23
Figure 7-22 The three $T_{dc}(t)$ traces of the representative scenarios for LOCAs 4-inch to 8-inch.....	7-24
Figure 7-23 The three P(t) traces of the representative scenarios for LOCAs 4-inch to 8-inch.....	7-24
Figure 7-24 $T_{dc}(t)$ and P(t) plots of the 16-inch LOCA.....	7-25
Figure 7-25 Tdc trends of three variations of the two SRVs simultaneously stuck open bin. ..	7-26
Figure 7-26 Probability distribution of representative scenarios of SRV stuck open and not reclosed (full power).....	7-28

Figure 7-27 Cumulative distribution function of SRV stuck open and not reclosed (full power)	7-28
Figure 7-28 Probability distribution of representative scenarios of SRVs stuck open and not reclosed (hot zero power)	7-30
Figure 7-29 Cumulative distribution function for SRVs stuck open and not reclosed (hot zero power)	7-30
Figure 7-30 Uniform probability distribution of a valve stuck open area	7-31
Figure 7-31 Probability distribution of the total open area of two valves stuck open	7-32
Figure 7-32 $T_{dc}(t)$ of one SRV stuck open and reclosed at 50 and 100 minutes	7-33
Figure 7-33 $T_{dc}(t)$ of two SRVs stuck open and reclosed at 50 and 100 minutes	7-34
Figure 7-34 T_{sen} probability distribution for LOCAs 1.4-inch to 4-inch	7-39
Figure 7-35 T_{sen} cumulative probability distribution and identification of the representative scenarios for LOCAs 1.4-inch to 8-inch	7-40
Figure 7-36 The five $T_{dc}(t)$ representative scenarios for LOCAs 1.4 inch to 4 inch	7-40
Figure 7-37 The five $P(t)$ representative scenarios for LOCAs 1.4 inch to 4 inch	7-41
Figure 7-38 T_{sen} probability distribution for LOCAs 4-inch to 8-inch	7-42
Figure 7-39 T_{sen} cumulative distribution and identification of representative scenarios for LOCAs 4-inch to 8-inch	7-42
Figure 7-40 The three T_{dc} traces of the representative scenarios for LOCAs 4-inch to 8-inch	7-43
Figure 7-41 The three P traces of the representative scenarios for LOCAs 4-inch to 8-inch	7-43
Figure 7-42 T_{dc} and P traces of the representative scenario for LOCAs greater than 8-inch	7-44
Figure 8-1 T_{sen} and CPFs trends of varying LOCA sizes for Oconee-1	8-3
Figure 8-2 $T_{dc}(t)$ of the nominal scenarios of different LOCA sizes for Oconee-1	8-4
Figure 8-3 $P(t)$ of the nominal scenarios of different LOCA sizes for Oconee-1	8-4
Figure 8-4 $h_{dc}(t)$ of the nominal scenarios of different LOCA sizes for Oconee-1	8-5
Figure 8-5 Impact of HPI state on T_{sen} and CPF	8-6
Figure 8-6 Effect of HPI partial failure on T_{sen} and CPF	8-6
Figure 8-7 Impact of decay heat on T_{sen} and CPF for Oconee-1	8-7
Figure 8-8 $T_{dc}(t)$ of 5.7-inch surge line LOCA comparing full power with low decay heat for Oconee-1	8-8
Figure 8-9 $P(t)$ of 5.7-inch surge line LOCA comparing full power with low decay heat for Oconee-1	8-8
Figure 8-10 $h_{dc}(t)$ of 5.7-inch surge line LOCA comparing full power with low decay heat Oconee-1	8-9
Figure 8-11 Impact of season on T_{sen} and CPF	8-10
Figure 8-12 $T_{dc}(t)$ for 5.7-inch surge line LOCA comparing spring/fall with winter for Oconee-1	8-10
Figure 8-13 $P(t)$ for 5.7-inch surge line LOCA comparing spring/fall with winter for Oconee-1	8-10
Figure 8-14 $T_{dc}(t)$ for 8-inch surge line LOCA comparing spring/fall with winter for Oconee	8-11
Figure 8-15 $P(t)$ for 8-inch surge line LOCA comparing spring/fall with winter for	8-11
Figure 8-16 Impact of break location on CPF and T_{sen} for Oconee-1	8-12
Figure 8-17 RVVV impact on T_{sen} and CPF for Oconee-1	8-13
Figure 8-18 $T_{dc}(t)$ for 2.8-inch surge line LOCA comparing three different RVVV states	8-14
Figure 8-19 $P(t)$ for 2.8-inch surge line LOCA comparing three different RVVV states	8-14
Figure 8-20 $T_{dc}(t)$ for 4-inch surge line LOCA comparing three different RVVV states	8-15
Figure 8-21 $P(t)$ for 4-inch surge line LOCA comparing three different RVVV states	8-15

Figure 8-22 Impact of variation in heat transfer coefficient on T_{sen} and CPF for Oconee-1	8-16
Figure 8-23 Loop recirculation flow effect on T_{sen} and CPF	8-17
Figure 8-24 CPFs of varying pressurizer SRV reclosure times and HPI throttling times (full power)	8-18
Figure 8-25 CPFs of varying pressurizer SRV reclosure times and HPI throttling times (low decay heat).....	8-18
Figure 8-26 T_{sen} and mean CPF of the key influencing parameters for Oconee-1 2.8-inch LOCA.....	8-20
Figure 8-27 T_{sen} and CPF of the key influencing parameters for Oconee-1 4-inch LOCA	8-20
Figure 8-28 T_{sen} and CPF of key influencing parameters for Oconee-1 5.7-inch LOCA	8-21
Figure 8-29 T_{sen} and CPF for key influencing parameters for Oconee-1 8-inch LOCA.....	8-21
Figure 8-30 T_{sen} and CPF of influencing parameters for Beaver Valley 2.8-inch LOCA	8-22
Figure 8-31 T_{sen} and CPF for influencing parameters for Beaver Valley 4-inch LOCA.....	8-22
Figure 8-32 T_{sen} and CPF for influencing parameters for Beaver Valley 5.7-inch LOCA	8-23
Figure 8-33 T_{sen} and CPF for the key influencing parameters for Beaver Valley 8-inch LOCA.....	8-23
Figure 8-34 Lowest T_{dc} versus CPF for the Oconee sensitivity studies	8-24
Figure 8-35 Lowest dT_{dc}/dt versus CPF for the Oconee sensitivity studies.....	8-24
Figure 8-36 Lowest dT_{dc}/dt versus CPF Oconee sensitivity studies	8-25
Figure 8-37 CPF versus LOCA size for Oconee, Beaver Valley, and Palisades	8-25
Figure A-1 Range of variation of energy source (decay heat + RCPs).....	A-3
Figure A-2 $T_{dc}(t)$ comparing high power with hot zero power decay heat (RCPs on)	A-4
Figure A-3 $T_{dc}(t)$ comparing high power with hot zero power decay heat (RCPs off).....	A-4
Figure A-4 Steam generator secondary side pressures for two and one TBVs stuck open per steam generator.....	A-6
Figure A-5 Steam generator secondary side tube exit and RCS downcomer temperatures for two and one TBV(s) stuck open per steam generator	A-7
Figure A-6 Estimated ΔT by reflecting ΔP through saturation line	A-7
Figure A-7 T_{dc} for 1.71-inch and 1.54-inch surge line breaks	A-8
Figure A-8 Level dependent steam generator condensation surface	A-15
Figure B-1 Generic relationship between $T_{dc}(t)$ and $h_{dc}(t)$	B-2
Figure B-2 Range of $h_{dc}(t)$ for external natural circulation conditions	B-4
Figure B-3 Nu number dependence on $T_{dc}(t)$ for the forced and natural circulation correlations,.....	B-4
Figure B-4 $h(\delta T)$ determined from local buoyancy circulation fluid-to-surface δT	B-5
Figure B-5 Temperature distribution in vessel wall	B-5
Figure C-1 h_{eff} as a function of liquid flow velocities in tubes	C-3
Figure C-2 Temperature difference across steam generator tubes vs. tube side liquid velocity	C-3
Figure C-3 Primary side temperature exiting steam generator as function of h	C-4

Tables

Table 4-1	Inventory and Heat Capacity of Oconee-1 Primary System	4-6
Table 4-2	MSLB steam generator energy removal	4-11
Table 4-3	Energy source/sink magnitudes for Oconee-1	4-14
Table 4-4	Fluid circulation time constants for Oconee-1	4-15
Table 4-5	PTS event classification matrix	4-25
Table 4-6	RCP and HPI nominal states	4-25
Table 4-7	Thermal hydraulic runs for binning PRA event sequences and their frequencies	4-26
Table 4-8	Summation of event frequencies from the PTS event classification matrix	4-28
Table 5-1	Ability of RELAP5 to evaluate inventory dependent two-phase flow states	5-2
Table 5-2	Bounding range of break sizes for critical flow (Oconee-1)	5-9
Table 6-1	Representative values and corresponding probabilities of key influencing parameters for uncertainty analysis of Oconee-1	6-4
Table 6-2	Key influencing parameters matrix for primary system breaks for Oconee-1 Default location is surge line except as indicated for cold leg LOCA (T_{sen} in K)	6-6
Table 6-3	RELAP5 runs for validating the linearly additive assumption for multiple parameters (2.8 inch surge line LOCA)	6-9
Table 7-1	Representative values and corresponding probabilities of the key influencing parameters for Oconee-1	7-2
Table 7-2	Matrix of influencing parameters T_{sen} for LOCAs in Oconee-1 (T_{sen} in K)	7-3
Table 7-3	Influencing parameters for LOCAs 1.5-inch to 4-inch	7-4
Table 7-4	Boundary conditions of the five representative scenarios for LOCAs 1.5-inch to 4 inch	7-6
Table 7-5	Influencing parameters of LOCAs 4-inch to 8-inch	7-7
Table 7-6	Boundary conditions of the five representative scenarios of LOCAs 4-inch to 8-inch	7-7
Table 7-7	Boundary conditions of the representative scenario of LOCAs greater than 8-inch	7-10
Table 7-8	Influencing parameters for pressurizer SRV stuck open without reclosure	7-12
Table 7-9	Representative scenarios for pressurizer SRV stuck open and remaining open and their probabilities (full power)	7-12
Table 7-10	Representative scenarios for pressurizer SRV stuck open and remaining open and their probabilities (hot zero power)	7-12
Table 7-11	The six combinations for T_{dc} uncertainty representation of pressurizer SRV stuck open and reclosed scenarios	7-14
Table 7-12	Representative scenarios and their probabilities for pressurizer SRV stuck open and later reclosed (full power)	7-15
Table 7-13	Representative scenarios and their probabilities for pressurizer SRV stuck open and later reclosed (hot zero power)	7-15
Table 7-14	T_{sen} for Beaver Valley based on NRSA	7-18
Table 7-15	Representative values and probabilities for LOCAs 1.4-inch to 4-inch	7-18
Table 7-16	Influencing parameters for each break size from 1.4 inch to 4 inch	7-19
Table 7-17	Boundary conditions of the five uncertainty representative scenarios for LOCAs 1.4-inch to 4-inch	7-20
Table 7-18	Representative values and probability of break sizes for LOCAs 4-inch to 8-inch	7-22
Table 7-19	Influencing parameters for LOCAs 4-inch to 8-inch	7-22
Table 7-20	Boundary conditions of the three representative scenarios of LOCAs 4-inch to 8-inch	7-22
Table 7-21	Boundary conditions of representative scenario for LOCAs greater than 8-inch	7-25
Table 7-22	Representative values and probabilities for SRV stuck open without reclosure	7-27

Table 7-23 Influencing parameters for pressurizer SRV stuck open (full power).....	7-27
Table 7-24 Boundary conditions of the three representative scenarios for one pressurizer SRV stuck open without reclosure (full power)	7-29
Table 7-25 Representative values and probabilities of influencing parameters for SRV stuck open without reclosure (hot zero power)	7-29
Table 7-26 Boundary conditions for the three representative scenarios for SRV stuck open without reclosure (hot zero power).....	7-31
Table 7-27 The two representative scenarios and their probabilities for SRVs stuck open and remaining open	7-32
Table 7-28 Conditional probabilities of the representative scenarios of one SRV stuck open and reclosed (high decay heat).....	7-34
Table 7-29 Conditional probabilities of the representative scenarios of two SRVs stuck open and reclosed (high decay heat).....	7-35
Table 7-30 Representative values and probabilities of influencing parameters for pressurizer SRV stuck open and reclosed.....	7-35
Table 7-31 Conditional probabilities of representative scenarios of one SRV stuck open and reclosed.....	7-36
Table 7-32 Conditional probabilities of representative scenarios of two SRVs stuck open and reclosed.....	7-36
Table 7-33 Representative scenarios and probabilities for pressurizer SRVs stuck open without reclosure	7-37
Table 7-34 Representative scenarios and probabilities for one pressurizer SRV stuck open and later reclosed (high decay heat).....	7-37
Table 7-35 Representative scenarios and probabilities for one pressurizer SRV stuck open and later reclosed (low decay heat)	7-37
Table 7-36 Representative scenarios and probabilities for two pressurizer SRVs stuck open and later reclosed (full power).....	7-38
Table 7-37 Representative scenarios and probabilities for two pressurizer SRVs stuck open and later reclosed (low decay heat)	7-38
Table 7-38 T_{sen} matrix for LOCAs (T_{sen} in K).....	7-39
Table 7-39 Boundary conditions of the five representative scenarios for LOCAs 1.4-inch to 4-inch	7-40
Table 7-40 Boundary conditions of the three representative scenarios for LOCAs 4-inch to 8-inch	7-43
Table 7-41 Boundary conditions of the representative for LOCAs greater than 8 inch.....	7-44
Table 8-1 Sensitivity assessment matrix for Oconee-1.....	8-2
Table 8-2 Temperature of the emergency core cooling system at different seasons	8-9
Table A-1 Classification of uncertainties according to their impact.....	A-2
Table A-2 Classification of PTS relevant transients based on propagation of uncertainties.....	A-6
Table A-3 Classification of two-phase transients	A-11
Table E-1 RELAP5 sensitivity calculations for surge line LOCA.....	E-1
Table E-2 RELAP5 sensitivity studies for cold leg LOCAs	E-2
Table E-3 Summary of PFM Analysis of RELAP5 Sensitivity Calculations for Oconee-1	E-2
Table F-1 Scenario descriptions of RELAP5 calculations for Oconee-1 (Arcieri, 2001).....	F-1
Table F-2 Placement of the Oconee-1 scenarios calculated by RELAP5 in the PTS classification matrix.....	F-9

EXECUTIVE SUMMARY

This report describes the thermal hydraulic uncertainty analysis and process used as input to determining overall uncertainty for pressurized thermal shock (PTS) risk. The uncertainty analysis was performed for the Oconee, Beaver Valley, and Palisades plants. A top-down approach was used to identify the key factors affecting thermal stress and pressure stress applied to reactor vessel wall. Sensitivity analyses were performed to rank these factors and to identify the uncertainty representative scenarios.

The analysis was coordinated with probabilistic risk assessment (PRA) model development to specify and identify the “scenario bins” which were PTS risk significant for further detailed uncertainty analysis. Each plant’s PTS PRA model contained more than ten thousand PTS risk scenarios. These scenarios were grouped (or binned) into a number of categories (or “Bins”) based on their thermal hydraulic similarities to PTS challenge. Example bins were small break loss of coolant accidents (LOCA), medium LOCA, large LOCA, safety/relief valve (SRV) stuck open, steam generator overfeed, and main steam line break. A few scenarios, typically between 3 and 5, from each Bin were identified to represent its uncertainty. The probabilities of these representative scenarios were calculated along with their time histories of temperature, pressure, and heat transfer coefficient in the downcomer region [i.e., downcomer temperature (T_{dc}), downcomer pressure (P_{dc}), and downcomer convective heat transfer coefficient (h_{dc})] were transferred to the probabilistic fracture mechanics (PFM) group for calculating the final PTS risk.

Identification of the uncertainty representative scenarios considered factors beyond those which have been considered in the PRA model. Thus, each representative scenario can be specified with great detail for RELAP5 calculation. The following summarizes the thermal hydraulic uncertainty analysis method.

STEP 1: Construct PTS Event Classification Matrix

Thermal stress and *pressure stress* are the two stressors that affect the probability of RPV failure. The main factors affecting thermal stress at high-level are:

- Heat capacities of the reactor coolant system (RCS)
- Heat sources to RCS
- Heat sinks to RCS such as break
- RCS energy distribution
- Rate of heat transfer from RPV structure to downcomer fluid

The main factors affecting the pressure stress are:

- Change in RCS coolant inventory (e.g., loss of RCS inventory due to breach)
- Change in net energy lost by RCS
- Steam condensation in RCS

- HPI filling the RCS until it is water solid with pressure determined by the pressurizer SRV

PFM studies provided useful information to screen the PTS risk-significant scenarios including:

- T_{dc} lower than 300°F in order to fail RPV wall due to temperature dependent characteristics of materials properties
- PTS risk was more sensitive to change in T_{dc} than change in P_{dc} except for stuck open pressurizer SRV reclosure cases
- P_{dc} effect was significant when scenarios involving RCS repressurization

A wide range of events were screened to identify the event categories which were PTS risk significant. It was concluded that only three event categories, individually or combined, could significantly reduce T_{dc} to have PTS risk. These three event categories were primary system breach, secondary system breach, and secondary system overfed. A PTS event classification matrix was developed based on above conclusion to facilitate the analysis.

The PTS event classification matrix facilitated uncertainty analysis from two perspectives: firstly, through well defined event classification the number of uncertainty parameters needed to be considered was reduced; and secondly, the matrix provided a framework for preliminary event screening based on event frequencies.

STEP 2: Prioritize analysis effort

The main purpose of this step was to identify the high PTS-risk event categories in order to concentrate the analysis effort. An iterative process between the PRA, PFM, and thermal hydraulics work groups was required in this step.

In the PTS event classification matrix, the event category of primary system having greater than 1.5 inches breach and secondary system remaining integral contributed about 95% of the frequency of PTS-risk scenarios. The PFM group found that this event category had the most significant conditional PTS challenge. Thus, the TH uncertainty analysis effort was focused on this event class.

For finer analysis, the primary system breach was divided into scenarios of LOCA and PZR valve stuck open. The LOCA scenarios were further sub-classified into three groups based on the break size: 1.5 ~ 4 inches, 4 ~ 8 inches, and larger than 8 inches.

STEP 3: Assess sensitivity of individual parameter on thermal stress

This step measured the sensitivity of each key factor on T_{dc} in order to assess the combined sensitivity of multiple factors. A measurement system needed to be developed for measuring the sensitivity. From the thermal hydraulic perspective, thermal stress was dependent on the downcomer temperature and rate of change of temperature. Since there were no known rules specifying how these two parameters affecting thermal stress, for simplicity, a sensitivity indicator, T_{sen} , was defined as the average $T_{dc}(t)$ over the first 10,000 seconds of a given transient.

The *one-factor-at-a-time* method was used to calculate an individual parameter's sensitivity. This was done typically by applying the parameter's lower bound, nominal, and upper bound values separately while maintaining other parameters at their nominal values or state to calculate T_{sen} . The parameter's sensitivity was determined by the differences of the values of T_{sen} .

STEP 4: Assess the parameters' combined effect on thermal stress

This step was based on the sensitivity results obtained in Step 3 to assess the combined effect of multiple parameters on thermal stress. A linear additive method was used for aggregating multiple parameters' effects on thermal stress. This was based on the fact that the heat capacitance of the RCS downcomer remained nearly constant. Thus, the fluid temperature in downcomer was dependent on the net heat/energy change in this region. Since each parameter's effect can be seen as depositing or extracting energy into or from the downcomer, the linear additive method was a reasonable approach.

STEP 5: Identify the uncertainty representative scenarios

This step identified a few thermal hydraulic scenarios to represent the uncertainty of an event category. The results generated in Step 4 (i.e., T_{sen} and probability values for a specific scenario) were first plotted as a probabilistic density function (PDF) diagram, which was then converted to a cumulative density function (CDF).

The importance of parameters could be ranked based on the sensitivity assessment results calculated in STEP 3. Higher ΔT_{sen} indicates lower TWCP since less thermal stress is imposed on the RPV wall. The importance ranking of the key parameters is inversely corresponding to their ranking in ΔT_{sen} . It is important to note that ΔT_{sen} only represents effect of thermal stress and not pressure stress. Pressure stress was specifically considered in the scenarios involving RCS repressurization.

Both $T_{dc}(t)$ and $dT_{dc}(t)/dt$ impact the determination of CPF. In general, a more rapid T_{dc} decrease is worse, but the relationship is not strong. The timing of variation in T_{dc} and dT_{dc}/dt is another important factor. Scenarios with the lowest T_{dc} usually have larger CPFs, however, this is not always true. Trends of T_{sen} and CPF show coherence for breaks $>\sim 4$ inch. Some incoherence occurs for smaller sized LOCAs $< \sim 4$ inch. In small LOCA scenarios, the pressure effect might not be negligible and, in general, the outcome is more sensitive to other parameters such as break location. The use of T_{sen} assumes that the pressure effect is of second order importance. Second, T_{sen} is calculated based on the averaged T_{dc} for a long period of time (10,000 seconds).

An important conclusion is, that short of running FAVOR, there is no simple way to accurately predict the CPF of a scenario based on examining the thermal hydraulic input.

ACKNOWLEDGEMENTS

The authors wish to thank a number of individuals whose help greatly benefited this report. From the national laboratory and industrial sectors this includes Mr. William Arcieri (Information Systems Laboratories), Mr. Robert Beaton (ISL), and Mr. Mohammad Pour-Gol Mohammad (UMD) for performing many of the RELAP5 simulation runs; Dr. Alan Kolaczowski (Science Applications International Corporation), Mr. Donnie Whitehead (Sandia National Laboratory), and Dr. William Galyean (Idaho National Laboratories) for providing insights on operator response; Dr. Terry Dickson (Oak Ridge National Laboratory) and Dr. Mark Kirk (Nuclear Regulatory Commission) for help in characterization of material properties affected by thermal and pressure stresses.

The authors also express their appreciation of several thorough reviews of this document at various stages of its development by a number of prominent experts including Dr. David Johnson (ABS Consulting), Dr. Eric van Walle, Dr. Thomas Murley (Consultant), Professor Ivan Catton (UCLA), Dr. Upendra Rohatgin (Brookhaven National Laboratory), and Mr. Helmut Schultz, Gesellschaft für Anlagen- und Reaktorsicherheit (GRS) mbH, Germany.

ABBREVIATIONS

AFW	auxiliary feedwater
B&W	Babcock and Wilcox Company
CC	Combustion Engineering, Inc.
CDF	cumulative distribution function
CFT	core flood tank (accumulator)
CPI	conditional probability of crack initiation
CPF	conditional probability of vessel failure
CSAU	code scaling, applicability, and uncertainty
ECC	emergency core cooling
FAVOR	Fracture of Vessel
HPI	high pressure injection
HZP	hot zero power
IPTS	Integrated Pressurized Thermal Shock study
IRM	interruption-resumption mode
LOCA	loss of coolant accident
LPI	low pressure injection
MMFW	main feedwater
MSIV	main steam isolation valve
MSLB	main steamline break
NRSA	nominal range sensitivity analysis
OTSG	once-through steam generator
PDF	probability density function
PFM	probabilistic fracture mechanics
PIRT	phenomena Identification and ranking technique
PORV	power operated relief valve
PRA	probabilistic risk assessment
PTS	pressurized thermal shock
PWR	pressurized water reactor
RCP	reactor coolant pump
RCS	reactor coolant system
RVVV	reactor vessel vent valve
RELAP5	Reactor Leak And Power Excursion Code Modification 5
SRV	safety/relief valve
TBV	turbine bypass valve

NOMENCLATURE

Cp	specific heat
H	enthalpy
h	convective heat transfer coefficient, W/m ² -K
P	pressure
p	probability
Q	heat, J
T	temperature, K
t	time, s
W	mass, kg
$h_f(T_i)$	enthalpy at entrance to downcomer \bar{T}_i (MJ/C)
$h_f(T_o)$	liquid enthalpy at exit of downcomer \bar{T}_o (MJ/C)
\dot{Q}_{pump}	energy generated by RCPs (MW)
\dot{Q}_{brk}	energy lost from the primary system break (MW)
\dot{Q}_{SG}	energy transferred to or from the steam generators (MW)
$M_{prim,f}$	mass of primary liquid (kg)
$M_{Int.met}$	mass of internal metal (kg)
$M_{Ext.met}$	mass of external metal, i.e. pressure boundary (kg)
$Cp(T_{av})$	heat capacities of respective materials at T_{av}
δ_{mcp}	variation of the effective metal heat capacity
Fac	fraction of pressure boundary that adds to the effective heat capacity
δ	uncertainties associated with the respective terms.

Subscripts

Brk	break
CL	cold leg
Dec	decay heat
dc	downcomer
f	fluid
HL	hot leg
sen	sensitivity
SG	steam generator

1. INTRODUCTION

1.1 Background

Prior to 1978, it was postulated that the most severe thermal shock scenarios were large loss of coolant accidents (LOCAs). The combination of rapid decrease in temperature and the coldness alone could cause vessel failure (through-wall crack). The Rancho Seco event (March 20, 1978) raised concerns that secondary side induced overcooling combined with repressurization of the reactor coolant system could cause worse conditions because of the combination of low temperatures and high pressures. This would maximize the tensile stress imposed on the inside surface of the reactor vessel.

Should events more serious than Rancho Seco occur with a highly embrittled vessel due to neutron irradiation, it was postulated that small flaws existing on or near the vessel surface could propagate through the wall. The U.S. Nuclear Regulatory Commission therefore, designated pressurized thermal shock (PTS) as an unresolved safety issue (A-49) [Rosenthal 2001].

Between 1983 and 1985, the NRC selected three pressurized water reactors (PWRs) for the Integrated Pressurized Thermal Shock (IPTS) analysis. The three plants were: Oconee Unit 1 (Babcock & Wilcox (B&W)), Calvert Cliffs Unit 1 (Combusting Engineering (CE)) and H.B. Robinson Unit 2 (Westinghouse).

The IPTS study of Calvert Cliffs-1 concluded [Selby, Ball et al. 1984]:

- Small break loss-of-coolant accidents (LOCAs) occurring during low decay heat conditions were the most significant risk contributors.
- Uncertainty in the vessel flaw density was the most important contributor to the overall uncertainty in the risk.
- The most important operator action in mitigating PTS risk was controlling repressurization after a rapid cooldown.

The H.B. Robinson study concluded [Selby, Ball et al. 1985]:

- Main steam line breaks (MSLB) involving blowdown of more than one steam generator (steam generator) were the most important risk contributors.
- Uncertainty in vessel flaw density was the most important contributor to uncertainty in the risk.
- The most important operator actions to mitigate the PTS risk were:
 - Closing main steam isolation valves (MSIVs) following a small or medium-sized MSLB down stream of MSIVs, and
 - Isolating auxiliary feedwater (AFW) to the broken steam generators following a MSLB.

The Oconee-1 study concluded [Burns, Cheverton et al. 1986]

- MSLB was the most significant risk contributor.
- Uncertainty in downcomer temperature was the most important contributor to uncertainty in the risk.

- The most important plant features that mitigate the PTS challenge were
 - Reactor vessel vent valves, and
 - Feedwater pumps tripping on high steam generator levels.
- The most important operator action to reduce the PTS challenge was isolating a steam generator during a MSLB.

A number of studies had been performed in understanding PTS related phenomena such as

- Fluid-fluid thermal mixing [Theofanous and Yan 1991; Bass, Pugh et al. 1999];
- Probabilistic fracture mechanics (PFM) sensitivity study using small break LOCA transients as the leading conditions for the Yankee Rowe reactor pressure vessel [Dickson, Cheverton et al. 1993],
- Impact of heat transfer coefficient uncertainty [Boyd and Dickson 1999], and
- International efforts of understanding PTS related materials characteristics [Ikonen 1995; Pugh and Bass 2001].

A recent thermal hydraulic re-evaluation of H.B. Robinson was performed [Palmrose 1999]. Four different initiating events were analyzed, 2-inch break in the hot leg, 2-inch break in the cold leg, MSLB at hot standby, and steam generator overfeed. The study indicated that small hot leg break LOCA and MSLB were the most important contributors to risk.

These prior studies presumed that a PTS challenge required low downcomer temperatures AND pressure stress.

1.2 Achievements and Observations

Assessment of PTS risk uncertainty must include collaboration of multiple disciplines, including probabilistic risk assessment (PRA), thermal hydraulics, and probabilistic fracture mechanics (PFM). This report discusses the methods and results in analyzing the thermal hydraulic contributions to PTS risk uncertainty. The report is not stand-alone, because actual uncertainty distributions are possible only when combined with PFM and PRA. This study focuses how thermal hydraulic distributions were generated, that were then used as boundary conditions to the PFM analysis. The following are achievements from this study:

Identified large break LOCA as a significant PTS contributor. The IPTS study narrowed the LOCA break spectrum to small breaks on the belief that pressure was necessary to generate a through-wall crack. The current study assessed the complete break spectrum, and identified break size as a dominant factor. PFM calculations of large LOCA sequences showed them to be a significant PTS risk contributor, and indicate that downcomer temperature alone could cause through-wall cracks.

Approached the uncertainty process from top-down rather than bottom-up. The Phenomena Identification and Ranking Technique (PIRT) process is generally viewed as bottom-up. Direct application of the Code Scaling, Applicability, and Uncertainty (CSAU) methodology, including PIRT, and was not possible as the basic approach to the current uncertainty analysis. A top-down approach was developed to identify the key parameters. This was then combined with the bottom-up PIRT process. Sensitivity studies were then performed to rank the important parameters.

A classification matrix was developed through the top-down approach to classify event categories for PTS risk analysis. The matrix classifies events according to clearly identifiable plant boundary conditions. The classification reduces the number of key parameters needed for analysis, which reduces analysis complexity to something manageable.

Developed a method to identify representative scenarios. A figure of merit was identified for measuring sensitivities of individual parameters. Justified assumptions were applied to assess the combined effects of multiple parameters. Representative scenarios were identified directly that were used as the basis for determining thermal hydraulic uncertainties. The thermal hydraulic uncertainty is expressed by the three thermal hydraulic parameters that are boundary conditions to the PFM analysis. They are downcomer fluid temperature (T_{dc}), pressure (P), and convective heat transfer coefficient between vessel inner wall and the downcomer fluid (h_{dc}). No numerical processing was required to generate artificial time histories of the three thermal hydraulic parameters relevant to PTS risk for the representative scenarios.

Performed a thorough parameter sensitivity assessment. The one-factor-at-a-time method was used to outline RELAP5 calculations to assess the sensitivity of each parameter. Between 100 and 200 RELAP5 calculations were performed for each plant. The PFM code FAVOR was used to determine the conditional probability of vessel failure (CPF) of these RELAP5 calculations. The results provided rich information to understand the relationship between thermal hydraulic behavior and PFM.

Key observations were:

For events with similar thermal hydraulic signatures, the effect of uncertainty in pressure (P) on PTS uncertainty is small compared with the impact of downcomer temperature (T_{dc}) uncertainty.

The two categories of: 1) large LOCAs, and 2) pressurizer safety/relief valve (SRV) stuck open and later reclosed, are the most risk significant.

For pressurizer SRV stuck open and later reclosed scenarios, the timing of SRV reclosure, and the timing of operator throttling HPI, both affect risk significantly.

Reducing HPI flow rate in small LOCA scenarios reduces their risk contribution significantly.

1.3 Limitations

The following restrictions apply:

- The PFM code FAVOR input requirements dictated that classes of scenarios be represented by selected representative scenarios. That is, discrete time-histories $T_{dc}(t)$, $P(t)$ and $h_{dc}(t)$ are required as opposed to distributions. The thermal hydraulic inputs to PFM analysis are, therefore, deterministic time histories of T_{dc} , P , and h_{dc} of representative scenarios, along with the PRA frequency of the individual representative scenarios.
- The thermal hydraulic uncertainty analysis focused on the risk dominant event categories. The scenarios analyzed were chosen to represent a huge number of scenarios in the PRA model (181,258 for Oconee, 8,298 for Beaver Valley, and 3,425 for Palisades)

- FAVOR was under development during the thermal hydraulic uncertainty method development phase, so PFM calculations were unavailable to aid the effort. The relationship between thermal hydraulic behavior and its PFM impacts could not be assessed without FAVOR calculations. To screen thermal hydraulic transients in terms of assessing their PTS significance from the PFM perspective, a screening criterion of $T_{dc} < 150C$ (300F) was adopted. The screening criteria used were qualitative (e.g., repressurization is significant to PTS).

1.4 Tasks and Process

PTS uncertainty analysis is complex since it involves a variety of sources of uncertainty, such as the PRA model construction, human factors, thermal hydraulic analysis, plant design, PFM modeling, and their various interfaces. It requires collaboration of professionals in different disciplines to achieve the goal. This project developed a systematic way of analyzing PTS uncertainty. In doing so, the project consisted of a joint effort by three groups, under the direction of NRC staff.

The PRA group was composed of NRC, SNL, INEEL, and SAIC. This group was responsible for interacting with plant staff to construct a PRA model for PTS scenarios. In order to manage the huge number of event sequences generated in the PRA model for further thermal hydraulic uncertainty analysis, a limited number of *bins* were specified to group sequences having similar thermal hydraulic characteristics. The probability of a bin is the cumulative probability of the grouping of sequences.

The thermal hydraulic group included two subgroups. One assessed and applied the thermal hydraulic code used for the analyses, RELAP5/MOD3, and included NRC, Information Systems Laboratory (ISL), Oregon State University (APEX experiments), and University of Maryland. The second developed methods to quantify thermal hydraulic uncertainty. This involved identifying representative scenarios that served to determine the thermal hydraulic uncertainty through FAVOR analysis. The group included experts from the NRC and the University of Maryland.

The PFM group included NRC, Oak Ridge National Laboratory, and University of Maryland. This group was responsible for FAVOR development and computations.

PTS uncertainty includes three categories of uncertainty associated with the above three groups. Figure 1-1 shows the conceptual process to aggregate the uncertainties. The block on the left hand side represents the event trees constructed based on the PRA model. To reduce such a huge number of sequences to a manageable number, *bins* (typically ~100) were identified. Sequences with similar thermal hydraulic responses were binned together, so each bin represented a group of similar events whose frequency was an aggregate of the frequencies of many scenarios comprising the bin. The binning was iterative between PRA, thermal hydraulics, and PFM, to ensure the number, scope, and definition of bins was adequate to cover the entire risk space.

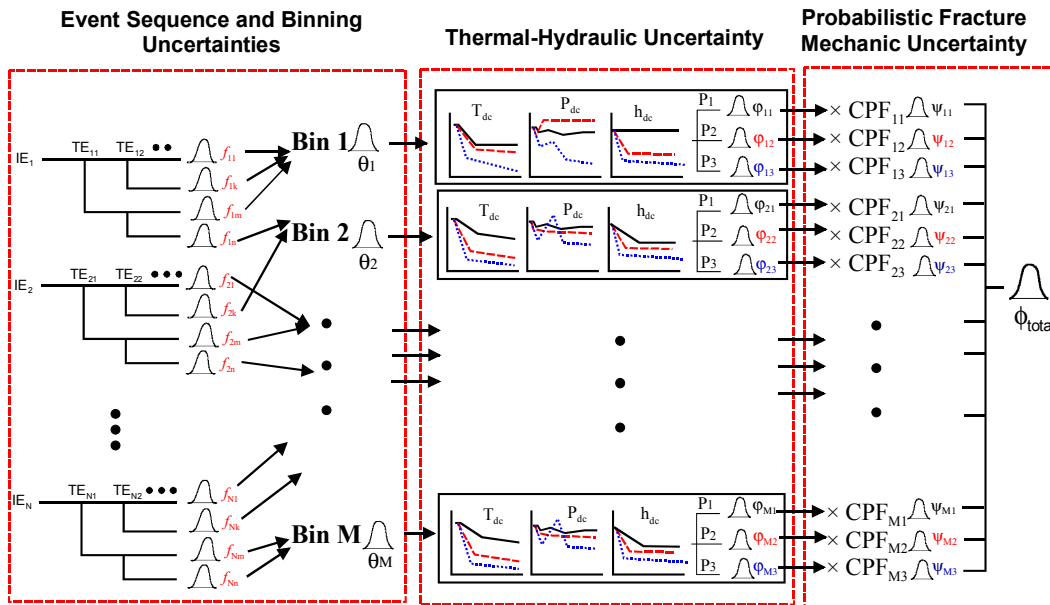


Figure 1-1 Conceptual model of the PTS uncertainty analysis process

Each bin represents a cluster of similar events that exhibit some range of thermal hydraulic response. The range and uncertainty of thermal hydraulic response within a given bin must be characterized; the thermal hydraulic uncertainty analysis assessed the uncertainty of thermal hydraulic behavior (i.e., T_{dc} , P , and h_{dc}) within a bin.

Multiple *scenarios* were selected to *represent* each bin. The total probability of the bin was apportioned among the *representative scenarios*. Typically three to five scenarios were identified to characterize each bin. RELAP5 was used to calculate the representative scenarios to generate time histories of T_{dc} , P , and h_{dc} , which along with the *probability distribution* of the bin, are the inputs required for PFM analysis. The *probability distribution* is that which is generated by PRA to characterize the family of event sequences that make up a given bin. PFM analysis is based on the time history of T_{dc} , P , and h_{dc} of each representative scenario, to calculate conditional probability of vessel failure (CPF). FAVOR employs post processing to combine CPFs with event frequencies (probabilities) all representative scenarios to generate a total PTS risk number.

Thermal hydraulic uncertainty was performed for risk dominant categories of events (bins). Uncertainty was not analyzed for the bins that contributed minimally to risk. For such bins, conservative representative scenarios were selected to represent the bins. Bins that did not contribute to risk were eliminated (Figure 1-2).

PRA uses a bottom-up approach to build PRA models (i.e., event trees). The process differed from the top-down approach used by the thermal hydraulic group. In the end, the two approaches reached the same results in event classification, with the exception of minor differences in the scope of some event categories. For example, LOCAs were divided into small (< 2-inch), medium (2 to 6 inch), and large LOCAs (> 6 inch) in the PRA model, based on historical definitions. The thermal hydraulic analysis divided LOCAs into <1.5 inch, 1.5 to 4 inch, 4 to 8 inch, and > 8 inch, based on their important thermal hydraulic similarities. As a result of the somewhat different definitions, the probability of a PRA bin could be split into two thermal hydraulic event categories, and a thermal hydraulic category could share probabilities from more than one PRA bin.

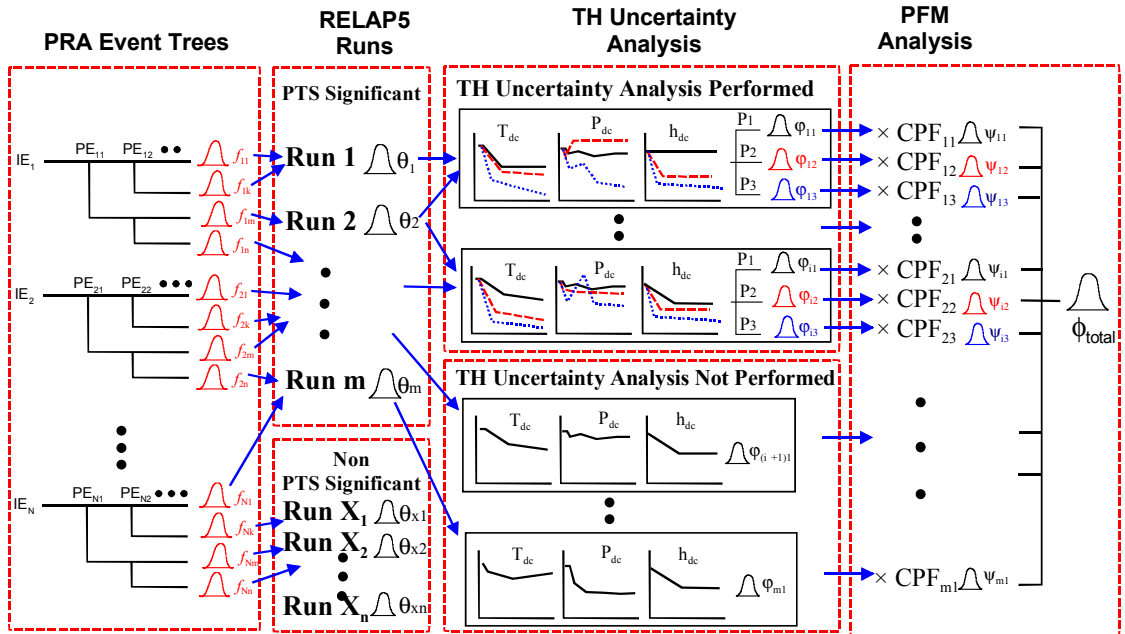


Figure 1-2 Implemented model of PTS uncertainty analysis process

Chapter 2 reviews the most recent PTS study of H.B. Robinson. Chapter 3 summarizes the task flow for thermal hydraulic uncertainty assessment, which included: identification of factors affecting downcomer temperature and pressure; event classification; identification of the key influencing parameters at the system level; determination of the scope of uncertainty analysis; sensitivities of influencing parameters; uncertainty assessment; and selection of representative scenarios.

Chapter 4 discusses: identification of factors affecting downcomer temperature and pressure stress; event classification; identification of the key influencing parameters at the system level; and determination of the scope of uncertainty analysis. A top-down approach was used to identify the factors affecting downcomer temperature and pressure stress. The process parameters and phenomena at the system level are discussed and their impacts are assessed. A classification matrix is constructed to facilitate the analysis effort. The matrix classifies events based on the main factors affecting downcomer temperature and pressure. The boundary conditions of each cell within the matrix is clearly defined, which reduces the number of influencing parameters needed to be considered for the analysis and dramatically reduces the analysis effort.

Thermal hydraulic uncertainty analysis is based on RELAP5. The use of a code combines *physical modeling uncertainty* with *parameter uncertainty*. *Parameter uncertainty* is defined as relating to the boundary conditions characterizing a given plant and transient. Parameter uncertainty is represented in the RELAP5 input deck. Physical modeling uncertainty is defined as relating to physical models and numerics of RELAP5. Chapter 5 discusses RELAP5 modeling uncertainty from known weaknesses and inherent limitations in the code. Some of them are treated explicitly and some of them are not treated in this report, but are addressed elsewhere. For example, fluid-fluid mixing in the cold leg and downcomer, and downcomer plumes cannot be modeled by a one-dimensional code.

Chapter 6 discusses parameter sensitivity. LOCA is identified as the most risk significant category. The parameters affecting PTS risk for LOCAs are identified, and their sensitivities are

assessed. A *figure of merit* (T_{sen}) was chosen as a *sensitivity indicator* to measure parameter sensitivities. T_{sen} was determined by RELAP5 by averaging T_{dc} over the first 10,000 seconds of the calculation, to obtain a single valued indication of downcomer temperature. Use of T_{sen} allowed representative scenarios to be determined without performing untenable numbers of RELAP5 and FAVOR calculations. A calculational matrix was developed for each plant to determine T_{sen} for each influencing factor, using the *one-factor-at-a-time* method. Hundreds of RELAP5 calculations were performed to obtain values for T_{sen} for the three plants.

Chapter 7 discusses analysis results of Oconee-1, Beaver Valley, and Palisades. Medium LOCA, Large LOCA, and pressurizer SRVs stuck open and later reclosed scenarios are concluded to be the dominant initiators for PTS risk. Chapter 8 discusses the relationship between T_{sen} and CPF. In this analysis, the pressure stress uncertainty is limited for each category. The PTS uncertainty is mainly dependent on the uncertainty of downcomer temperature. T_{sen} is used as a surrogate downcomer temperature indicator. It is used to select the representative scenarios. The appropriateness of T_{sen} selection is discussed.

Chapter 8 discusses the appropriateness of using T_{sen} as the sensitivity indicator. Values obtained for T_{sen} are compared to corresponding values of CPF.

Appendix A discusses system response to perturbations, which can be damped, proportional, or augmented. The key factors of different types of effects are discussed. This classification of perturbation-response is seen in the numerous sequences analyzed by RELAP5, and is an indicator of plant behavior with respect to PTS.

Appendix B supports the argument that h_{dc} uncertainty has a lesser contribution to PTS uncertainty, relative to temperature and pressure. Appendix B is an independent analysis that reached the same conclusion as Boyd and Dickson [Boyd and Dickson 1999] as well as several earlier studies, namely that heat flux from the vessel wall is conduction limited. The evaluation of temperature gradients within the wall then depends principally on the fluid temperature $T_{dc}(t)$, and the uncertainties associated with the evaluation of $h_{dc}(t)$ have a reduced influence.

Appendix C addresses uncertainty in steam generator heat transfer. It concludes that steam generators are "over designed" when the reactor is tripped. That is, the heat transfer area is sized for greater than 100% power while decay heat levels are ~1% power, providing a factor of 100 on heat transfer area. The uncertainty in heat transfer, therefore, is trivial. The secondary side becomes the heat source in many transients to moderate the decrease in T_{dc} with the primary system coupled to the secondary.

Appendix D places the thermal hydraulic representative scenarios in the PTS event classification matrix for Oconee-1.

Appendix E is the C++ computer code developed to calculate effects on T_{sen} from the varied combinations of multiple factors. The results provide a foundation for identifying representative scenarios to characterize the range of behavior within a given bin.

Appendix E lists the vessel conditional probability of failure (CPF) results calculated by the FAVOR code for the parameter sensitivity study from a study done to validate the appropriateness of use of T_{sen} .

Appendix F lists the RELAP5 calculations performed by ISL and their placement in the PTS event classification matrix.

2. LITERATURE REVIEW AND STUDY RESTRICTIONS

This chapter reviews the H.B. Robinson (HBR) PTS uncertainty study [Palmrose 1999], which was the most recent PTS uncertainty study prior to the current effort. It was intended to update the earlier IPTS study using uncertainty methodology. The HBR-2 study applied a slightly modified Code Scaling, Applicability, and Uncertainty (CSAU) methodology [Boyack, Catton et al. 1990] to assess thermal hydraulic uncertainty.

The original and modified processes of the CSAU methodology are shown in Figures 2.1 and 2.2 respectively. The CSAU methodology was the first method to determine code uncertainty for thermal hydraulic applications. The method was used to develop a regulatory guide for best-estimate analysis and to demonstrate the feasibility of such analysis, in support of the NRC rule revision to 10 CFR 50.46 in 1988 allowing best-estimate methods of LOCA. The revised rule also required quantifying the uncertainty of the best-estimate results for comparison with the prescribed acceptance limits. The CSAU methodology was first used to assess peak clad temperature (PCT) uncertainty in a large break LOCA.

The HBR study reanalyzed four events from the IPTS study: 2-inch hot leg LOCA, 2-inch cold leg LOCA, MSLB from hot zero power (HZP), and steam generator overfeed. For each scenario, the PIRT process was applied to develop PIRT tables identifying and ranking phenomena by importance. For each phenomenon, values for upper bound, nominal, and lower bound were identified.

From this, a matrix of uncertainty calculations was developed to identify baseline thermal hydraulic runs. In the original CSAU method, a response surface methodology was used to combine the one-factor-at-time results of individual runs. The HBR study instead placed important parameters into common groups based on their impact on PTS. Two groups were created for parameters of similar impact: a) injection flow rate (HPI and accumulator flows); and b) injection temperature (Refueling Water Storage Tank (RWST) and accumulator temperatures).

Three parameters could not be grouped and were discussed separately: a) vessel wall thermal conductivity; b) flow distribution and mixing in downcomer; and c) break flow. The first two were the subject of a sensitivity study that investigated both plumes and h_{dc} . In this study, downcomer temperature variation was analyzed using REMIX and COMMIX. From the calculations, three plumes were generated (nominal, strong, and weak), the effects of which were evaluated using an early version of FAVOR. The study indicated that the impact of possible plumes on vessel failure probability was small [Dickson 1997]. Similar conclusions were reached regarding uncertainty in heat transfer coefficient.

An uncertainty calculation matrix was developed for the two parameter groups. The calculation matrix typically included a nominal run, upper and lower bounding runs, and a few intermediate runs. In total, six RELAP5 runs were performed to assess PTS uncertainty of 2-inch hot leg LOCA. Different thermal hydraulic calculation codes, such as TRAC-P, REMIX, and COMMIX, were used to validate RELAP5 results.

Finally, a numerical method was used to manipulate the results of the baseline RELAP5 runs, to generate new T_{dc} , P , and h_{dc} time histories. These new scenarios were generated by selecting

the data with the lowest T_{dc} and highest P from all the baseline runs, to obtain upper and lower bounds, with the intention of combining the lowest temperature with the highest pressure for PTS challenge. The mean scenario was the numerical average of all the baseline runs. Uniform distribution was assumed for all parameters. The lower, mean, and upper bound scenarios represented the 5th, 50th, and 95th percentiles for thermal hydraulic uncertainty, and were used for the PFM calculations.

The uncertainty scenarios representing the 5th, 50th, and 95th percentiles for thermal hydraulic uncertainty were, therefore, numerically manipulated products rather than real scenarios. For example, the 95th percentile scenarios had the lowest T_{dc} and highest P of all baseline scenarios. In reality, scenarios with lower T_{dc} usually have lower P . The HBR study's approach also did not include the impact of repressurization on PTS risk. The category, SRV stuck open and later reclosed was one of the risk dominant groups in the current study.

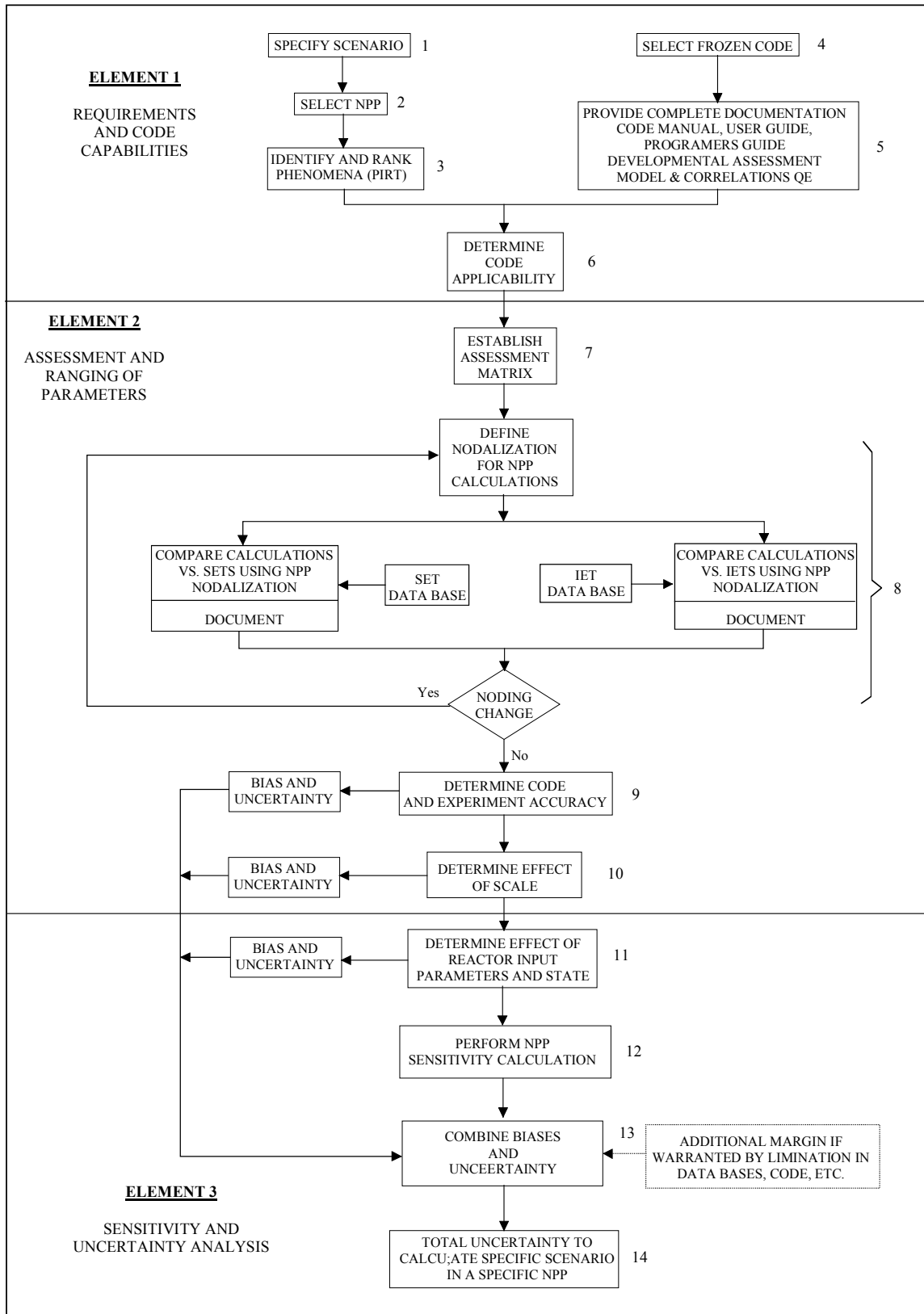


Figure 2-1 Code Scaling, Applicability, and Uncertainty (CSAU) methodology

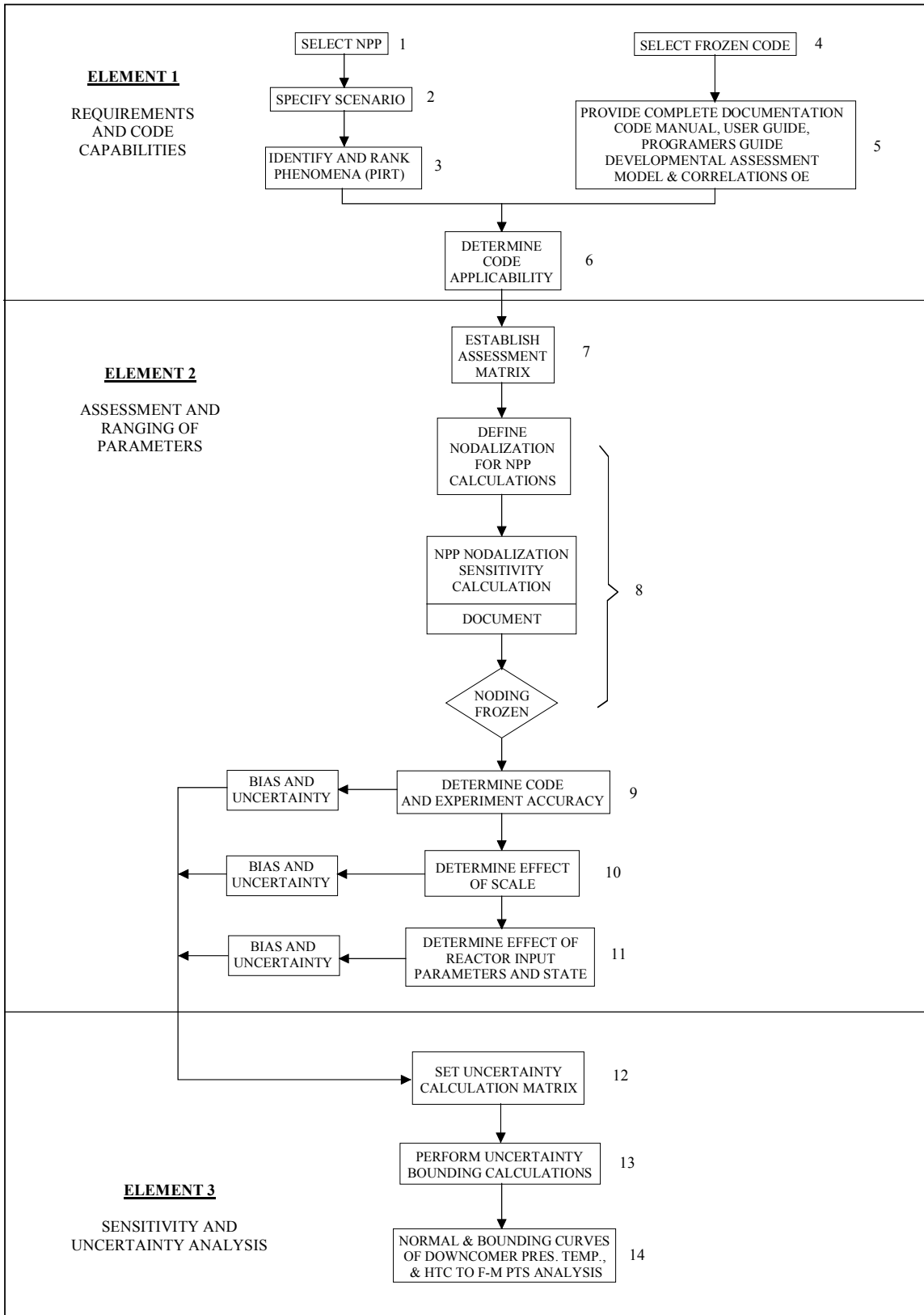


Figure 2-2 Process of the H.B. Robinson Unit-2 PTS uncertainty methodology

3. THERMAL HYDRAULIC UNCERTAINTY ASSESSMENT PROCESS

This Chapter summarizes the task flow for thermal hydraulic uncertainty assessment. It includes: identification of factors affecting downcomer temperature and pressure, event classification and identification of the key influencing parameters at the system level, determination of uncertainty analysis scope, sensitivities assessment, uncertainty assessment, and selection of representative scenarios. These tasks are divided into nine steps, with iterations between some steps. The purpose of these steps is to facilitate the analysis effort. Steps 1 to 3 are the foundation for understanding PTS and plant design factors that influence PTS analysis. The “real” uncertainty analysis starts at Step 4. Some steps required PRA and PFM inputs. The following paragraphs provide an introduction to these steps. The detailed process of each step is discussed in the rest of this report.

Step 1 Apply basic principles and plant-specific design characteristics to identify key influencing factors

Thermal hydraulic uncertainty for PTS consists of three parameters: T_{dc} , P , and h_{dc} . The impact of h_{dc} on the evaluation of temperature gradients within the vessel wall was studied previously [Boyd and Dickson 1999], where it was concluded that heat flux was controlled primarily by the internal, conductive resistance, that is, heat transfer is conduction limited. The impact of $h_{dc}(t)$, as well as the computational uncertainties associated with $h_{dc}(t)$, is therefore limited. Appendix B is an independent analysis done as part of this study that reached the same conclusion. Therefore, the uncertainty assessment focused on the remaining two parameters, $T_{dc}(t)$ and $P(t)$.

The basic factors affecting an open system’s temperature are the heat capacity of the system and the heat sources and heat sinks introduced into the system. Downcomer temperature is affected by the secondary system. Reactor coolant system (RCS) flow (i.e., forced circulation, natural circulation, and flow stagnation) is an influencing factor, which in turn is affected by the state of the secondary system. Some plant-specific design features affect the fluid temperature distribution inside the vessel and, consequently T_{dc} . For example, the reactor vessel vent valves (RVVVs) of the B&W reactor allow in-vessel natural circulation of hot water/steam from the upper plenum to the upper downcomer. From there, the flow can mix with cold leg flows and cause an increase in $T_{dc}(t)$. The key factors influencing T_{dc} are in summary,

- Heat capacity
- Heat source
- Heat sink
- RCS coolant flow rate
- Vessel internal fluid/stream energy distribution

The factors that affect the pressure (dP/dt) of a constant volume system are the mass and energy change of the system. For the RCS, change in mass is from flow of coolant in and out of the system. The change in RCS energy is dependent on the heat sources and heat sinks of the system. Besides mass and energy, thermal non-equilibrium steam condensation occurring in RCS could change reactor pressure. The key factors influencing $P(t)$ are, in summary,

- Change in RCS coolant inventory
- Change in heat source and heat sinks
- Steam condensation in RCS

Some of the influencing parameters of $T_{dc}(t)$ and $P(t)$ are identified from the plant design, while some require more elaboration to identify the basic parameters. For example, a primary system break would induce a heat sink to RCS. The basic parameters relating to primary system break are break size and break location.

Step 2 Construct PTS event classification matrix

Consider the heat capacity at initial conditions of the primary and secondary systems. A large heat sink must be induced to have a PTS scenario. From examining such scenarios, a PTS event classification matrix is constructed. Three categories of events frame the matrix: primary system breaks, secondary system depressurization, and steam generator overfeeding. An additional factor, HPI state, is considered in all scenarios, since energy and inventory are dependent on HPI state.

The event classification matrix facilitates uncertainty analysis in three ways. First, the matrix provides a framework to perform preliminary screening in order to focus on PTS-significant categories. Second, through well-classified categories with clearly defined boundary conditions, the number of influencing parameters to be considered can be reduced (screening step). Third, the matrix provides a framework to perform scenario propagation. The classification matrix is especially helpful in identifying operator actions, which can be an important factor contributing to PTS risk and uncertainty.

Step 3 Screen categories of events and scenarios to identify those with PTS potential

The PTS event classification matrix provides a framework for preliminary screening to eliminate the PTS-insignificant categories. Initial screening includes low event frequency and low fracture mechanics challenge. Since frequencies of the initiating events that construct the matrix can be estimated, the frequencies of event categories involving one or several combinations of initiating events can be estimated as well. The screening criterion used for event frequency was $1E-8$ per reactor year (from PRA). For screening the fracture mechanics challenge screening, the categories and sequences for which T_{dc} did not drop below 150C (300F), or cause a cooldown ramp rate ($dT_{dc}(t)/dt$) greater than 56C/hr (100F/hr) were screened out from further analysis.

Step 4 Select risk-dominant categories for uncertainty analysis

From the remaining (not screened out) categories, representative scenarios are identified. The CPFs for these representative scenarios are calculated. The CPFs along with the event frequencies determine the risk contribution of the category. The relative risk of different categories is used to prioritize the uncertainty analysis to concentrate on the categories with greatest contribution to overall risk. For the three plants analyzed, *primary system break causing loss of subcooling* (LOCA) is the dominant category contributing to PTS-risk, and so, thermal hydraulic uncertainty analysis focused on this category alone.

Step 5 Refine risk-dominant categories to reduce variations in RCS pressure

The event categories defined in step 4 are coarse, containing a wide range of T_{dc} and P outcomes, and require discretization. The uncertainty and variability of P for events that contribute to PTS is smaller than contributions from T_{dc} uncertainty for a given category, but remain nontrivial. When event categories are refined to reduce contributions from P variation, the uncertainty analysis can then be based on T_{dc} alone.

For example, the category of primary system break causing loss of subcooling includes two types of scenarios: LOCAs and SRVs stuck open. For LOCAs, sensitivity analysis indicated that break sizes >1.5 inch were required for the RCS to lose subcooling. Very small break were, therefore, screened out from the break spectrum. The remaining LOCA break spectrum was subdivided into three groups, 1.5 to 4 inch, 4 to 8 inch, and >8 inch. With this refinement, variations in pressure are now reduced within each category.

For pressurizer SRV stuck open scenarios, the RCS repressurizes if the valve recloses. In such situations, the uncertainty in P must be considered. The pressurizer SRV stuck open scenarios are divided into two groups, based on whether or not the valve recloses later in time.

Thus, five new categories are generated from the original category of LOCA. These categories are also referred to as **bins**. Only one bin requires treating both T_{dc} and P uncertainties; the other four are focused on T_{dc} uncertainty alone.

- 1) LOCAs 1.5 to 4 inch
- 2) LOCAs 4 to 8 inch
- 3) LOCAs >8 inch
- 4) Pressurizer SRV stuck open and remains open
- 5) Pressurizer SRV stuck open and later recloses (treat both T_{dc} and P uncertainties)

Step 6 Identify sources of uncertainty and corresponding ranges

For each bin (category of events) in Step 5, identify the key parameters influencing T_{dc} (and P if necessary). The system parameters relating to the five T_{dc} -dependent factors and three P-dependent factors from Step 1 must be identified. The influencing factors affecting T_{dc} and P are:

- Heat capacity: initial conditions of liquid mass, steam mass, and structure mass of the primary system and secondary system
- Heat sources: decay heat, reactor coolant pump heat, structure heat, and pressurizer heater
- Heat sinks:
- Break size, break location (i.e., elevation and HL vs. CL), break flow rate, pressurizer SRV reclose timing
- Emergency core cooling (ECC) injection temperature, flow rate
- Energy transferred to and from the secondary system. Depressurization and overfeeding of the secondary system induce excessive heat sink to RCS.
- RCS coolant flow rate: RCP state, loop flow resistance
- Vessel internal fluid energy distribution: reactor vessel vent valves (B&W), bypass flow

Sources of uncertainty include both physical models and parameter (boundary conditions). For each factor, its range of variation must be identified. This range is discretized by its lower bound, nominal value, and upper bound, with appropriate probabilities assigned. It is important to identify common causes for different parameters. For example, the HPI, accumulator, and LPI coolant temperatures vary with seasonal differences.

Step 7 Perform sensitivity analysis of each influencing factor

A matrix was formulated to assess the sensitivity of each influencing factor using the Nominal Range Sensitivity Analysis (NRSA) method [Cullen and Frey 1999; Frey and Patil 2002], which can be called the one-factor-at-a-time (1-FAT) method. Break size is an independent factor, while the sensitivities of all other factors are dependent on break size. Each influencing factor was, therefore, evaluated at various break sizes.

Based on the ranges in values identified in Step 6 for each influencing factor, each factor's importance was assessed by RELAP5 calculations. For example, the importance of winter conditions was assessed by comparing RELAP5 results (i.e., T_{sen}) using ECC injection temperatures of spring/fall versus winter. The difference in T_{sen} was the importance measure.

Step 8 Determine the aggregate uncertainty and select representative scenarios

The assumption was made that the effects of individual influencing factors were linear and were, therefore, additive. If this proved to be true, then the combined effect of multiple sources of uncertainty could be readily determined, using T_{sen} as the importance measure. The assumption, naturally, does not work for scenarios where different influencing factors are interdependent. The linearly additive assumption was found to be valid for LOCAs, where the break is the dominant heat sink.

A small computing program (see Appendix D) was written to integrate the effect of all combinations of influencing factors. The sensitivity of the combination is the cumulative sensitivities of its convective. The probability of a combination is the product of the individual probabilities of its components. These combinations were plotted as a probabilistic density function (PDF) versus T_{sen} as shown in the left hand side of Figure 3-1.

The PDF was then transformed into a cumulative distribution function (CDF), plotted in the right hand side of Figure 3-1. Using the CDF plot, representative scenarios are then identified, as follows. In the CDF plot, first the tails of the distribution less than the 5th percentile and greater than the 95th percentile were dropped. Then the remaining distribution range from the 5th percentile to the 95th percentile was divided equally into several sections, the number of which depended on the detail required. The probabilities of the truncated tails were distributed to the lower bound and upper bound representative scenarios. For each sector, a representative scenario was defined at the mean of the distribution.

For example, a sector's probabilities for the lower and upper bounds are p_L and p_H , respectively. The representative scenario is selected at the $(p_L + p_H)/2$ position. The probability for this representative scenario is $(p_H - p_L)$. The representative scenario's T_{sen} was identified by graphing the x any y values on the CDF curve. Based on T_{sen} , the exact combinations of the representative scenarios can be identified from all the combinations (see the right hand side of Figure 3-1).

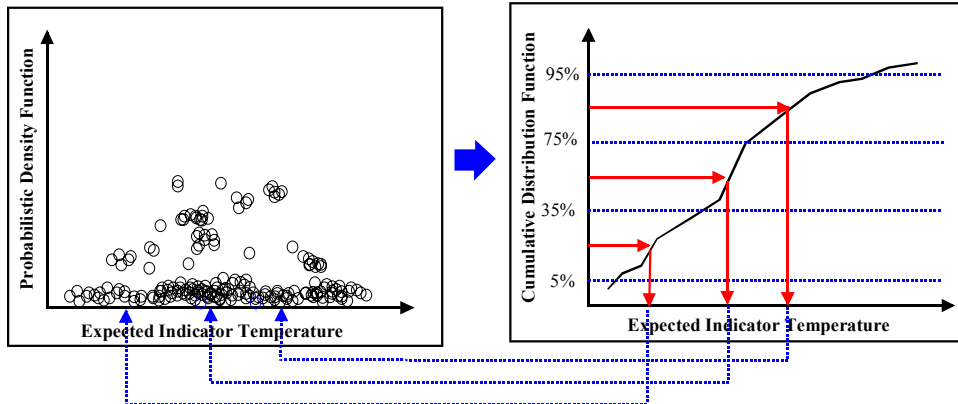


Figure 3-1 Probability density and cumulative distribution function diagrams for identifying representative scenarios

For example, assume for the moment that only two parameters contribute to uncertainty, break location and season. The season affects ECC temperature. The year is broken down into summer (probability = 25%), spring/fall (50%), and winter (25%). Break location can be either hot leg (50%) or cold leg (50%). The scenario, hot leg LOCA in the spring/fall, is the nominal reference. The value of T_{sen} for this scenario is called T_0 . $T_{sen}(T_0)$ is determined by RELAP5 calculation. As well, RELAP5 is used to calculate the remaining possibilities,

- 1) Nominal: hot leg spring/fall (0.250)
- 2) Hot leg – winter (0.125)
- 3) Hot leg – summer (0.125)
- 4) Cold leg – spring/fall (0.250)
- 5) Cold leg – summer (0.125)
- 6) Cold leg - winter (0.125)

The six one-factor-at-a time permutations provide six values of T_{sen} . The computing program from Appendix D is run to generate a PDF (left hand side of Figure 3-4), which is then transformed to a CDF (right hand side of Figure 3-4).

Step 9 Estimate the frequency distribution for each representative thermal hydraulic run

The total bin probability was subdivided and apportioned to the sectors it contained. A frequency distribution is generated for each bin, from which the frequency of a given sector was determined. The representative scenarios identified in Step 8 comprise the event frequency of their bin. Thus, the frequency of a representative scenario is the frequency of the bin (from PRA) times the fraction of bin frequency assigned to the representative scenario. In some cases, there were some differences in bin definition between the PRA group and the thermal hydraulic approach, in which case an adjustment factor was needed to make them consistent.

RELAP5 was used to calculate each representative scenario to generate the time histories of T_{dc} , P , and h_{dc} . In this way, the entire LOCA break spectrum was discretized to a degree sufficient to represent the actual continuum in a manner that could be then analyzed by FAVOR.

4. IMPORTANT SYSTEM CHARACTERISTICS AND PTS CLASSIFICATION MATRIX

Quantification of the uncertainties of T_{dc} , P , and h_{dc} required a careful assessment of their relative importance and their inter-dependence. These parameters vary in time, and their uncertainty band varies as well. Furthermore, for some types of transients, these parameters are not independent, consequently neither are their uncertainties. Chapter 4.1 discusses this from the thermal hydraulic perspective.

Irrespective of how the PTS significant transient scenarios are initiated, their evolution is dominated by the mass/energy exchange rates imposed on the fluid of the primary system. Therefore, terms in the mass/energy balance of the primary system fluid could be used as classification criteria. The large number of 'event' based scenarios can be classified into a significantly smaller number of categories. Chapter 4.2 illustrates a simple plant model to identify the factors that affect T_{dc} and P . Chapter 4.3 discusses the influencing factors from the perspective of T_{dc} , and Chapter 4.4 does the same from the perspective of P . Chapter 4.5 presents the PTS event classification matrix developed for this study to facilitate analysis.

4.1 PTS Driving Forces from a Thermal Hydraulic Perspective

PTS transients are initiated by some malfunction that cools down the RCS. PTS is a combination of sufficiently low wall temperatures with a sufficiently high total stress. Thermal hydraulic results are employed by PFM to determine stress and temperature in the vessel wall. Both wall temperature gradients and pressure contribute to vessel wall stress. The local temperature throughout the vessel wall is also very important because of its effect on material toughness.

When a pre-existing flaw propagates, the two possibilities that immediately follow are: 1) crack arrest, that is, the crack reaches a zone of low stress and high temperature and stops; or 2) through-wall cracking, that is, vessel failure. For a crack to arrest implies that crack ran until reaching a zone of high temperature and low tensile, or even compressive, thermal stress, as the crack approached the outer wall. Pressure effects may or may not play an important role as well. Often, however, for the crack to propagate through-wall implies high vessel pressure. The FAVOR code defines a through wall crack as 90% of the total vessel wall thickness.

Together, T_{dc} and h_{dc} determine the heat flux from the inner vessel wall to the downcomer fluid, which in turn determines the time-dependent wall temperature gradients. The relative importance of the two variables (T_{dc} and h_{dc}) is assessed by considering the thermal characteristics of the vessel. The vessel wall is ~0.22 m (8.5 inch) carbon steel, clad on the inside by a thin layer of stainless steel. The thermal conductivity of the steel is of moderate magnitude. Time periods on the order of hundreds of seconds are required for surface thermal effects to penetrate into the interior.

A quantitative measure of this characteristic is the Biot number, which is the ratio of internal to external resistance to heat transfer. For the vessel wall, this index is always well above 1. For typical values of h_{dc} , ~2000 W/m²C (350 BTU/hr-ft²-F) the Biot number can exceed 10. Note that forced flow (RCPs on) is not relevant to PTS scenarios, rather, the conditions in the

downcomer are characterized by natural circulation or “flow stagnation”). This indicates that primarily the internal resistance of the steel determines the heat flux from the vessel wall. The external resistance ($1/h_{dc}$) has relatively little effect.

A recent study evaluated the effect of h_{dc} [Boyd and Dickson 1999]. Additionally, a quantitative assessment covering the entire range of fluid conditions is presented here in Appendix B. For example, the time by which the centerline temperature changes by 10% of the equilibrium value is ~470s for a high value of h_{dc} , and ~480s for a low value. The two studies thus concur that for physically reasonable values of h_{dc} , the associated uncertainty contributed by h_{dc} is small. The uncertainty in h_{dc} was not, therefore, propagated further in this study, however, it was treated separately within the current PTS re-evaluation [Bessette, 2004].

Considering RCS pressure, a distinction must be made between the two classes of transients:

Transients for which pressure is determined by boundary conditions imposed on the primary system (e.g. PORV pressure settings, or by operator control). Primary system pressure is then independent of downcomer fluid temperature.

Transients for which a two-phase region develops and persists in the coolant loops. For these conditions, pressure is equal to the saturation pressure of the hottest fluid in the circuit, in which case $P = P_{sat}(T_{sat})$. P is not independent of T_{dc} ; the degree of dependence varies. If a sizable circulation rate is maintained, that is forced or natural circulation flow,

$$T_{hot} \sim T_{cold} = T_{dc}$$

and thus P and T_{dc} are coupled along the saturation line. For transients that involve “flow stagnation,” T_{dc} lags behind T_{hot} by a subcooling margin, which depends on the relative flows of ECC, loop natural circulation (if any), break flow, depressurization rate, and in-vessel natural circulation.

The system pressure has some uncertainty for both classes of transients. A *thermal hydraulic uncertainty*, however, exists only for the second class of transients. Uncertainties for transients of the first type reduce to human factors issues of how the operator controls the RCS pressure. Take the example of a stuck open pressurizer SRV that later recloses. HPI will refill the RCS, and if HPI flow is not controlled, the pressure reaches the pressurizer PORV set point. The uncertainty of $P(t)$ is dominated by operator action to control HPI. This is termed a controlled pressure sequence. If a scenario falls into the controlled pressure class of events, then a “nominal” pressure trace is evaluated, that is, uncertainty in pressure is attributed to uncertainty in operator action, since this is the dominant aspect of the transient. Operator action is part of the event tree and not part of thermal hydraulic uncertainty.

The conclusion of this brief review is that of the three “PTS relevant variables”, $T_{dc}(t)$ has the largest impact. T_{dc} depends both on the boundary conditions characterizing the transient, and the code used to analyze the transient. $T_{dc}(t)$ is, therefore, subject both to imposed boundary conditions (input deck) and to code (RELAP5) related uncertainties, namely, physical models and numerics. These are termed *parameter uncertainty* and *model uncertainty*, respectively. This will be discussed further in subsequent Chapters.

Fluctuations of T_{dc} in time need not be considered if they are short in comparison to the thermal time constant of the vessel wall. This conclusion, which is based on the magnitude of the vessel thermal time constant, has important consequences. As will be shown, most of the

thermal hydraulic time constants that characterize the primary system (e.g. the fluid circulation time constant, and the thermal time constant across the steam generator tubes) are shorter than the thermal time constant of the vessel wall. This means that from the PTS point of view, a computed result obtained by a mass/energy balance, rather than instantaneous mass/energy transfer rates, is adequate in most cases.

System codes such as RELAP5 perform balance (conservation) calculations accurately. This does not imply that “code related” uncertainties are not present. Such uncertainties exist in any computation of mass/energy exchange rates. However, if the time constants characterizing these rates are smaller than the thermal time constant of the vessel wall, the actual transfer rates, as long as they are in the appropriate range, contribute little to the uncertainty of the result. What matters is the equilibrium state of the system, which is determined by the heat capacity and the magnitude of the sink and source terms. The uncertainty of the computed result is then directly related to the uncertainty of these parameters.

4.2 Simple Nuclear Power Plant System Model

Figure 4-1 shows a generic schematic of a nuclear plant that groups basic components into control volumes,

Downcomer and pump discharge side of cold legs

Vessel minus downcomer

Hot legs, primary sides of steam generators, and pump suction sides of cold legs

Pressurizer and surge line.

The combined component blocks 1 through 3 represent the normal circulating side of the primary system. The diagram indicates the location of the principal energy source and sink, namely, core power or decay energy (\dot{Q}_{dec}) and the energy transferred to the steam generators (\dot{Q}_{SG}). In addition, the locations at which mass/energy interchange can take place during transients are shown. This includes:

HPI and accumulator injection into the primary system.

Cold or hot leg break.

Pressurizer PORVs and SRVs.

RCPs, which greatly affect loop circulation, and also are a significant energy source.

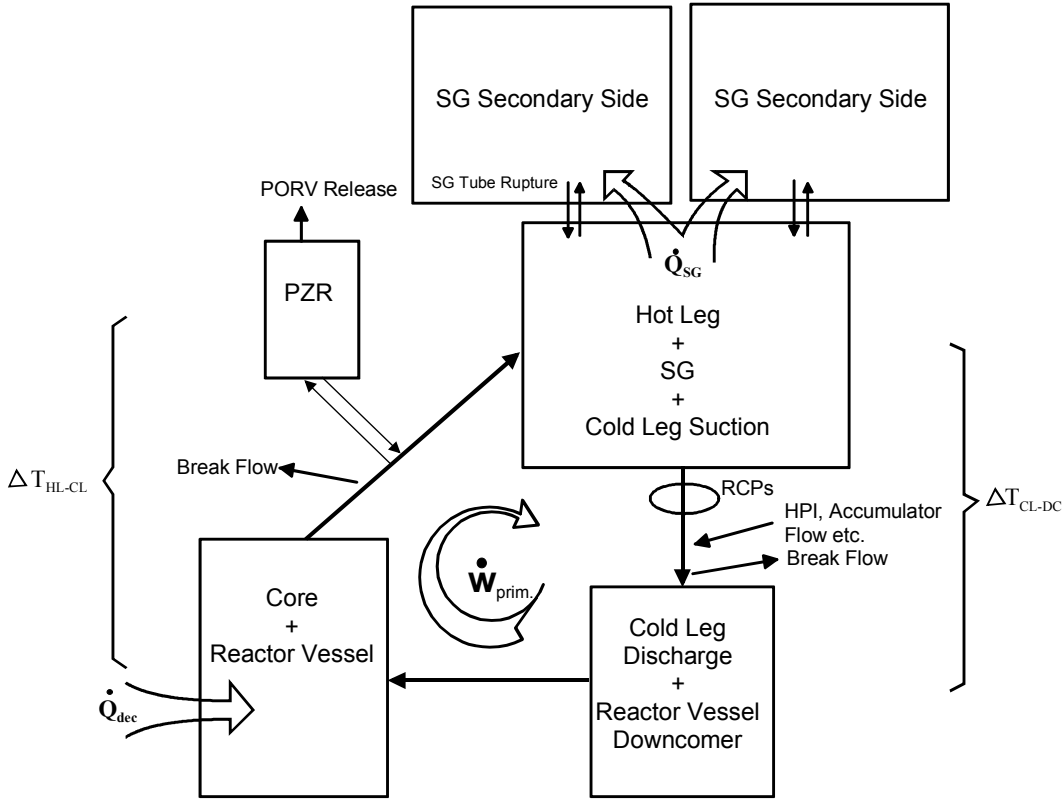


Figure 4-1 Schematic of PWR heat capacities and mass/energy sink/source terms

For forced or natural circulation flows, the RCS temperature distribution is relatively uniform, and all volumes have a similar temperature. The two variables T_{dc} and h_f are related as described in the convection equation. From the thermal hydraulic point of view we can derive the generic T_{dc} change rate from the following equation.

$$\frac{dT_{dc} \pm \delta}{dt} = \frac{(\dot{Q}_{dec} \pm \delta_{dec}) - (\dot{w}_{hpi} \pm \delta_{hpi}) \times \{ [h_f(T_i) \pm \delta_h] - [h_f(T_o) \pm \delta_h] \} + (\dot{Q}_{pump} \pm \delta_Q) - (\dot{Q}_{brk} \pm \delta_Q) - (\dot{Q}_{SG} \pm \delta_Q)}{[M_{prm,f} \times Cp_f(T_{av}) + (M_{Int.met} + Fac \times M_{Ext.met}) \times Cp_{met}(T_{av})] \pm \delta_{mcp}} \quad (4.1)$$

where:

- \dot{Q}_{dec} decay heat (MW)
- \dot{w}_{hpi} ECC flow rate (kg/s)
- $h_f(T_i)$ liquid enthalpy at entrance to downcomer \bar{T}_i (MJ/C)
- $h_f(T_o)$ liquid enthalpy at exit of downcomer \bar{T}_o (MJ/C)
- \dot{Q}_{pump} energy generated by SG RCPs (MW)
- \dot{Q}_{brk} energy lost from the primary system break (MW)

\dot{Q}_{SG}	energy transferred to or from the steam generators (MW)
$M_{prim,f}$	mass of primary liquid (kg)
$M_{Int.met}$	mass of internal metal (kg)
$M_{Ext.met}$	mass of external metal, i.e. pressure boundary (kg)
$Cp(T_{av})$	heat capacities of respective materials at T_{av}
δ_{mcp}	variation of the effective metal heat capacity
Fac	fraction of pressure boundary that adds to the effective heat capacity
δ	uncertainties associated with the respective terms.

Equation 4.1 is a general expression for the magnitude of dT_{dc}/dt . The uncertainty in dT_{dc}/dt comes from the heat sources and sinks identified in Equation 4.1. The most important energy sink is the break flow through the primary system break. Operator actions or component failures can change magnitudes of parameters and timing of events. The exchange rate with the steam generators \dot{Q}_{SG} can be positive or negative. The influencing factors for T_{dc} and P are discussed in detail in sections 4.3 and 4.4.

4.3 Downcomer Temperature Influencing Factors

The primary circuit of a PWR can be considered as a series of volumes and heat capacities. Coolant circulates through these volumes, and energy is added or subtracted as the flow moves through them. Volume temperature depends on,

- Relative magnitude of the heat sources or sinks, and
- Rate of energy addition or subtraction (relative to the circulation rate)

Heat capacity, heat sinks, heat sources, energy distribution, and RCS coolant flow rate are the factors affecting downcomer temperature. Varying these factors will, therefore, encompass all possible transient scenarios. Boundary conditions can be imposed either by an accident or by operator action, or they can be triggered and/or modulated by the state of the primary system (e.g. initiation and flow rate of HPI). The schematic shown in Figure 4-1 provides the basis for classifying the PTS significant transients, analyzing how uncertainties are associated with boundary conditions, and transforming thermal hydraulic analysis into uncertainties of the thermal hydraulic parameter T_{dc} .

Five T_{dc} influencing factors with their relevant convective/system state and phenomena are:

- Heat capacities
 - Primary system heat capacity, including liquid, steam, structures
 - Secondary system heat capacity, including liquid, steam, structures
- Heat sources
 - Decay heat
 - RCPs

- Heat sinks
 - Primary system break
 - Steam generators
 - HPI
 - Core flood tank/Accumulator
 - LPI
- RCS coolant flow rate
 - RCPs
 - Natural circulation
 - Flow stagnation
- Vessel energy distribution
 - In vessel natural circulation, mixing of hot water or steam from upper plenum into colder water in downcomer through bypass or RVVVs
 - Boiling and condensation

The component/system states and the phenomena of the above five groups are discussed in the following sections. Other parameters that were considered, but which were found to have that have little impact on T_{dc} , are not included in the above list. For example, the pressurizer heaters generate about 1.6 MW, which has trivial impact on T_{dc} .

4.3.1 Heat Capacities

The primary circuit of the simple plant model described in section 4.2 is depicted as a series of interconnected volumes. The capacitance of these volumes, together with the rate of fluid circulation, limits the rate at which both average and local fluid temperature can change.

Table 4-1 shows the overall mass and heat capacity of the Oconee-1 primary system for single phase and two phase conditions. The heat capacities change somewhat as a function of temperature, but the change is moderate. At a temperature of 230C (440F) the values decrease by ~5%. The numbers are large, which implies that only large energy removal rates can produce rapid temperature decreases.

Table 4-1 Inventory and Heat Capacity of Oconee-1 Primary System

State of Primary	Liquid		Vapor			Combined (MJ/K)	
	Mass (kg)	Heat Cap. (MJ/K)	Mass (kg)	Heat Cap. (MJ/K)	Evap Energy (MJ)	Vapor + Liquid	Vapor + Liquid + Metal
Liquid Solid	2.57E5*	1360**	--	--	--	1360	1690
25% Steam	1.93E5	1080	3170	16	4760	1030	1360
50% Steam	1.29E5	680	6350	32	9520	710	1040

*Without pressurizer

**Evaluated at $p = 7.2$ MPa (1045 psia), $T_{HL} = 290$ C, $T_{CL} = 260$ C

The steam generators provide additional heat capacity. The amount is substantial when the secondary system becomes a heat source, and in some transients will moderate the rate of decrease of T_{dc} . For Oconee-1, after the reactor trips, the steam generator secondary side water levels are maintained at about 30 inches if the RCPs are on, and at 240 inches if the RCPs are tripped. The heat capacity of one steam generator with water levels of 30 inches and 240 inches are 121 MJ/C and 282 MJ/C, respectively. These values are (per steam generator) about 12% and 27% of the RCS heat capacity, for a condition where 50% of the RCS inventory is filled with steam.

4.3.2 Heat Sources

The decay heat level is dependent on the duration of reactor operation. Figure 4-2 shows three decay heat trends following reactor tripped for: infinite operation; 10 hours of operation; and during power ascension. The decay heat trends of having been operated for an infinite time interval and of hot zero power are used as the upper and lower bounds for this study. Each of the four RCPs generates about 5.5 MW when running, for a total of 22 MW. Tripping RCPs not only reduces the heat source by 22 MW, but also changes the RCS circulation flow from forced to natural circulation. Flow stagnation may follow shortly for many transients.

4.3.3 Heat Sinks

The three important heat sinks that impact T_{dc} are discussed: primary system break, secondary system malfunction, and ECC injection.

4.3.3.1 Primary System Breaks

Primary system breaks include LOCA (hot leg or cold leg), steam generator tube rupture, or primary system valves stuck open (pressurizer PORV or SRV). Oconee-1 has a 1.1-inch pressurizer PORV, and two 1.8-inch pressurizer SRVs. Figures 4.3 shows energy flows for several break sizes, Figure 4-4 shows energy flows for open pressurizer valves, and Figure 4-5 shows the energy flow for a steam generator tube rupture. These results are from RELAP5. The calculations assumed that there were no other system failures, no operator actions, and no valve reclosure once the valve is stuck open.

4.3.3.2 Secondary System Malfunction

The steam generators of a nuclear power plant are designed to be capable of removing ~140% of full power. This means that for accident conditions where power is limited to decay heat, the steam generators are 'over-designed'. In effect, the available heat transfer surface is ~100 times larger than required. This large heat transfer area between the primary and secondary acts in two ways, depending of the class of events:

- a) Secondary side breaks and malfunctions. The steam generator conditions control the RCS fluid conditions.
- b) Primary side breaks. The steam generators switch from a heat sink to a heat source as primary system temperature falls. For a while, the generators supply heat to the primary until the two systems decouple.

The observations are the basis for a classification of uncertainties presented in Table 4-2. A consequence of the first class of events is that a large number of PTS-relevant scenarios are initiated or compounded by steam generator malfunction. A schematic representation of the boundary conditions that can be imposed on the once-through steam generator (OTSG) and their locations is shown in Figure 4-6. This figure illustrates that, though the possible ways in which malfunctions could occur is large, the impact that they have on the steam generator can be reduced to the variation of four independent boundary conditions. These are: feedwater flow rate (\dot{W}_{fw}), feedwater temperature (T_{fw}), flow area available for the exiting steam (A_{flow}), and the location at which feed water is introduced. The effects that these boundary conditions have on the primary system is determined by a thermal hydraulic analysis that combines their influence into a single time varying parameter - the steam generator energy transfer rate ($\dot{Q}_{SG}(t)$).

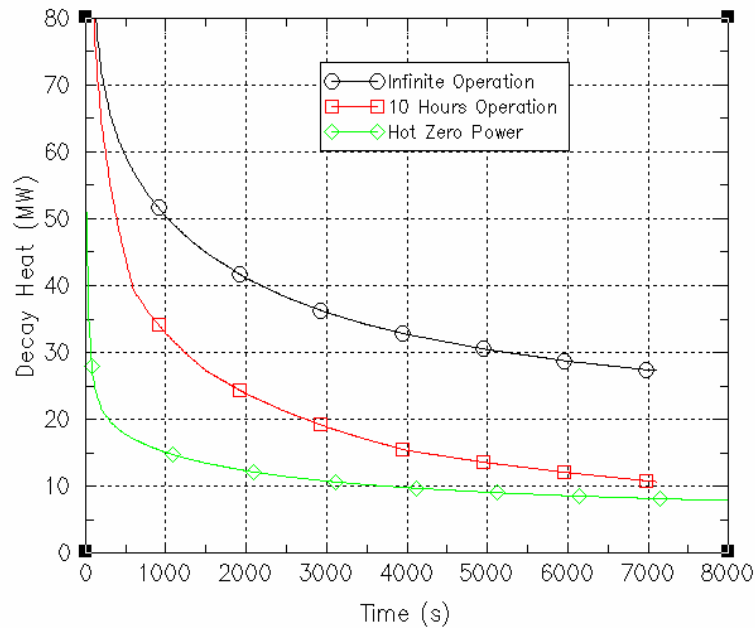


Figure 4-2 Decay heat for infinite operating time, 10 hours, and power ascension

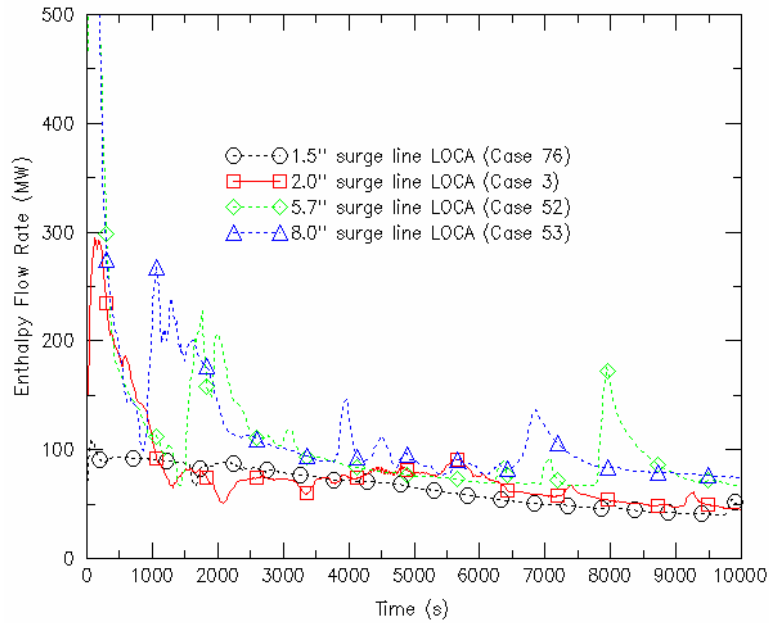


Figure 4-3 Energy flows for different size surge line breaks

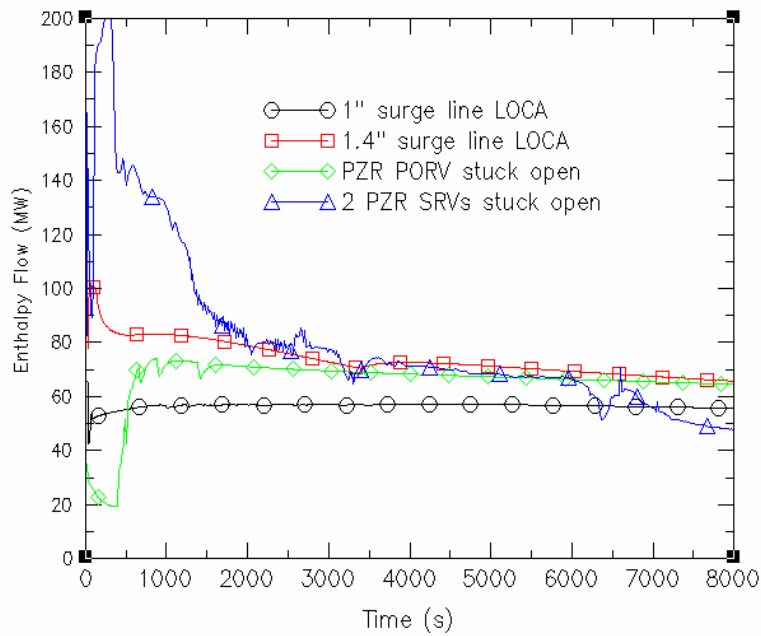


Figure 4-4 Energy flows for different size surge line breaks and SRVs stuck open

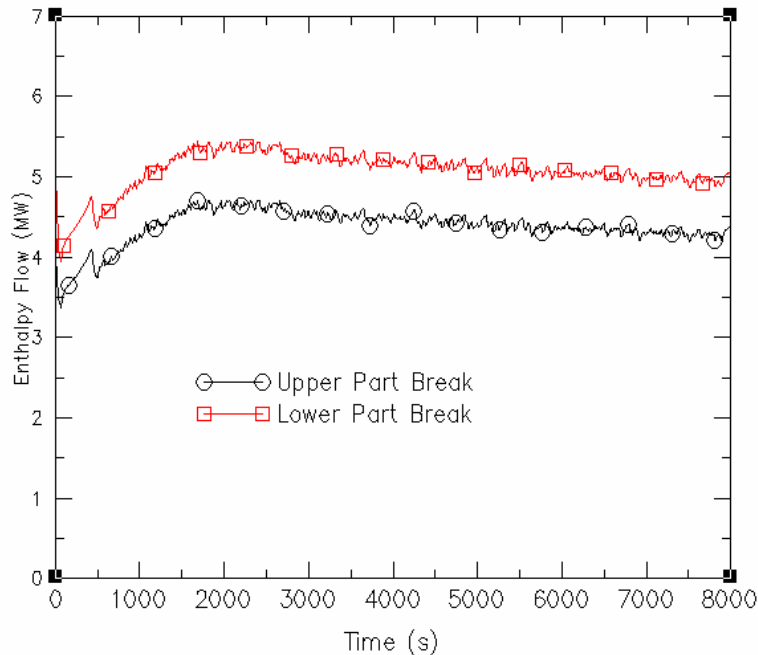


Figure 4-5 Energy flows for single steam generator tube rupture

A quantitative overview of the temperature difference between the secondary and primary systems for a range of operational conditions is presented in Appendix C. For a broad range of conditions, the temperature difference from primary to secondary across the steam generators, ranges from less than 0.5C for forced flow, to ~3C for natural circulation flow. The analysis includes the uncertainties associated with the evaluation of h_{eff} across the steam generator tubes.

For MSLBs, the energy removal capacity of the liquid inventory in the steam generators is of interest. Table 4-2 shows the total energy that can be removed during the initial blowdown phase of a MSLB for representative OTSGs and U-tube steam generators. During blowdown, energy is removed primarily by flashing of the liquid in the secondary side. The remaining liquid is then boiled off. The maximum boiling rate is limited by the rate at which the primary system flow can supply the necessary energy. The last column was obtained by assuming that the boiling heat transfer coefficient on the secondary system is large, and the resistance to heat transfer consists of the resistance of the tube metal and of the convective resistance of the primary system.

As shown in Table 4-2, though the total amount of energy that can be removed in this manner is sizable, due to the very large heat capacity of the primary system, the resulting temperature decrease is relatively modest. This leads to the conclusion that even for MSLBs, the important cool down phase occurs after the highly dynamic events immediately following the rupture. The initial cool down caused by the flashing of the steam generator inventory provides an initial temperature drop, but does not produce temperatures which are PTS-relevant. The exception is if feedwater flow is uncontrolled and therefore, continues to supply water to the broken steam generator.

Table 4-2 MSLB steam generator energy removal

	Initial SG mass (kg)	Mass after depressurization (kg)	Energy to evaporate remaining liquid	δT of RCS due to evaporate	Energy removal rate (MW)
OTSG (Oconee)	27,200	18,240	4080 MJ	-24C	19.5
U-tube SG (Zion)	43,000	28,300	6340 MJ	-28C	60.9

Secondary system malfunctions causing large amounts of heat transfer from the primary system to the secondary system include secondary system break or excessive feedwater flow. The Oconee-1 main steam lines are 31.5-inch diameter. Each main steam line has two 4.3-inch turbine bypass valves (TBVs), and eight 4.4-inch steam generator safety/relief valves. Figure 4-7 shows the magnitude of heat transfer rate from the primary system to the secondary system of one steam generator at different sizes of secondary system break. Continued feedwater flow was assumed, which is why the MSLB is similar to the two valve cases out in time. The initial blowdown of the MSLB case is not evident because of the time scale.

Figure 4-8 shows the heat transfer rate for two steam generator overfeed cases, by AFW and by MFW. The AFW water source is the condensate storage tank with nominal temperature 20C (70F). The MFW water source is the main condenser, and the flow passes through the feedwater heaters, so its temperature starts at 230C (450F) and decreases over time. The AFW sprays onto the upper tubes. The difference in temperatures of the two water sources causes a larger heat transfer rate for AFW overfeed than for MFW overfeed.

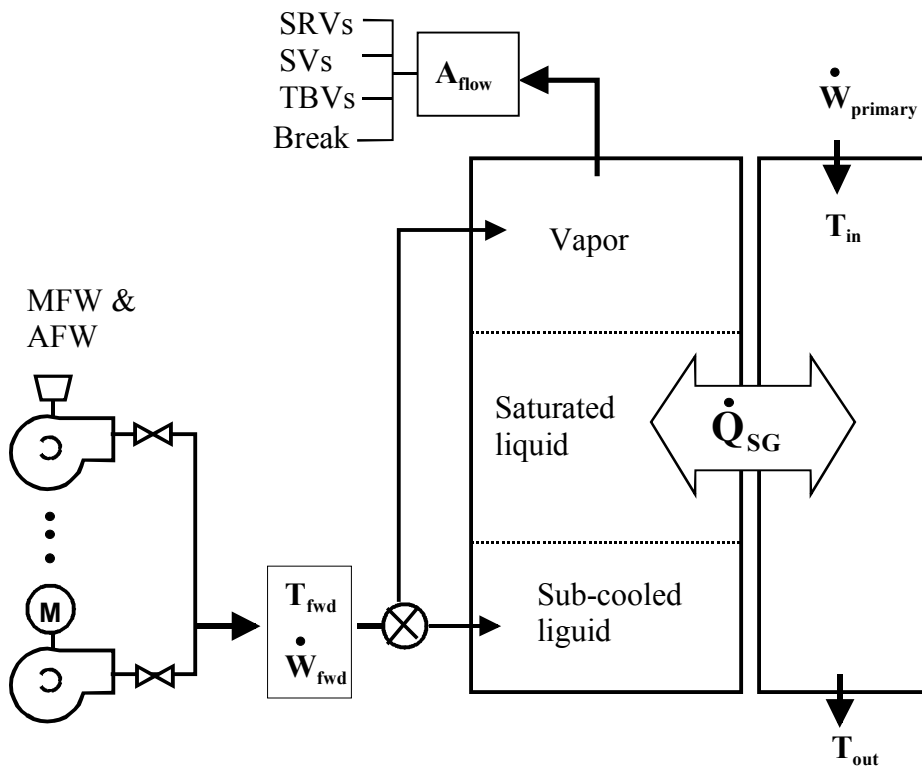


Figure 4-6 Types and locations of boundary conditions for OTSG

c) ECC injection

The RCS heat capacities shown in Table 4-1 can be compared to energy sources/sinks after a reactor trip. Table 4-3 shows the decay energy source at three time periods after reactor trip (from infinite irradiation) and four representative HPI flow rates. HPI flow is inversely proportional to system pressure and therefore has a low value at the high pressure of the PORV set point (~30 kg/sec for Oconee-1). A simple time dependent scenario is assumed in which the pressure decreases from 60 to 20 bar (~ 900 to ~300 psi) in 3000 s. The table shows the corresponding HPI flows and sensible heat sink provided by the HPI water. The comparison shows the capacitance of HPI flow is almost twice as large as the decay energy, so it alone will remove decay heat and cool the RCS.

The second to the last column in Table 4-3 shows downcomer fill times. This is the time in which the HPI could fill an empty downcomer, absent any other system flows.

The last column in the table is an estimate of the energy removal capacity of the steam generators for a condition where the difference between primary and secondary temperatures ($T_{prim} - T_{sec}$) is 6C (10F). The heat sink offered by the steam generator exceeds \dot{Q}_{dec} by a factor of three.

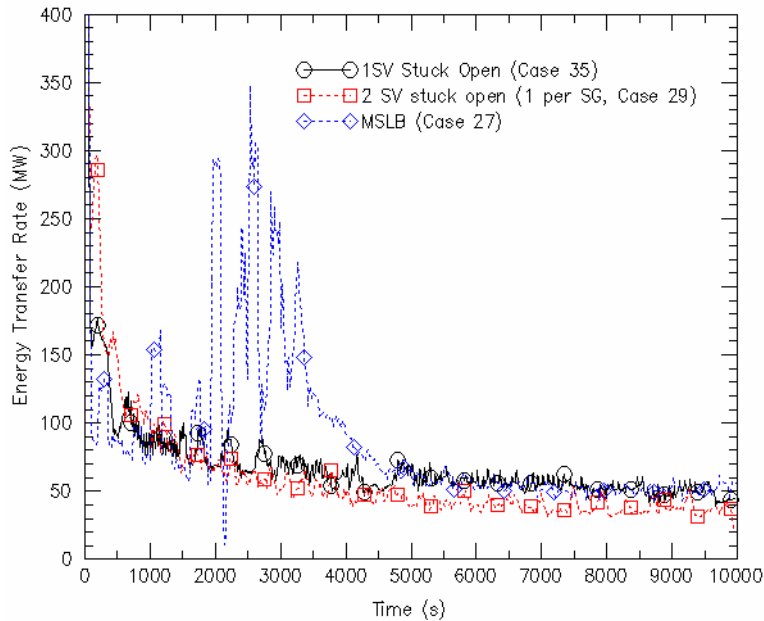


Figure 4-7 Heat transfer rate from the primary to the secondary system of a steam generator for different secondary system breaks.

Note: continued feedwater flow was assumed, which is why the MSLB is similar to the two scenarios of stuck open valves out in time. The initial blowdown of the MSLB case is not evident because of the time scale.

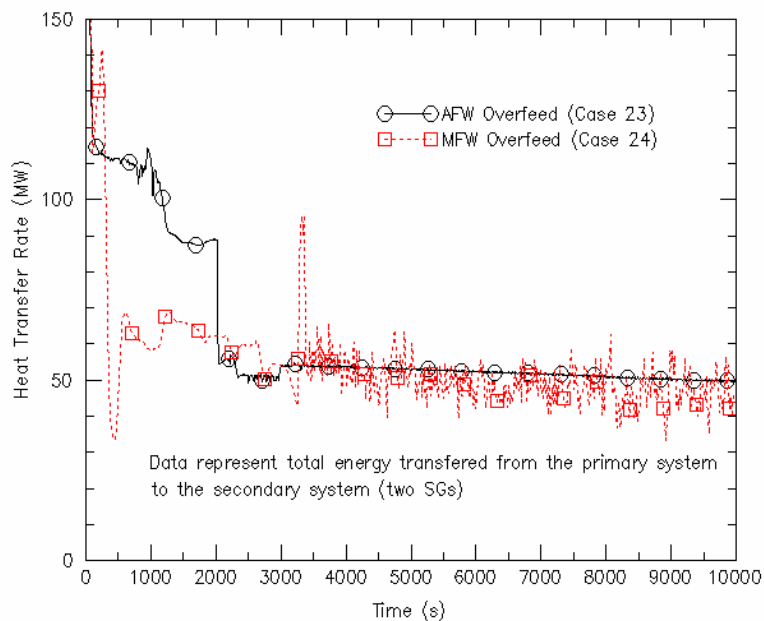


Figure 4-8 Heat transfer rate from the primary system to the secondary system of a steam generator when the steam generator is overfed by MFW and AFW.

Note: No operator actions are involved.

Table 4-3 Energy source/sink magnitudes for Oconee-1

Time after trip (s)	System P* Bar (psi)	HPI flow rate (kg/s) 3 pumps	Energy source/sink (MW)		Downcomer + Cold Leg fill time (s)	SG energy removal rate for $\delta T= 6C$ (MW)
			\dot{Q}_{decay}	\dot{Q}_{HPI}^*		
1000	60 (870)	67	48	-70	400	150
2000	46 (670)	71	40	-74	380	125
4000	20 (290)	77	33	-81	350	115
2000	170 (2460)**	30	40 + 22***	-31	900	325

*
$$\dot{Q}_{HPI} = \dot{w}_{HPI} \times [h_f(T_{SAT}) - h_f(T_{HPI})]$$

** pressurizer PORV setting

*** decay heat + pump power

The core flood tanks (CFTs) and the low pressure inject (LPI) also supply water to act as a heat sink, at rates much higher than HPI. CFTs are activated when RCS pressure is below 4.25 MPa (600 psi). Oconee-1 has two CFTs each holding 57 m₃ (2020 ft³) of water. As the HPI, the CFT flow rate is dependent on the primary system pressure.

Once RCS drops below 1.5 MPa (200 psi) LPI delivers flow at approximately six times the rate of HPI. Due to its lower pressure, LPI was not considered as a PTS influencing factor in the past PTS uncertainty studies.

4.3.4 RCS Coolant Flow Rate

The downcomer cool down rate depends on the circulation flow in the RCS. Flow rates are very large when the RCPs are on. Flow rates are moderate during natural circulation, and low during flow stagnation. Table 4-4 shows for pumped and natural circulation flow conditions; flow rates, associated inventory exchange time constants, and component velocities. The system exchange time is the time it takes for a fluid particle to complete a transit of the RCS. The system exchange time constant can influence T_{dc}. When RCPs are running, the RCS loops are well mixed (globally and locally).

Figure 4-9 shows the four permutations of: RCPs on and off; and decay heat high and low. The scenario is a pressurizer PORV stuck open and reclosed 400 seconds later, and the results are shown in terms of T_{dc}. HPI remained on after the pressurizer PORV is reclosed. The highest temperature was for RCPs on and high decay heat, as to be expected. The lowest temperature was for RCPs off and low decay heat. For this scenario, the PORV was sufficient to remove the decay heat and natural circulation was lost. For the high decay heat/RCPs tripped case, natural circulation was maintained, so the downcomer did not cool significantly. The effects of pump heat and decay heat combine together as heat sources in the analyses.

For scenarios where the secondary system is the dominant heat sink, changing from forced circulation to natural circulation does not affect T_{dc}. Figure 4-10 shows T_{dc} trends of varying HPI and RCP states of steam generator overfeed scenarios (steam generator water level maintained at 100% wide range level). It shows the impact of HPI as a sink is approximately equal to the RCPs as a source.

Table 4-4 Fluid circulation time constants for Oconee-1

	Flow Rate (kg/s)	System Exchange Time	u_{cl} (m/s)	u_{dc} (m/s)
RCPs On	17,900	14 s	15.5	7.0
Natural Circulation 1- ϕ Q_{dec} @ 1000s	420	610 s	0.33	0.15
Q_{dec} @ 4000s	290	860 s	0.22	0.11
Natural Circulation 2- ϕ $\alpha = 0.25$	83	40 min	0.06	0.3
Natural Circulation 2- ϕ $\alpha = 1$	24	95 min	0.02	0.008

4.3.5 Vessel Energy Distribution

In-vessel natural circulation is possible during LOCAs in which flow stagnation occurs. The flow path is from the upper plenum, through the RVVVs (B&W) or bypass (CE, W) into the upper downcomer. From there, mixing can occur in the cold legs and lower downcomer with ECC injection flows. The hot water and /or steam from the upper plenum can moderate the drop in downcomer temperature. During LOCAs, the primary system will partly void, and a vapor-liquid interface can form at the loop elevation that could interrupt the liquid continuous internal flow path and bring about changes in the break flow rate and local fluid composition. For OTSG type plants like Oconee these flow states will be especially pronounced if the break energy flow is smaller than \dot{Q}_{dec} or for transients during which HPI fails on demand.

Figures 4.11 and 4.12 illustrate the unique geometrical features of an OTSG type plant like Oconee. Figure 4-11 is a side view of a scaled integral system test facility, which clearly exhibits the vertical characteristics of the OTSG flow geometry. The key geometric features that influence the response of reduced inventory states are:

The tall vertical riser of the hot leg (HL) which turns through an 180° angle (the ‘candy cane’) before entering the superheated end of the OTSG. The candy cane is the highest elevation of the primary system. As RCS pressure decreases, hot water at this location will be the first to flash because of the absence of additional gravity head. If sufficient vapor is generated to fill the upper portion of the candy cane, flow through the hot leg will be interrupted.

The large vertical dimension of the OTSG and the lowered loop design results in a large rise distance in the cold leg at the suction side of RCPs. Before the cold leg (CL) turns into the horizontal segment that enters the downcomer, it rises above the cold leg entrance to the vessel, so that there is a short descending segment. The HPI nozzles are located in this segment.

Six RVVVs located in the core barrel above the loop (HL and CL) elevation. These are flapper type valves attached to the outside of the core barrel that under normal operation are closed. When the core-to downcomer pressure differential reverses, they open allowing hot water and/or steam to penetrate directly into the upper region of the downcomer.

Figure 4-13 shows the enthalpy delivered from the upper core to the downcomer through RVVVs at various sizes of LOCA based on RELAP5 calculations. It shows that the energy transfer rate is generally not overly large, but may still affect T_{dc} .

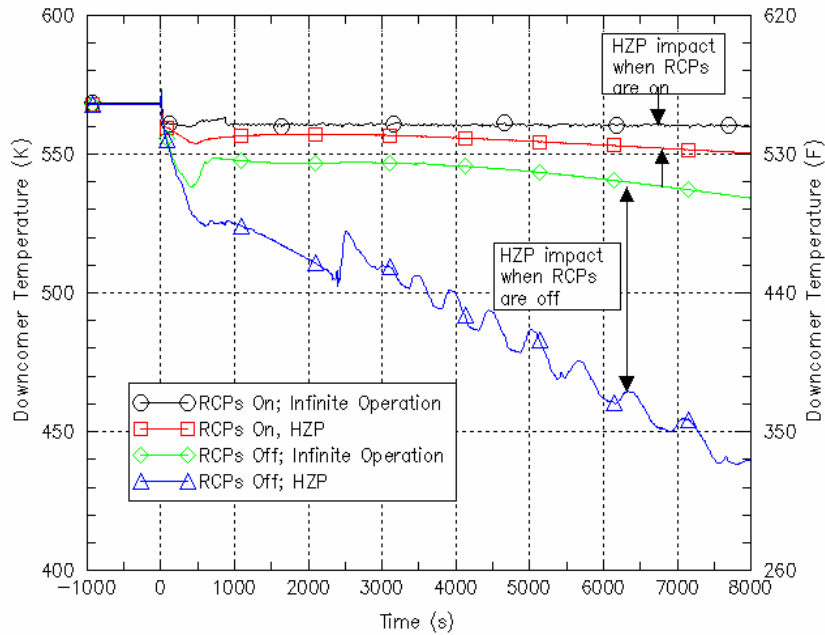


Figure 4-9 Downcomer temperatures for feed-and-bleed scenarios where decay heat and RCP state are varied (pressurizer PORV opens and stays open for the first 400 seconds)

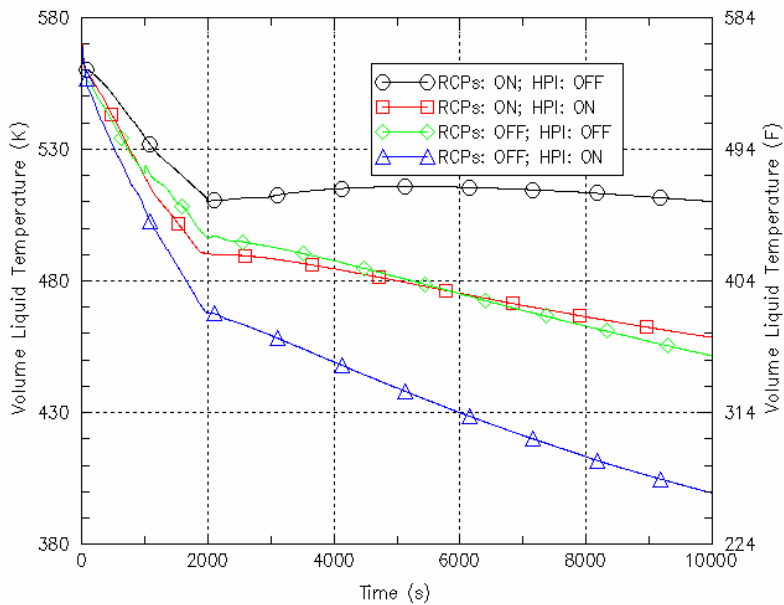


Figure 4-10 $T_{dc}(t)$ for different combination of RCP and HPI states for overfeeding of both steam generators

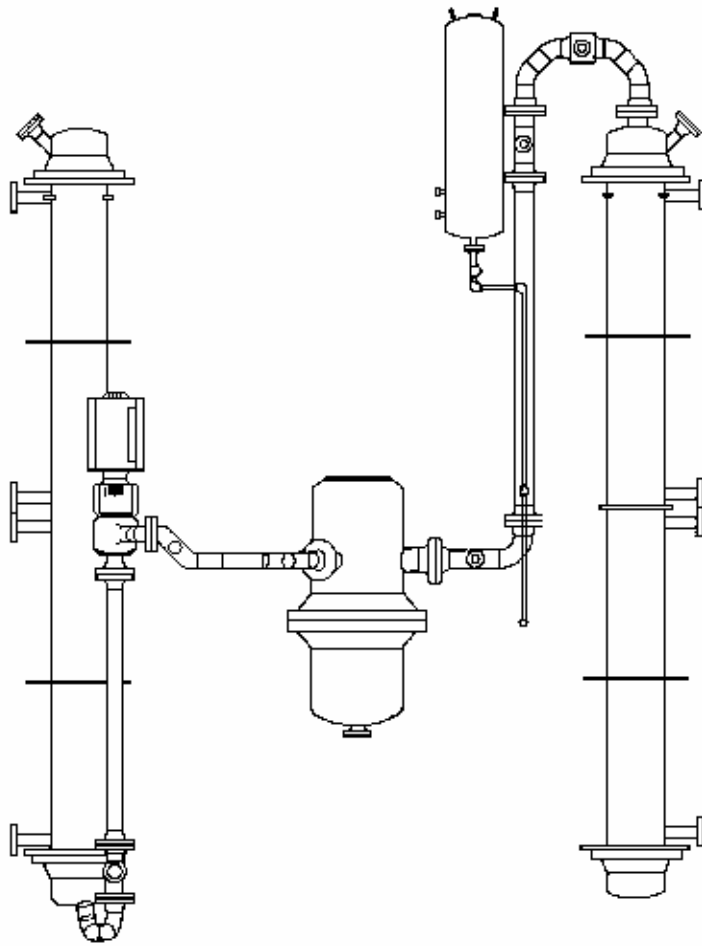


Figure 4-11 Side view the B&W reactor coolant system geometry (OTSG)

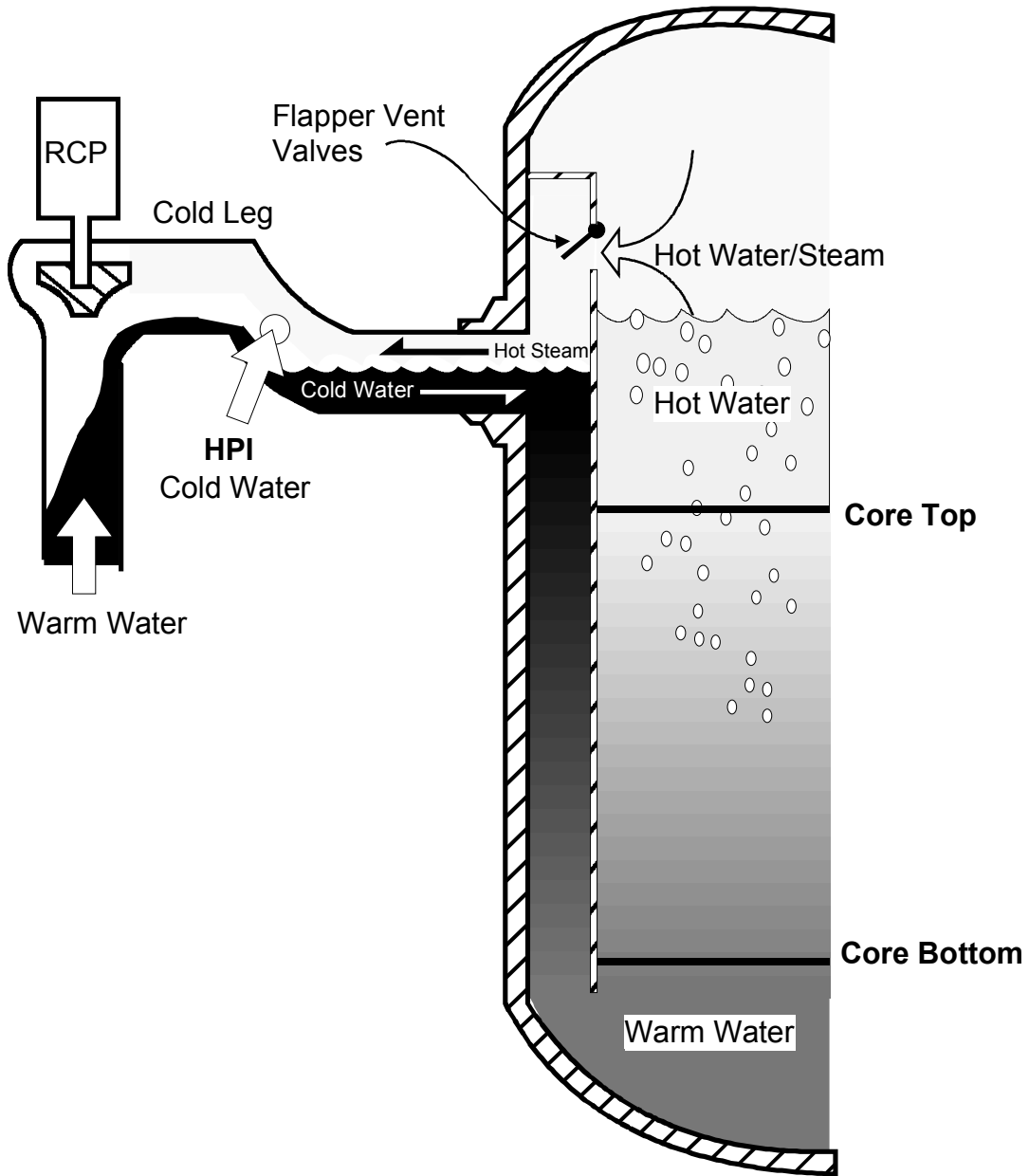


Figure 4-12 Interfaces between cold water, hot water, and steam in reactor pressure vessel and cold leg

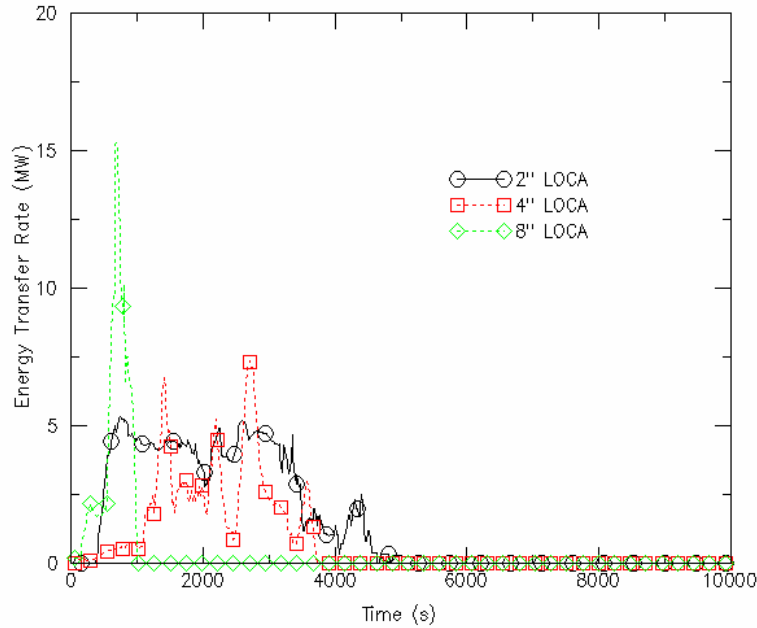


Figure 4-13 Energy flow through RVVVs to the downcomer region for different sizes of LOCA based on RELAP5 calculations

$$\dot{Q}_{RVVVs} = \dot{w}_{RVVVs} \times [h_f(T_{Rx\ upper\ plenum}) - h_f(T_{dc})]$$

4.4 Pressure Influencing Factors

The influencing factors affecting P are classified into three categories:

- Change in RCS coolant inventory
 - HPI
 - Primary system break
- Change in RCS energy
 - Heat sources
 - Heat sinks
- Short term rapid RCS steam condensation
 - Pressurizer spray
 - Mixing of ECC water with hot water or steam (condensation) in upper downcomer and cold leg
 - Boiling-condensation

These three categories and their related system factors are discussed in the following:

4.4.1 Change in RCS Coolant Inventory

HPI is the first ECC system to inject coolant in RCS cooldown scenarios. Figure 4-14 shows the RCS pressures for different break sizes. For Oconee-1, HPI is able to maintain inventory control and RCS subcooling for LOCAs up to about 1.5 inch.

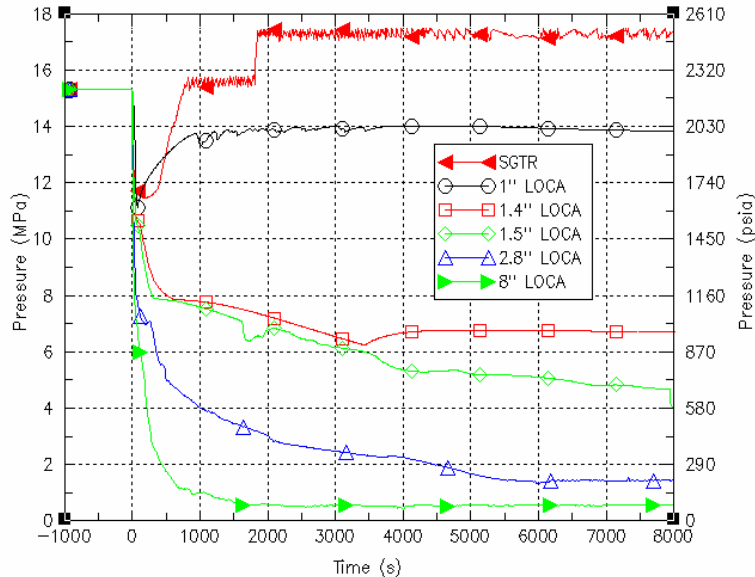


Figure 4-14 RCS pressures for different sizes of surge line LOCA.

4.4.2 Change in RCS Energy

The RCS can be viewed as a control volume containing water and steam. Energy added or removed from the control volume changes its energy, consequently P is affected as well. However, in comparison with the effect of changing RCS inventory, the change of RCS energy has less impact on P.

4.4.3 Short Term Rapid RCS Steam Condensation

Rapid steam condensation phenomena may occur in the cold leg or upper downcomer during LOCAs. Rapid condensation is difficult to predict. When it occurs, pressure decreases, and large flows are induced for a short period of time. The effect is to tend bring the RCS towards thermal equilibrium, and to increase T_{dc} and decrease P, both of which render the transient more benign from a PTS perspective. Following the condensation, the tendency is for the system trajectory to trend towards nonequilibrium conditions again. The condensation cycle may be repeated.

4.5 PTS Event Classification Matrix

From the above, a PTS event classification matrix is created to facilitate thermal hydraulic uncertainty analysis. The matrix uses key influencing factors affecting T_{dc} and P, as discussed in sections 4.3 and 4.4, as its framework. Variation in the value or state of an influencing has a significant effect on PTS risk. Less critical PTS risk-related parameters are discussed within that framework.

When a scenario has a system/component state change, causing the scenario's classification to change from one sub-category to another, this scenario is placed in the sub-category with the largest heat sink. For example, a scenario with stuck open and reclosed SRV is placed in the category where SRV is stuck open without being reclosed, since this creates a greater heat sink than if SRV is closed.

PTS requires rapid T_{dc} decrease, along with temperature dropping below 150C (300F). Only primary system breaks, or secondary system breaks combined with overfeed, reach these two criteria. All PTS events must include either primary system break, or a secondary system failure, or both. The primary system state and secondary system state are used as the two-dimensional framework of the matrix.

Figures 4.15 show the effect secondary side breaks compared to decay heat on RCS temperature. Figure 4-16 is a similar comparison for LOCAs compared to decay heat. The two figures show that the heat sinks caused significant breaks in either primary system or secondary system depressurization dominate over decay heat.

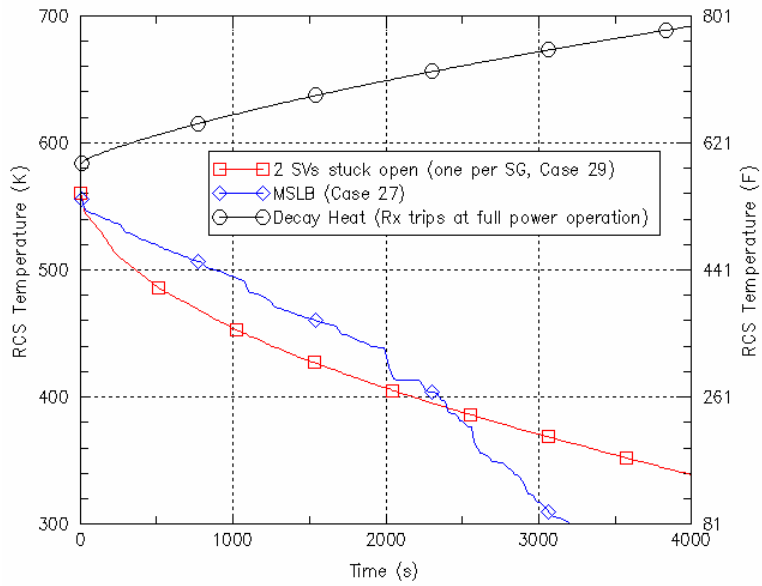


Figure 4-15 RCS temperature trends for two secondary side breaks compared to heatup from decay heat (RCS heat capacity 1690 MJ/K)

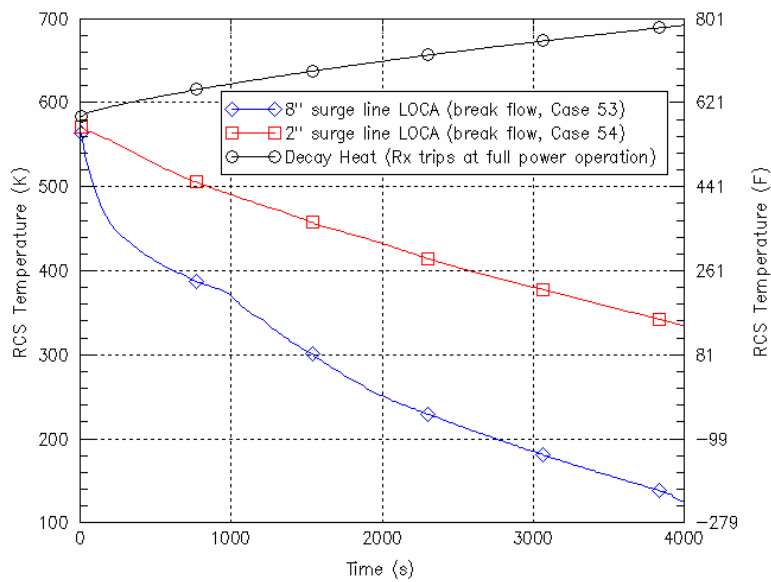


Figure 4-16 RCS temperature trends for two LOCA break sizes (2-inch, 8-inch) compared to heatup from decay heat (RCS heat capacity 1690 MJ/K)

Table 4-5 shows the PTS event classification matrix. The primary system state categorized as: intact, break without losing RCS subcooling, and break causing RCS loss of subcooling. RCS loss of subcooling is defined as loss of subcooling in the hot leg, causing the RCPs to be tripped. RCS subcooling is dependent on whether HPI can compensate for the break flow. For Oconee-1, HPI can compensate for breaks up to 1.5-inch. This study uses the criterion of whether HPI flow is greater than the break flow for scenario classification.

The classification of scenarios for PTS serves two purposes. First, the state of the RCPs can be determined. The RCPs are tripped when the RCS loses subcooling. For scenarios where HPI flow exceeds break flow, RCS subcooling is maintained and, as a result, the RCPs stay on. For scenarios where break flow exceeds HPI flow, the RCPs are tripped. Second, the operators will not throttle HPI if the break flow is greater than HPI flow. This reduces the uncertainty of in operator action for controlling HPI. HPI control and RCP state are two important parameters in PTS risk. Classification in this way eliminates two parameters from uncertainty analysis.

Secondary system failure includes secondary system breaks (e.g., MSLB, valves stuck open) and steam generator overfeed (by MFW and AFW). As discussed above, steam generators become a heat source to the RCS for LOCAs where the break is the dominant heat sink. The second way a steam generator acts as a heat source is when there is a break in one generator such that the RCS cools below the intact steam generator. In that event, the intact steam generator transfers heat back to the RCS. For a MSLB, the broken steam generator is the RCS heat sink. The intact steam generator becomes a heat source that moderates the decrease of T_{dc} . The heat capacity of a steam generator is significant. A scenario in which two steam generators were broken would induce two heat sinks. Since two broken steam generators are worse than one, this type of event is given a category of its own.

Figure 4-17 shows the difference in total net energy transferred from the primary system to the secondary system for the two-steam generator-SRVs-stuck-open events. Comparing the two SRVs are at the same steam generator and at different steam generator (one valve in each steam generator), the primary system transferred a larger amount of energy to the secondary system in the latter case (one valve at each steam generator).

Sensitivity studies of steam generator overfeed scenarios show that overfeed alone is not PTS significant. There is no need to distinguish whether one or two steam generators have been overfed. Only when feedwater flow is continued to a broken steam generator does feedwater play a role.

The above discussion frames the dominant sources affecting T_{dc} . The uncertainty in pressure also needs to be considered in all situations. HPI flow rate is the dominant parameter affecting P uncertainty for certain categories of events. Four different HPI states are modeled: full injection without (operator) throttling, controlled flow (throttled), HPI not demanded or failed, and HPI failed-and-recovered. These four different HPI states are a subset of each relevant category (see Table 4-5).

Table 4-6 shows the expected RCP and HPI states for different categories of the PTS event classification matrix. In the situation where the primary system is intact or HPI flow exceeds break flow, RCPs are not tripped. Failure of either HPI or RCPs would invalidate statements in Table 4-6. However, failure of either component has low probability. Also, failure of HPI reduces PTS risk by leading to higher values of T_{dc} and lower values of P.

Table 4-7 places the PRA-generated bins in the thermal hydraulic event classification matrix. The value in the bracket of each bin is the total frequency of all the scenarios grouped into the bin. The summed frequency for the bin indicates the importance of the group of scenarios the probability perspective. About 100 bins were generated. Some of them were eliminated from further analysis either because of low frequency low PFM consequence. Table 4-7 lists the 47 remaining bins that passed the screening.

Table 4-8 shows the summed event frequencies of the bins in each category. The risk-dominant category, for which thermal hydraulic uncertainty analysis was performed, is primary system break causing RCS loss of subcooling, with nominal secondary system state. This category contains about 94% of the total PTS-risk scenarios. The other categories are secondary system break and a combination of primary system break and secondary system break. The FAVOR code was used to calculate the CPFs of the different bins. The selected event categories dominate PTS-risk from PFM perspective.

Figure 4-18 shows the principles of PRA event tree construction. The event trees are constructed from a bottom-up approach in a process that is independent from constructing the PTS event classification matrix. In fact, however, the top events from the PRA process are consistent with the main parameters used in constructing the PTS event classification matrix, which was developed top-down. The end-point consistency between the PRA bottom-up approach and the thermal hydraulic top-down approach provides confidence in overall process.

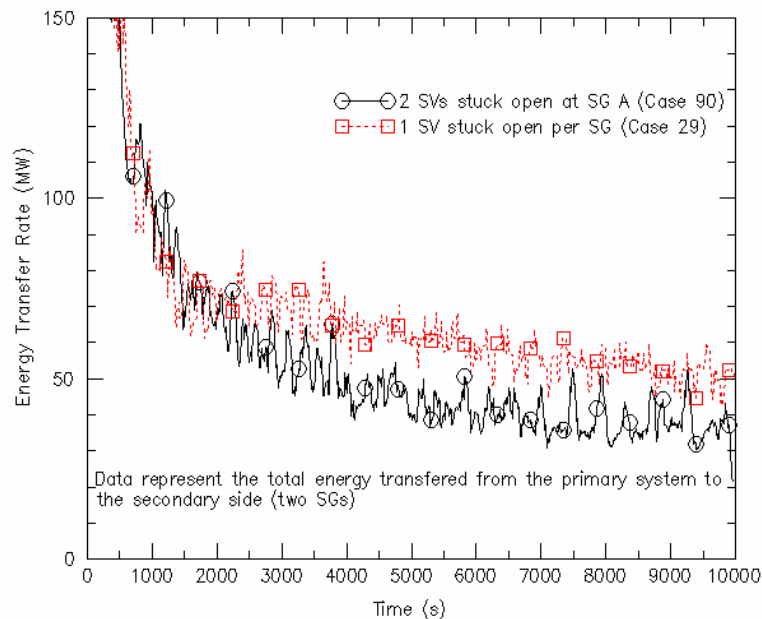


Figure 4-17 Energy transfer from the primary to secondary for two scenarios where both steam generators are broken. One scenario has one stuck open valve on each generator. The second scenario has two stuck open valves on each generator.

Table 4-5 PTS event classification matrix

Primary Side State Secondary State	Intact	Primary System Break	
		HPI > Break Break < 1.5 inch	HPI < Break Break > 1.5 inch
Nominal	1.1.1.1 Not PTS concern	A2 B1 1	A3 B1 1
		A2 B1 2	A3 B1 2
		A2 B1 3	A3 B1 3
		A2 B1 4	A3 B1 4
One SG Break	A1 B2 1	A2 B2 1	A3 B2 1
	A1 B2 2	A2 B2 2	A3 B2 2
	A1 B2 3	A2 B2 3	A3 B2 3
	A1 B2 4	A2 B2 4	A3 B2 4
Two SG Break	A1 B3 1	A2 B3 1	A3 B3 1
	A1 B3 2	A2 B3 2	A3 B3 2
	A1 B3 3	A2 B3 3	A3 B3 3
	A1 B3 4	A2 B3 4	A3 B3 4
SG(s) Overfeed	A1 B4 1	A2 B4 1	A3 B4 1
	A1 B4 2	A2 B4 2	A3 B4 2
	A1 B4 3	A2 B4 3	A3 B4 3
	A1 B4 4	A2 B4 4	A3 B4 4
SG(s) Break + SG(s) Overfed	A1 B5 1	A2 B5 1	A3 B5 1
	A1 B5 2	A2 B5 2	A3 B5 2
	A1 B5 3	A2 B5 3	A3 B5 3
	A1 B5 4	A2 B5 4	A3 B5 4

- 'A' is the primary system state. A has three variables defined as: intact = 1; HPI recoverable break = 2; HPI unrecoverable break = 3. Primary system 'intact' includes small leakage compensated by normal make-up.
- 'B' is the secondary system state. B has five variables defined as: nominal = 1; one steam generator broken = 2; two steam generators broken = 3; steam generator(s) overfeed = 4; and combinations of steam generator(s) broken and overfeed = 5.
- Last digit at end of each legend is HPI state. HPI state has 4 variations defined as: HPI actuated and not throttled = 1; HPI actuated and throttled = 2; HPI fails or not demanded = 3; HPI fails and later recovered = 4.

Table 4-6 RCP and HPI nominal states

Primary System Secondary System	Intact	Primary System Break	
		HPI > Break Break Size < 1.5 inch	HPI < Break Break Size > 1.5 inch
Nominal (1)	Not PTS concern	RCPs do not trip HPI actuated HPI throttling required	RCPs Trip HPI actuated HPI not throttled
One SG Break (2)	RCPs do not trip		
Two SG Break (3)	HPI may or may not actuate		
SG(s) Overfeed (4)	HPI throttling required if actuated		
SG Break + Overfeed (5)			

Table 4-7 Thermal hydraulic runs for binning PRA event sequences and their frequencies

Primary Side State Secondary system State	Intact	Breached	
		Break Size <~ 1.5" Break flow compensated by HPI	Break Size > ~1.5" Breach flow cannot be compensated by HPI
Nominal	1.1.1.2	4.5.1.1	[2.6e-4] <u>3</u> (2" surge line) [6.2e-6] <u>70</u> (#3, HZP) [3.0e-5] <u>52</u> (5.656" surge line) [6.0e-7] <u>73</u> (#52 + HZP) [4.0e-6] <u>53</u> (8" surge line) [8.0e-8] <u>132</u> (#53 + HZP) [4.0e-4] <u>34</u> (PZR-SRV, 2.54") [7.6e-5] <u>106</u> (2.828" surge line + HZP) [2.9e-5] <u>41</u> (PZR-SRVs reseal at 100 minutes) [1.8e-6] <u>42</u> (#41 + HZP)
			[1.1e-3] <u>83</u> (PZR SRV SO. SRV reseated at 100 min, HPI throttled 1 min after 5F subcooling and 100" PZR level) [2.0e-4] <u>92</u> (#83 + HZP) [3.4e-5] <u>84</u> (PZR SRV SO. SRV reseated at 100 min, HPI throttled 10 min after 5F subcooling and 100" PZR level) [6.2e-6] <u>93</u> (#84 + HZP) [1.1e-3] <u>85</u> (PZR SRV SO. SRV reseated at 50 min, HPI throttled 1 min after 5F subcooling and 100" PZR level) [2.0e-4] <u>94</u> (#85 + HZP) [3.4e-5] <u>86</u> (PZR SRV SO. SRV reseated at 50 min, HPI throttled 10 min after 5F subcooling and 100" PZR level) [6.2e-6] <u>95</u> (#86 + HZP)
One SG Breach	[2.1e-6] <u>27</u> (MSLB) [4.0e-7] <u>101</u> (#27 + HZP) [1.2e-6] <u>37</u> (1 SG SV SO + HZP)	[5.6e-8] <u>8</u> (1" surge line + 1 SG SV SO) [1.0e-7] <u>28</u> (F&B, 1SG SV SO) [1.1e-7] <u>30</u> (#28 + HZP)	
		[4.8e-7] <u>12</u> (1" surge line, 1SG SV SO) [7.0e-7] <u>90</u> (2 SG SVs SO, HPI throttled @ 20 min after it can be throttled) [2.1e-7] <u>102</u> (#90 + HZP) [6.1e-5] <u>91</u> (SGA TR+ 1SGB SV SO and reseated @ 10 min after initiation + RCP tripped @ 1 min + HPI throttled @ 10 min after it can be throttled) [5.0e-8] <u>103</u> (#91 + HZP) [2.3e-7] <u>99</u> (MSLB + HPI throttled 20 min after it can be throttled) [2.3e-7] <u>100</u> (#99 + HZP)	
Two SGs Breach	[1.4e-5] <u>36</u> (2SVs SO) [2.6e-6] <u>38</u> (#36 + HZP)	[2.7e-7] <u>29</u> (2 SG SVs SO) [5.0e-9] <u>31</u> (#29 + HZP)	

		[3.1e-8] <u>15</u> (1" + 4 TBVs fully SO + No HPI) [1.8e-8] <u>74</u> (#15 + HZP)	[3.1e-6] <u>81</u> (2" surge line, 4 TBVs opened @ 15 min)
		[2.7e-8] <u>44</u> (1" LOCA + HPI F&R @2250s, 4 TBVs fully open) [1.3e-7] <u>75</u> (#44 + HZP) [3.1e-6] <u>82</u> (1" + 4 TBVs Opened @ 15 min, HPI recovered when CFTs are 50% discharged, HPI throttled @ 50 min)	[2.4e-7] <u>87</u> (PZR SRV SO, HPI fail, 4 TBVs opened @ 15 min, HPI was recovered when CFT was 50% discharged; HPI was throttled @ 20 min after being available) [4.2e-8] <u>96</u> (#87 + HZP) [7.4e-7] <u>88</u> (PZR SRV SO, HPI fail, 4 TBVs opened @ 15 min, HPI was recovered when CFT were 50% discharged; SRV reseated 5 min after HPI was recovered, HPI throttled 1 min after being available). [1.3e-7] <u>97</u> (#88 + HZP)
SG(s) Overfeed			
SG(s) breach + SG(s) Overfed	[1.2e-6] <u>89</u> (F&B + 4 TBVs are opened and HPI is throttled after RCS pressure reaches 2275 psi) [6.6e-8] <u>98</u> (#89 + HZP)		

HZP: Hot zero power
SG SV SO: SG safety valve stuck open
TBV: Turbine bypass valve
F&B: Feed-and-bleed (HPI injects coolant and RCS coolant leaks through the pressurizer PORV)
pressurizer SRV: pressurizer safety relief valve

The value inside the bracket is the bin's frequency.
The underlined digit is the identification of the bin corresponding thermal hydraulic run
The value inside the parentheses is the brief description of the thermal hydraulic run
*as a substitute of pressurizer SRVs stuck open without being reclosed (Case 34) plus HZP.

Table 4-8 Summation of event frequencies from the PTS event classification matrix
 (thermal hydraulic uncertainty analysis performed for the category in bold).

Primary State \ Secondary Side State	Intact	Break	
		Break < 1.5" HPI > Break	Break > 1.5" Break > HPI
Nominal	4.5.1.2		8.1 E-4 2.7 E-3
One SG Break	3.7 E-6	2.7 E-7 6.3 E-5	
Two SGs Break	1.7 E-5	2.8 E-7 4.9 E-8 3.3 E-6	3.1 E-6 1.2 E-6
SG(s) Overfed			
SG(s) Break + SG(s) Overfed	1.3 E-6		

General Functional Event Tree for PTS					
Initiator	Primary Integrity	Secondary Pressure	Secondary Feed	Primary Flow/Press	
			ok	not PTS (1)	
				ok/controlled	minor PTS at most
				overfeed/pressurized/ no flow	possible significant PTS
		ok	overfeed		
				underfeed/lost	core damage; not PTS
			underfeed/lost	go to Primary Integrity failed (Feed & Bleed) (2)	
	ok				
				ok/controlled	minor PTS at most
				overfeed/pressurized/ no flow	possible significant PTS
			not isolate/overfeed		
		depressurizing		underfeed/lost	core damage; not PTS
			underfeed/lost	go to Primary Integrity failed (Feed & Bleed) (3)	
		see note (4)			
(1) not considered a PTS concern regardless of primary flow/pressure					
(2) loss of feed to both SGs; procedures call for Feed & Bleed which is equivalent to entering tree at Primary Integrity "failed"					
(3) like (2) above except secondary depressurization has further lowered RCS temp					
(4) logic is identical to rest of tree above except choices also exist for Primary Flow/Pressure even for Secondary Pressure and Feed "ok" state and PTS effects are generally potentially greater for all scenarios					

Figure 4-18 Overview of the PRA event tree approach in modeling PTS scenarios

5. MODEL UNCERTAINTY CHARACTERISTICS

This chapter discusses sources and characteristics of uncertainty, to provide a basis for developing a simple and acceptable method to quantify the thermal hydraulic contributions to PTS uncertainty. It was not the intention that the method provide a detailed uncertainty method for the best-estimate codes. Section 5.1 discusses the important phenomena that contribute to uncertainty in RELAP5 calculations. Section 5.2 discusses, in particular, uncertainty associated with calculation of critical flow. Section 5.3 discusses flow oscillations and flows driven by numerics. Section 5.4 lists the specific items relating to physical modeling uncertainty treated in this study. The discussion of physical modeling uncertainty is limited to the applicability of RELAP5 for PTS analyses. We considered the following issues:

1. One-dimensional, volume averaging. Three-dimensional fluid flows (e.g., plumes) are treated by a one-dimensional approximation. This was considered as a possible concern in the cold leg and downcomer region, where nonuniform fluid temperatures could occur, which could be important to the current analyses. Comparing RELAP5 results with experimental data, such as the Oregon State University APEX program, and with Computational Fluid Dynamics (CFD), the one-dimensional approximation was found to be reasonable [Bessette 2004].
2. Numerics. Nonphysical results may occur from numerical solutions. Comparison of RELAP5 with experimental data indicated the influence of numerics to the current studies to be relatively limited and understood.
3. Empirical correlations. Important uncertainties relating to use of empirical correlations (e.g., calculation of critical flow) are discussed in later Chapters. The important correlations are treated explicitly.
4. Nodalization. The Ocone-1 input deck originated with the IPTS study (Fletcher et al., 1984), and has been used in several subsequent studies [Hanson, Meyer et al. 1987], [Determan and Hendrix 1991], [Quick 1994]. For the current study, the downcomer nodalization was modified, along with other updates [Arcieri, Beaton et al. 2001]. The uncertainty contributed by the nodalization is considered to be small.

5.1 Important Phenomena Contributing to Uncertainty of RELAP5 Calculations

The answer to the question, “what is the contribution of thermal hydraulic uncertainties to the overall uncertainty of P and T_{dc} ” is relatively complicated. It is difficult to provide an overall answer because it is such a broad question. For example, Table 5-1 shows the RCS circulation modes.

The ability of RELAP5 and other system codes to calculate thermal hydraulic physical phenomena varies significantly for the above outlined modes of energy/mass transfer and inventory loss. RELAP5 is a one-dimensional code, employing volume averaging. Regimes characterized by stratified flows and influenced by three-dimensional geometry will not be properly reproduced. For example, the intermittent periods of flow stagnation during the interruption-resumption mode (IRM) depends on the mixture level in the reactor vessel relative

to the hot leg entrance elevation. Such inherently three-dimensional flows cannot be represented adequately by a one-dimensional code. On the other hand, if vapor-liquid separation in horizontal channels is not a dominant phenomenon, or if separation is nearly complete and leads to single phase (vapor or liquid) flows (e.g. the boiler-condenser mode), then system response is reproduced moderately well.

Table 5-1 Ability of RELAP5 to evaluate inventory dependent two-phase flow states.

Phenomena	Plant type	Ability of RELAP5 to model	Effect on T_{dc} and P_{dc}
Flow interruption by vapor in candy cane	OTSG	Poor	Short term increase of P_{dc} and decrease of T_{dc}
Interruption-resumption flow	OTSG	Not able	Periodic fluctuation of P_{dc} promotes mixing therefore higher average T_{dc}
Boiler-condenser mode	OTSG	Good	Significantly lower P_{dc} . Low loop flow thus lower T_{dc}
Mixing of core and downcomer through RVV)	OTSG, & U-tube	Moderate	Increases T_{dc} . Small effect on P_{dc}
Reflux condensation	U-tube	Poor	Reduces P_{dc} . Reduces C.L. flow therefore lower T_{dc}
Temporary heat sink loss due to mismatch of SG levels	OTSG	Moderate	Short term P_{dc} increase & flow stagnation. Short term T_{dc} decrease
Heat sink loss due to $P_{prim} < P_{sec}$ Caused by $\dot{Q}_{dec} < \dot{Q}_{brk}$	U-tube & OTSG	Moderate. Bounded by choked flow limits.	P_{dc} rises & flow stagnates, lower T_{dc}

Not all uncertainties associated with two-phase flow phenomena and their computation influence the PTS relevant parameters unfavorably. Several of the phenomena (e.g. operation in the IRM and internal circulation through the RVVVs) generate more mixing and thus higher downcomer fluid temperatures. A list of the characteristic two-phase flow phenomena along with a qualitative assessment of system code capability to evaluate them is presented in Table 5 -1. The table is meant to be inclusive and does not take into account the probability a phenomenon occurs. The question, "how do the computational shortcomings noted influence uncertainty," must be answered by weighing their relevance to PTS. In this respect, most of the phenomena noted either have short time constants (short compared to the PTS relevant time constants) or, from the PTS perspective, have a beneficial effect. Especially beneficial are flow states that are inherently dynamic. They lead to chugging and condensation-induced flow surges that churn the primary system inventory and promote mixing.

Transients for which $\dot{Q}_{dec} < \dot{Q}_{brk}$ lead to flow stagnation, since the energy out the break exceeds decay heat, the steam generators are not needed. The major contribution to the thermal hydraulic uncertainty for such transients is the computation of the mass/energy loss term through the break. The computational uncertainties can be separated into two major

components. First is the uncertainty introduced by the fluid conditions of the break node. This uncertainty is strongly dependent on the location (especially the elevation) of the break. Second are the modeling uncertainties associated with the computation of critical flow. These two items are interrelated.

5.2 Uncertainties Associated with Critical Flow

Modeling of critical flow has been important to reactor safety analysis from the very beginning. Consequently extensive benchmarking and verification efforts of computational models have been carried out. Reviews of these studies are available in a number of survey papers [Weisman and Tentner 1978; Rosdahl and Caraher 1986]. A recent example is by Queral et al. [Queral, Mulas et al. 2000], which includes quantitative comparisons of Marviken data with the two models used in RELAP5, Ransom-Trapp [Ransom and Trap 1980] and Henry-Fauske [Henry and Fauske 1971]. Extensive critical flow data should make it possible to provide a reasonable assessment of modeling uncertainty. That is true for situations where the boundary conditions are accurately known, however, this condition does not apply for random breaks. To evaluate the uncertainty associated with random breaks requires considering the wide spectrum of locations, sizes and types of possible breaks that are actually possible, as well as code calculational error. Though two-phase critical flow is modeled adequately (on the order of ± 10 to 15%) for well known fluid conditions and specific physical characteristics of the break, this accuracy cannot be expected generically.

Whether or not flow stagnation occurs depends on the relative magnitudes of primary system mass/energy source and sink terms. Over the duration of a small break LOCA, these terms are a "moving target" because they change with time and pressure. Also, the choked flow mass/energy loss term has large aleatory and epistemic (modeling) uncertainties. Simplifying a complex problem is desirable, however, when dealing with a parameter depending on several time-varying conditions, simplification has inherent limits. Critical flow through a random break is such a parameter.

An overview of the variation in break flow is provided in Figures 5.1 to 5.7. The figures present computed critical flow mass/energy rates as a function of upstream pressure, quality, and break size. To span the entire possible range of modeling uncertainty, two 'limiting' models as well as two 'best-estimate' models are used in the computations. The models differ principally in the assumptions determining the approach to thermal equilibrium in the "throat" of the break opening. For two-phase fluids, an approach to thermal equilibrium in a decreasing pressure gradient requires both mass and energy transfer between the phases. These processes take time, therefore, how close they come to equilibrium depends on the spatial distribution of the pressure gradient along the flow path.

The two limiting models employ bounding assumptions that bracket this range. The Homogeneous Equilibrium Model (HEM) provides the lower limit. As the name implies, this model assumes that, as the fluid flows from the upstream pressure to the throat pressure, the two phases remain in thermal and mechanical equilibrium. HEM results in the lowest possible density of the fluid at the throat and, therefore, the lowest mass flux. The upper limit is set by the bounding assumption that the fluid composition does not change at all as it moves through the pressure gradient of the break. In effect, as the name by which this model is identified implies, its state remains 'frozen'. The fluid density at the throat and, therefore, the flow rate are maximized. The actual flow rate will fall somewhere between the two limits. For sharp orifice

breaks and low qualities, the flow rate will be closer to the frozen model, whereas for longer nozzles and higher qualities, it will fall closer to HEM.

The figures also show two 'best estimate' models implemented in RELAP5. Up to ~1998, RELAP5 for over a decade used the Ransom-Trapp model. The RELAP5 version released in ~1998 included the option to use the older Henry-Fauske model. In the RELAP5 version released in June 1999, Henry-Fauske became the default model. The two models differ in their approach to evaluating thermal and mechanical equilibrium (characterized by the 'slip' ratio) at the throat of the break. As illustrated in the figures, when the upstream condition is saturated or subcooled water, the results are closer to the frozen model. By comparison, Ransom-Trapp allows more equilibration and, therefore, generally falls below the rates computed by Henry-Fauske.

Recent studies [Queral, Mulas et al. 2000] using large scale data concluded that the Henry-Fauske model is preferable. The conclusion is justified if the break geometry approximates orifice conditions, however, it should not be applied uncritically to a random break. In fact, if the break flow has more time to equilibrate (e.g. SGTR), then the Ransom-Trapp model may be preferable. The spread between the results obtained from the two best-estimate models provides an illustration of the modeling uncertainty associated with computation of critical flow.

Figures 5.1 and 5.2 show computed mass and energy flow rates for a 2-inch break as a function of upstream pressure. Besides the two limiting and two best estimate models, the range of the relevant terms is superimposed on the figures. The HPI flow rate (Figure 5-1) depends on RCS pressure, and can vary from ~40 kg/s at the PORV set point pressure up to ~80kg/s at low RCS pressures (~20 bar). The range of \dot{Q}_{dec} (Figure 5-2) depends on time after scram. For Oconee-1, \dot{Q}_{dec} decreases from ~50 MW 15 min after shutdown, to ~28 MW 2 hours after shutdown.

During a LOCA, the RCS pressure will initially drop rapidly to the saturation pressure (~72 bar). What happens next depends on the relative mass/energy source and sink terms. Figures 5.1 and 5.2 show that for a 2-inch break with HPI actuated, the RCS inventory depends on the nature of the break. For breaks with critical flow approaching HEM (e.g. L/D >10), inventory loss is minimized and the RCS may refill and repressurize. However, net energy loss (Figure 5-2) will proceed, so that RCS temperature will continue to drop to the range 540K to 505K are reached. Whether and at what rate cool down and depressurization is calculated (and whether flow stagnation occurs), depends on the choice of critical flow models, and thus on the combined effects of *model* and *type of break* uncertainties.

A more comprehensive overview of the effective range of break sizes associated with the range in critical flow models is obtained by plotting mass/energy flow rate as a function of break flow. Figures 5.3 to 5.6 show the mass/energy flow rates for two representative pressures: 70 bar (~1028 psi) the saturation pressure at operating conditions; and 20 bar (290 psi). The figures illustrate that the spread caused by model uncertainties is wide. Figures 5.3 and 5.4 can be used for estimating the size of the largest break which, independent of model uncertainties and the physical characteristics of the break, would lead to depressurization, as well as the smallest break for which, given that HPI is operating, depressurization would not occur. Similarly, Figures 5.5 and 5.6 show for 20 bar how far the inventory and pressure can decrease before the source/sink terms reach a new balance.

Table 5-2 is a summary of break size ranges as estimated from Figures 5.1 to 5.6. The first row (P = 70 bar) is an estimate of the range of break sizes that lead to flow stagnation. The second

row ($P = 20$ bar) is an indication of how far depressurization will proceed. The break size range is quite wide, extending from an equivalent diameter of ~ 3.2 -inch down to ~ 0.65 -inch. This reflects both the large differences that are possible in the characteristics of the break, and the margin of uncertainty associated with the modeling of critical flow. The estimates apply for conditions where the fluid upstream from the break is saturated liquid.

The break flow depends on the fluid conditions just upstream of the break, and these change with time during a transient, and so it a “moving target.” For low elevations the fluid could be subcooled longer leading to larger flows, while at higher elevations it could become saturated sooner which would reduce the flow rates. As void fraction upstream of the break changes, break flow is affected. Figure 5-7 illustrates, showing calculated break flow rates as a function of the upstream fluid vapor fraction for a constant pressure of 70 bar. Depending on the model employed, the flow rate decreases by a factor of three to six as the upstream fluid condition passes from saturated liquid to steam. As expected, the models converge as α approaches 1.

The trends in the range $0 < \alpha < 1$ point out some unphysical aspects of the models. The frozen model, which is the upper bound for saturated water, are seen to fall below those obtained from both best-estimate models. This is caused by the frozen model assumption that both phases are accelerated to the same throat velocity. On the other hand, the nonequilibrium best estimate models use a slip ratio that minimizes momentum by preferentially accelerating the lighter phase. A computational shortcoming not evident in the figure is that for several intermediate α values, the Ransom-Trap model as implemented in RELAP5 produces oscillations. The values shown in the figure are averages.

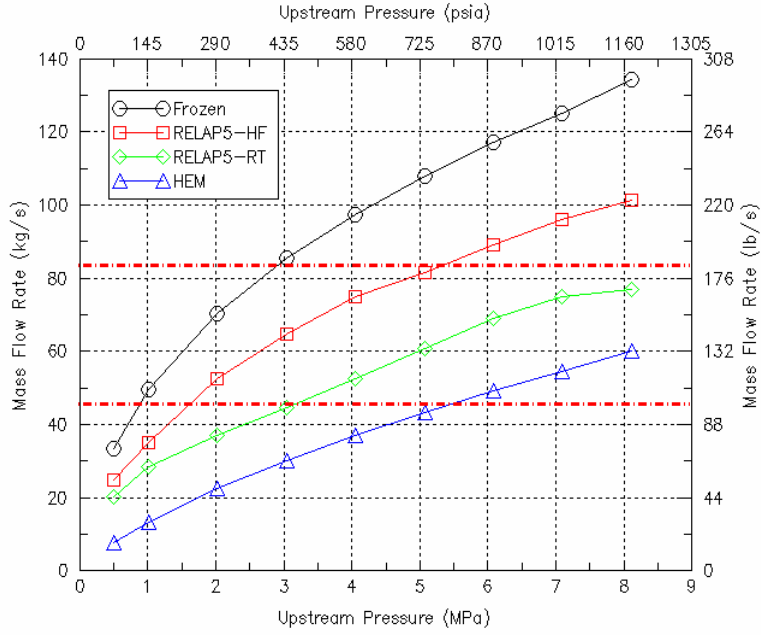


Figure 5-1 Critical mass flow rate vs. pressure (saturated liquid 2-inch break). *Region between two dashed lines is where flow stagnation could occur.*

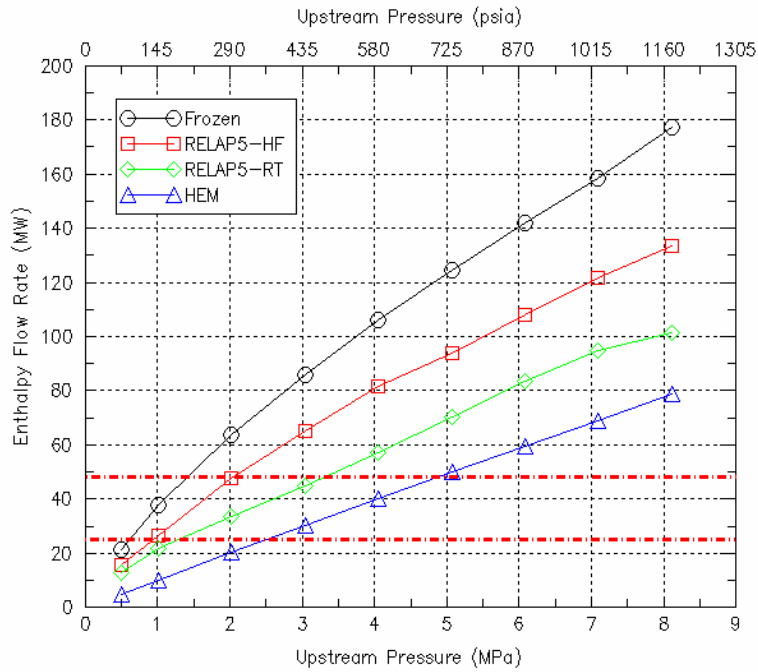


Figure 5-2 Critical flow energy discharge rate vs. pressure (saturated liquid 2-inch break) *Region between two dashed lines is where flow stagnation could occur.*

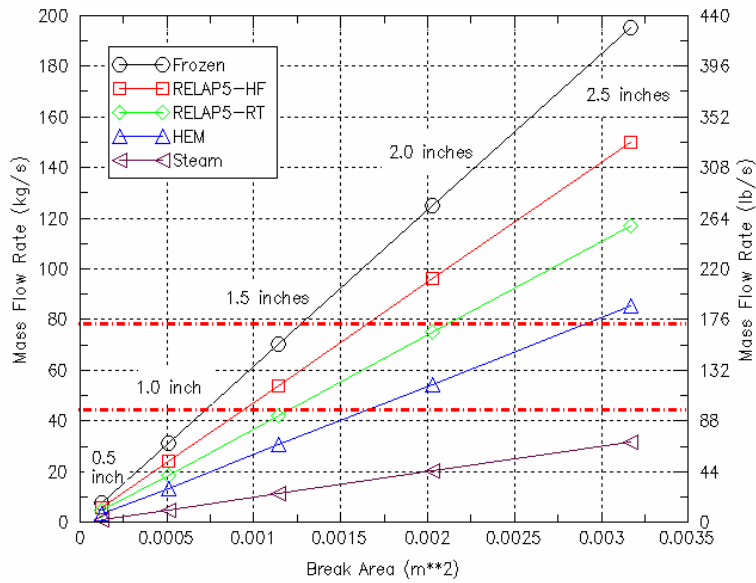


Figure 5-3 Critical mass flow rate as function of break area P = 7 MPa (1028 psia), TSAT = 559K (546F) Region between two dashed lines is where flow stagnation could occur.

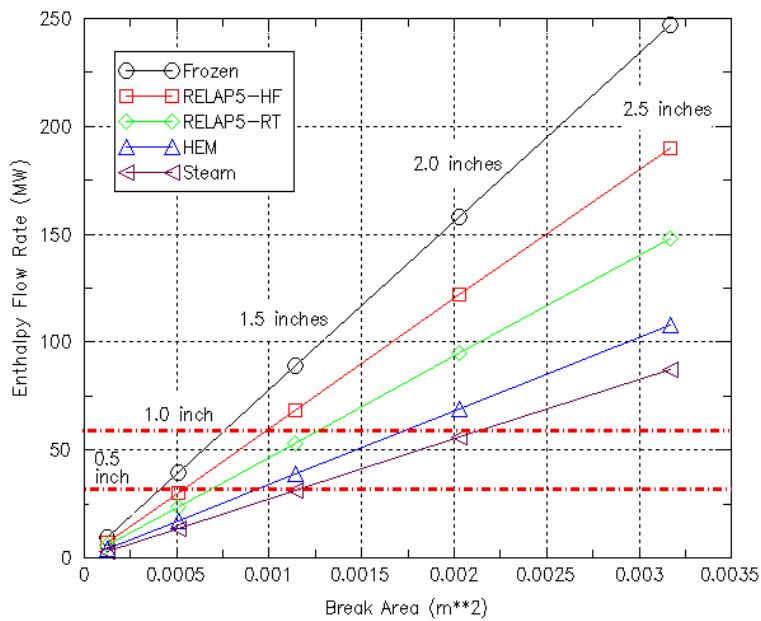


Figure 5-4 Critical flow energy discharge rate as function of break area P = 7 MPa (1028 psia), TSAT = 559K (546F) Region between two dashed lines is where flow stagnation could occur.

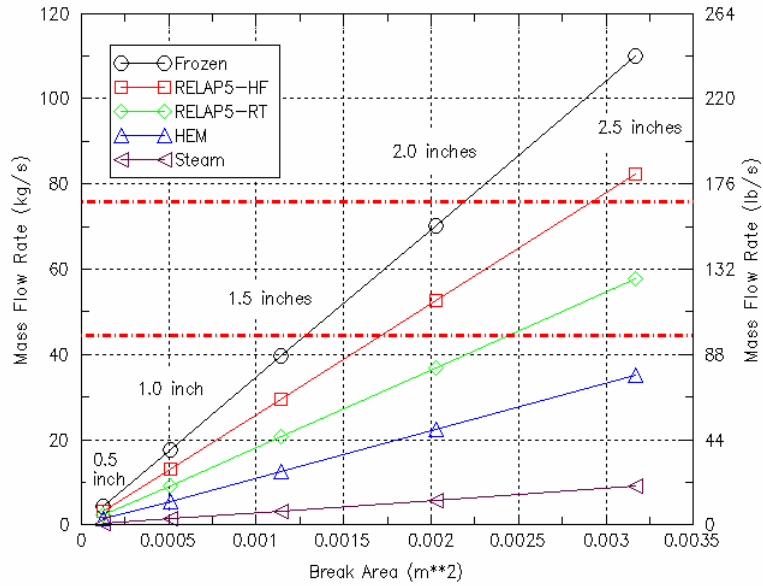


Figure 5-5 Critical flow mass flow rate as function of break area P = 2 MPa (290 psia), TSAT = 486K (414F) Region between two dashed lines is where flow stagnation could occur..

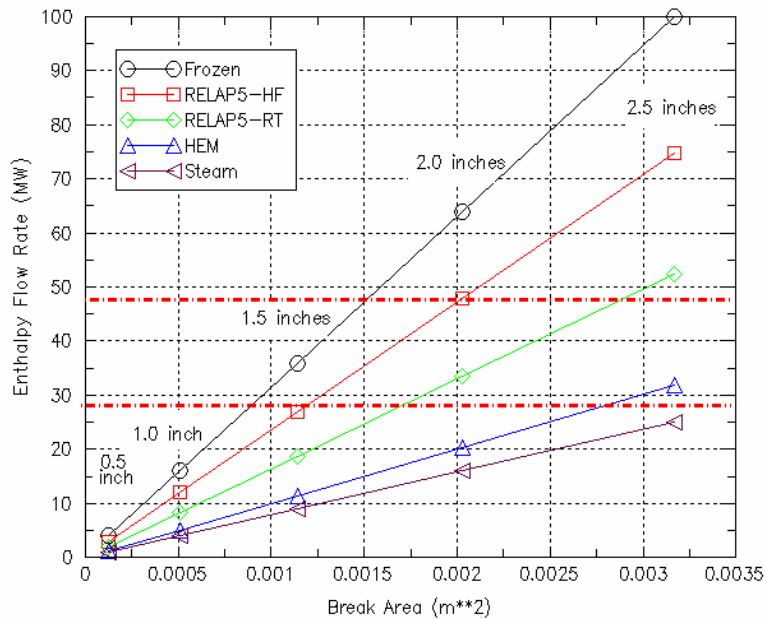


Figure 5-6 Critical flow energy discharge rate as function of break area P = 2 MPa (290 psia), TSAT = 486K (414F) Region between two dashed lines is where flow stagnation could occur.

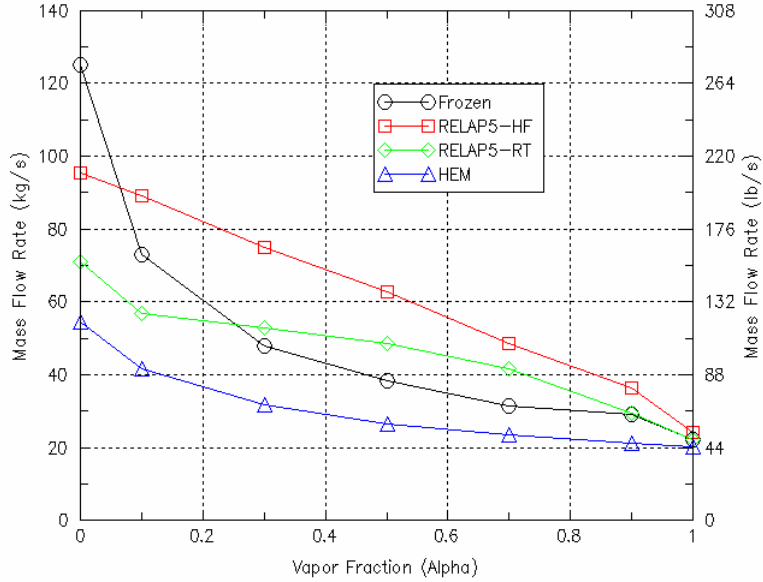


Figure 5-7 Critical mass flow rate as function of void fraction (saturated liquid 2 inch break) P = 7 MPa (290 psia)

Table 5-2 Bounding range of break sizes for critical flow (Oconee-1)

		Low flow limit: HEM		High flow limit: Frozen	
		Mass Flow $\dot{W}_{brk} > \dot{W}_{HPI}$	Energy Flow $\dot{Q}_{brk} > \dot{Q}_{HPI}$	Mass Flow $\dot{W}_{brk} > \dot{W}_{HPI}$	Energy Flow $\dot{Q}_{brk} > \dot{Q}_{HPI}$
70 bar	Area (cm ²)	30 – 17	17 – 10	12 – 8	7 - 4
	D (in)	2.4 – 1.4	1.4 - .8	1 - 0.65	0.6 – 0.4
20 bar	Area (cm ²)	40 - 36	21 -18	21 - 18	14 - 9
	D (in)	3.2 - 2.9	1.7 - 1.4	1.7 - 1.4	1.2 - 0.7

5.3 Flow Oscillations and Numerical Flows

A fundamental code development issue code has been that the six equation set used to describe the mass/energy/momentum balances of both phases is “ill-posed”. This is a broad subject that has been dealt with in depth in many excellent studies [Mahaffy 1981; Ransom and Hicks 1984]. In RELAP5, several steps are taken to reduce the consequences of this problem. The most relevant are: incorporation of numerical viscosity in the time advancement algorithm that dampens high frequency oscillations; and prioritization of the precision with which the conservation equations are evaluated. The priority is to conserve mass and energy. Transfer of

mass/energy between volumes, therefore, always takes place at the same time in the time advancement scheme (implicit method). The transfer of momentum is assigned a lower priority, and includes some explicit components.

Such prioritization is necessary because one of the most persistent and commonly occurring unphysical phenomena associated with volume-averaged system codes are numerically induced oscillations. They can occur for a variety of conditions and have a range of causes. A commonly occurring type of oscillation is driven by discontinuous transitions of fluid condition dependencies between flow regimes and/or transitions between empirical correlations. This is exacerbated since both the flow regimes and the correlations are chosen explicitly.

For many years, significant code development effort has been directed toward incorporating various time and spatial averaging schemes to reduce the magnitude of this generic problem and thus make the code more robust. These efforts have been largely successful and in the present version of the code, numerical oscillations rarely grow to such an extent as to terminate its operation. RELAP5 is presently remarkably robust, however, the price of this achievement is that the code has become less transparent. This is especially true regarding numerical oscillations, as in many cases it is difficult to diagnose their precise cause and to distinguish them from oscillations which have a physical basis.

The important question regarding numerically induced phenomena is how, and to what extent, they influence the computed parameters of interest, and thus contribute to their uncertainty. The two main PTS relevant parameters P and T_{dc} depend on the overall system mass/energy balance and on the distribution of the mass/energy within the system. The priority assigned in the evaluation of the conservation equations assures that, in spite of potential numerical fluctuation of flows, mass and energy are conserved. However, the distribution of both quantities within the system can be influenced by unphysical flows. This can happen in two basic ways:

- 1) Unphysical variation of the circulation flow rate in time.

Unphysical flow mixing, that is, fluid is moved back and forth between adjoining regions, for example, the core and downcomer.

There is an additional way that improperly evaluated internal flows can impact the parameters of interest. Namely, they could affect the magnitude of the energy/mass sink and source terms, particularly the outflow rate through breaks. There is a limited range of system inventory states in which the geometric discontinuities of the RCS (e.g. elevation of the hot legs) can induce significant changes in flow and local fluid composition. Such geometric discontinuities can, in turn, influence the computed break flow rate, especially if the break occurs at higher elevations.

Two examples are presented to illustrate: a computed oscillation that has a physical basis but is enhanced by the volume-averaging feature of the code; and a numerically induced flow in parallel channels.

5.3.1 Oscillation With A Physical Basis

Oscillations are dynamic events. Chugging and condensation-induced flow surges can churn the primary system inventory and promote mixing. In general, more mixing can be expected in the actual three-dimensional plant than in a simulation provided by a one-dimensional model. In this respect, the limitations of RELAP5 are more likely to be in the *conservative* direction, that is,

they will underestimate the degree of inter-region mixing. Of particular interest in this respect is the code's ability to evaluate the mixing that occurs between the core region and the downcomer.

Figure 5-8 shows the RELAP5 computed downcomer cooldown rates for a feed-and-bleed transient, accompanied by loss of the steam generator heat sink (due to failure of feedwater). T_{dc} oscillates with a period of ~ 200 s and an amplitude of ~ 3 K. The answer to the question, "is this physical or numerical," is that it is probably a mixture of both. Though the figure depicts a two-phase condition, the flow phenomena apply for single phase as well. HPI flow enters the cold legs upstream of the downcomer entrance. There it mixes with the warmer circulating loop flow and proceeds towards the downcomer. The average temperature and density of the fluid stream entering the downcomer depends on the relative flow rates of the two streams. At low loop flow the mixed flow will be cooler, whereas and at higher loop flow it will be warmer.

A component of the driving force for natural circulation flow is the density difference between the downcomer fluid and the fluid inside the core barrel in the core region. We pick up the development of a cycle depicted in Figure 5-8, at the point in time that T_{dc} decreases. As the downcomer fluid cools, its density increases, increasing the in-vessel natural circulation driving force. Circulation flow then increases, and the fluid temperature in the cold leg starts to rise because the constant HPI flow rate now mixes with a larger volume of warm loop flow. When this warmer water starts to penetrate into the downcomer, the in-vessel driving force is decreased, and the circulation flow drops. There is thus a negative feedback with a time lag between loop flow and temperature.

Figure 5-9 shows the coolant velocities in all cold legs. As illustrated, the velocities remain positive in all cold legs and vary in magnitude from ~ 0.6 to ~ 0.3 m/s. Finally, Figure 5-10 shows an expanded time segment on which the temperature oscillations in the downcomer and the cold leg velocities are superimposed. This illustrates that there is a small phase shift between the two cycles and thus substantiates the proposed explanation.

In the presented example, the calculated oscillation has a physical basis, however, this does not guarantee that the actual phenomenon would have the same period or magnitude. Because of the volume-averaged character of the code, the HPI and circulation streams are fully mixed, whereas in reality thermal stratification would occur. The question of how this impacts PTS analysis can be answered by considering the oscillation period and the vessel thermal time constant (~ 200 s vs. ~ 400 s). The difference is sufficiently large that a time average of T_{dc} is adequate. This is obtained by the overall energy mass balance, and depends on the average rate of loop flow and HPI flow. Therefore the oscillation, including its possible numerical component, does not contribute an additional uncertainty.

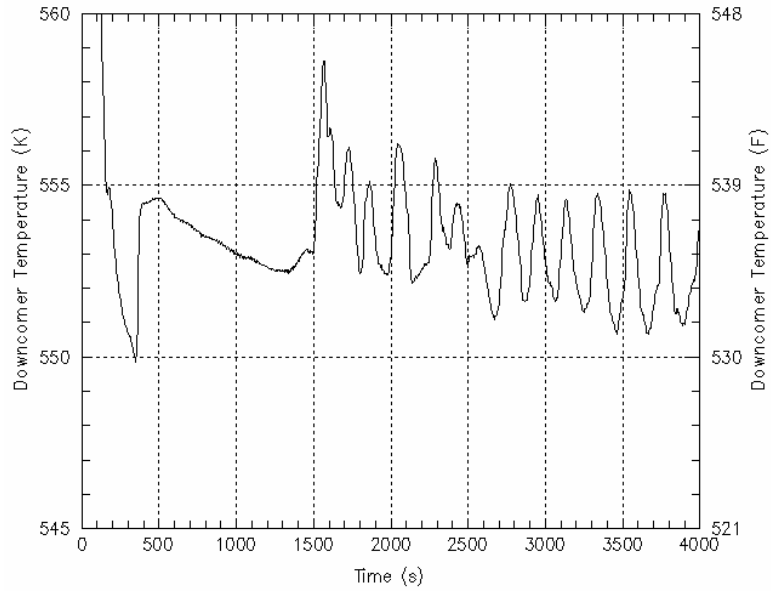


Figure 5-8 T_{dc} oscillation during feed-and-bleed transient with loss of heat sink

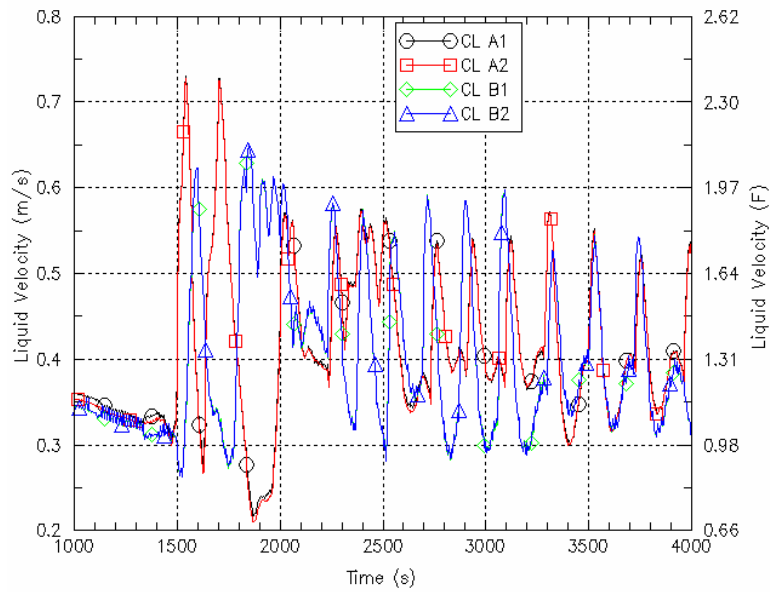


Figure 5-9 Cold leg flow velocities (feed and bleed transient with loss of heat sink)

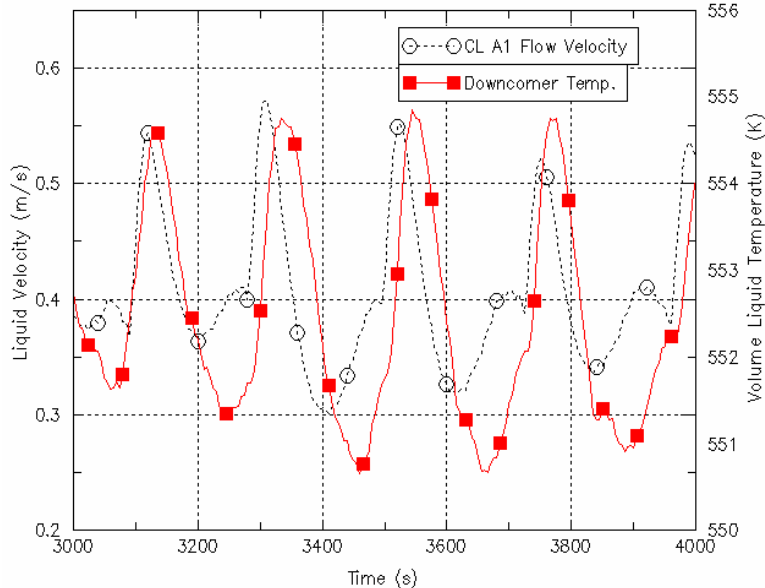


Figure 5-10 T_{dc} and cold leg velocities (feed and bleed transient with loss of heat sink)

5.3.2 Numerically Induced Flow

The influence of numerics on the evaluation of flows becomes more pronounced as the physical driving forces decrease. This can become especially apparent if the plant's flow geometry includes parallel flow channels with the same resistance. In Oconee-1, the two cold legs that connect to each steam generator provide just such an example. Anomalous flows in the cold legs may occur when the RCPs are tripped and natural circulation ceases (flow stagnation). Then, the physical driving force is small.

This numerical problem was observed in previous calculations [Riemke and Johnsen 1994], including the IPTS studies. The explanation is that the iterative algorithm used to invert matrices treats nodes sequentially. The inevitable sequential nature introduces asymmetries (through numerical round off) even for flow geometries that are in other respects completely symmetric. When dissipative terms are small (low flow), the round off differences can accumulate during the iteration process and produce macro differences in the computed flows.

An illustration of such flows is presented in Figure 5-11, which shows flow rates in cold legs A1 and A2 for a 1.71-inch break after natural circulation stops. Figure 5-12 shows the flow rate in hot leg A for two break sizes: the 1.71-inch break utilized in Figure 5-11 and a somewhat smaller 1.54-inch break. As Figure 5-12 shows, for the larger break size the recirculation flow along the hot leg decreases to zero at ~500 s, at which point there is no longer loop natural circulation flow. The quite sizable flow rate of ~100 kg/s in the negative direction (vessel to steam generator) in cold leg A1 is offset by an equivalent flow in the positive direction (steam generator to vessel) in cold leg A2. Both cold legs are at the same elevation thus there is no physical driving force for this flow. The conclusion [Riemke and Johnsen 1994], it that the flow is generated by round off errors and the asymmetry of the matrix inversion routine.

The magnitude of this influence on the downcomer temperature is illustrated in Figure 5-13. It shows two computed T_{dc} traces, which differ only in the presence of the numerical flow circulating along both cold legs. For the lower trace, specifying a very large reverse flow resistance for the RCP eliminates this flow. As long as flow is in the positive steam generator-to-vessel direction, the added resistance does not alter the computed result, however, it prevents the development of an unphysical reverse flow.

5.4 Treatment of Model Uncertainty

Even with the limitations above, RELAP5 can simulate PTS scenarios well. Only for certain phenomena does RELAP5 have large uncertainty. These phenomena and their treatments are listed as follows:

- Two-phase choked flow. It is complex to change RELAP5 internal flow rate modeling from one model to another. Instead, a variation of 30% of the break flow covers the critical flow uncertainty.
- RVVV state. The uncertainty is due to how RELAP5 models in-vessel natural circulation between the upper plenum and the downcomer. The uncertainty in-vessel circulation is bounded by the RVVV states if fully closed and fully open.
- Flow driven by numerics. Applying high reverse flow resistance in the RCPs eliminates unrealistic recirculation flow between the two parallel cold legs of the same loop.
- Flow resistance. The shear force at the interface between liquid and steam in two-phase scenarios could affect coolant flow rate. There is uncertainty in RELAP5 modeling the drag force. A 200% flow resistance is used to model the uncertainty.
- Heat transfer coefficient. Heat transfer between metal structures and coolant depends on the heat transfer coefficient determined by RELAP5. It is difficult to change the actual heat transfer models in RELAP5. Instead, a 30% variation (increase and decrease) in the heat transfer coefficient is used to evaluate the uncertainty.

The physical model uncertainties above and the boundary condition uncertainties, discussed in Chapter 6, are combined to assess the aggregate thermal hydraulic uncertainty.

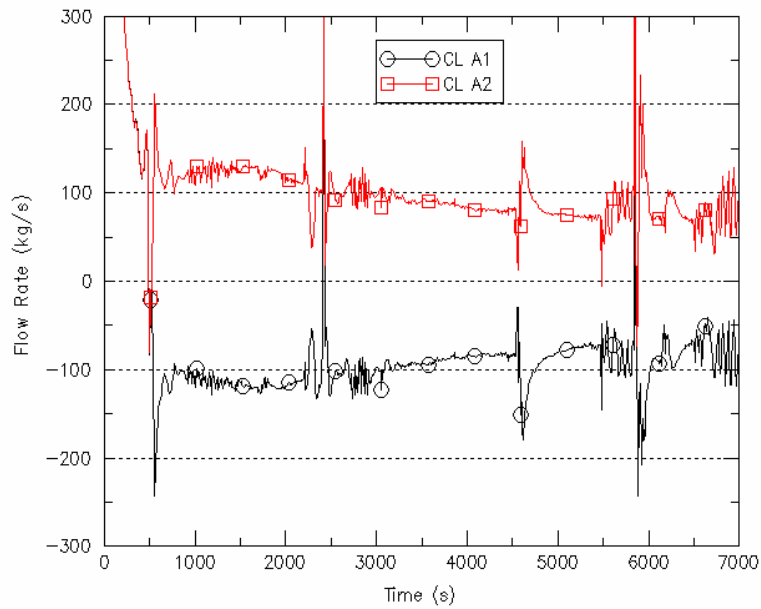


Figure 5-11 Flow rates in cold legs A1 and A2 for a 1.71-inch break

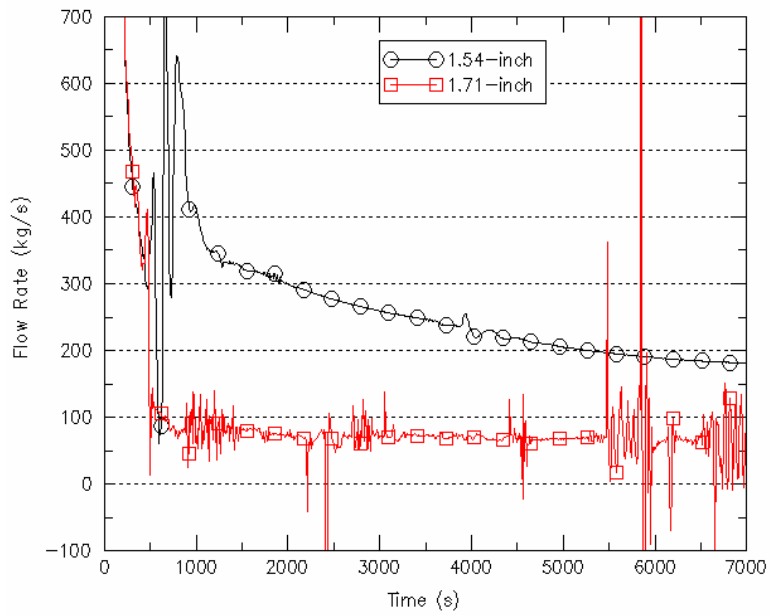


Figure 5-12 Flow rates in hot leg A for two LOCAs with different break sizes

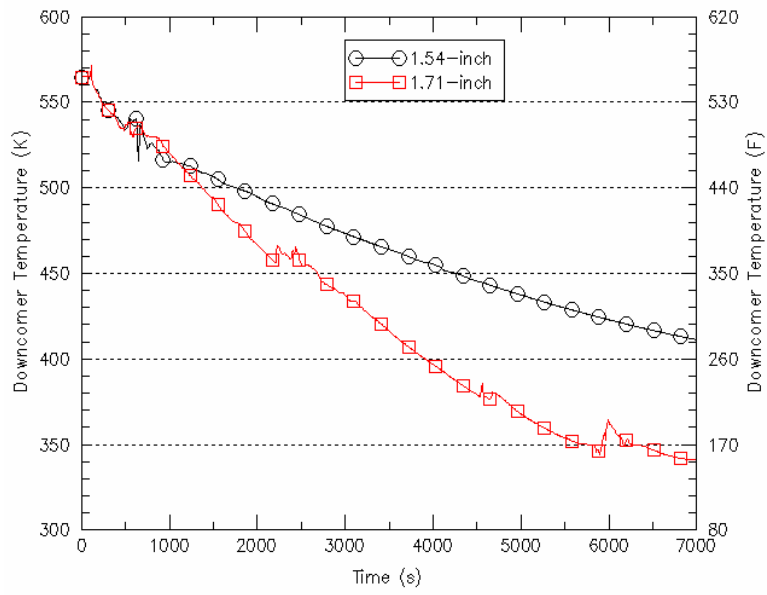


Figure 5-13 Effect of numerical parallel channel flow on T_{dc}

6. PARAMETER UNCERTAINTY

The parameters affecting PTS risk differ from one category of events to another. This chapter focuses on the category of loss of coolant accidents (LOCA), with nominal secondary system response. LOCAs are characterized by two-phase conditions within the coolant loops of the RCS. The RCS pressure equals to the saturation pressure of the hottest fluid in the loops (pressurizer no longer controls pressure), usually at the top of the vessel or the steam generators. As a result, P is no longer independent of T_{dc} . The exception is the subcategory consisting of scenarios in which a pressurizer SRV is stuck open and later reclosed. For SRV scenarios, the coolant loops become subcooled again following valve reclosure, and P becomes a function of operator control of HPI. One parameter dominates the uncertainty in $P(t)$ during refill and repressurization; the timing of HPI throttling.

Section 6.1 discusses preliminary screening of parameters affecting T_{dc} to identify system level parameters. The discussion follows the five influencing factors described in Chapter 4 for T_{dc} . Section 6.2 describes the *discrete probabilistic distribution* (DPD) method and its implementation. Section 6.3 discusses the selection of a *figure of merit*. The figure of merit is an importance indicator to PTS risk and is used to measure the magnitude, or sensitivity, of each influencing parameter. As such, the figure of merit T_{sen} is used to characterize the difference between the nominal and the upper and lower bounds of each influencing parameter. A large number of RELAP5 calculations were performed to characterize the sensitivity of each influencing parameter. Section 6.4 discusses sensitivity study results and DPD representation for all key influencing parameters, to assess aggregate uncertainty. The *linearly additive* method is used to combine the uncertainties of individual parameters. Section 6.4 also justifies the use of linearly additive assumption. Section 6.5 discusses rankings of key influencing parameters.

6.1 Identification of T_{dc} Influencing Parameters

The five T_{dc} influencing factors identified in Chapter 4 are discussed, as well as the uncertainty related features from Chapter 5.

1) Heat capacities

This includes the amounts of liquid, steam, and structure in the primary system and secondary system. These parameters are reflected in the RELAP5 input deck for the plant. The uncertainty in this category is expected to be small.

2) Heat sources

- a) Decay heat. Decay heat is dependent on the operating time and reactor power prior to the start of the event. Three decay heat curves were used to represent the uncertainty: full power infinite operation; 0.7% of full power, and 0.2% of full power. The 0.7% and 0.2% curves represent hot standby shortly after scram, and hot standby after a refueling outage, respectively. For Oconee-1, only two of the three curves were used, corresponding to full power operation and 0.2% power. When three curves are used, PRA assigns probabilities of 98% to power operation, one percent to the 0.7% decay power, and one percent to the 0.2% decay power. When two curves are used, the

probabilities assigned are 98% to full power operation, and 2% to low decay heat (0.2%) end of refueling conditions.

- b) RCPs. Some plants have automatic trip while others rely on operator action to trip the reactor coolant pumps. In general, the RCP trip criterion is loss of subcooling. In the PRA model, the probability of RCP trip upon loss of subcooling is very high. In this study it is assumed that the RCPs are tripped as intended.
- c) Structural Heat. As discussed in Chapter 5, heat transfer from structures to fluid is affected by the heat transfer coefficient calculated by RELAP5. An uncertainty of $\pm 30\%$ on heat transfer coefficient was used.

3) Heat sinks

- a) Primary system break. Break location and break size are the key parameters. The thermal hydraulic response of the RCS is significantly different for hot leg breaks compared to cold leg breaks. The pressurizer SRV is another break location that causes loss of subcooling. The LOCA break sizes that cause loss of subcooling range from ~ 1.5 -inch to a double-ended LOCA. For scenarios involving pressurizer SRV stuck open, the break size ranges from the valve open area that creates break flow greater than HPI flow, to the maximum valve open area. For a fixed break size, as mentioned in Chapter 5, there is uncertainty in the calculation of critical flow. An uncertainty of $\pm 30\%$ was used.
- b) Steam generators. The boundary conditions for LOCAs specify nominal secondary system conditions. For LOCAs, the primary system break is the dominant heat sink. The steam generators will become heat sources to RCS. The uncertainty in heat transfer from the secondary system to the primary system is small (Appendix C).
- c) HPI, accumulator (core flood tank), and LPI. Four important factors that affect ECC injection: system function state (fail on demand), flow rate, ECC temperature, and timing of actuation:
 - i) System function state concerns failure upon demand. Complete or partial failure of an ECC injection system reduces injection flow significantly, with corresponding reduction of PTS consequence. ECC systems have small failure probabilities, for example, the failure probability of HPI is about $2E-3$ per demand. When combined with the frequency of the initiating event, scenarios with ECC failures have very low frequencies. From the PFM perspective, failure of ECC injection reduces the $T_{dc}(t)$ cooldown and corresponding PTS risk. Therefore, such scenarios have negligible PTS risk. Sensitivity studies of HPI failure were performed, but HPI failure, as well as accumulator and LPI failures, are not included in the uncertainty analysis because the sequences are low probability and low consequence.
 - ii) Flow rates of the three ECC injection systems are primarily dependent on the RCS pressure. The flow rate versus pressure curves for HPI and LPI are part of the input deck. These pump curves are the main source of uncertainty. A $\pm 10\%$ variation on HPI flow was applied to treat this uncertainty. The uncertainty in accumulator flow was addressed by varying accumulator pressure. Uncertainty in LPI flow was not considered, since LPI injection begins at low pressure (1.4 MPa), which was believed to be below the pressure of PTS significance.

- iii) ECC injection temperature varies through year for the three injection systems. Three sets of temperature were chosen to represent summer, spring/fall, and winter conditions. The associated probabilities used were 0.25, 0.5, and 0.25, respectively. When the refueling water storage tank (RWST) is empty, ECC suction is switched to the containment sump. The sump water is at a higher temperature (~350K) than the RWST, so the injection temperature increases. Sump recirculation begins later in the scenarios, and was determined to have no impact on PTS risk.
- iv) Actuation of ECCS depends on the system logic. Low pressurizer pressure is usually the ECCS actuation signal. The uncertainty on this pressure setting is small. The timing of accumulator injection depends on the pressure of the accumulator relative to the RCS. A variation of ± 50 psi was applied to the accumulator pressure to account for uncertainty in timing (and flow rate).

4) RCS coolant flow rate

- a) RCP state. The RCP state was discussed above under *heat source*.
- b) RCS loop flow resistance. RCP trip upon loss of subcooling was assumed. Thereafter, natural circulation or flow stagnation ensues. Uncertainty in mass flow rate under these conditions was treated by varying the nominal resistance by a factor of two (increased by 100%) to assess the impact of modeling uncertainty.

5) Vessel energy distribution

- a) RVV state. As discussed in Chapter 5, flow through the RVVVs could cause mixing of hot water/steam from the upper plenum in the downcomer and cold legs. The impact of in-vessel natural circulation is to increase T_{dc} . To bound the uncertainty in natural circulation, the RVVVs were modeled as fully closed and fully open.
- b) Interruption-resumption and boiler-condenser modes. These two natural circulation modes occur at very specific primary and secondary side conditions, and the phenomena last only for a short period of time. Their impact on PTS risk is considered small.

6.2 Finite Discrete Uncertainty Representation

The *Discrete Probabilistic Distribution* (DPD) method was used to represent a parameter's continuous distribution by discrete values. Each discrete value has an associated probability. Representative values were selected that usually included lower bound, nominal, and upper bound. Selection of representative values was discussed in Section 6.1, and Table 6-1 lists the values and probabilities of these parameters.

Table 6-1 Representative values and corresponding probabilities of key influencing parameters for uncertainty analysis of Oconee-1

	Factors	Value 1 (Lower Bound)	Value 2 (Nominal)	Value 3 (Upper Bound)
		Probability	Probability	Probability
Parametric (Boundary Condition) Uncertainty	Break Size	N number of representative break sizes	--	--
		Proportional to percent of break flow represented	--	--
	Break Location	Cold Leg	Hot Leg	--
		0.5	0.5	--
	Decay Heat*	Nominal	0.7%	0.2%
		0.98	0.01	0.01
	Season**	Winter	Spring/Fall	Summer
0.25		0.50	0.25	
High Pressure Injection Flow	90%	Nominal	110%	
	0.1	0.8	0.1	
Core Flood Tanks Pressure	- 50 psi	Nominal	+ 50 psi	
	0.1	0.8	0.1	
Sump recirculation	If break size > ~ 4"	If break size < ~4"		
	1.0	0.0		
RELAP5 Model Uncertainty	Reactor Vessel Vent Valve State	Fully closed	Nominal	Fully open
		0.25	0.5	0.25
	Convective Heat Transfer Coefficient	70%	Nominal	130%
		0.1	0.8	0.1
	Flow Resistance	200%	Nominal	--
0.1		0.9	--	
Critical Flow (Break flow)	70%	Nominal	130%	
	0.25	0.50	0.25	
Numerical flow	High CL reverse flow resistance	--	--	
	1.0	--	--	

* Applied only for LOCA. PRA model treats HZP explicitly for pressurizer SRV stuck open

**Winter $T_{HPI} = 4C (40F)$ $T_{ACC} = 21C (70)$ $T_{LPI} = 4C(40F)$

**Summer $T_{HPI} = 29C (85F)$ $T_{ACC} = 38C (100F)$ $T_{LPI} = 29C (85F)$

**Spring/fall $T_{HPI} = 21C (70F)$ $T_{ACC} = 27C (80F)$ $T_{LPI} = 21C (70F)$

6.3 Sensitivity Indicator

The *figure of merit*, or *sensitivity indicator* is based on $T_{dc}(t)$, since this variable has the greatest significance to PTS consequence amongst the three thermal hydraulic parameters. $T_{dc}(t)$ is averaged over the 10,000 s duration of the RELAP5 calculations performed for the different sensitivity studies. **The averaged value of $T_{dc}(t)$ is termed T_{sen} .** T_{sen} is a quantitative measure of the sensitivity of a given parameter. As such, T_{sen} is used to measure the difference between the nominal value of a parameter and its upper and lower bound values. It is also used to select *representative scenarios* for carry out the thermal hydraulic uncertainty determination. The values obtained for T_{sen} are meaningful primarily by comparison to each other, as a measure of the relative sensitivity of various parameters and their ranges of uncertainty.

The *nominal range sensitivity analysis* (NRSA) method [Cullen and Frey 1999; Frey and Patil 2002] was used to evaluate the sensitivity (T_{sen}) of individual parameters. The NSRA process starts with the calculation of a base case scenario, with all parameters at their nominal (most probable) values. Additional calculations are performed changing the value of one-and-only-one parameter, while keeping the other parameters at their nominal values. The difference between the new result and the base result is the sensitivity of the parameter with respect to the figure of merit (T_{sen}). This process continues until the sensitivities of all the parameters are assessed. This method is also called *one-factor-at-a-time* (1-FAT).

To apply the NRSA method for a given initiating event, all parameters are assigned nominal values. A RELAP5 calculation is performed to obtain the base case value of T_{sen} , which is the reference value ($T_{\text{sen, ref}}$). An influencing parameter is selected, its nominal value is changed to its upper bound value, and the RELAP5 calculation is repeated to obtain $T_{\text{sen}} = T_{\text{sen, upper}}$. The difference

$$T_{\text{sen, upper}} - T_{\text{sen, ref}}$$

is the sensitivity of upper bound value from the nominal. This is repeated for the lower bound value of the same influencing parameter.

$$T_{\text{sen, lower}} - T_{\text{sen, ref}}$$

This is repeated for all influencing parameters. The total number of sensitivity cases is “N+N-1”,

$$N_1 + \sum_2^M (N_i - 1) \quad (6.1)$$

where,

M is the total number of parameters,

N_i is the number of representative values of the i -th parameter.

For example, four parameters (M) with three representative values each (N_i) (lower bound, nominal, and upper bound), the number of RELAP5 sensitivity runs is nine ($3 + 2 + 2 + 2$).

For LOCAs, the sensitivities of the different influencing parameters are strongly dependent on the break size. The variation in $T_{\text{dc}}(t)$ is less for large breaks than for small. Thus, the broad category of LOCAs must be subdivided. For each subcategory, a reference value $T_{\text{sen, ref}}$ was obtained for the different break sizes. Table 6-2 shows T_{sen} of the key parameters for Oconee-1. Not all parameter variations were calculated. The uncalculated data were estimated by interpolation or extrapolation, or judgment.

Table 6-2 Key influencing parameters matrix for primary system breaks for Oconee-1
Default location is surge line except as indicated for cold leg LOCA (T_{sen} in K)

		Break Size (inch)					
		1.5"	2"	2.8"	4"	5.7"	8"
Parameters, Values							
Nominal		414	394	388	363	329	317
Season	Winter	402	--	374	--	314	314
	Summer	--	--	395	--	336	317
ACC Pressure	+ 50 psi	--	--	386	--	--	--
	- 50 psi	--	--	389	--	--	--
HPI State and Flow Rate	110%	401	--	380	--	--	--
	90%	416	--	402	--	--	--
	HPI Failed and Recovered @~7000s	--	--	491	--	--	317
	HPI Failed and Recovered @~1000s	--	--	400	--	--	--
	HPI Failed and Recovered @~2000s	--	--	416	--	--	--
	HPI 100% Failed	--	--	500	403	328	319
	HPI 25%Failed	446	453	442	--	--	--
	HPI 50%Failed	514	511	467	--	--	--
Decay Heat	HZP	398	--	349	--	321	312
RVVV State	Closed	--	--	362	345	--	--
	2/6 Open	--	--	406	--	--	--
	4/6 Open	--	--	410	--	--	--
	Open	--	--	413	371	--	--
Numerics	High CL Reverse Flow Resistance	400	372	370	356	--	311
H	130%	--	400	396	--	331	--
	70%	--	387	380	--	324	--
Loop Resist	200%	--	395	--	--	--	--
	200% Bypass Flow Area	--	396	--	--	--	--
	Bypass Closed	--	375	--	--	--	--
Heat Structure	No heat structure	--	369	--	--	--	--
Break Location	Cold Leg	--	455	412	376	345	317

*Winter $T_{HPI} = 4C (40F)$ $T_{ACC} = 21C (70F)$ $T_{LPI} = 4C (40F)$
 Summer: $T_{HPI} = 29C (85F)$ $T_{ACC} = 38C (100F)$ $T_{LPI} = 29C (85F)$
 Spring/fall: $T_{HPI} = 21C (70F)$ $T_{ACC} = 27C (80F)$ $T_{LPI} = 21C (70F)$

6.4 Uncertainty Assessment and Identification of Representative Scenarios

The effect of changing a parameter's value from its nominal value to another is determined by the difference in T_{sen} of the two scenarios.

$$\Delta T_{sen(i,j)} = T_{sen(i,j)} - T_{sen,ref} \quad (6.2)$$

where

$\Delta T_{sen(i,j)}$ is the sensitivity of parameter-i changing its value from nominal to the j-th representative value

$T_{sen(i,j)}$ is T_{sen} of changing parameter-i's value from its nominal value to j-th representative value.

$T_{sen,ref}$ is T_{sen} of the nominal scenario

Since the vessel water level does not fall below the bottom of cold leg, the downcomer is always full, and the heat capacity of the fluid in the downcomer is roughly constant. Parameters affecting T_{dc} are heat sources or heat sinks. Physically, it is intuitively reasonable that the

combined impact of multiple factors on T_{dc} would be close to a simple summation of each parameter's individual effect,

$$\Delta T = \sum_{i=1}^M \Delta T_{sen,(i,j)} \quad (6.3)$$

where,

ΔT is the combined sensitivity of multiple parameters. M is the total number of key parameters

$\Delta T_{sen,(i,j)}$ is the individual parameter's sensitivity at its j -th representative value. The value j is a random number.

The combined effect of multiple parameters is calculated from Equation 6.3. For example, changing the ECC injection temperature from spring/fall (nominal) to winter changes T_{sen} by x degrees; changing decay heat from full power operation (nominal) to low decay heat changes T_{sen} by y degrees. Combining winter temperature and low decay heat effects, one simply adds $x + y$ to obtain the combined affect on T_{sen} . The probability of a combination is the product of each parameter's probability

$$\text{Prob} [\Delta T] = \prod_{i=1}^M \text{Prob} (T_{sen,(i,j)}) \quad (6.4)$$

where,

$\text{Prob} [\Delta T]$ probability of the combined scenario

M total number of key parameters

$\text{Prob} [T_{sen,(i,j)}]$ probability of the i -th parameter at its j -th representative value

For the above example, the probability of the event occurring during winter is α , and during low decay heat operation is β . The probability of the combination is $\alpha\beta$. Equations 6.2 to 6.4 are applied to determine the respective probabilities of all combinations of sensitivity studies. Each combination has a T_{sen} and a probability, which can be plotted as probabilistic density function (PDF) versus T_{sen} , as shown on the left of Figure 6-1. The PDF can be transformed into a cumulative density function (CDF) versus T_{sen} , shown on the right of Figure 6-1.

Representative scenarios are identified from the CDF diagram. First, the number of scenarios is determined based on how large the range is of T_{sen} . Starting from the total CDF, the two 5% tails are truncated since the T_{sen} of the two tails could have a large deviation from the linearly additive assumption. The remaining 90% of the CDF space is subdivided into equal areas, according to the predetermined number of representations. The probability apportioned to each representative scenario is 90% divided the number of representative scenarios. To account for the probability of the two truncated tails of the distribution, 5% is added to the probabilities of the upper bound and lower bound scenarios. The larger the range, the more subdivisions are required to obtain a reasonable representation.

For each subdivision of the CDF, a T_{sen} is identified by using the mean percentile of the subdivision, as shown in the CDF diagram to the right of Figure 6-1. Representative scenarios are identified as the particular combination of parameters and their values that yields that particular value of T_{sen} . Each representative scenario represents a subdivision; the discrete representative scenarios represent the range of behavior.

A RELAP5 calculation is performed for each representative scenario to obtain $T_{dc}(t)$, $P(t)$, and $h_{dc}(t)$. An appropriate PRA frequency is assigned to each representative scenario. The thermal hydraulic boundary conditions and PRA data are input to the FAVOR PFM calculation. The representative scenarios so determined are used to evaluate thermal hydraulic uncertainty through FAVOR PFM analysis.

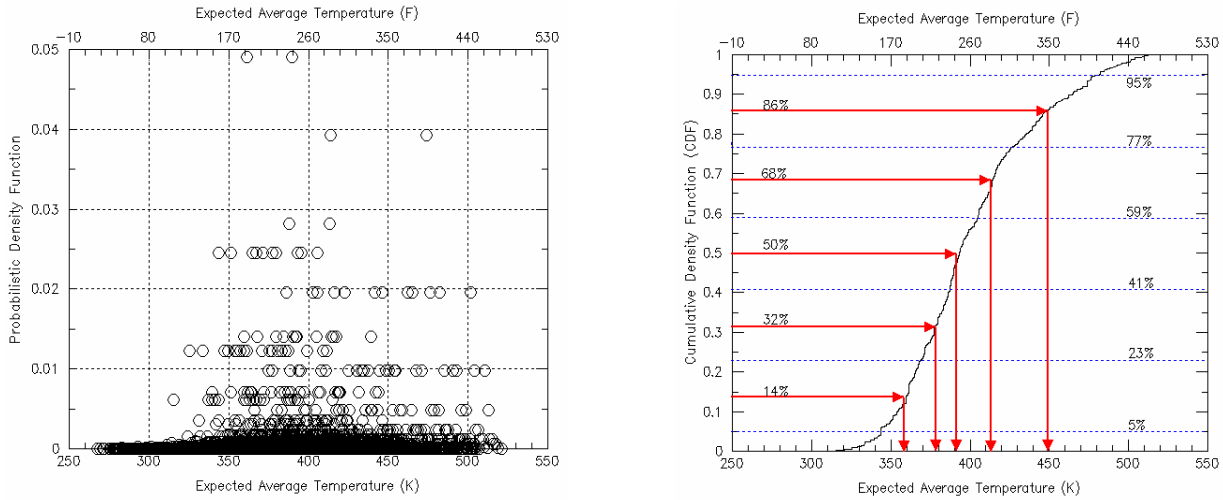


Figure 6-1 Probability density and cumulative density functions for a category of LOCAs .

To validate the linear additive assumption, a 2.8-inch surge line LOCA scenario was selected. The nominal 2.8-inch break served as reference ($T_{sen, ref}$). Five different combinations of parameters were selected,

- 1) $T_{sen} = T_{sen, ref} - 100F$
- 2) $T_{sen} = T_{sen, ref} - 50F$
- 3) $T_{sen} = T_{sen, ref}$
- 4) $T_{sen} = T_{sen, ref} + 50F$
- 5) $T_{sen} = T_{sen, ref} + 100F$

Thus, a 200F (110K) range of T_{sen} was covered. A combination of parameters was identified that corresponded to each of the five values of T_{sen} . RELAP5 calculations were performed for the five cases identified to obtain values of $T_{sen, RELAP5}$. These values were compared with the linearly additive model. Table 6-3 shows results for the five comparisons. Figure 6-2 is the corresponding plot. The 45° line in Figure 6-2 is the ideal solution in which the linearly additive assumption yields the same values as RELAP5. The deviation is seen as the difference between the solid points and the line. We conclude that the linearly additive assumption is reasonable.

Table 6-3 RELAP5 runs for validating the linearly additive assumption for multiple parameters (2.8 inch surge line LOCA).

No.	Description (other parameters assigned nominal values)	Linear model T_{sen} (K)	RELAP5 T_{sen} (K)	$T_{sen, RELAP5} - T_{sen, model}$ (K)
1	Winter; $P_{ACC} + 50$ psi; 70% A_{brk} ; RVVVs closed; 70% h	331.7	345.3	13.6
2	Summer; RVVVs Close; 200% flow resistance	360.0	362.3	2.7
3	$P_{ACC} + 50$ psi; 110% HPI; 70% Break flow; 130% h	387.6	391.4	3.8
4	Summer; $P_{ACC} + 50$ psi; 90% HPI; 130% break; RVVVs fully open; 200% flow resistance	415.5	406.9	-8.6
5	Summer; 90% HPI; 70% Break flow; RVVVs fully open; 130% h	438.2	448.8	10.7

Note: The RELAP5 calculated average first 10,000 seconds T_{dc} of a nominal 2.8 inch surge line LOCA is $388K = T_{sen}$

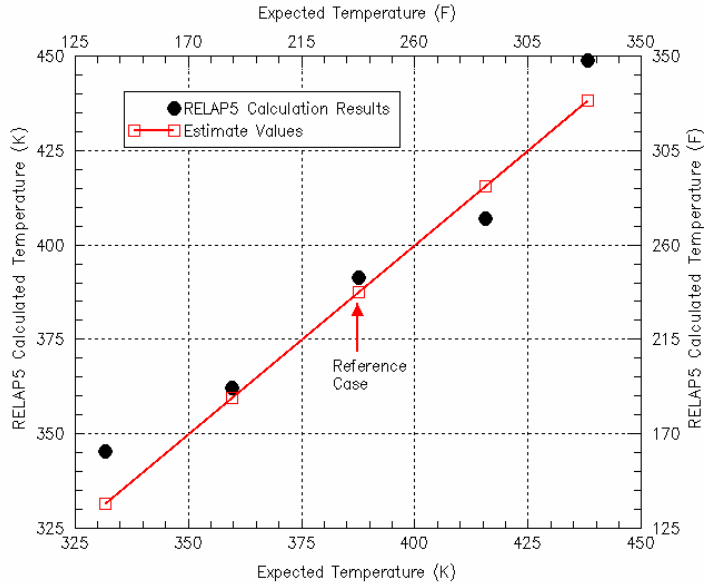


Figure 6-2 Linearly additive assumption compared with RELAP5 calculations for a 2.8-inch surge line LOCA.

6.5 Parameters Rankings

The results in Table 6-2 can be used to assess parameter importance for the designated category in terms of T_{dc} . The impact on P by the timing of HPI throttling for RCS repressurization (SRV) scenarios is not included.

Figures 6.3 to 6.5 show the ranking of key influencing parameters for break sizes of 2.8, 5.7, and 8 inch (4 E-3, 1.6 E-2, and 3.2 E-2 m²), respectively. For breaks greater than 8-inch, the PTS consequence is not sensitive to uncertainty of any parameters. The higher ΔT_{sen} indicates a positive effect (higher downcomer temperature). For example, HPI failure for a 2.8-inch break increases T_{sen} more than 100K. Some observations are,

- Parameter importance rank varies at different break sizes.
- Relative importance of two parameters could be different at different break sizes.
- Some parameters change their PTS impact vector direction when the break sizes changed.
- Parameters' sensitivities decrease when break size increased.

For example, Figure 6-3 shows that HPI failure increased T_{sen} more than 100C for a 2.8-inch break, however, HPI failure had little impact when break size is greater than 5.7-inch (1.6E-2 m²) (Figures 6.5, and 6.6). As a second example, consider the comparison of a 2.8-inch LOCA at HZP, which causes T_{sen} to decrease ~40C compared to full power decay heat. However, HZP is insignificant when the break size is greater than 5.7-inch. These two examples show that the sensitivity is strongly dependent on the break size.

For small LOCA scenarios the RCS remains at high pressure preventing CFTs and LPI from injecting when HPI fails. In this case, T_{sen} is higher than the nominal scenario. However, for a certain range of break sizes, HPI failure induces a faster depressurization and faster accumulator and LPI injection. As a result, T_{sen} for HPI failure is lower for this break range than nominal.

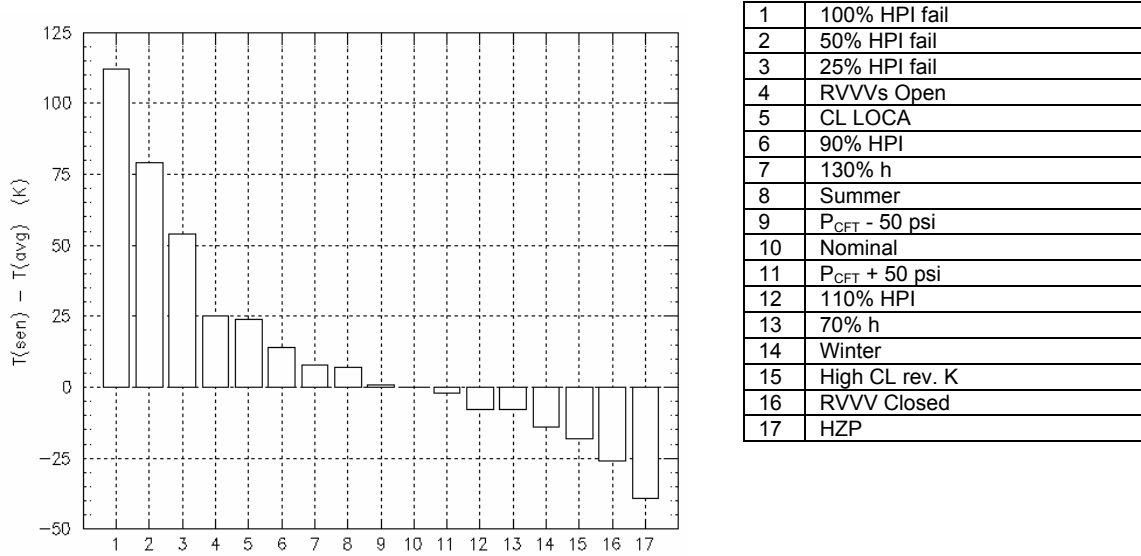


Figure 6-3 Parameter rankings for 2.8-inch LOCA (base case location is surge line)

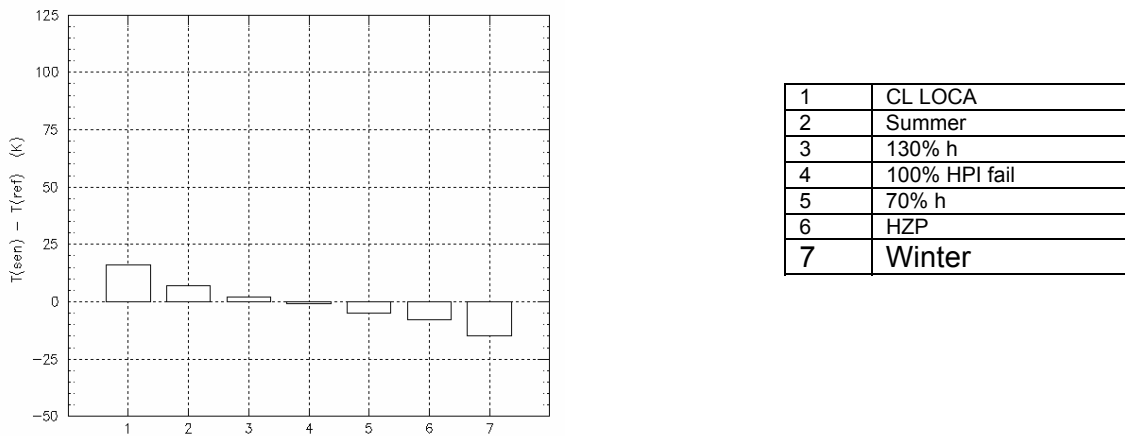


Figure 6-4 Parameter rankings for 5.7-inch LOCA (base case location is surge line)

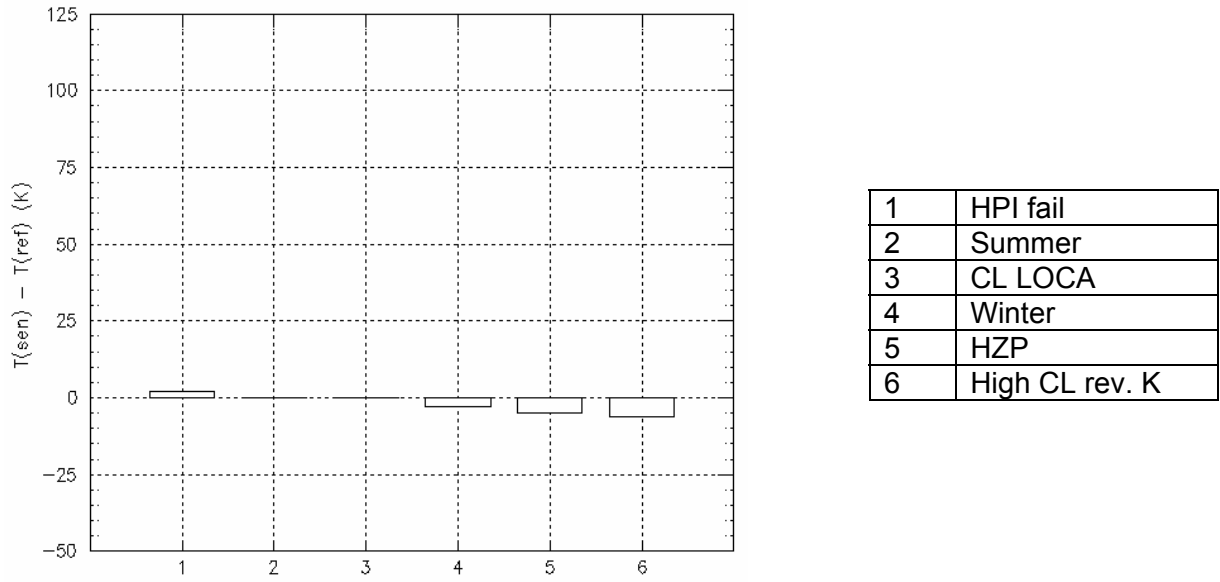


Figure 6-5 Parameter rankings for 8-inch LOCA (base case location is surge line)

7. RESULTS OF THERMAL HYDRAULIC UNCERTAINTY ASSESSMENT

This chapter presents uncertainty analysis results for Oconee-1, Beaver Valley, and Palisades. For all three plants, uncertainty analyses were performed for the category of loss of RCS subcooling due to primary system break, with nominal secondary system state. The minimum break size and SRV open area that induce break flow greater than HPI flow, causing RCS loss of subcooling, are similar for all three plants. This category includes LOCAs and stuck open SRVs, and is divided into five subcategories,

- 1) LOCA break sizes ~1.5-inch to 4-inch ($\sim 1 \text{E-}3 \text{ m}^2$ to $8 \text{E-}3 \text{ m}^2$)
- 2) LOCA break sizes 4-inch to 8-inch ($8 \text{E-}3 \text{ m}^2$ and $3.2 \text{E-}2 \text{ m}^2$)
- 3) LOCA break sizes > 8-inch ($3.2 \text{E-}2 \text{ m}^2$)
- 4) Pressurizer SRVs stuck open and remaining open, with total valve area greater than ~1.5-inch ($\sim 1 \text{E-}3 \text{ m}^2$)
- 5) Pressurizer SRVs stuck open and reclosed, with total valves open area greater than ~1.5-inch ($\sim 1 \text{E-}3 \text{ m}^2$)

The uncertainty of each subcategory was assessed separately, with representative scenarios identified for each subcategory. Representative values of key parameters and their probabilities are shown in Table 7-1.

7.1 Oconee-1 Representative Scenarios for Thermal Hydraulic Uncertainty

Table 7-2 shows T_{sen} values calculated by RELAP5 for Oconee-1. The values obtained were used for uncertainty assessment. The data not listed were estimated by interpolation, extrapolation, or judgment based on thermal hydraulic behavior.

Table 7-1 Representative values and corresponding probabilities of the key influencing parameters for Oconee-1

	Factor	Lower Bound Probability	Nominal Probability	Upper Bound Probability
Boundary Condition Uncertainty	Break Size	N number of representative break sizes	--	--
		Proportional to represented percentage of break flow	--	--
	Break Location	Cold Leg	Hot Leg	--
		0.5	0.5	--
	*Decay Heat	Nominal	0.7%	0.2%
		0.98	0.01	0.01
	Season	Winter	Spring/Fall	Summer
0.25		0.5	0.25	
High Pressure Injection Flow	90%	Nominal	110%	
	0.1	0.8	0.1	
Accumulator Pressure	- 50 psi	Nominal	+ 50 psi	
	0.1	0.8	0.1	
Sump recirculation	If break size > ~ 4"	If break size < ~4"		
	1.0	0.0		
RELAP5 Model Uncertainty	RVVV State	Fully closed	Nominal	Fully open
		0.25	0.5	0.25
	Heat Transfer Coefficient	70%	Nominal	130%
		0.1	0.8	0.1
	Flow Resistance	200%	Nominal	--
0.1		0.9	--	
Critical Flow	70%	Nominal	130%	
	0.25	0.5	0.25	
Numerical Flows	High CL reverse flow resistance	--	--	
	1.0	--	--	

*For Oconee, only one low decay heat curve is used

Table 7-2 Matrix of influencing parameters T_{sen} for LOCAs in Oconee-1 (T_{sen} in K)

		Break Size (inch)					
		1.5"	2"	2.8"	4"	5.7"	8"
Value							
Nominal		414	394	388	363	329	317
Season	Winter*	402	--	374	--	314	314
	Summer*	--	--	395	--	336	317
CPF	$P_{CFT} + 50$ psi	--	--	386	--	--	--
	$P_{CFT} - 50$ psi	--	--	389	--	--	--
HPI State and Flow Rate	110% HPI RCPs off	401	--	380	--	--	--
	90% HPI	416	--	402	--	--	--
	HPI Failed and Recovered (@~7000 s)	--	--	491	--	--	317
	HPI Failed and Recovered (@~1000 s)	--	--	400	--	--	--
	HPI Failed and Recovered (@~2000 s)	--	--	416	--	--	--
	100 % HPI Failed	--	--	500	403	328	319
	25% HPI Failed	446	453	442	--	--	--
	50% HPI Failed	514	511	467	--	--	--
Decay Heat	HZP	398	--	349	--	321	312
Vent Valve State	Vent Valve Close	--	--	362	345	--	--
	Vent Valve 2/6 Open	--	--	406	--	--	--
	Vent Valve 4/6 Open	--	--	410	--	--	--
	Vent Valve 6/6 Open	--	--	413	371	--	--
Numerical Mixing	High CL Reverse Flow Resistance	400	372	370	356	--	311
Convective Heat Transfer	130% h	--	400	396	--	331	--
	70% h	--	387	380	--	324	--
Flow Resistance	200% Loop Flow Resistance	--	395	--	--	--	--
	200% Bypass Flow Area	--	396	--	--	--	--
	Zero Bypass Flow Area	--	375	--	--	--	--
Heat Structure	No heat structure	--	369	--	--	--	--
Break Location	Cold Leg LOCA	--	455	412	376	345	317

Base case break location is surge line

*Winter: $T_{HPI} = 4C (40F)$, $T_{CFT} = 21C (70F)$, $T_{LPI} = 4C (40F)$
 Summer: $T_{HPI} = 29C (85F)$, $T_{CFT} = 38C (100F)$, $T_{LPI} = 29C (85F)$
 Spring/fall: $T_{HPI} = 21C (70F)$, $T_{CFT} = 27C (80F)$, $T_{LPI} = 21C (70F)$

7.1.1 1.5-inch to 4-inch LOCA

To characterize this range of breaks, three specific break sizes were selected: 1.5-inch, 2.8-inch, and 4-inch (1E-3, 4E-3, and 8E-3 m², respectively). Each has 1/3 of the total probability for the break size range. Table 7-3 lists the parameters included for each break size. Some parameters have insignificant effect at certain break sizes and are not included in the analysis. The numbers in parentheses in the first column in Table 7-3 are the number of representative values of the parameter, whose values are shown in Table 7-1.

For example, break location has two variations: hot leg and cold leg. For a 1.5-inch break, there are 972 combinations of parameters, since this *bin* contains two parameters with two variations, plus five parameters with three variations (i.e. $2^2 \times 3^5 = 972$). The 2.8-inch LOCA has 5832 combinations ($2^3 \times 3^6$), and the 4-inch LOCA has 324 combinations ($2^2 \times 3^4$). In total, there are 7128 combinations (972 + 5832 + 324). The event descriptions, probabilities, and expected T_{sen} of the 7128 scenarios were calculated based on the linearly additive method. Figures 7.1 and 7.2 are the PDF and CDF plots of the 7128 combinations.

From the CDF shown in Figure 7-2, five representative scenarios were selected: the 14th, 32nd, 50th, 68th, and 86th percentiles of the distribution. The five values of T_{sen} were found by projecting the five percentiles to values of T_{sen} as shown in Figure 7-2 (from the horizontal arrows to vertical arrows). The difference in T_{sen} between the lower (14th) and upper (86th) percentiles is ~80K. This range (80K) is less than that used to verify the assumption of linearity (110K) (Figure 6-2), so the linearly additive assumption is applicable.

Table 7-3 Influencing parameters for LOCAs 1.5-inch to 4-inch

Parameter	Break Size		
	1.5"	2.8"	4"
Break Location (2)	√	√	√
Decay Heat (2)	√	√	√
Season (3)	√	√	√
HPI Flow Rate (3)	√	√	Insignificant
CFT pressure (3)	Insignificant	√	Insignificant
RVVV state (3)	√	√	√
Convection Heat transfer (3)	√	√	√
Flow Resistance (2)	Insignificant	√	Insignificant
Break Flow (3)	√	√	√

Numbers in parentheses are number of representative values of the parameter

The probabilities of the five representative scenarios were calculated based on the individual parameter's probability from Table 7-1. First, the two tails (<5th, >95th) of the distribution were truncated. Their probabilities were later added to the most similar representative scenarios after these representatives were identified. The remaining 90% of the distribution, between the 5th and 95th percentiles, was divided evenly into 5 regions. For each of the five regions, the mean percentile was selected, giving five representative values of T_{sen} . Each sector has a fractional probability of 0.18 (0.90/5). The 14th and the 86th percentiles also represent the respective

truncated tails, therefore, to each of them was added an additional 5% probability. The corresponding probabilities of the 14th, 32nd, 50th, 68th, and 86th representative scenarios were then 0.23, 0.18, 0.18, 0.18, and 0.23. Table 7-4 lists the five representative scenarios and their probabilities. Figures 7.3 and 7.4 are the time histories of T_{dc} and P of the five representative scenarios, as calculated by RELAP5.

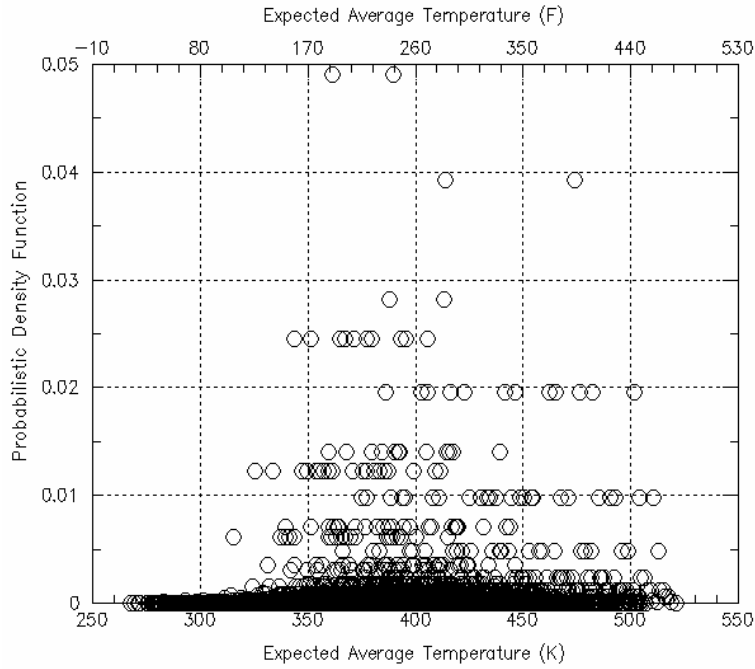


Figure 7-1 Probability distribution for T_{sen} for LOCAs 1.5-inch to 4-inch (7128 combinations in total)

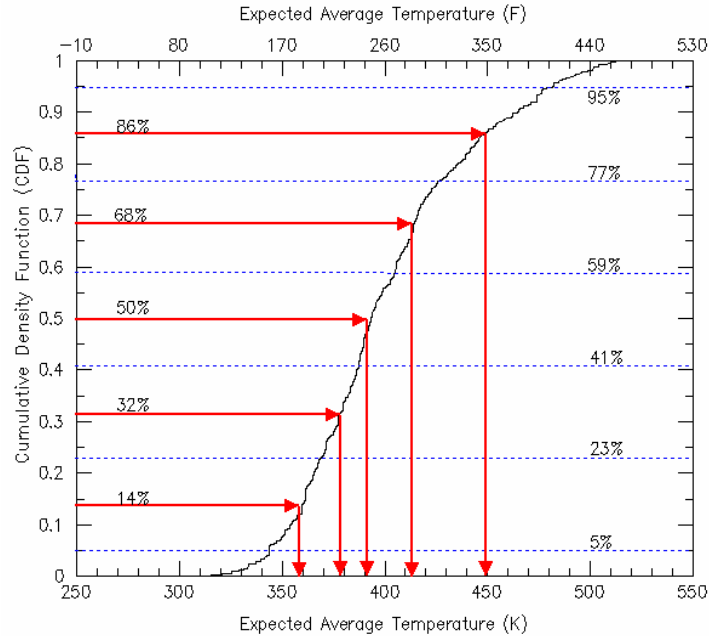


Figure 7-2 Cumulative density function and identification of representative scenarios for LOCA 1.5-inch to 4-inch

Table 7-4 Boundary conditions of the five representative scenarios for LOCA 1.5-inch to 4 inch

#	Bin #	Probability	Scenario Description
1	145	0.23	1-inch cold leg break, break flow increased 30%, winter*
2	142	0.18	2.8-inch surge line break, 70% break flow
3	141	0.18	2.8-inch surge line break, 130% break flow
4	172	0.18	4-inch cold leg break
5	154	0.23	4-inch surge line break, 70% break flow, RVVVs closed

7.1.2 4-inch to 8-inch LOCA

Three specific break sizes were selected to characterize this range of breaks: 4-inch, 5.7-inch, and 8-inch (8 E-3 m², 1.6 E-2 m², and 3.2 E-2 m² respectively). Table 7-5 shows the parameters included in the thermal hydraulic uncertainty assessment. The total sample size is 336 (2²×3⁵ + 2×3 + 2×3). For the three break sizes, three influencing factors were considered to be most important: break location, season, and decay heat. The PDF and CDF diagrams for the three breaks and their parametric variations are shown in Figures 7.5 and 7.6, from which the three representative scenarios were selected (Figure 7-6). These three scenarios happened to be the base case (nominal) scenarios: 4-inch, 5.7-inch, and 8-inch surge line LOCAs. Their probabilities are 0.35, 0.30, and 0.35, respectively. The scenario descriptions of these three representative scenarios and their corresponding thermal hydraulic bins are shown in Table 7-6. Their T_{dc} and P plots are shown in Figures 7.7 and 7.8, respectively.

Table 7-5 Influencing parameters of LOCAs 4-inch to 8-inch

Parameter	Break Size		
	4-inch	5.7-inch	8-inch
Break Location (2)	√	√	√
Decay Heat (2)	√	Insignificant	Insignificant
Season (3)	√	√	√
HPI Flow Rate (3)	Insignificant	Insignificant	Insignificant
RVVV state (3)	√	Insignificant	Insignificant
Convective Heat Transfer (3)	√	Insignificant	Insignificant
Flow Resistance (2)	Insignificant	Insignificant	Insignificant
CFT Pressure (3)	Insignificant	Insignificant	Insignificant
Break Flow (3)	√	Insignificant	Insignificant

Numbers in parentheses are the number of representative values of the parameter.

Table 7-6 Boundary conditions of the five representative scenarios of LOCAs 4-inch to 8-inch

#	Bin #	Probability	Scenario Description
1	178	0.35	4-inch surge line break
2	160	0.30	5.7-inch surge line break
3	164	0.35	8-inch surge line break

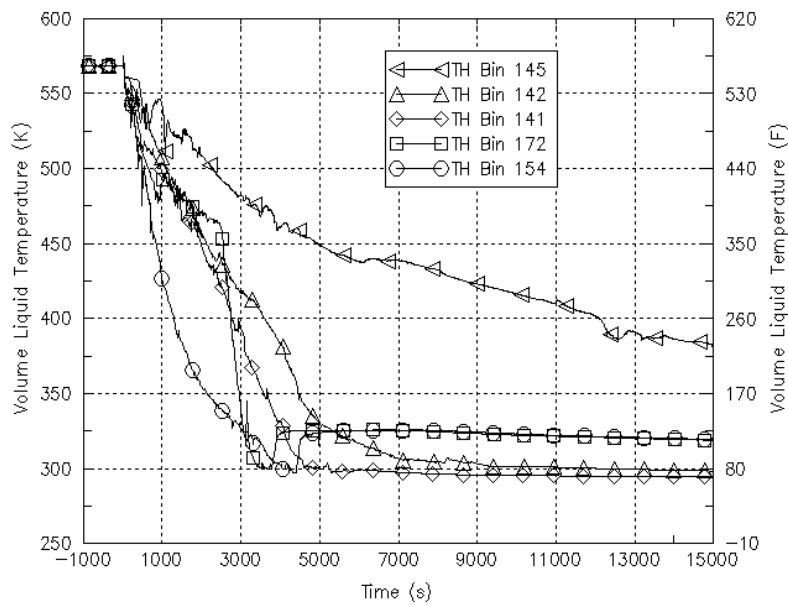


Figure 7-3 The five T_{dc} traces of representative scenarios of LOCAs 1.5-inch to 4-inch

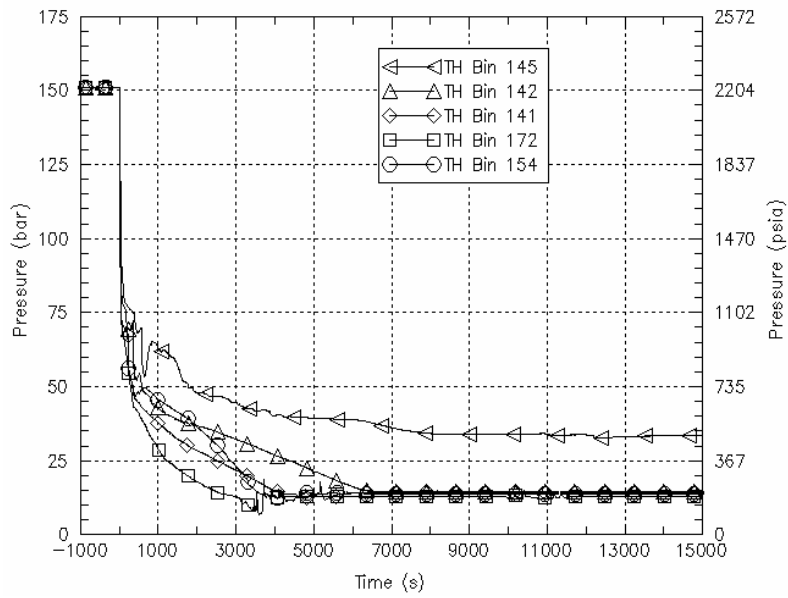


Figure 7-4 The five P traces of representative scenarios of LOCAs 1.5-inch to 4-inch

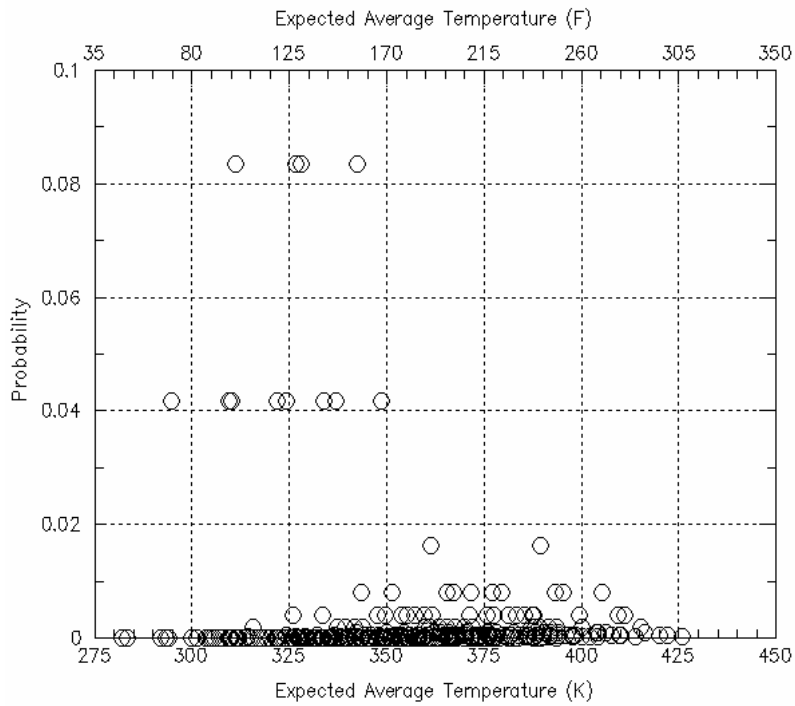


Figure 7-5 Probability distribution of Tsen of LOCAs 4-inch to 8-inch (336 combinations in total)

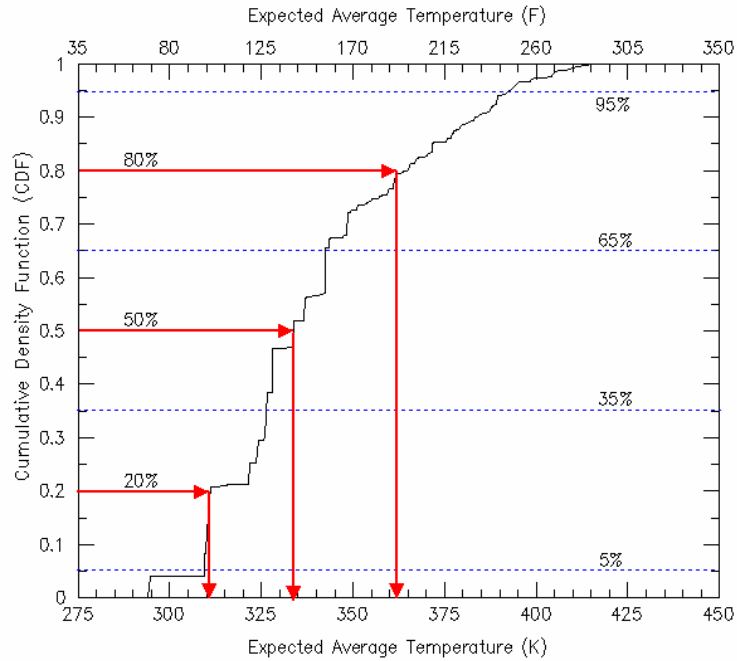


Figure 7-6 Cumulative distribution function and identification of representative scenarios of LOCAs 4-inch to 8-inch

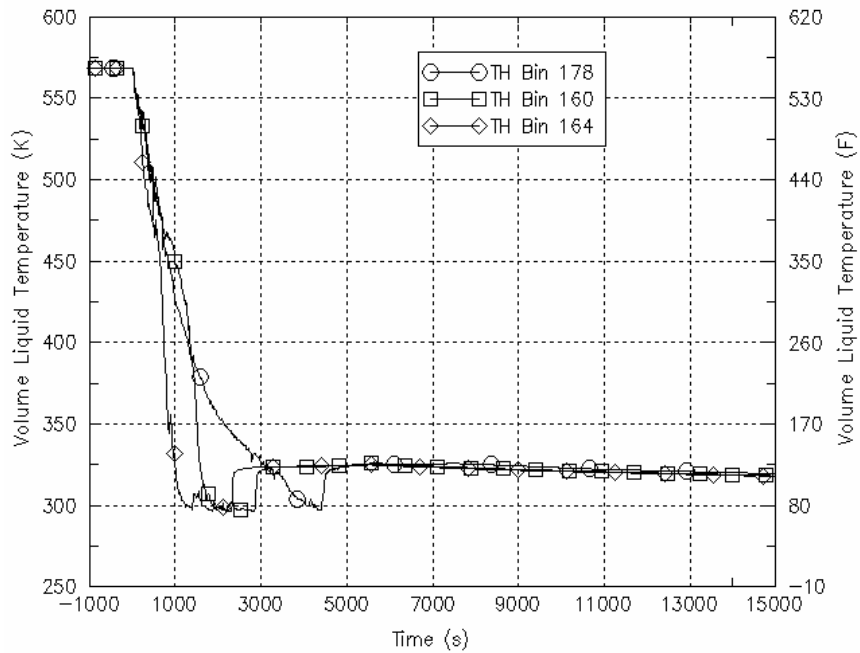


Figure 7-7 The three T_{dc} traces of the representative scenarios of LOCAs 4-inch to 8-inch

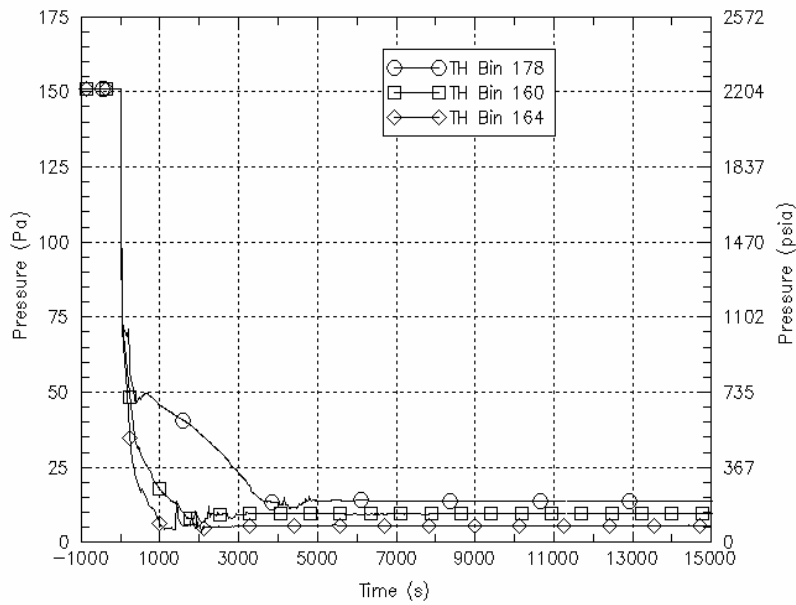


Figure 7-8 The three P traces of the representative scenarios of LOCAs 4-inch to 8-inch

7.1.3 Greater than 8-inch LOCA

T_{dc} uncertainty is very limited for LOCAs greater than 8-inch. Only one representative scenario is selected in this category: 16-inch hot leg break (Table 7-7). The T_{dc} and P time histories are shown in Figure 7-9.

Table 7-7 Boundary conditions of the representative scenario of LOCAs greater than 8-inch

#	Bin #	Probability	Scenario Description
1	156	1.0	16-inch hot leg break

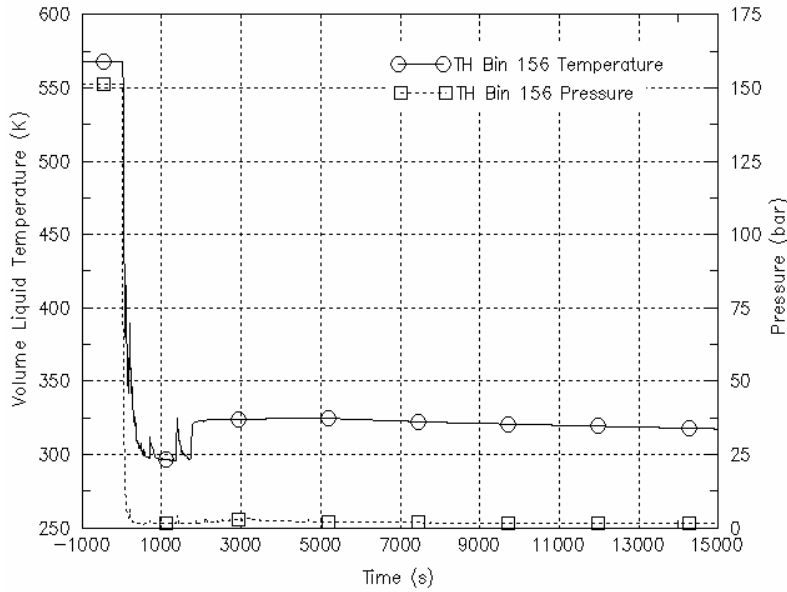


Figure 7-9 $T_{dc}(t)$ and $P(t)$ plots for 16-inch LOCA

7.1.4 Pressurizer SRV Stuck Open Without Valve Reclosure

The total pressurizer SRV stuck open area must be greater than 1.5-inch (8 E-3 m^2), for break flow to exceed HPI flow. The Oconee-1 pressurizer has one 1.1-inch PORV (6.1 E-4 m^2) and two 1.8-inch SRVs (1.8 E-2 m^2). The probability of two valves simultaneously stuck open events is too small to be considered, according to the PRA assessment. The PORV capacity is too small to be PTS concern. Thus, this category includes only the scenario of one SRV stuck open, with opening area >1.5 -inch, with the valve remaining open until the end of the scenario.

The process of identifying representative scenarios for uncertainty evaluation is similar to the LOCA process above. There are some differences in the list of influential factors in this category. First, unlike LOCAs, the break location is specific; the SRV is at the top of pressurizer. Second, the SRV has a unique flow resistance that differs in comparison with the same size LOCA. Third, the PRA model treats decay heat explicitly, so decay heat uncertainty is not considered in the thermal hydraulic uncertainty analysis.

Two break flows representing the lower and upper bounds of valve opening area were analyzed to provide base case values of $T_{sen.ref}$: 1.5-inch and 1.8-inch (8 E-3 m^2 and 1.8 E-2 m^2). The sensitivities obtained from the equivalent size breaks in the LOCA analysis were used (Table 7-2). The key influencing parameters are listed in Table 7-8. Three representative scenarios were identified from the 486 possible combinations, whose scenario descriptions are shown in Tables 7.9 and 7.10 for full power and low decay heat conditions, respectively. The $T_{dc}(t)$ and $P(t)$ plots are shown in Figures 7.10 and 7.11, respectively.

Table 7-8 Influencing parameters for pressurizer SRV stuck open without reclosure

	Break Sizes	
	1.5 inch	1.8 inch
Decay Heat (1)	Explicitly modeled by PRA	Explicitly modeled by PRA
Season (3)	√	√
HPI Flow Rate (3)	√	√
RVVVs State (3)	√	√
Convective Heat Transfer (3)	√	√
Flow Resistance (1)	Insignificant	Insignificant
CFT Pressure (1)	Insignificant	Insignificant
Break Flow (3)	√	√

Numbers in parentheses are the number of representative values of the parameter

Table 7-9 Representative scenarios for pressurizer SRV stuck open and remaining open and their probabilities (full power)

#	Bin #	Probability	Scenario Description
1	148	0.35	SRV open area = 1.5", h = 130%
2	147	0.30	Summer
3	146	0.35	SRV open area = 70%, Summer, RVVVs Closed

Table 7-10 Representative scenarios for pressurizer SRV stuck open and remaining open and their probabilities (hot zero power)

#	Bin #	Probability	Scenario Description
1	171	0.35	SRV open area = 1.5", h = 130%
2	170	0.30	Summer, low decay heat
3	169	0.35	SRV open area = 70%, Summer, RVVVs Closed

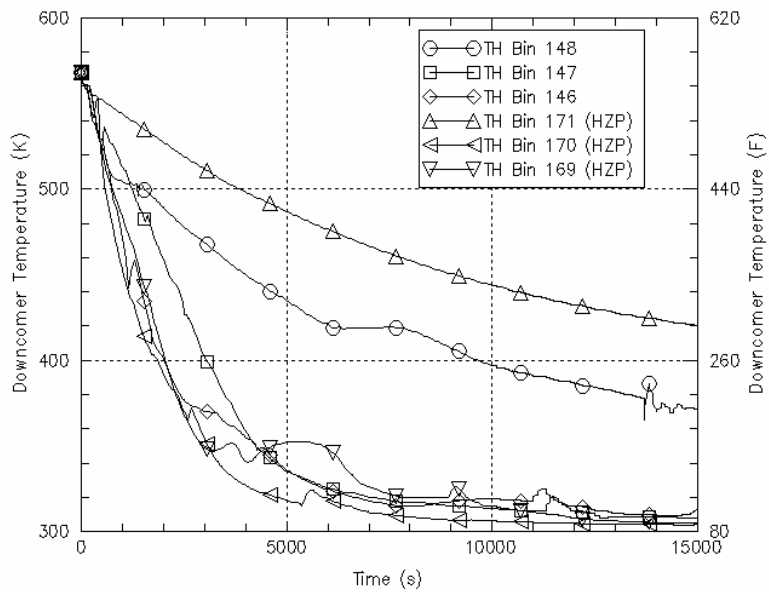


Figure 7-10 $T_{dc}(t)$ for the six representative scenarios for pressurizer SRV stuck open and remaining open

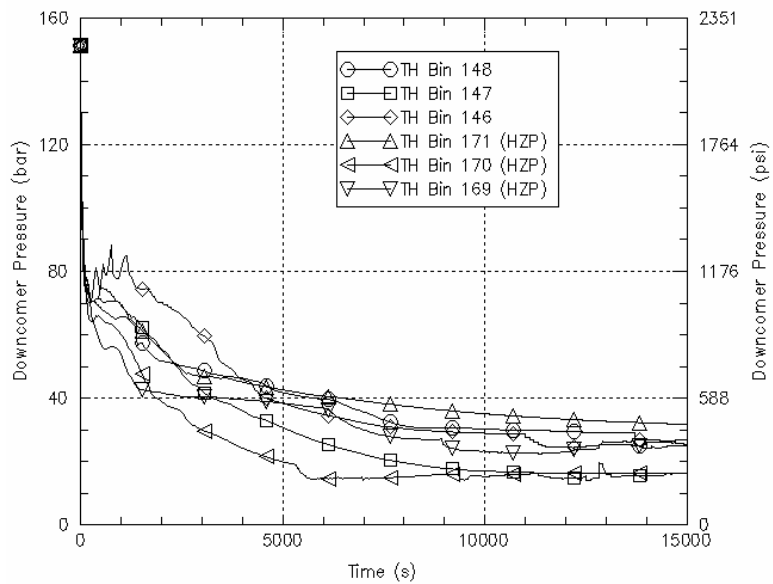


Figure 7-11 $P(t)$ for the six representative scenarios for pressurizer SRV stuck open and remaining open

7.1.5 Pressurizer SRV Stuck Open and Later Reclosed

Reclosing a stuck open SRV has two important effects. First, it removes the dominant heat sink. When that happens the decline in T_{dc} will slow or even reverse. Second, although the break is closed, HPI is still on. Operator action is required to throttle HPI to prevent RCS repressurization. The repressurization has a significant contribution to PTS risk. Unlike previous event categories analyzing only T_{dc} uncertainty, this category must include both T_{dc} and P uncertainties. P uncertainty depends mainly on the time at which HPI is throttled. The PRA group specified three times for HPI throttling: 1 minute, 10 minutes, and never, with respective probabilities of 97%, 2%, and 1%.

Beside the T_{dc} uncertainty analyzed in Section 7.1, the timing of pressurizer SRV reclosure is an additional factor contributing to T_{dc} uncertainty. In the PRA model, two times were used: 50 minutes and 100 minutes. Each was assigned a probability of 0.5. The effects of the other influencing factors were represented by the three representative scenarios (20th, 50th, and 80th percentiles in Section 7.1.4). Combined with the two reclosure times, there are six (2 × 3) combinations in total to represent the downcomer temperature uncertainty.

Since SRV reclosure changes the course of T_{dc} , the T_{sen} in Table 7-2 are not appropriate for the analysis. Instead the lowest T_{dc} is a more appropriate indication. Table 7-11 lists the six combinations and their differences in terms of their lowest T_{dc} . It shows that the SRV reclosure timing dominates T_{dc} uncertainty. In order to reduce the number of representative scenarios, two out of six variations were selected to represent T_{dc} uncertainty: SRV reclosed at 50 min and 100 min, with all other factors at their nominal values.

The two representative scenarios for T_{dc} need to be combined with three representative scenarios for P. Since the PRA model differentiates high decay heat from low decay heat, there are six representative scenarios each for high decay heat (Table 7-12) and low decay heat (Table 7-13). Figures 7.12 and 7.13 are plots of $T_{dc}(t)$ and P(t) for the six high decay heat scenarios, while Figures 7.14 and 7.15 are similar plots for low decay heat.

Table 7-11 The six combinations for T_{dc} uncertainty representation of pressurizer SRV stuck open and reclosed scenarios

#	$\Delta T_{min}(K)$	Description
1	-8	20 th percentile + SRV reclosed at 100 min
2	0	50 th percentile + SRV reclosed at 100 min
3	6	80 th percentile + SRV reclosed at 100 min
4	76	20 th percentile + SRV reclosed at 50 min
5	83	50 th percentile + SRV reclosed at 50 min
6	90	80 th percentile + SRV reclosed at 50 min

Table 7-12 Representative scenarios and their probabilities for pressurizer SRV stuck open and later reclosed (full power)

#	Bin #	Probability	Scenario Description
1	112	0.485	SRV reclosed @ 100 min; HPI throttled 1 min after permitted
2	113	0.01	SRV reclosed @ 100 min; HPI throttled 10 min after permitted
3	109	0.005	SRV reclosed @ 100 min; HPI not throttled
4	114	0.485	SRV reclosed @ 50 min; HPI throttled 1 min after it permitted
5	115	0.01	SRV reclosed @ 50 min; HPI throttle 10 min after permitted
6	149	0.005	SRV reclosed @ 50 min; HPI not throttled

Table 7-13 Representative scenarios and their probabilities for pressurizer SRV stuck open and later reclosed (hot zero power)

#	Bin #	Probability	Scenario Description
1	121	0.485	SRV reclosed @ 100 min; HPI throttled 1 min after permitted
2	122	0.01	SRV reclosed @ 100 min; HPI throttled 10 min after permitted
3	165	0.005	SRV reclosed @ 100 min; HPI not throttled
4	123	0.485	SRV reclosed @ 50 min; HPI throttled 1 min after permitted
5	124	0.01	SRV reclosed @ 50 min; HPI throttled 10 min after permitted
6	168	0.005	SRV reclosed @ 50 min; HPI not throttled

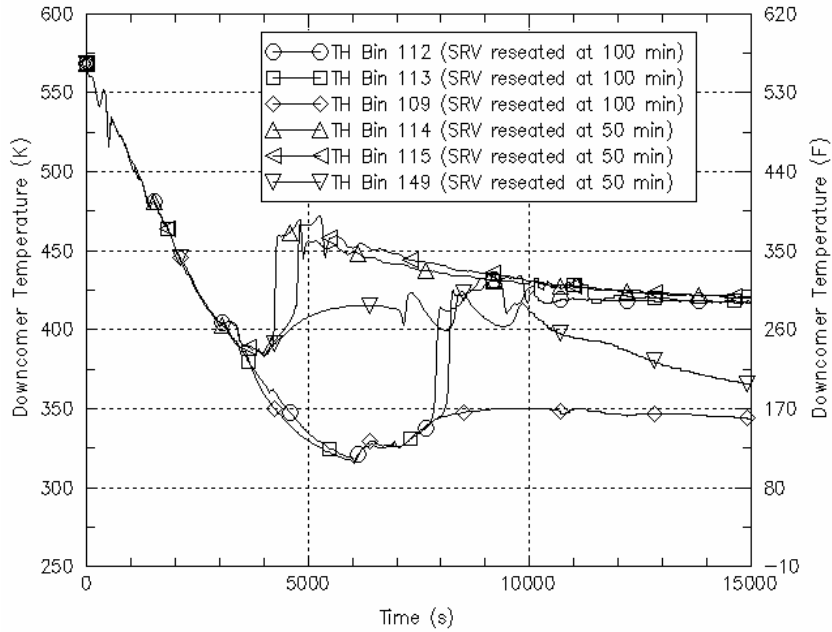


Figure 7-12 $T_{dc}(t)$ for representative scenarios for pressurizer SRV stuck open and later reclosed (full power)

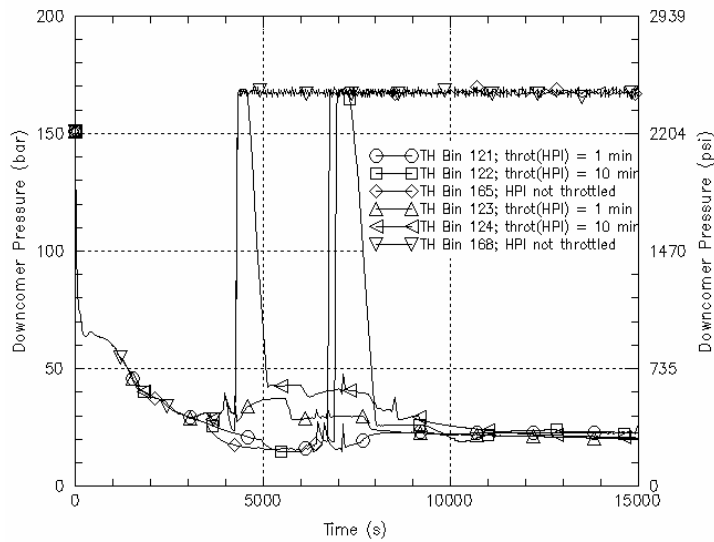


Figure 7-13 $P(t)$ for representative scenarios for pressurizer SRV stuck open and later reclosed (full power)

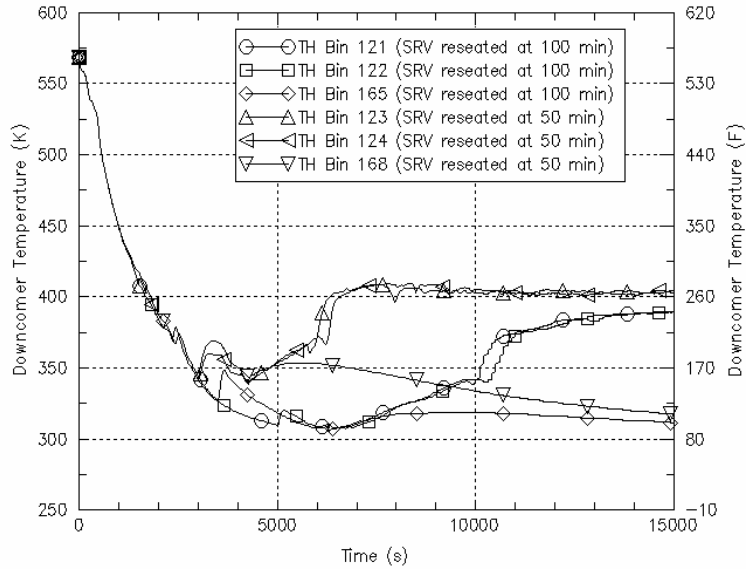


Figure 7-14 $T_{dc}(t)$ for pressurizer SRV stuck open and later reclosed (hot zero power)

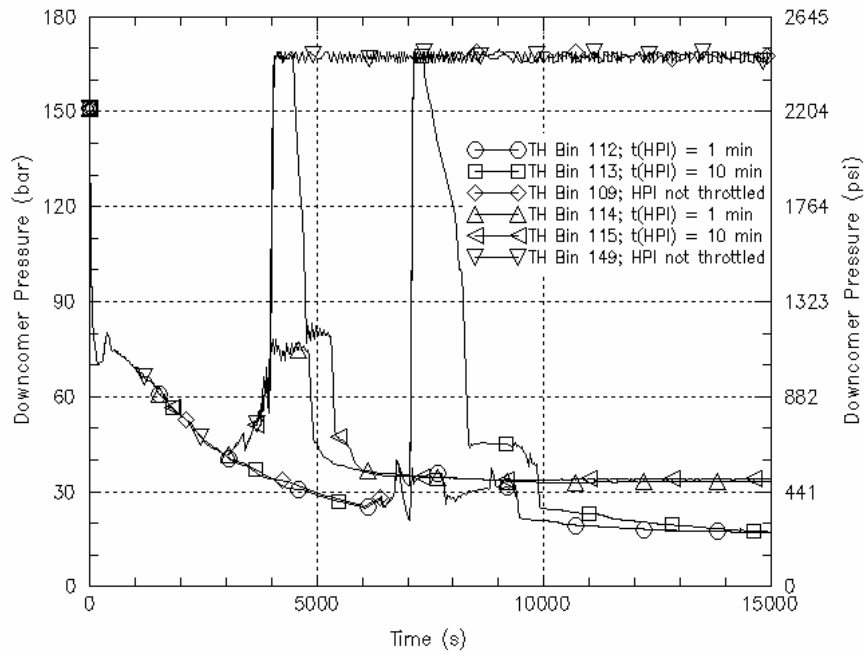


Figure 7-15 $P(t)$ for pressurizer SRV stuck open and later reclosed (hot zero power)

7.2 Beaver Valley Representative Scenarios for Thermal Hydraulic Uncertainty

The same process utilized to identify Oconee-1 uncertainty representative scenarios was applied to identify the representative scenarios for Beaver Valley. Table 7-14 shows the values of T_{sen} calculated by RELAP5 for Beaver Valley. The probability of each representative value is listed in Table 7-1. The classification of events is identical to the Oconee-1 analysis.

Table 7-14 T_{sen} for Beaver Valley based on NRSA

	Break Size (inches in diameter)							
	1.4"	2"	2.8"	4"	5.7"	8"	SRV 2.1"	2 SRVs 3"
Nominal	459	377	336	319	313	300	393	349
Winter*	457	366	333	318	316	297	388.2 ^{&}	346 ^{&}
Summer*	460	370	344	331	318	303	393 ^{&}	355 ^{&}
110% HPI	--	362	334	--	--	--	379 ⁺	345 ^{&}
90% HPI	466	373	341	--	--	--	396 ^{&}	354 ^{&}
HPI 100% Failed	521	496	432	--	--	--	--	--
Low Decay Heat 0.7%	360	348	325	312	304	299	351 ^{&}	334 ^{&}
Low Decay Heat 0.2%	353	337	320	309	302	298	341 ^{&}	322 ^{&}
130% h	462	374	342	324	--	300	396 ^{&}	355 ^{&}
70% h	455	362	331	321	--	--	385 ^{&}	345 ^{&}
130% Break Flow	--	329	325	307	300	301	--	327 ^{&}
70% Break Flow	--	359	359	323	306	306	--	359 ^{&}
Cold Leg LOCA	455	453	415	369	347	340	--	--

*Summer: $T_{HPI} = 55F$ $T_{ACC} = 105F$ $T_{LPI} = 55F$

*Spring/fall: $T_{HPI} = 50F$ $T_{ACC} = 90F$ $T_{LPI} = 50F$

*Winter: $T_{HPI} = 45F$ $T_{ACC} = 75F$ $T_{LPI} = 45F$

⁺ Extrapolated data

[&] Interpolated data

7.2.1 1.4-to 4-inch LOCA

Table 7-15 shows the probabilities for different representative break sizes used in the analysis. Table 7-16 lists the parameters that are included in the analysis. There are 1296 combinations in total for the four representative break sizes. The PDF and CDF distributions are shown in Figures 7.16 and 7.17. Five representative scenarios are identified as shown in Figure 7-17. The scenario descriptions and scenario probabilities are shown in Table 7-17. $T_{dc}(t)$ and $P(t)$ are shown in Figures 7.18 and 7.19, respectively.

Table 7-15 Representative values and probabilities for LOCAs 1.4-inch to 4-inch

Factors	Value 1	Value 2	Value 3	Value 4
	Probability	Probability	Probability	Probability
Break Size	1.4"	2.0"	2.8"	4.0"
	0.15	0.25	0.30	0.30

Table 7-16 Influencing parameters for each break size from 1.4 inch to 4 inch

Parameter	Break Size (inches in diameter)			
	1.4"	2.0"	2.8"	4"
Break Location (2)	√	√	√	√
Decay Heat (3)	√	√	√	√
Season (3)	√	√	√	√
HPI Flow Rate (3)	√	√	√	Insignificant
Convective Heat Transfer (3)	√	√	√	√
Break flow (3)	Insignificant	√	√	√

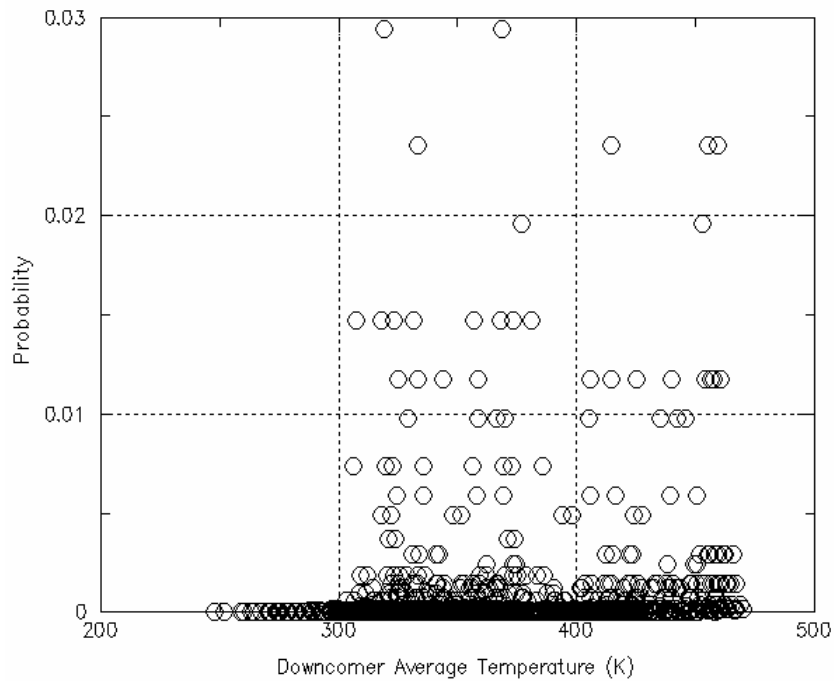


Figure 7-16 Probability distribution of representative scenarios of LOCAs 1.4-inch to 4-inch

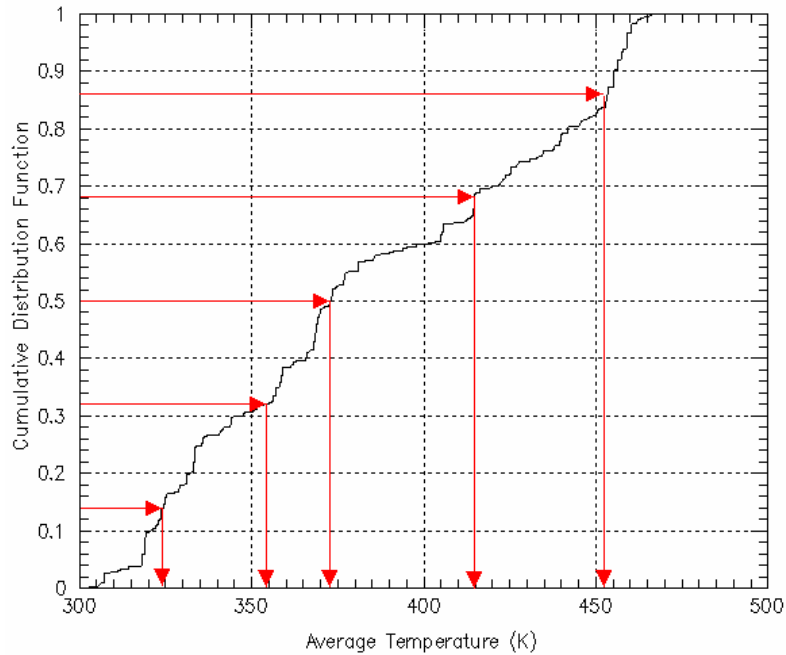


Figure 7-17 Cumulative distribution function and the five representative scenarios of LOCA 1.4-inch to 4-inch

Table 7-17 Boundary conditions of the five uncertainty representative scenarios for LOCA 1.4-inch to 4-inch

#	Bin #	Probability	Scenario Description
1	2	0.23	1.4" cold leg LOCA, winter
2	115	0.18	2.8" cold leg LOCA
3	3	0.18	2" surge line LOCA, 90% HPI flow
4	114	0.18	2.8" surge line LOCA, summer; 130% h
5	56	0.23	4" surge line LOCA, 0.7% decay heat

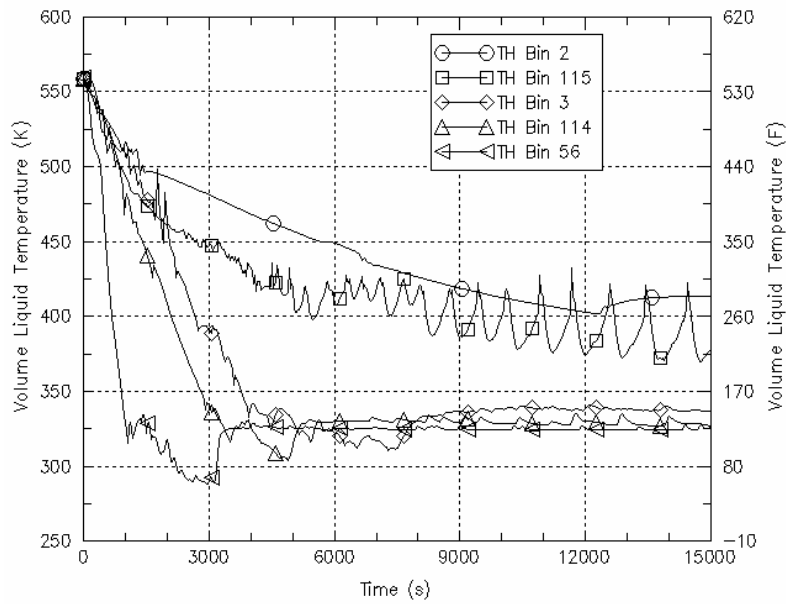


Figure 7-18 $T_{dc}(t)$ of the five representatives scenarios for LOCAs 1.4-inch to 4-inch .

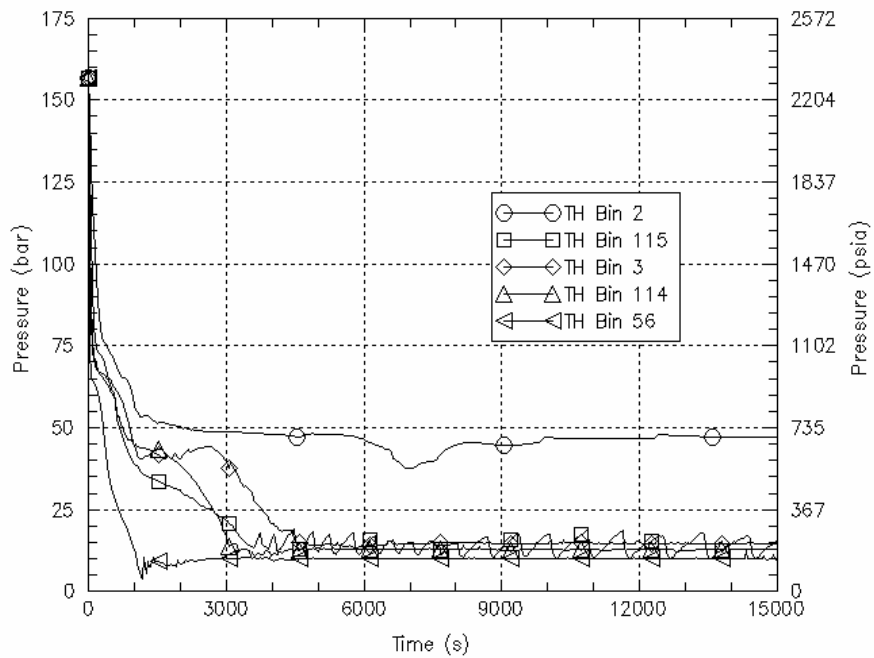


Figure 7-19 $P(t)$ of the five thermal hydraulic uncertainty representatives for LOCAs 1.4-inch to 4-inch

7.2.2 4-inch to 8-inch LOCA

Table 7-18 shows the probabilities for different representative break sizes of the category of LOCA with break sizes between 4-inch and 8-inch. Table 7-19 shows the parameters used in the calculations. The total number of combinations is 270. Figures 7.20 and 7.21 are the PDF and CDF diagrams. The descriptions and probabilities of the three representative scenarios are shown in Table 7-20. $T_{dc}(t)$ and $P(t)$ are shown in Figures 7.22 and 7.23, respectively.

Table 7-18 Representative values and probability of break sizes for LOCAs 4-inch to 8-inch

Factors	1	2	3
	Probability	Probability	Probability
Break Size	4"	5.7"	8"
	0.35	0.30	0.35

Table 7-19 Influencing parameters for LOCAs 4-inch to 8-inch

Parameter	Break Size (inches in diameter)		
	4"	5.7"	8"
Break Location (2)	√	√	√
Decay Heat (3)	√	√	√
Season (3)	√	√	√
HPI Flow Rate (3)	Insignificant	Insignificant	Insignificant
Convective Heat Transfer (3)	√	Insignificant	Insignificant
Break Flow (3)	√	√	√

Numbers in parentheses are the number of representative values of the parameter

Table 7-20 Boundary conditions of the three representative scenarios of LOCAs 4-inch to 8-inch

ID	Bin #	Probability	Scenario Description
1	117	0.35	5.7" cold leg LOCA, summer
2	116	0.30	5.7" cold leg LOCA; 70% break flow
3	7	0.35	8" surge line LOCA; 70% break flow

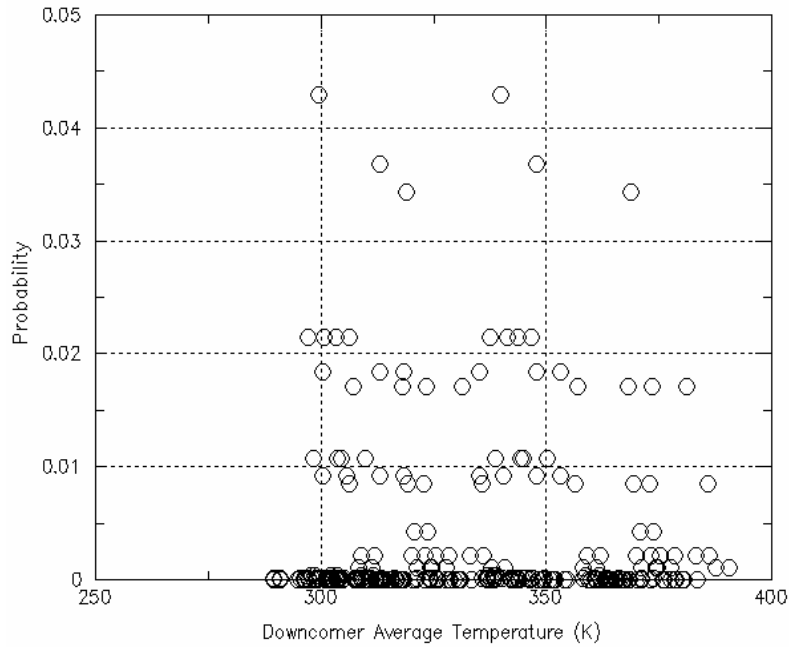


Figure 7-20 Probability distribution of the representative scenarios of LOCAs 4-inch to 8-inch

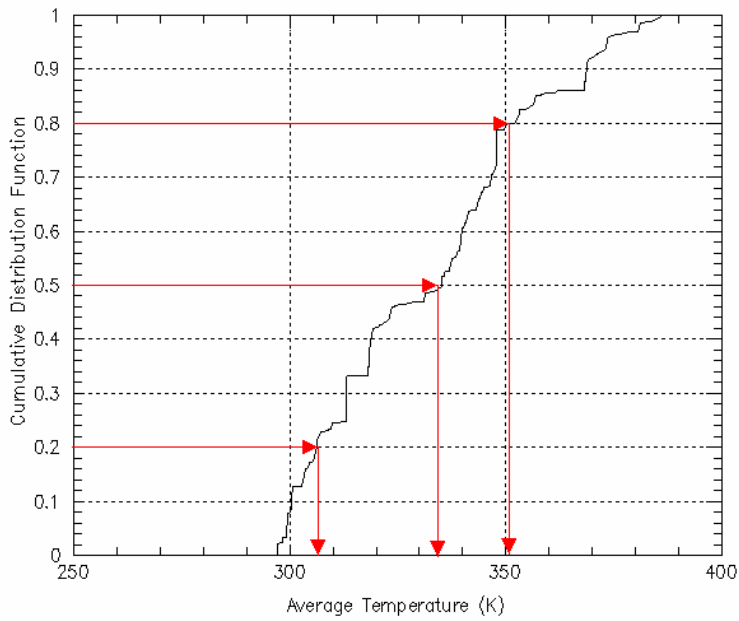


Figure 7-21 Cumulative distribution function and the three representative scenarios for LOCAs 4-inch to 8-inch

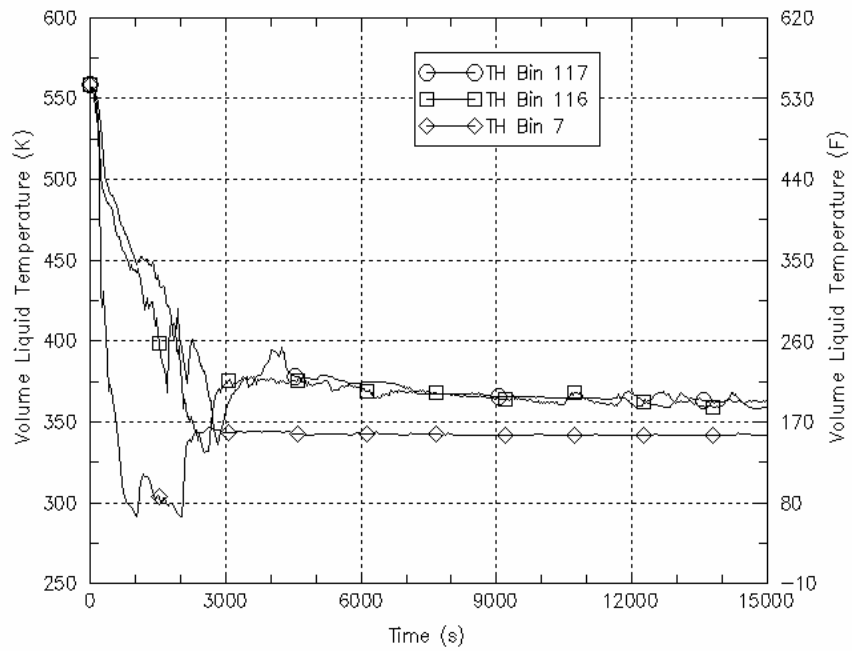


Figure 7-22 The three $T_{dc}(t)$ traces of the representative scenarios for LOCAs 4-inch to 8-inch

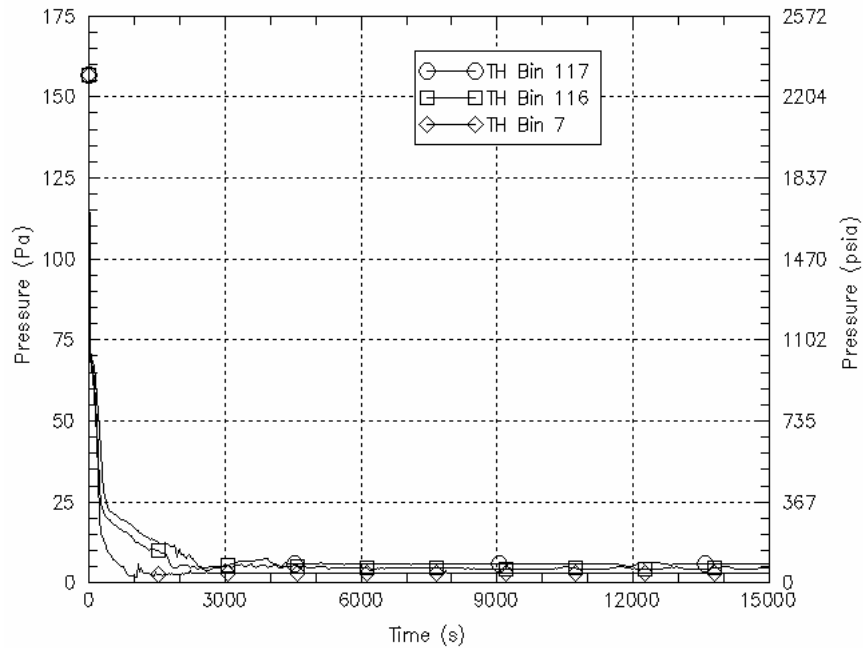


Figure 7-23 The three $P(t)$ traces of the representative scenarios for LOCAs 4-inch to 8-inch

7.2.3 Greater Than 8-inch LOCA

One representative scenario is used: 16-inch (1.3E-1 m²) hot leg LOCA. Table 7-21 is the event description. The T_{dc}(t) and P(t) plots are shown in Figure 7-24.

Table 7-21 Boundary conditions of representative scenario for LOCAs greater than 8-inch

#	Bin #	Probability	Scenario Description
1	9	1.0	16" hot leg LOCA

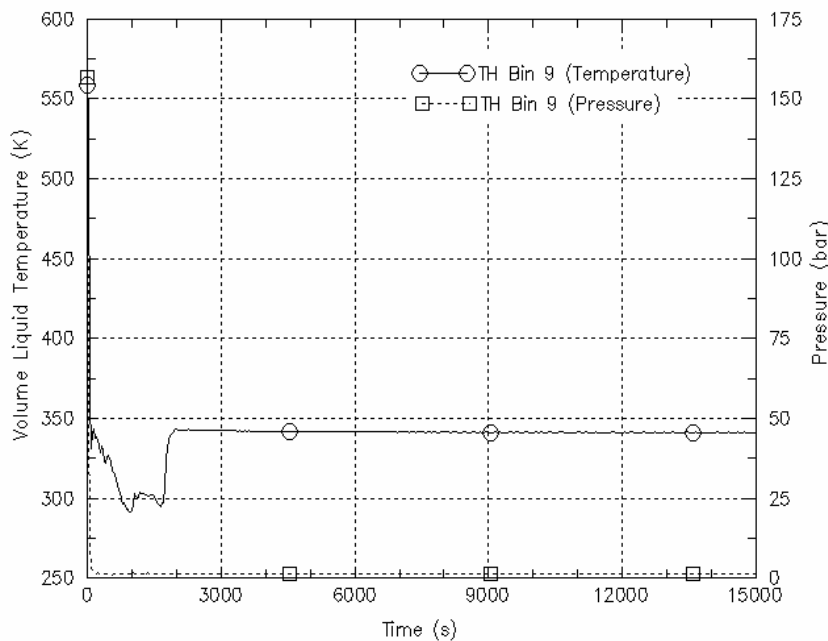


Figure 7-24 T_{dc}(t) and P(t) plots of the 16-inch LOCA

7.2.4 Pressurizer Valve(s) Stuck Open and Remaining Open

For Beaver Valley, in contrast to Oconee-1, the PRA model indicated that the probabilities of more than one SRV stuck open scenarios cannot be neglected. The analysis becomes more complex when there are two types of valves, pressurizer PORV and pressurizer SRV, and the two have different flow capacities. In addition, there are scenarios in which no valves reclosed, one valve reclosed, and two valves reclosed, that dramatically increase analysis complexity compared with Oconee-1. The PRA model distinguished between scenarios with high decay heat and low decay heat, however, the difference between the two 0.7% and 0.2% low decay heat situations was not explicitly treated. Thus, this uncertainty analysis separated high decay heat from low decay heat.

Full Power (high decay heat)

The PRA model considered three valve opening combinations:

- 1) One SRV stuck open
- 2) Two SRVs stuck open
- 3) PORVs stuck open

The scenarios involving two valves stuck open include: neither valve reclosed; $\frac{1}{2}$ valves reclosed; and both valves reclosed. The $T_{dc}(t)$ for neither valve reclosed and $\frac{1}{2}$ valves reclosed are compared in Figure 7-25, which shows little difference between the two. Therefore, these two scenarios are grouped together based on the T_{dc} similarity shown in Figure 7-25.

For scenarios of two valves stuck open and remaining open, the valve opening area is stochastic and should be continuously distributed. The total area of two simultaneously stuck open valves could be smaller than one fully opened valve.

The scenarios involving one valve stuck open and reclosed along with both valves stuck open and reclosed are discussed in Section 7.2.5,

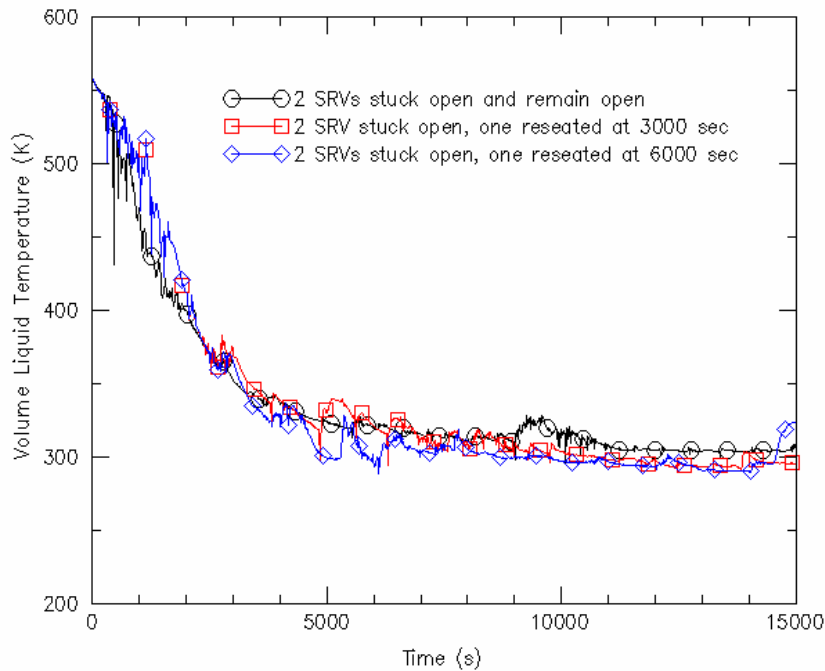


Figure 7-25 Tdc trends of three variations of the two SRVs simultaneously stuck open bin.
Note: The three scenarios have one valve remaining stuck open until the end of the scenario. The difference is in the second valve either reclosed at 50 minutes, reclosed at 100 minutes, or never reclosed.

The base frequencies of one SRV, two SRVs, and two PORVs stuck open are 1.6 E-3, 1.6 E-5, and 3.3 E-6, respectively. The relevant frequencies of the variations of the SRV stuck open scenarios are (according to the PRA information):

- 1) One SRV stuck open and stays open: $1.6 \text{ E-3} \times 0.25 = 4.0 \text{ E-4/year}$
- 2) Two SRVs stuck open and stay open: $1.6 \text{ E-5} \times 6.25 \text{ E-2} = 1.0 \text{ E-6/year}$
- 3) Two SRVs stuck open with one reclosed: $1.6 \text{ E-5} \times 3.75 \text{ E-1} = 6.0 \text{ E-6/year}$
- 4) Two PORVs stuck open and stay open: $3.3 \text{ E-6} \times 0.5 = 1.65 \text{ E-6/year}$

**The probability of the valve being reclosed is 75%

The uncertainty analysis of above four scenarios is similar to the LOCA analysis. The probabilities of one SRV stuck open, two SRVs stuck open, and two PORVs fully open are 97.88%: 1.71%: 0.41%. Since the one SRV stuck open scenario dominates the probability, for simplicity, the break size is represented by two values: one SRV fully stuck open and two SRVs fully stuck open with probability of 97.9% and 2.1% as shown in Table 7-22. The results obtained from such a simplification are conservative.

Table 7-22 Representative values and probabilities for SRV stuck open without reclosure

#	Break Size	Probability
1	2.2 E-3 m ² , one SRV fully open	0.979
2	4.6 E-3 m ² , two SRVs fully open	0.021

Table 7-23 lists the influencing parameters for uncertainty analysis. Applying the probabilities in Table 7-1, the PDF and CDF plots are shown in Figures 7.26 and 7.27. Figure 7-26 shows that there is a probability gap between one and two valve stuck open scenarios. One valve stuck open scenarios share about a probability of 98%. The PDF is used to identify the representative scenarios. A representative scenario of two valves stuck open, even with relatively low probability, is specified as a representative scenario as shown in Figure 7-27. Table 7-24 shows the probabilities and descriptions of the two representative scenarios.

Table 7-23 Influencing parameters for pressurizer SRV stuck open (full power)

Key Parameters for each break size	1 SRV Fully Open	2 SRVs Fully Open
Season (3)	√	√
HPI Flow Rate (3)	√	√
Convective Heat Transfer Rate (3)	√	√
Break flow (3)	--	√

Numbers in parentheses are number of representative values of the parameter

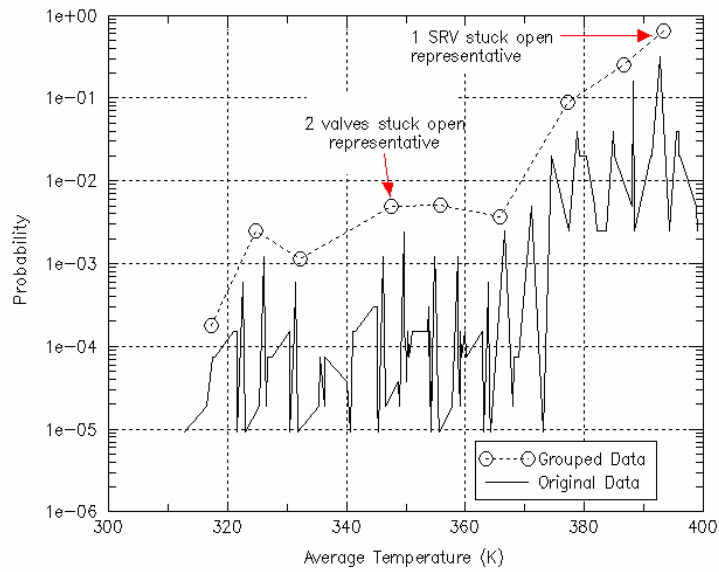


Figure 7-26 Probability distribution of representative scenarios of SRV stuck open and not reclosed (full power)

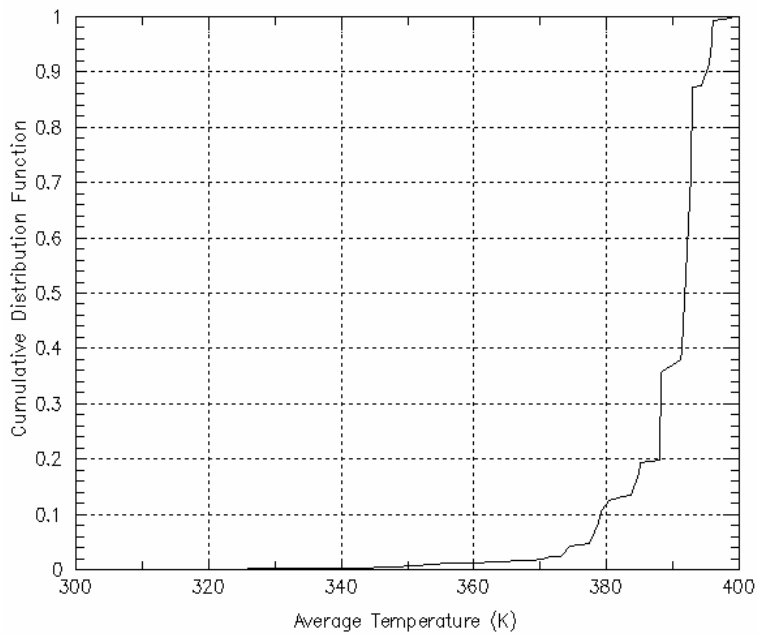


Figure 7-27 Cumulative distribution function of SRV stuck open and not reclosed (full power)

Table 7-24 Boundary conditions of the three representative scenarios for one pressurizer SRV stuck open without reclosure (full power)

#	Description	Distributed Probability
U1	1 PRZ SRV Stuck Open	97.9%
U2	2 PRZ SRV Stuck Open	2.1%

Hot Zero Power (low decay heat)

For the scenarios of SRVs stuck open with low decay heat, the thermal hydraulic uncertainty assessment is similar to that for high decay heat. Two decay heat curves were used for Beaver Valley: 0.7% and 0.2% of full power. The probability of each is 0.5. Table 7-25 shows the representative values and probabilities of break size and decay heat. Figures 7.28 and 7.29 are the PDF and CDF diagrams. Two representative scenarios were identified and shown in Table 7-26. Factors of 0.564 ($= 1 - 0.0107/0.0245$) and 0.782 ($= 1 - 0.0107/0.0490$) need to be multiplied for one and two SRVs stuck open scenarios respectively, since we are only interested in the stuck open area greater than $1E-3 \text{ m}^2$ (1.5 inches in diameter) instead of the full spectrum of valve open area.

Table 7-25 Representative values and probabilities of influencing parameters for SRV stuck open without reclosure (hot zero power)

Parameter	1	2
	Probability	Probability
Break Size	$2.2 \text{ E-}3 \text{ m}^2$	$4.6 \text{ E-}3 \text{ m}^2$
	One SRV	Two SRVs
Decay heat	0.979	0.021
	0.7%	0.2%
	0.5	0.5

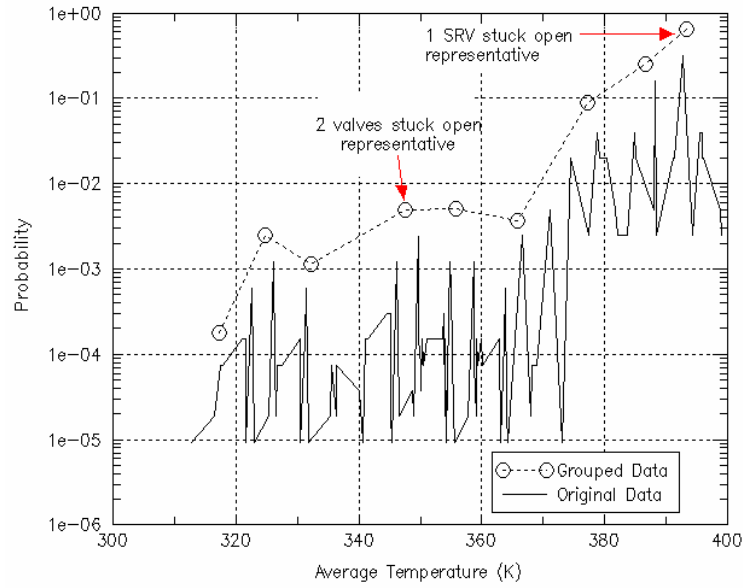


Figure 7-28 Probability distribution of representative scenarios of SRVs stuck open and not reclosed (hot zero power)

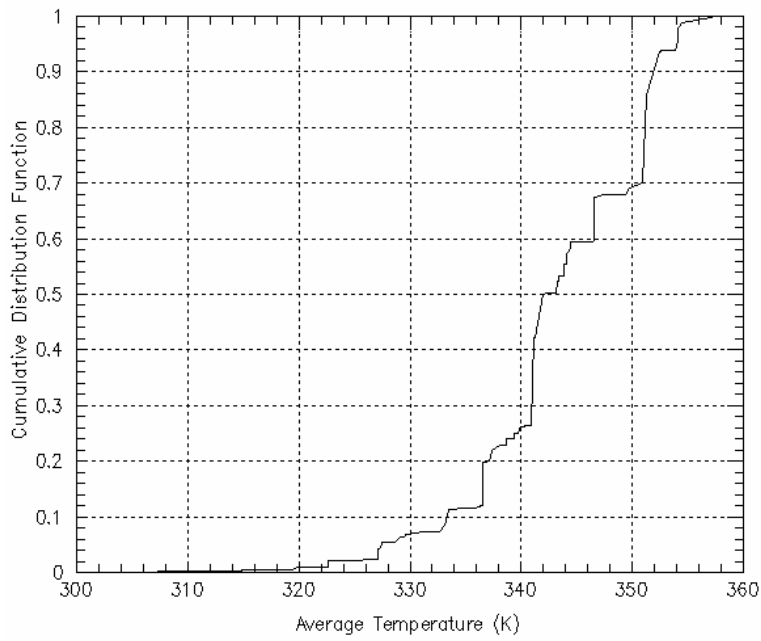


Figure 7-29 Cumulative distribution function for SRVs stuck open and not reclosed (hot zero power)

Table 7-26 Boundary conditions for the three representative scenarios for SRV stuck open without reclosure (hot zero power)

Bin #	Description	Distributed Probability
U3	1 SRV Stuck Open (fully open; 0.2% decay heat	97.9%
U4	2 SRVs Stuck Open (fully open); 0.2% decay heat	2.1%

The above analysis mixes scenarios of one valve and two valves stuck open, however, in the PRA event tree the one valve stuck open and two valves stuck open scenarios are explicitly modeled. The thermal hydraulic uncertainty analysis is based on the total valve open area, whereas the PRA model is based on the number of valves stuck open. Two partially open valves have a total area that is not necessarily larger than a single fully open valve. To assign the correct probability to the two representative scenarios in Table 7-27, the probabilities in the PRA model need to be adjusted.

A uniform distribution is assumed for valve opening area. For one valve stuck open, Figure 7-30 shows the probability distribution of valve opening area from zero to its maximum size ($2.2 \text{ E-}3 \text{ m}^2$). The area **A** $< 1\text{E-}3 \text{ m}^2$ is not of interest to the PTS, since in this range HPI flow can compensate for valve flow. The area **B** remains, ranging between $1\text{E-}3 \text{ m}^2$ and the maximum valve open area. Thus, a factor of $0.564 \left(\frac{B}{A+B} \right)$ is obtained to multiply the PRA probability of one SRV stuck open without reclosure.

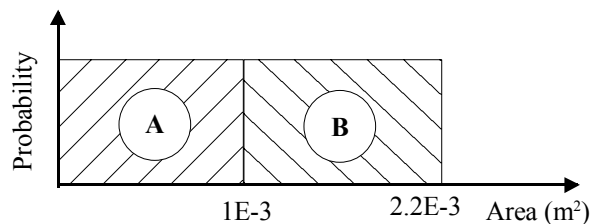


Figure 7-30 Uniform probability distribution of a valve stuck open area. Region B is relevant to PTS while A is not.

For scenarios of two stuck open valves, the effective area ranges from zero to two valves fully open. The probability distribution is a triangle, as shown in Figure 7-31, assuming the probability of a valve's opening area is uniformly distributed. In Figure 7-31, the region **C** is not of interest due to its small open area ($< 1\text{E-}3 \text{ m}^2$). The scenario of one SRV fully open represents region **D**. The scenario of two valves fully open represents region **E**. A factor of 0.5

$\left(\frac{E}{C+D+E} \right)$ is applied to the PRA frequency for two valves stuck open, to reflect the fraction of the region, **E**. This adjusted frequency is applied to the PRA probability of two valves simultaneously stuck open (U4 in Table 7-26). Region **D** has a probability of $0.4 \left(\frac{D}{C+D+E} \right)$, and is represented by one valve stuck open (U3 in Table 7-26). Table 7-27 shows the equations for adjusting the PRA probabilities to be consistent with thermal hydraulic uncertainty definition.

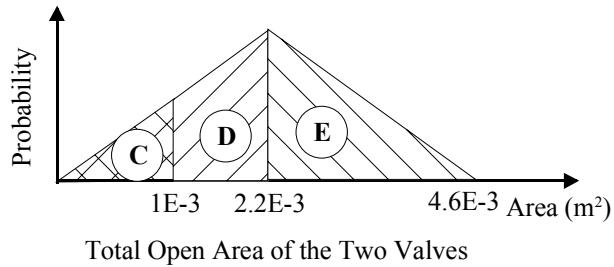


Figure 7-31 Probability distribution of the total open area of two valves stuck open

Note: Region C is not of PTS concern. Region D is represented by one SRV fully open. Region E is represented by two SRVs fully open.

Table 7-27 The two representative scenarios and their probabilities for SRVs stuck open and remaining open

Description	Probability
1 SRV fully stuck open	$0.564 \times \text{Probability (1 SRV SO \& remains open)}$ $+ 0.4 \times \text{Probability (2 SRVs SO \& at least one valve remains open)}$
2 SRVs fully stuck open	$0.5 \times \text{Probability (2 SRVs SO \& at least one valve remains open)}$

7.2.5 One and Two Pressurizer SRVs Stuck Open and Reclosed

This category includes the assumption that two valves stuck open and reclosed simultaneously. As discussed above, the SRV reclosure scenarios must include two additional key parameters: time of reclosure and time of HPI control. Unlike Oconee-1, HPI does not have flow control valves; HPI pumps are either on or off, though they can be stopped individually. Two valve reclosure times were specified in the PRA model: 50 minutes and 100 minutes. Each was given a probability of 0.5. Figures 7.32 and 7.33 show that both the valve reclosure time and the number of stuck open valves are important. Thus, four representative scenarios are specified:

- 1) 1 SRV stuck open and reclosed at 50 minutes
- 2) 1 SRV stuck open and reclosed at 100 minutes
- 3) 2 SRVs stuck open and reclosed at 50 minutes
- 4) 2 SRVs stuck open and reclosed at 100 minutes

The uncertainty in pressure is dominated by HPI control. Three representative timings were specified in the PRA model, along with probabilities,

- 1) HPI shutoff within 1 minute of permitted: 0.906
- 2) HPI shutoff between 1 minute and 10 minutes of permitted: 0.092
- 3) HPI never shutoff: 1E-3

Combining T_{dc} uncertainty and P uncertainty, Tables 7.28 and 7.29 are the representative scenarios and probabilities for one valve and two valves stuck open and reclosed, respectively. For low decay heat, Table 7-30 shows the influencing parameters values and probabilities. The representative scenarios for one and two valves stuck open and reclosed are listed in Tables 7.31 and 7.32, respectively. Tables 7.33 to 7.37 list the representative scenarios and estimated frequencies for all SRV stuck open scenarios.

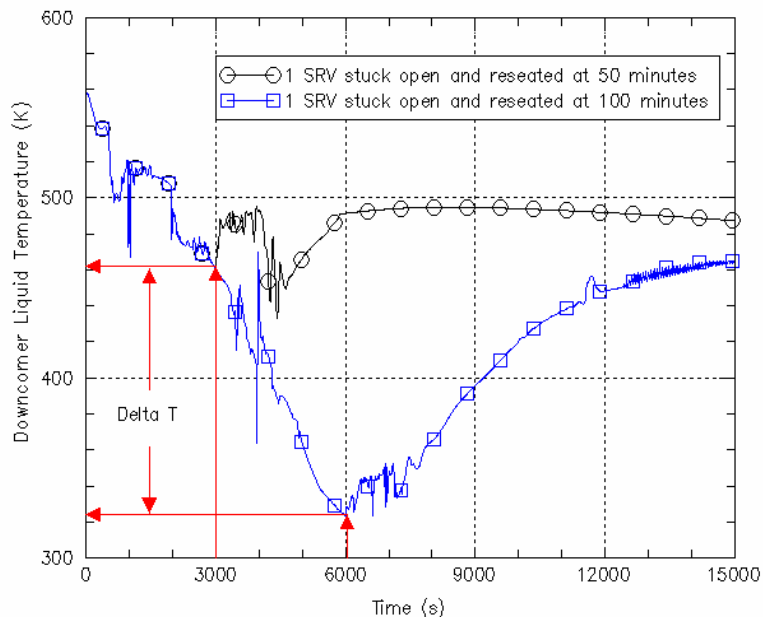


Figure 7-32 $T_{dc}(t)$ of one SRV stuck open and reclosed at 50 and 100 minutes

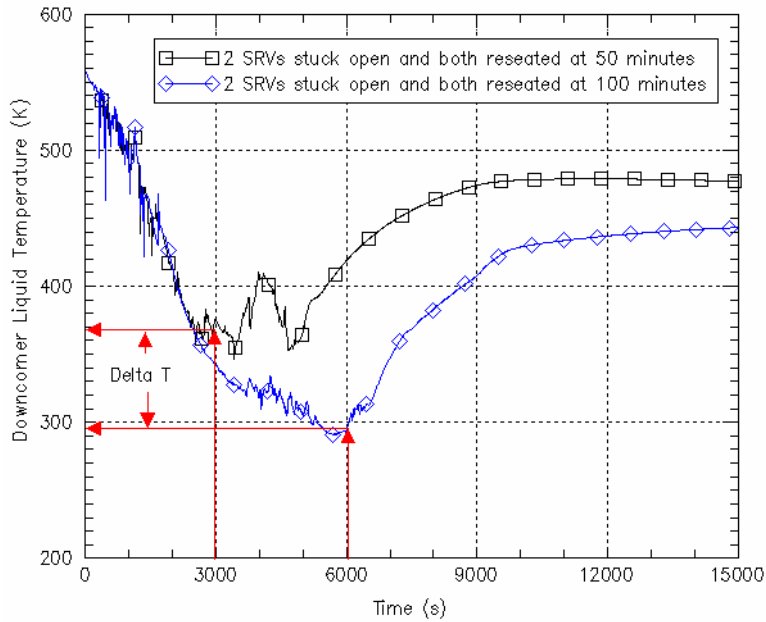


Figure 7-33 $T_{dc}(t)$ of two SRVs stuck open and reclosed at 50 and 100 minutes

Table 7-28 Conditional probabilities of the representative scenarios of one SRV stuck open and reclosed (high decay heat)

#	Reclose time (min) [Probability] (A)	HPI shutoff time (min) [Probability] (B)	Decay Heat (C)	Distributed Probability (A×B×C)	Descriptions
U9	50 [0.5]	1 [0.906]	Nominal [1.0]	4.53E-01	SRV reclose at 50 min; HPI shutoff at 1 min
U10		10 [0.092]		4.60E-02	SRV reclose at 50 min; HPI shutoff at 10 min
U11		Infinite [1E-3]		5.00E-04	SRV reclose at 50 min; HPI not shutoff
U12	100 [0.5]	1 [0.906]		4.53E-01	SRV reclose at 100 min; HPI shutoff at 1 min
U13		10 [0.092]		4.60E-02	SRV reclose at 100 min; HPI shutoff at 10 min
U14		Infinite [1E-3]		5.00E-04	SRV reclose at 100 min; HPI not shutoff

Table 7-29 Conditional probabilities of the representative scenarios of two SRVs stuck open and reclosed (high decay heat)

#	Reclose time (minute) [Probability](A)	HPI throttling time (min) [Probability] (B)	Decay Heat (C)	Distributed Probability (A×B×C)	Description
U21	50 [0.5]	1 [0.906]	Nominal [1.0]	4.53E-01	SRV reclose at 50 min; HPI shutoff at 1 min
U22		10 [0.092]		4.60E-02	SRV reclose at 50 min; HPI shutoff at 10 min
U23		Never [1E-3]		5.00E-04	SRV reclose at 50 min; HPI not shutoff
U24	100 [0.5]	1 [0.906]		4.53E-01	SRV reclose at 100 min; HPI shutoff at 1 min
U25		10 [0.092]		4.60E-02	SRV reclose at 100 min; HPI shutoff at 10 min
U26		Never [1E-3]		5.00E-04	SRV reclose at 100 min; HPI not shutoff

Table 7-30 Representative values and probabilities of influencing parameters for pressurizer SRV stuck open and reclosed

Parameter	1	2	3
	Probability	Probability	Probability
Break Size	4.6E-3m ² 1.0		
Decay Heat	Nominal 0.8	Low decay heat 0.2% 0.1	Low decay heat 0.7% 0.1
Valves Reclosure Time	50 minutes 0.5	100 minutes 0.5	
HPI Shutoff Time	1 minute 0.906	10 minutes 0.092	Not shutoff 1E-3

Table 7-31 Conditional probabilities of representative scenarios of one SRV stuck open and reclosed

(hot zero power)

#	Reclose time (minute) [Probability] (A)	HPI throttling time (minute) [Probability] (B)	Decay Heat [Probability] (C)	Distributed Probability (A×B×C)	Description (Low decay heat for all scenarios)
U15	50 [0.5]	1 [0.906]	0.2% power [1.0]	4.53E-01	SRV reclose at 50 min; HPI throttled in 1 min
U16		10 [0.092]		4.60E-02	SRV reclose at 50 min; HPI throttled in 10 min
U17		Infinite [1E-3]		5.00E-04	SRV reclose at 50 min; HPI not throttled
U18	100 [0.5]	1 [0.906]		4.53E-01	SRV reclose at 100 min; HPI throttled in 1 min
U19		10 [0.092]		4.60E-02	SRV reclose at 100 min; HPI throttled in 10 min
U20		Infinite [1E-3]		5.00E-04	SRV reclose at 100 min; HPI not throttled

Table 7-32 Conditional probabilities of representative scenarios of two SRVs stuck open and reclosed

(hot zero power)

#	Reclose time (minute) [Probability](A)	HPI throttling time (minute) [Probability] (B)	Decay Heat (C)	Distributed Probability (A×B×C)	Description (Low decay heat for all scenarios)
U27	50 [0.5]	1 [0.906]	0.2% power [1.0]	4.53E-01	SRV reclose at 50 min; HPI shutoff at 1 min
U28		10 [0.092]		4.60E-02	SRV reclose at 50 min; HPI shutoff at 10 min
U29		Infinite [1E-3]		5.00E-04	SRV reclose at 50 min; HPI not shutoff
U30	100 [0.5]	1 [0.906]		4.53E-01	SRV reclose at 100 min; HPI shutoff at 1 min
U31		10 [0.092]		4.60E-02	SRV reclose at 100 min; HPI shutoff at 10 min
U32		Infinite [1E-3]		5.00E-04	SRV reclose at 100 min; HPI not shutoff

Table 7-33 Representative scenarios and probabilities for pressurizer SRVs stuck open without reclosure

ID	Frequency	Scenario Description
14	2.23 E-4	1 SRV SO and remaining open, full power
72	5.14 E-7	1 SRV SO and remaining open, full power, no HPI
34	4.95 E-7	2 SRVs SO and remaining open, full power
65	1.04 E-9	2 SRVs SO and remaining open, full power, no HPI
66	1.18 E-7	2 SRVs SO and one reclosed at 50 minutes, full power
67	1.18 E-7	2 SRVs SO and one reclosed at 100 minutes, full power
83	3.51 E-6	2 PORVs SO and remaining open, full power
31	3.10 E-7	Open all pressurizer PORVs and HPI on with loss of feed water
94	4.10 E-5	1 SRV SO and remaining open, low decay heat
73	6.55 E-8	1 SRV SO and remaining open, low decay heat, no HPI, all ADVs opened 5 min after HPI fails to start
64	8.67 E-8	2 SRVs SO and remaining open, low decay heat
92	2.13 E-7	2 SRVs SO and one reclosed at 50 minutes, low decay heat
93	2.13 E-7	2 SRVs SO and one reclosed at 100 minutes, low decay heat
76	1.06 E-4	2 PORVs SO and remaining open, low decay heat

Table 7-34 Representative scenarios and probabilities for one pressurizer SRV stuck open and later reclosed (high decay heat)

ID	Frequency	Scenario Description
59	3.46E-4	1 SRV stuck open; reclosed at 50 min; HPI not throttled
95	1.34E-4	1 SRV stuck open; reclosed at 100 min; HPI throttled 1 min after permitted
96	1.87E-4	1 SRV stuck open; reclosed at 100 min; HPI throttled 10 min after permitted
60	2.15E-5	1 SRV stuck open; reclosed at 100 minutes; HPI not throttled
82	1.51E-6	1 SRV stuck open, no HPI, all ADVs open 5 min after HPI fails to start

Notes: 1 SRV stuck open and reclosed at 50 minutes and that HPI is throttled at 1 and 10 minutes are eliminated due to low event frequencies

Table 7-35 Representative scenarios and probabilities for one pressurizer SRV stuck open and later reclosed (low decay heat)

ID	Frequency	Scenario Description
99	2.59 E-5	1 SRV stuck open; reclosed at 50 min; HPI throttled 1 min after permitted; low decay heat
101	3.09 E-5	1 SRV stuck open; reclosed at 50 min; HPI throttled 10 min after permitted; low decay heat
97	3.74 E-6	1 SRV stuck open; reclosed at 50 min; HPI not throttled; low decay heat
98	2.59 E-5	1 SRV stuck open; reclosed at 100 min; HPI throttled 1 min after permitted; low decay heat
100	3.09 E-5	1 SRV stuck open; reclosed at 100 min; HPI is throttled 10 min after permitted; low decay heat
71	3.74 E-6	1 SRV stuck open; reclosed at 100 minutes; HPI not throttled; low decay heat

Table 7-36 Representative scenarios and probabilities for two pressurizer SRVs stuck open and later reclosed (full power)

ID	Frequency	Scenario Description
61	1.79 E-6	2 SRV stuck open; reclosed at 50 min; HPI not throttled
86	6.84 E-7	2 SRV stuck open; reclosed at 100 min; HPI throttled 1 min after permitted
87	9.98 E-7	2 SRV stuck open; reclosed at 100 min; HPI throttled 10 min after permitted
62	1.08 E-7	2 SRV stuck open; reclosed at 100 min; HPI not throttled
68	1.33 E-8	2 SRV stuck open; no HPI, all ADVs opened 5 minutes after HPI fails to start

The scenarios, two SRVs stuck open and reclosed at 50 minutes with HPI throttled at 1 min and 10 min were eliminated due to low event frequencies

Table 7-37 Representative scenarios and probabilities for two pressurizer SRVs stuck open and later reclosed (low decay heat)

ID	Frequency	Scenario Description
88	1.33E-7	2 SRV stuck open; reclosed at 50 min; HPI throttled at 1 min after permitted; low decay heat
90	1.65E-7	2 SRV stuck open; reclosed at 50 min; HPI throttled 10 min after permitted; low decay heat
69	2.09E-8	2 SRV stuck open; reclosed at 50 min; HPI not throttled; low decay heat
89	1.33E-7	2 SRV stuck open; reclosed at 100 min; HPI throttled 1 min after permitted; low decay heat
91	1.65E-7	2 SRV stuck open; reclosed at 100 min; HPI throttled at 10 min after permitted; low decay heat
70	2.09E-8	2 SRV stuck open; reclosed at 100 min; HPI not throttled; low decay heat

7.3 Palisades Thermal Hydraulic Uncertainty Representative Scenarios

This section discusses the determination of representative scenarios for thermal hydraulic uncertainty evaluation for Palisades. As instructed by the PRA group, the uncertainty study scope for the Palisades is limited to the LOCAs; pressurizer SRV scenarios were not analyzed. Table 7-38 shows the parameters sensitivities calculated by RELAP5. The probabilities of the representative values are listed in Table 7-1.

The LOCA spectrum is divided into three categories based on break size: between 1.4-inch to 4-inch (1.1 E-3 m^2 to 8 E-3 m^2), 4-inch to 8-inch (8 E-3 m^2 to 3.2 E-2 m^2), and greater than 8-inch (3.2 E-2 m^2). The process of identifying the thermal hydraulic representative scenarios was the same as the other two plants.

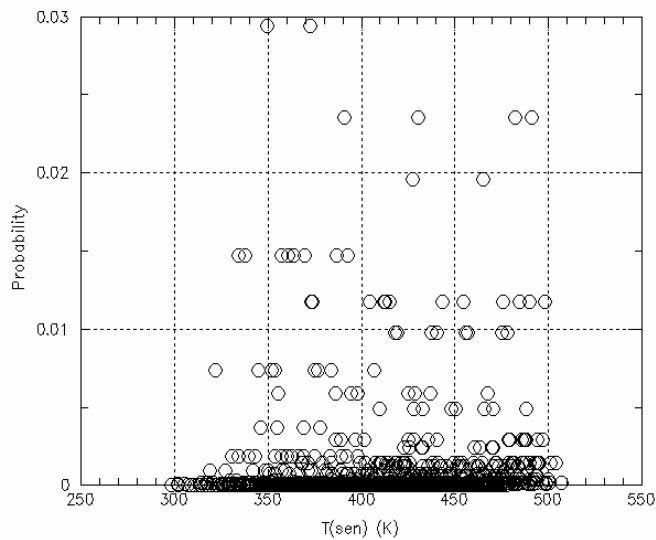
Table 7-38 T_{sen} matrix for LOCAs (T_{sen} in K)

Parameter	Break Size (inches in diameter)					
	1.4"	2"	2.8"	4"	5.7"	8"
Nominal	482	427	391	350	320	310
Winter*	476	419	374	334	304	294
Summer*	490	437	404	364	333	325
110% HPI	478	422	386	--	--	--
90% HPI	488	432	397	--	--	--
100 % HPI Failed	550	532	501	--	--	--
Low decay heat (0.7%)	450	406	364	333	319	310
Low decay heat (0.2%)	416	380	351	330	318	309
130% h	486	433	402	355	--	--
70% h	479	425	389	346	--	--
70% Break flow	--	440	415	370	334	313
130% Break flow	--	418	373	338	314	309
Cold Leg LOCA	491	465	430	373	352	332

*Winter $T_{HPI} = 4C (40F)$ $T_{LPI} = 4C (40F)$
 *Summer $T_{HPI} = 38C (100F)$ $T_{LPI} = 38C (100F)$
 *Spring/Fall $T_{HPI} = 21C (70F)$ $T_{LPI} = 21C (70F)$

7.3.1 1.4-inch to 4-inch LOCA

Figures 7.34 and 7.35 are the PDF and CDF plots. The representative scenario descriptions are shown in Table 7-39. Figures 7.36 and 7.37 are the $T_{dc}(t)$ and $P(t)$ of the representative



scenarios, respectively.

Figure 7-34 T_{sen} probability distribution for LOCAs 1.4-inch to 4-inch

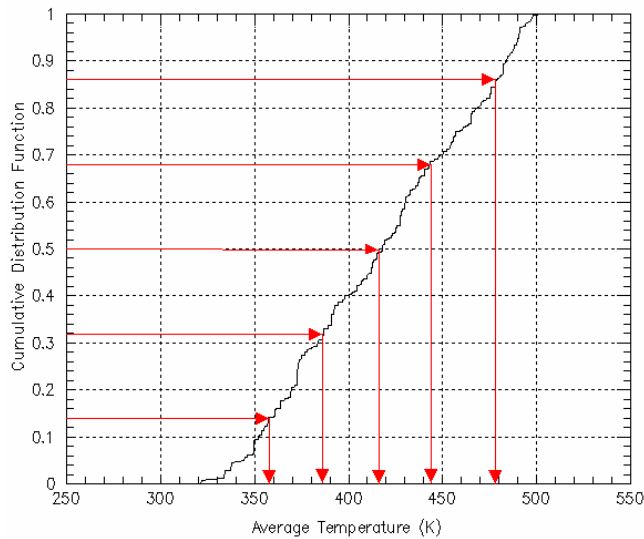


Figure 7-35 T_{sen} cumulative probability distribution and identification of the representative scenarios for LOCAs 1.4-inch to 8-inch

Table 7-39 Boundary conditions of the five representative scenarios for LOCAs 1.4-inch to 4-inch

#	Bin #	Probability	Scenario Description
1	2	0.23	1.4" surge line LOCA
2	61	0.18	2.8" surge line LOCA, summer
3	60	0.18	2" surge line LOCA, winter
4	59	0.18	4" cold leg LOCA, summer
5	58	0.23	4" cold leg LOCA, winter

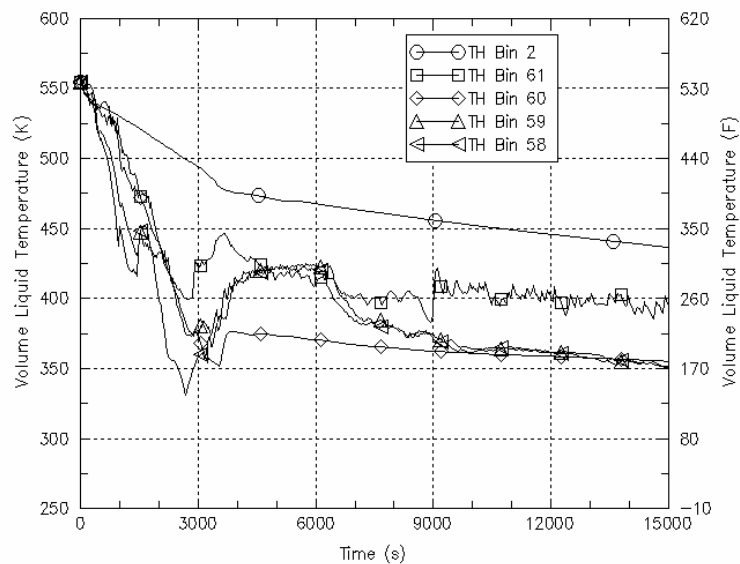


Figure 7-36 The five $T_{dc}(t)$ representative scenarios for LOCAs 1.4 inch to 4 inch

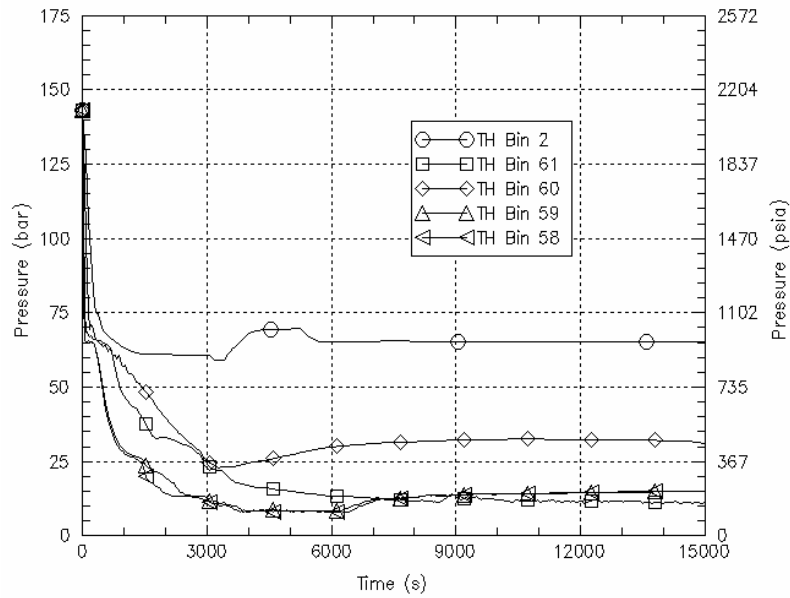


Figure 7-37 The five P(t) representative scenarios for LOCAs 1.4 inch to 4 inch

7.3.2 4-inch to 8-inch LOCA

Figures 7.38 and 7.39 are the PDF and CDF plots. The representative scenario descriptions are shown in Table 7-40. Figures 7.40 and 7.41 are the $T_{dc}(t)$ and $P(t)$ plots of the representative scenarios, respectively.

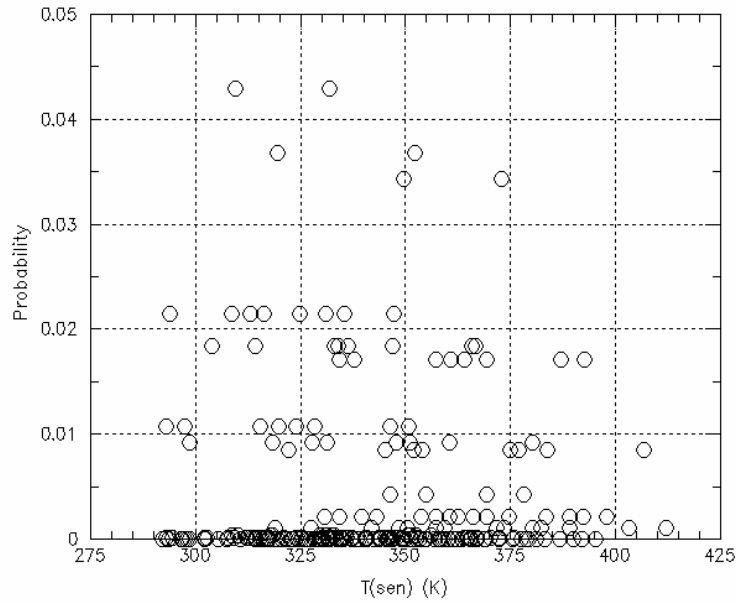


Figure 7-38 T_{sen} probability distribution for LOCAs 4-inch to 8-inch

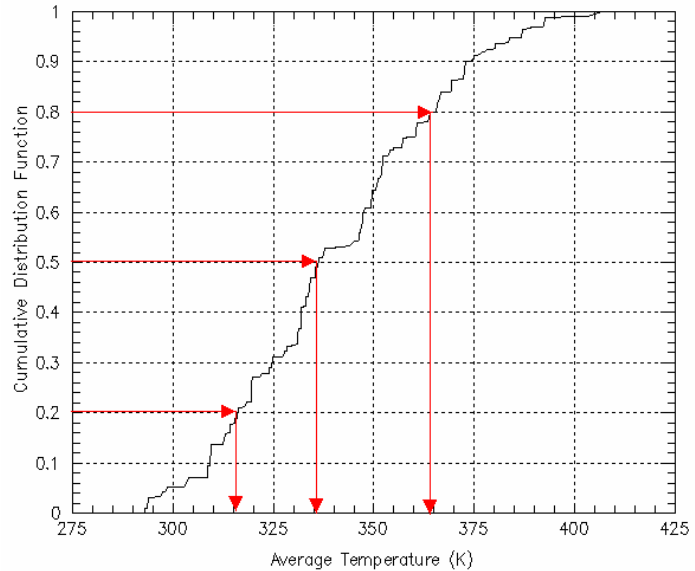


Figure 7-39 T_{sen} cumulative distribution and identification of representative scenarios for LOCAs 4-inch to 8-inch

Table 7-40 Boundary conditions of the three representative scenarios for LOCAs 4-inch to 8-inch

#	Bin #	Probability	Scenario Description
1	64	0.35	4-inch surge line LOCA, summer
2	63	0.30	5.7-inch cold leg LOCA, winter
3	62	0.35	8-inch cold leg LOCA, winter

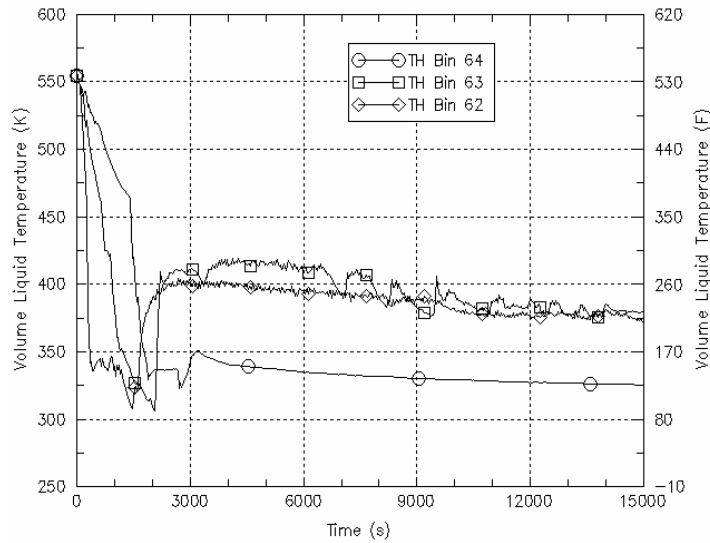


Figure 7-40 The three T_{dc} traces of the representative scenarios for LOCAs 4-inch to 8-inch

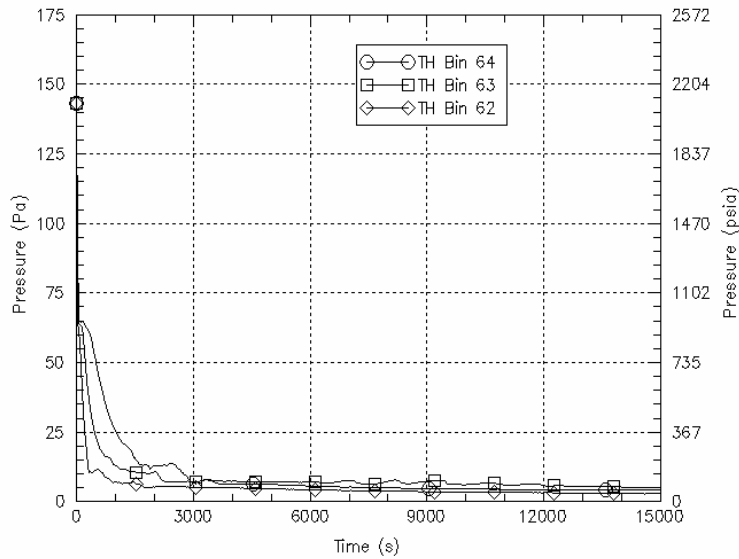


Figure 7-41 The three P traces of the representative scenarios for LOCAs 4-inch to 8-inch

7.3.3 Greater than 8 inch LOCA

The representative scenario is a 16-inch hot leg LOCA (Table 7-41). The $T_{dc}(t)$ and $P(t)$ are plotted in Figure 7-42.

Table 7-41 Boundary conditions of the representative for LOCAs greater than 8 inch

	Bin #	Probability	Scenario Description
1	40	1.0	16-inch surge line LOCA

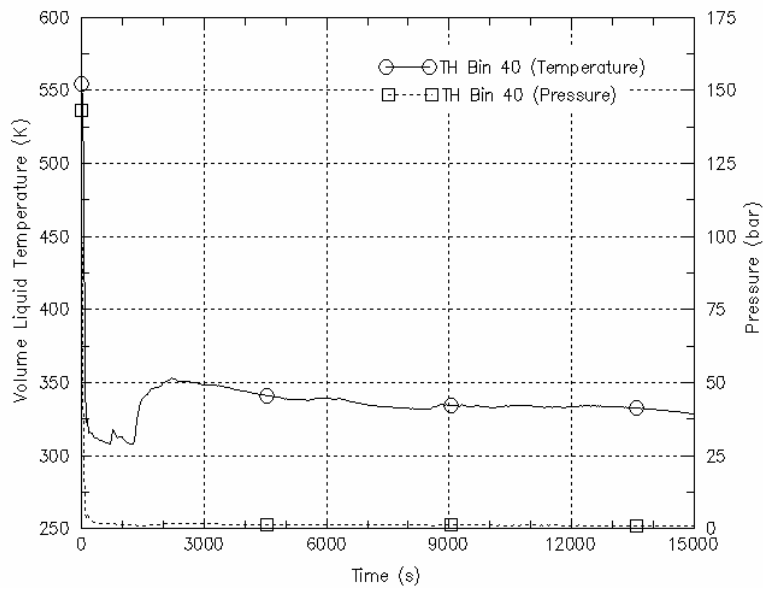


Figure 7-42 T_{dc} and P traces of the representative scenario for LOCAs greater than 8-inch

8. DISCUSSION

The figure of merit (sensitivity indicator, T_{sen}) was used to measure the sensitivity of a parameter. The value of T_{sen} was a measure of importance to PTS consequence. The averaged downcomer temperature, T_{sen} was used as the PTS sensitivity indicator for two reasons. First, from the TH perspective, downcomer temperature is the most direct indicator of fracture probability. Second, during the development of the thermal hydraulic uncertainty methodology, the PFM code, FAVOR, was not finished. The preferred approach would have been to use CPF as calculated by FAVOR as the sensitivity indicator, however, this was impossible. The FAVOR code became available after the thermal hydraulic uncertainty assessment method had been developed.

This being the case, it is important to examine the relationship between T_{sen} and CPF in order to validate the appropriateness of using T_{sen} for selecting representative scenarios for thermal hydraulic uncertainty evaluation. Section 8.1 shows the sensitivity assessment matrix for Oconee-1, comparing calculated values of T_{sen} and CPF. The data in the matrix form the basis for the subsequent discussions. Section 8.2 compares sensitivities of T_{sen} with CPF. Section 8.3 discusses parameters' importance rankings based on T_{sen} and CPF.

The FAVOR calculations used for this parameter sensitivity study are from December 2002. The CPIs and CPFs calculated by FAVOR are shown in Appendix F. Since then, FAVOR has been modified further. There might be inconsistencies between the CPFs used in this Chapter and those in the latest PFM results for the same scenario, in which case the latest PFM results should be used.

While the following discussion shows that many trends produce results that are obvious and expected, not all results appear at first glance to be self-consistent. An important conclusion is, that short of running FAVOR, there is no simple way to accurately predict the CPF of a scenario based on examining the thermal hydraulic input.

8.1 Sensitivity Assessment Matrix

Table 8-1 shows the sensitivity assessment matrix. Each cell contains two values; the top is T_{sen} , and the bottom is CPF. The parameter sensitivities were evaluated at six different sizes of LOCA: 1.5", 2", 2.3", 4", 5.7", and 8". The first row, "nominal", are the baseline scenarios, in which all parameters are at their nominal values for the specified break size. T_{sen} and CPF were calculated by RELAP5 and FAVOR, respectively. The CPFs were calculated based on the embrittlement map corresponding to 60 effective full power years (EFPY) of Oconee-1 operation. The following discusses the sensitivities of different parameters.

Table 8-1 Sensitivity assessment matrix for Oconee-1

Top value in each cell is T_{sen} . Bottom value in each cell is CPF.

#		Break Size, inches					
		1.5"	2"	2.8"	4"	5.7"	8"
1	Nominal	414 0	394 4 E-10	388 5.2 E-8	363 4.4E-7	329 7.4 E-7	317 7.7 E-7
2	Winter*	402 1 E-10	--	374 9.8 E-8	--	314 3.5 E-7	314 1.3 E-8
3	Summer*	--	--	395 2.5 E-8	--	336 2.0 E-8	317 2.9 E-8
4	$P_{CFT} + 50$ psi	--	--	386 1.2 E-9	--	--	--
5	$P_{CFT} - 50$ psi	--	--	389 6.0 E-8	--	--	--
6	110% HPI RCPs on	521 0	--	402 8.5 E-8	--	--	--
7	110% HPI RCP off	401 3 E-11	--	--	--	--	--
8	90% HPI	416 2 E-13	--	380 1.0 E-7	--	--	--
9	HPI Failed and Recovered @~7000 s	--	--	491 0	--	--	317 2.0 E-8
10	HPI Failed and Recovered @~1000 s	--	--	400 1.8 E-8	--	--	--
11	HPI Failed and Recovered @~2000 s	--	--	416 2.3 E-8	--	--	--
12	100% Failed	--	--	500 0	403 2.8E-7	328 8.6 E-7	319 1.5 E-7
13	HPI 25%Failed	446 0	453 2 E-12	442 2.1 E-8	--	--	--
14	HPI 50% Failed	514 0	511	467 6 E-11	--	--	--
15	Low Decay Heat	490 0	--	349 4.3 E-8	--	321 3.3 E-8	312 1.1 E-6
16	Vent Valve Close	--	--	362 0	345 0	--	--
17	Vent Valve 2/6 Open	--	--	406 0	--	--	--
18	Vent Valve 4/6 Open	--	--	410 0	--	--	--
19	Vent Valve 6/6 Open	--	--	413 0	371 4.7E-9	--	--
20	High CL Reverse Flow Resistance	400 1.4 E-9	372 1.6 E-8	370 9 E-9	356 1.1E-6	--	311 4.5 E-7
21	130% Convective Heat Transfer Coefficient	--	400 1 E-10	396 3.3 E-8	--	331 1.5 E-6	--
22	70% Convective Heat Transfer Coefficient	--	387 1 E-10	380 1.2E-7	--	324 9.1 E-8	--
23	200% Loop Flow Resistance	--	395 5 E-10	--	--	--	--
24	200% Bypass Flow Area	--	396 0	--	--	--	--
25	Zero Bypass Flow Area	--	375 0	--	--	--	--
26	No heat structure	--	369 4.5 E-8	--	--	--	--
27	Cold Leg LOCA	--	455 0	412 0	376 1E-11	345 5.2 E-9	317 1.2 E-7

8.2 Sensitivity Trends and Comparisons

This section discusses the sensitivity trends and comparisons between T_{sen} and CPF. In general, a lower T_{sen} corresponds to a larger CPF.

8.2.1 Break Size

The sensitivity of a parameter is dependent on break size. Table 8-1 can be used to examine the trend. It can also be used to compare sensitivities of different parameters at a fixed break size. Such comparisons were used for parameter importance ranking. Increasing break size decreases both the RCS temperature and pressure. The decrease in pressure reduces the stress on the vessel wall, which is in the favorable direction. For LOCAs, however, this is more than offset by the decreasing temperature in the downcomer. The trends of T_{sen} and CPF as a function of break size are shown in Figure 8-1 for the baseline scenarios

In earlier PTS studies [Boyd, 1998 #563; Burns, 1986; Fletcher, 1984], it was believed that PTS required both low downcomer temperature as well as relatively high pressure stress. Thus, earlier PTS studies focused on small break LOCAs and MSLBs. Large LOCA scenarios were not expected to be PTS significant due to lack of pressure stress, and were therefore excluded. Figure 8-1 shows that the CPF in fact increases with increased break size, which indicates that downcomer temperature alone can cause vessel wall failure. Figure 8-1 shows that CPF is sensitive to break size when the break size is less than 4 inch; CPF increases three orders of magnitude when the break size increases from 2-inch to 4-inch. Beyond 4-inch, the CPF remains relatively constant. Figures 8.2 to 8.4 plot $T_{dc}(t)$, $P(t)$, and $h_{dc}(t)$, respectively for the six LOCAs (1.5", 2", 2.3", 4", 5.7", and 8").

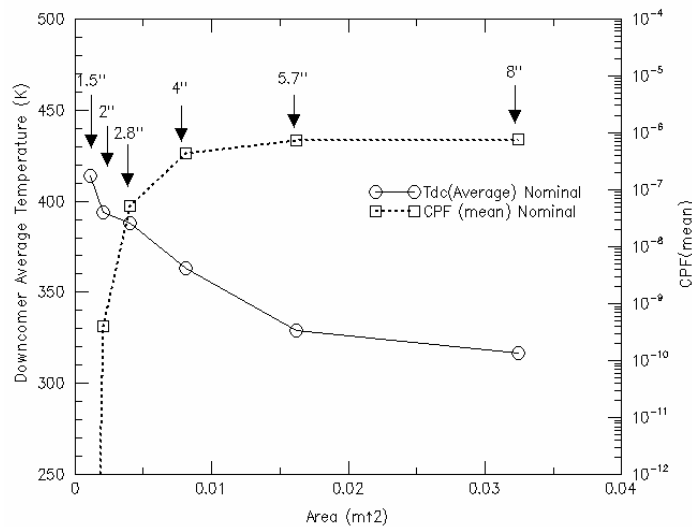


Figure 8-1 T_{sen} and CPFs trends of varying LOCA sizes for Oconee-1

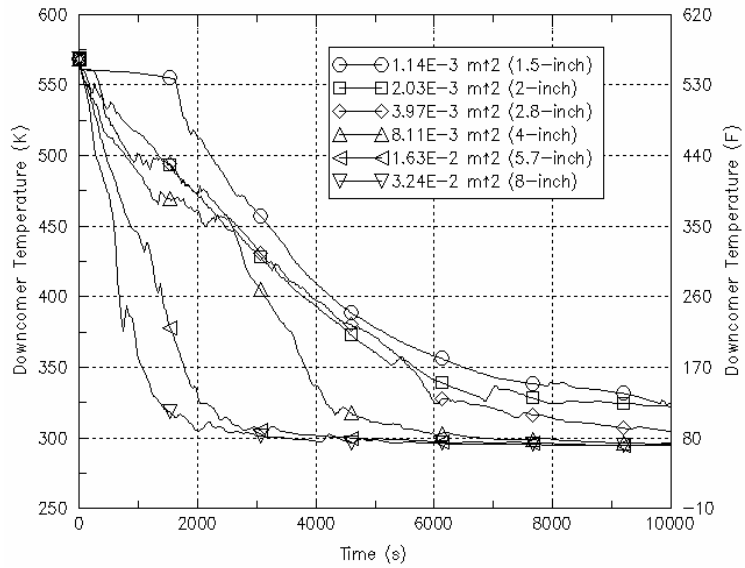


Figure 8-2 $T_{dc}(t)$ of the nominal scenarios of different LOCA sizes for Ocone-1

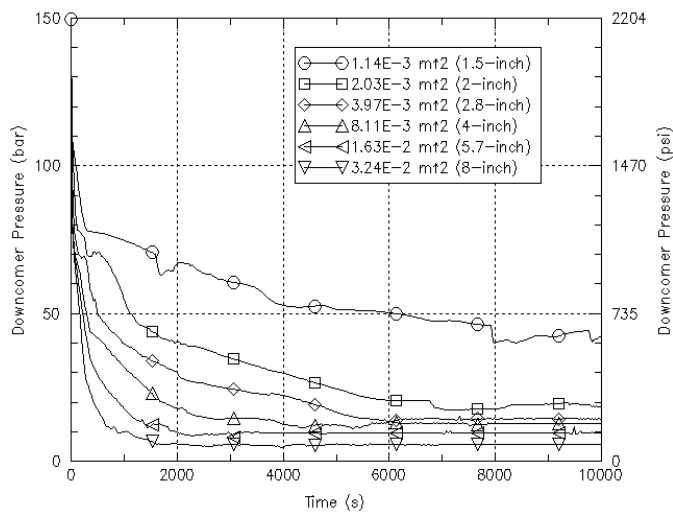


Figure 8-3 $P(t)$ of the nominal scenarios of different LOCA sizes for Ocone-1

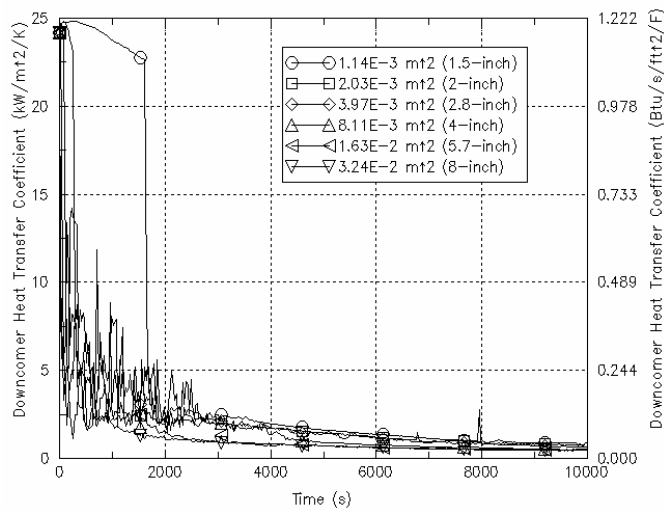


Figure 8-4 $h_{dc}(t)$ of the nominal scenarios of different LOCA sizes for Oconee-1

8.2.2 HPI State and HPI Flow Rate

HPI is an important heat sink in the early stages of a LOCA. HPI injection is located in the cold legs upstream from the downcomer, thus, its impact on T_{dc} is direct. HPI failure increases T_{sen} , especially for small LOCAs, in which high RCS pressure prevents accumulators and LPI from injecting.

Figure 8-5 shows the impact of HPI failure on T_{sen} and CPF. Two sets of T_{sen} and CPF curves are shown. One represents the nominal baseline scenarios without HPI failure. The other represents HPI failure scenarios. The differences between the two curves are the sensitivity of HPI failure. It shows that, from a T_{sen} perspective, when the break size is greater than 5.7-inch, the HPI state has no impact, and in terms of CPF, HPI has no effect for breaks greater than 4-inch. This is because for larger break sizes, accumulators and LPI dominate the downcomer cooldown.

On the other hand, Figure 8-5 also shows that CPF drops to zero if HPI fails for breaks smaller than 2.8 inch. Figure 8-6 shows HPI partially failed (nominal, 25% failure, 50% failure, and 100% failure) affecting CPF in the small LOCA region. For breaks smaller than 2.8 inch, reducing HPI flow by 50% reduces CPF by two orders of magnitude. Aside from the HPI function state (success, fail on demand, or fail during operation), this study used an uncertainty of 10% on HPI flow. For Oconee-1, as shown in Figure 8-6, the CPF for a 25% reduction in CPF was essentially the same as nominal (full HPI), therefore, the impact of the 10% variation used in the uncertainty analyses is negligible.

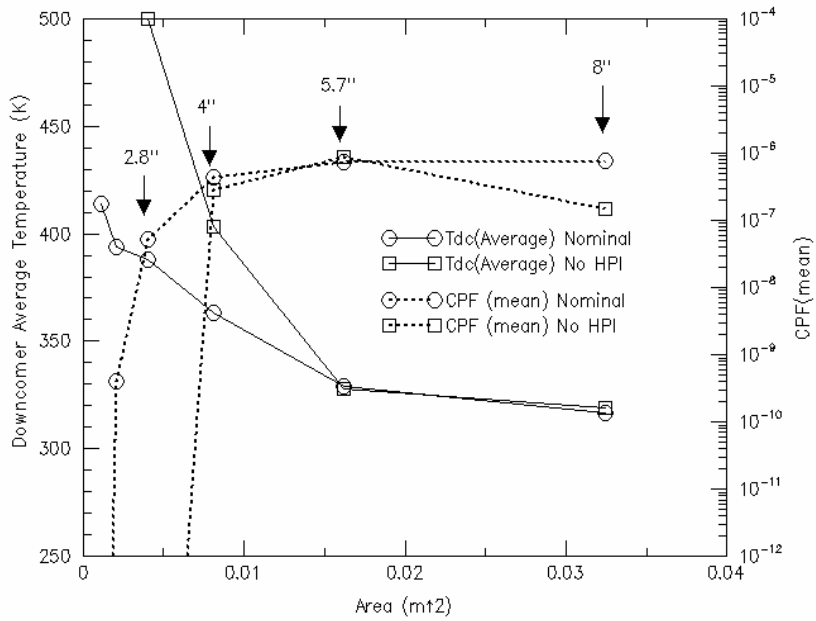


Figure 8-5 Impact of HPI state on T_{sen} and CPF

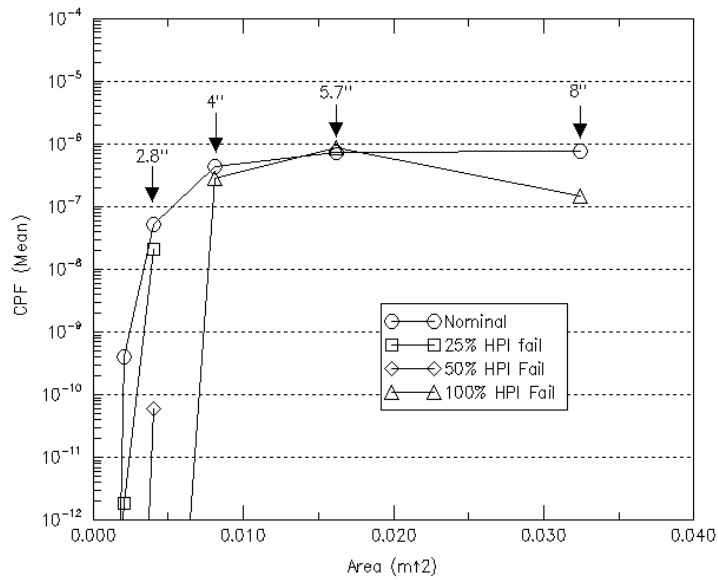


Figure 8-6 Effect of HPI partial failure on T_{sen} and CPF

8.2.3 Decay Heat

Decay heat is the major heat source after RCPs are tripped. Reduction of decay heat reduces RCS temperature, thus low decay heat (hot zero power (HZP)) is expected to increase CPF. Figure 8-7 shows mixed results. For a 5.7-inch LOCA, instead of increasing CPF, low decay heat decreased CPF more than an order of magnitude. Examining such a difference could provide insight to the relationship between thermal hydraulics and PFM. For this same 5.7-inch break, Figures 8.8 to 8.10 plot $T_{dc}(t)$, $P(t)$ and $h_{dc}(t)$ for the high and low decay heat scenarios. From the thermal hydraulic perspective, it is difficult to explain the CPF results. The PFM results suggest that both the absolute value and rate of change (T_{dc} and dT_{dc}/dt), are important in determining CPF. Such a combined effect is beyond the scope of this study.

Decay heat level affects the boundary in break size that causes loss of subcooling in the hot leg. For a 1.5 inch LOCA, subcooling is maintained for low decay heat. As a result, the RCPs are not tripped and the scenario is not PTS significant.

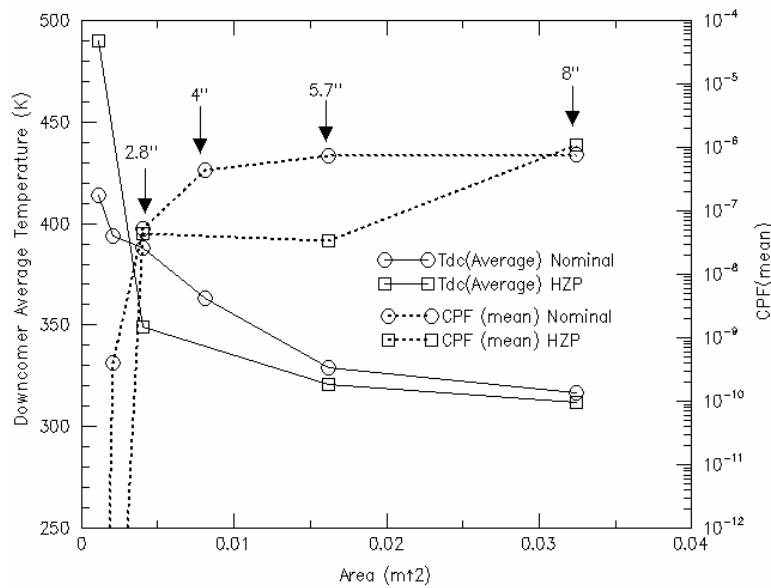


Figure 8-7 Impact of decay heat on T_{sen} and CPF for Oconee-1

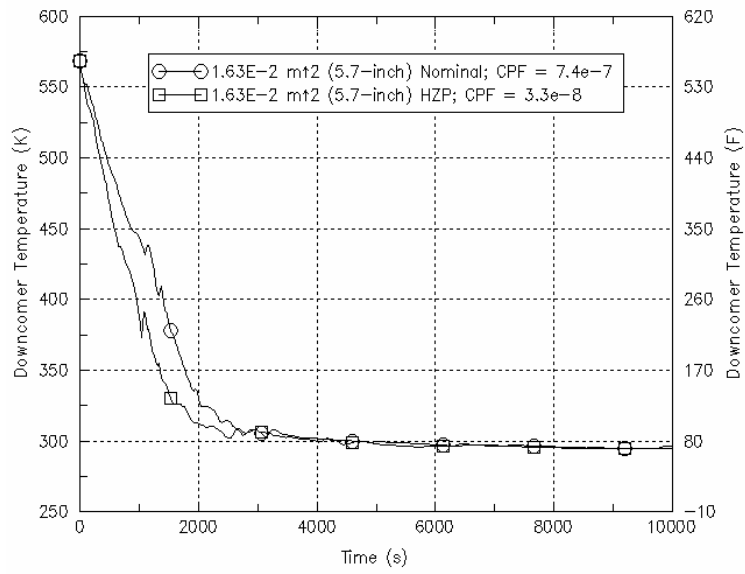


Figure 8-8 $T_{dc}(t)$ of 5.7-inch surge line LOCA comparing full power with low decay heat for Oconee-1

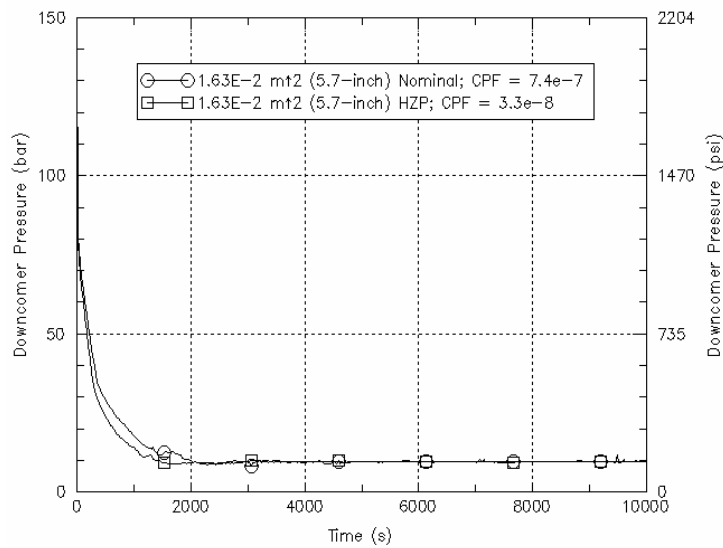


Figure 8-9 $P(t)$ of 5.7-inch surge line LOCA comparing full power with low decay heat for Oconee-1

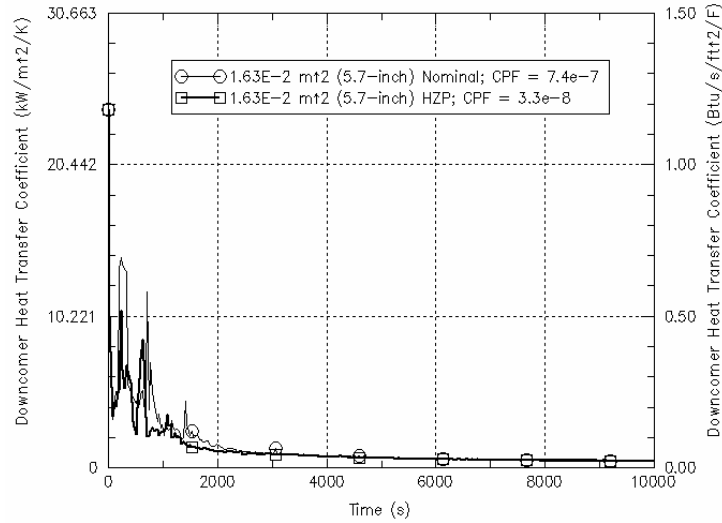


Figure 8-10 $h_{dc}(t)$ of 5.7-inch surge line LOCA comparing full power with low decay heat Oconee-1

8.2.4 Season

Season affects the ECC injection temperatures. The water source for HPI and LPI is the refueling water storage tank (RWST), which is located outside of containment. The RWST temperature depends on the environmental temperature. The CFTs are located inside the containment, and their temperature is less dependent on the environmental temperature, but still varies with the season. The continuous temperature distributions are represented by three sets of representative seasonal temperatures as shown in Table 8-2.

Table 8-2 Temperature of the emergency core cooling system at different seasons

System \ Season	Spring/Fall C (F)	Summer C (F)	Winter C (F)
HPI	21 (70)	29 (85)	4 (40)
CFT	27 (80)	39 (100)	21 (70)
LPI	21 (70)	29 (85)	4 (40)

Figure 8-11 shows the seasonal impact on T_{sen} and CPF. T_{sen} is lowest for winter and highest for summer, as to be expected. The CPF trends are generally consistent. The CPF for winter is lower than that for spring/fall for break sizes 5.7 inch and 8 inch, which conflicts with the T_{sen} trends, although the size of the differences are small. The largest deviation is in the 8-inch break, but this calculation mistakenly used the spring/fall LPI temperature for the winter condition, so the downcomer temperature ended up the same for the two cases. Figures 8.12 and 8.13 compare T_{dc} and P for the 5.7-inch break, while Figures 8.14 and 8.15 compare T_{dc} and P for the 8-inch break.

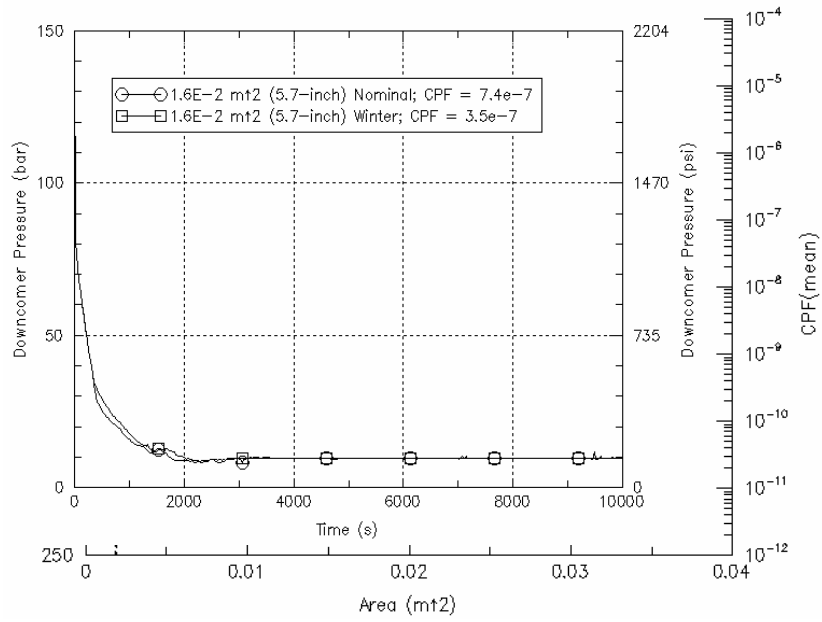


Figure 8-11 Impact of season on T_{sen} and CPF

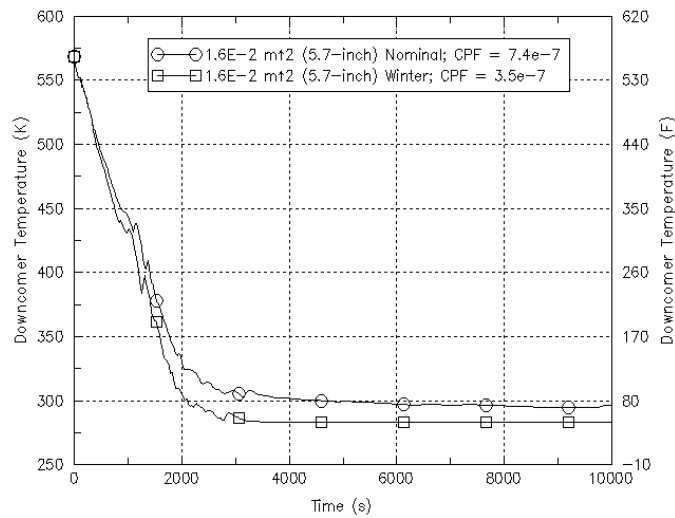


Figure 8-12 $T_{dc}(t)$ for 5.7-inch surge line LOCA comparing spring/fall with winter for Oconee-1

Figure 8-13 $P(t)$ for 5.7-inch surge line LOCA comparing spring/fall with winter for Oconee-1

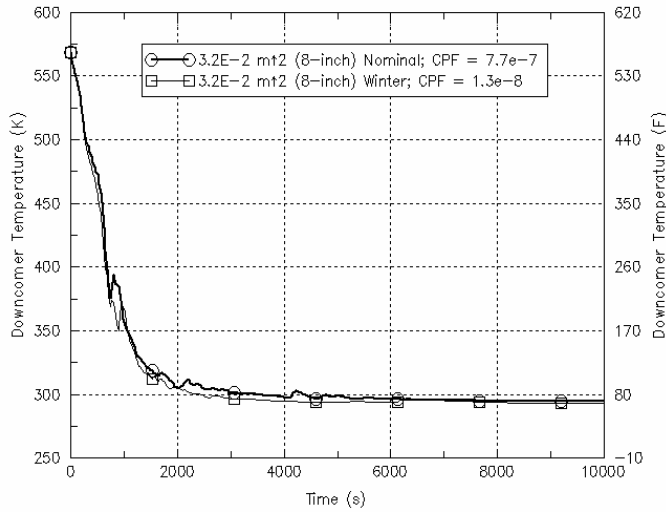


Figure 8-14 Tdc(t) for 8-inch surge line LOCA comparing spring/fall with winter for Oconee. The LPI temperature of the winter scenario mistakenly used the spring/fall LPI temperature that resulted in a final temperature 70F.

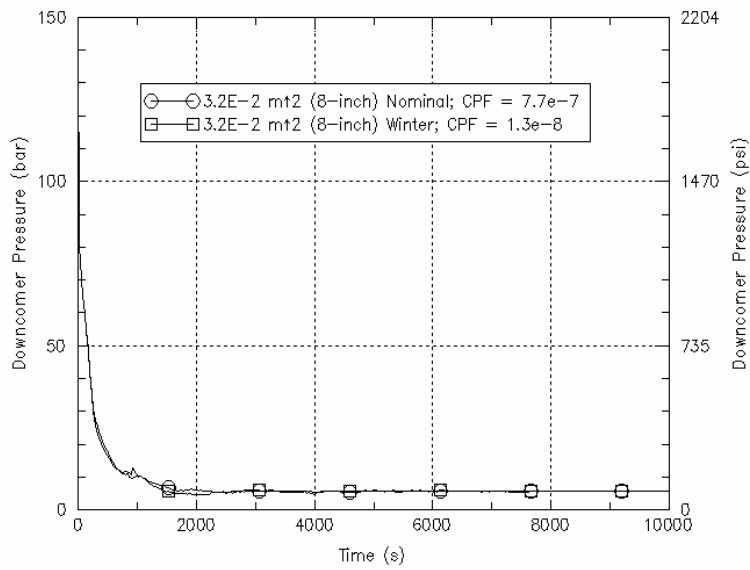


Figure 8-15 P(t) for 8-inch surge line LOCA comparing spring/fall with winter for Oconee-1

8.2.5 Break Location

Break location is divided into two groups, hot leg and cold leg. When the location is in the cold leg, the coolant in the vessel may flow from the core to the downcomer towards the break, thereby increasing T_{dc} . Also, the ECC injected into the broken cold leg tends to be bypassed out the break. In fact, some of the ECC injected into the intact cold legs has the potential to be bypassed as well. The enthalpy of the break flow is lower for cold leg than for hot leg breaks. Thus, cold leg LOCAs are expected to have a higher T_{dc} and a smaller CPF than hot leg LOCAs of same break size. Figure 8-16 shows that both the T_{sen} and CPF trends are as expected. It also shows consistency in that lower T_{sen} results in higher CPF, and a smaller variation in T_{sen} results in a smaller variation in CPF.

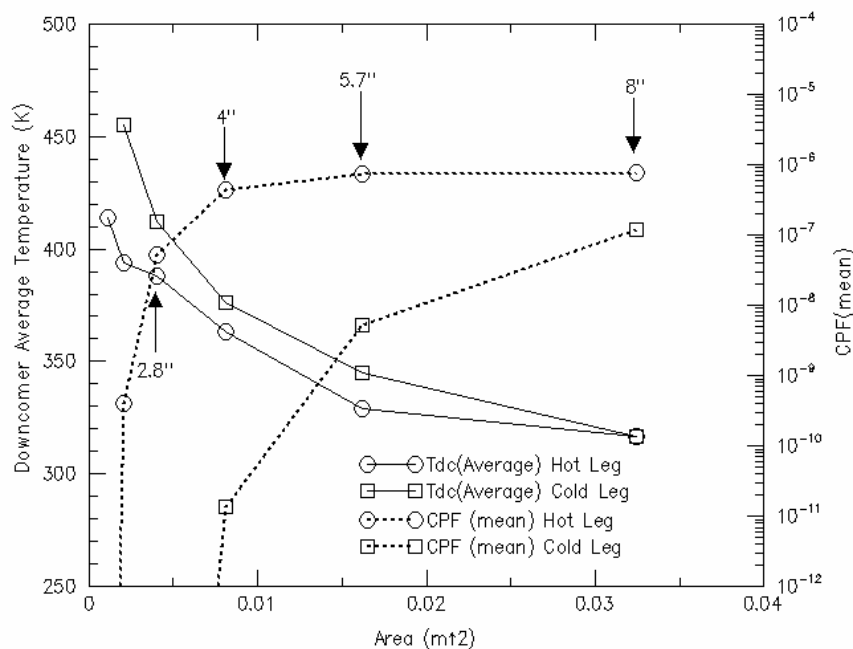


Figure 8-16 Impact of break location on CPF and T_{sen} for Oconee-1

8.2.6 Reactor Vessel Vent Valve State

Reactor vessel vent valves (RVVVs) are flapper type valves attached to the outside of the core barrel at an elevation just above the hot and cold legs. There are eight such valves with a total opening area of 0.8 m². Under normal operation they held shut by differential pressure. When the upper plenum-to-downcomer pressure differential is reversed, the RVVVs open, allowing hot water and/or steam to flow into the upper region of the downcomer. This tends to increase T_{dc} and decrease CPF.

The sensitivity of the RVVV state was assessed for two LOCA break sizes: 2.8-inch and 4-inch. The RVVV state was expected to have a lesser effect on CPF when the LOCA size was greater than 4-inch. The state (open or closed) of the RVVVs was fixed at the beginning of the

calculations, and the valves remained in the same state throughout the sequences. The T_{dc} and P trends of the different RVVV states for the two LOCAs are shown in Figures 8.16 to 8.19. Figure 8-16 shows that, as expected, opening the RVVVs increased T_{sen} , and closing them reduced T_{sen} . However, both the opened state and the closed state reduced CPFs, compared to the nominal sequence, so the trends between T_{sen} and CPF are not consistent.

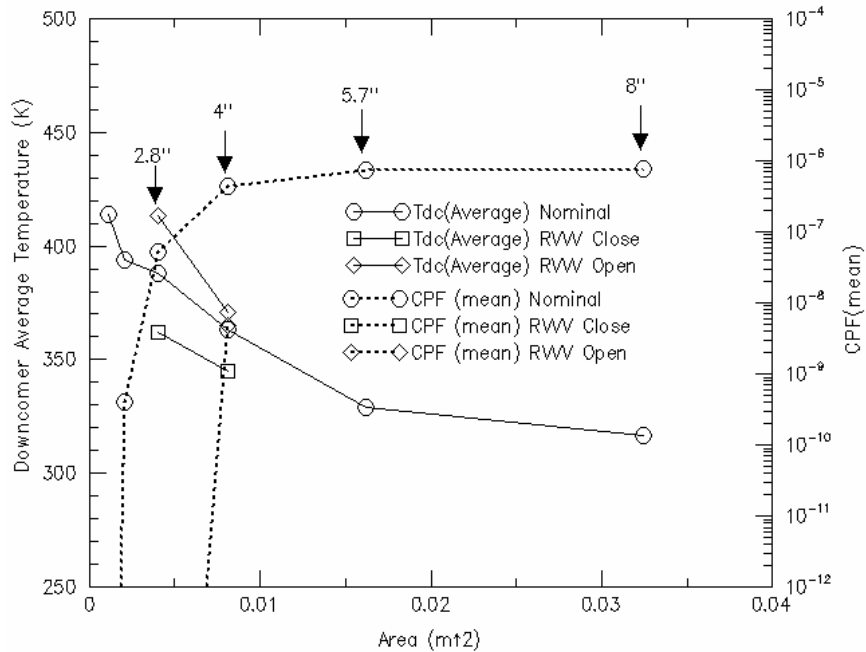


Figure 8-17 RVVV impact on T_{sen} and CPF for Oconee-1, CPFs for RVVV closed scenarios are zero

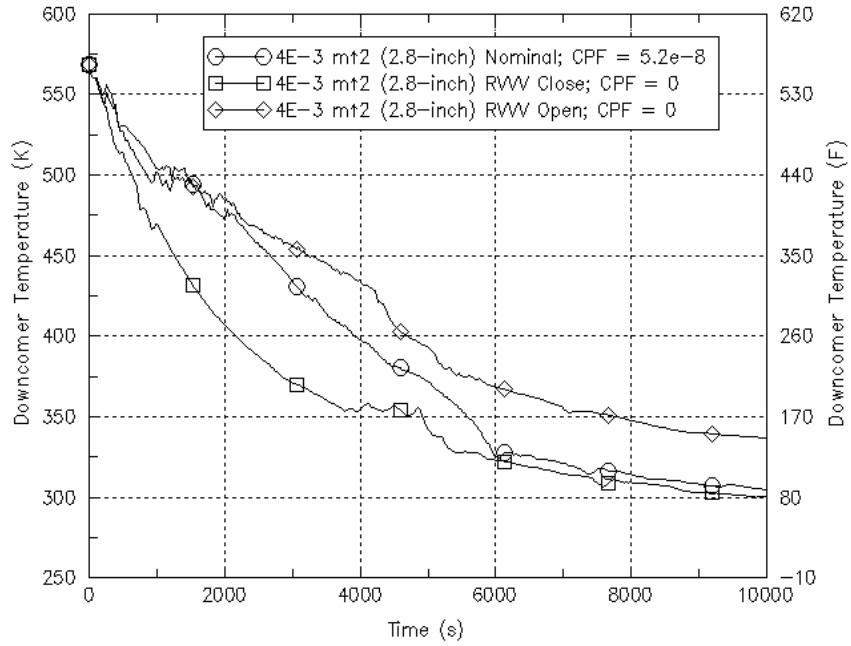


Figure 8-18 $T_{dc}(t)$ for 2.8-inch surge line LOCA comparing three different RVV states

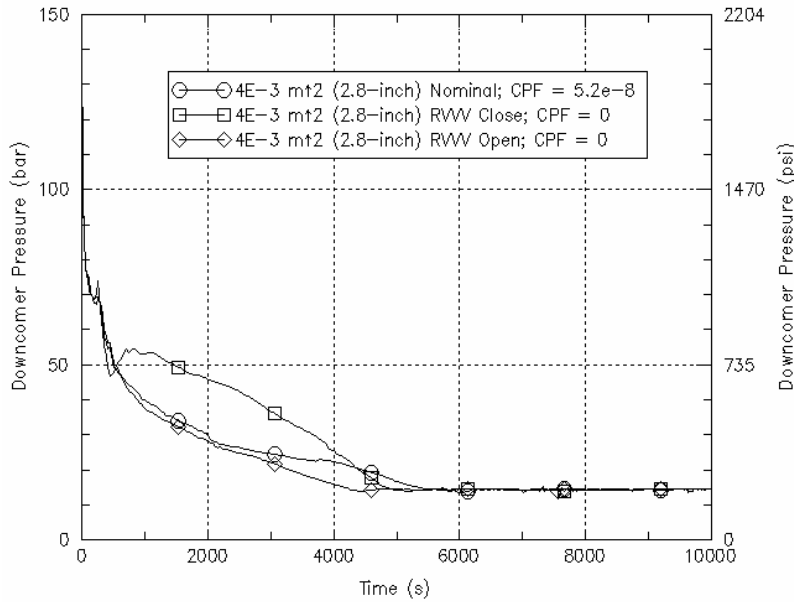


Figure 8-19 $P(t)$ for 2.8-inch surge line LOCA comparing three different RVV states

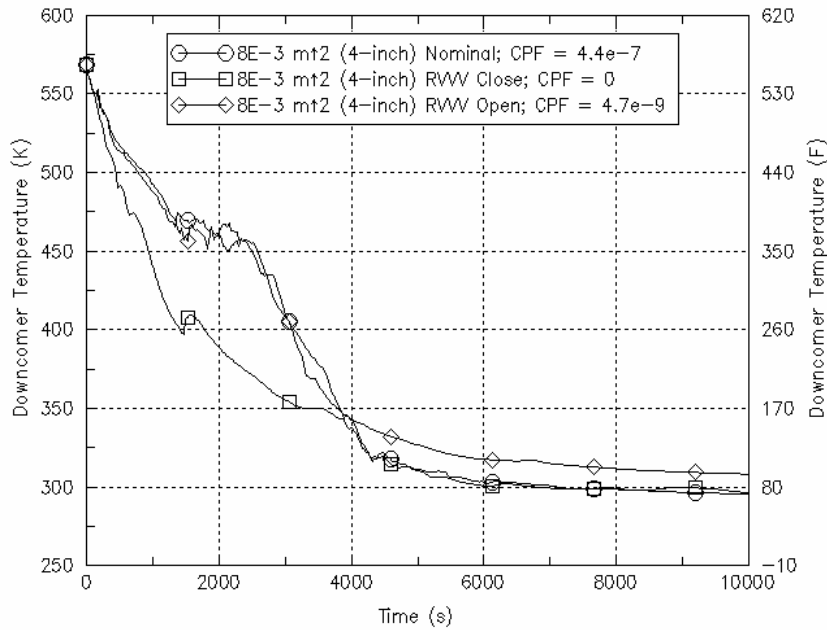


Figure 8-20 $T_{dc}(t)$ for 4-inch surge line LOCA comparing three different RVV states

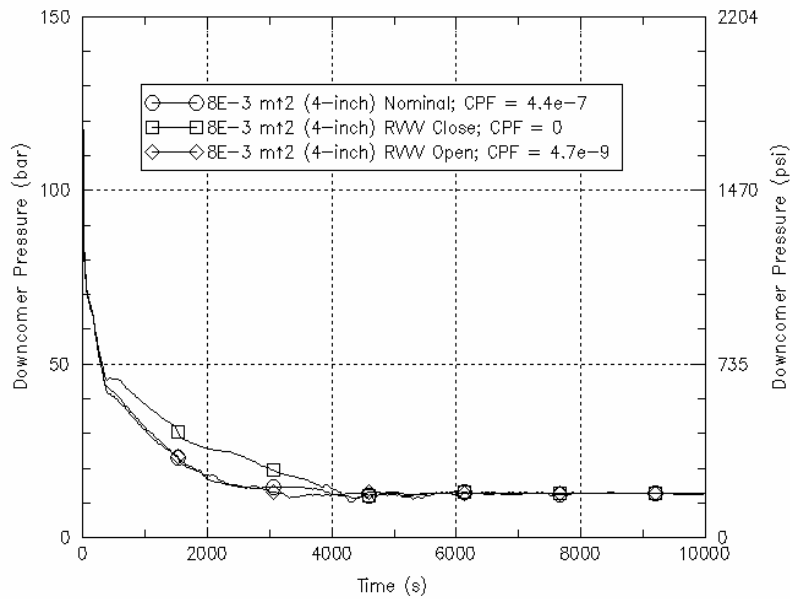


Figure 8-21 $P(t)$ for 4-inch surge line LOCA comparing three different RVV states

8.2.7 Convective Heat Transfer Coefficient

The convective heat transfer coefficient h affects the heat flux between the RCS coolant and structures. Before the initiating event, the coolant and structures are at the same temperature. After the initiating event, the coolant temperature decreases rapidly, causing heat transfer from structures to coolant. In the sensitivity assessment, h was varied by 30% from the nominal. Since h is calculated by RELAP5 based on the dynamics of convection and conduction heat

transfer, it requires changing the RELAP5 source code to assess h directly, which is difficult. Instead, the heat transfer area was changed as an alternative for simulating the uncertainty in h .

A larger h increases the heat flux from structures to coolant. This causes T_{dc} to be warmer, but also the vessel wall cools faster. However, RELAP5 is not coupled to FAVOR, which instead uses T_{dc} and h_{dc} as boundary conditions to calculate CPFs. Therefore, since T_{dc} is higher, the FAVOR calculation of is expected to be lower. Figure 8-21 plots the effect of h , showing the trends are consistent, but not pronounced.

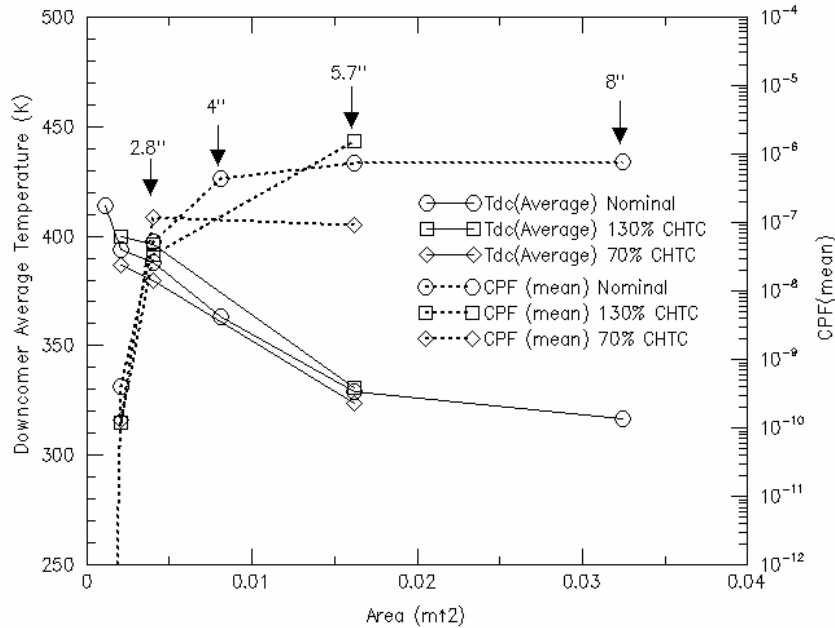


Figure 8-22 Impact of variation in heat transfer coefficient on T_{sen} and CPF for Oconee-1

8.2.8 Recirculation Flow

Recirculation flow in the cold legs is caused by numerical effects (Chapter 6). The recirculation flow causes the coolant in a cold legs and downcomer to be warmed since it mixes water from the cold legs and upper downcomer with the lower 1/3 of the lower steam generator in Oconee-1, or the steam generator outlet plenum in Palisades. Thus, loop recirculation flow is expected to increase T_{sen} and reduce CPF. The recirculation flow is stopped by applying damping in the form of large reverse flow coefficients in the RCPs (high K-factor). Figure 8-23 shows the loop recirculation effect on T_{sen} and CPF. The differences are not significant.

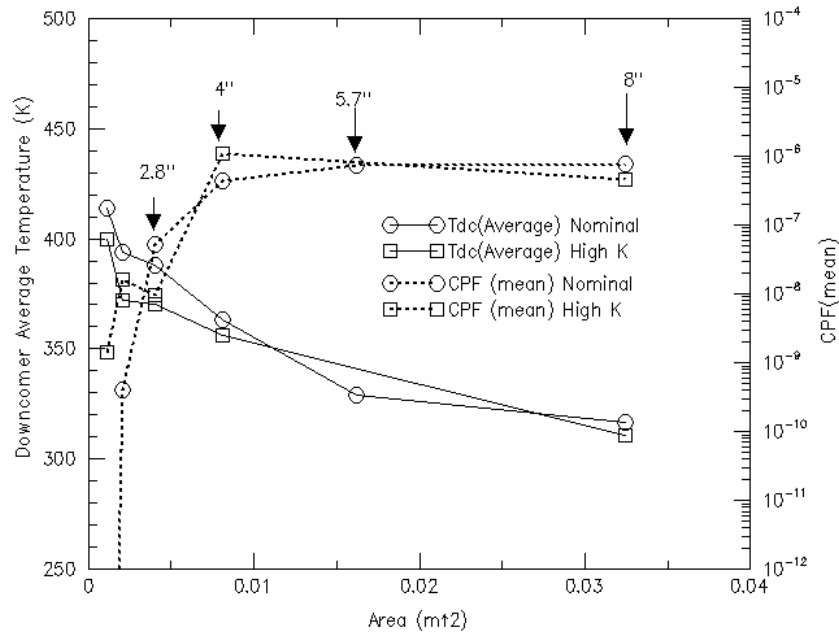


Figure 8-23 Loop recirculation flow effect on T_{sen} and CPF

8.2.9 Pressurizer SRV Reclose Timing and HPI Throttling Timing

The above discussed the influencing parameters for LOCAs where the break cannot be isolated. For the scenarios with isolable breaks, that is, pressurizer SRV stuck open scenarios, additional factors need to be considered, in particular, the time of valve reclosure and for control of HPI flow. Since these two factors are related, their effects are discussed together.

Figures 8.24 and 8.25 compare the CPFs for the combined effect of the pressurizer SRV reclosure time (50 min and 100 min) and the HPI throttling time, for high decay heat and low decay heat scenarios, respectively. Earlier valve reclosure (50 min) reduces CPF significantly, especially when combined with low decay heat. Early HPI throttling (1 min) reduces CPF by more than two orders of magnitude. If HPI is not throttled within 10 minutes of permitted, it is too late; subsequent throttling has no effect on CPF.

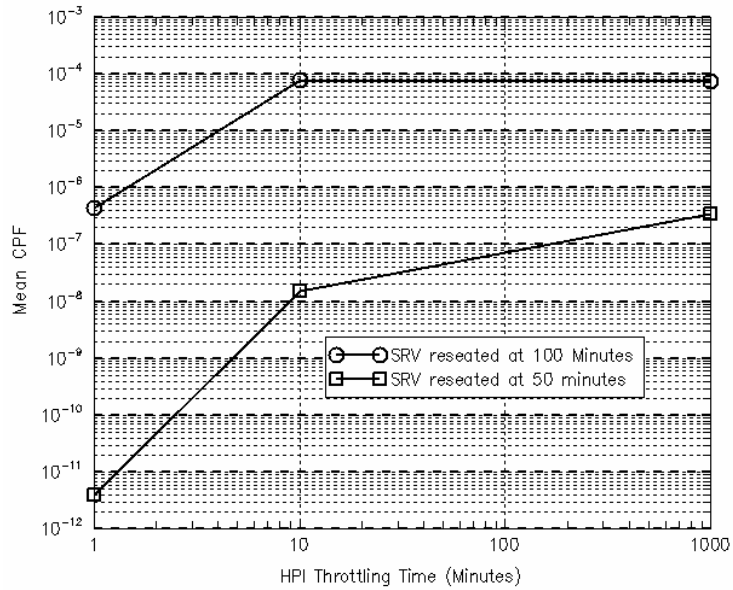


Figure 8-24 CPFs of varying pressurizer SRV reclosure times and HPI throttling times (full power)

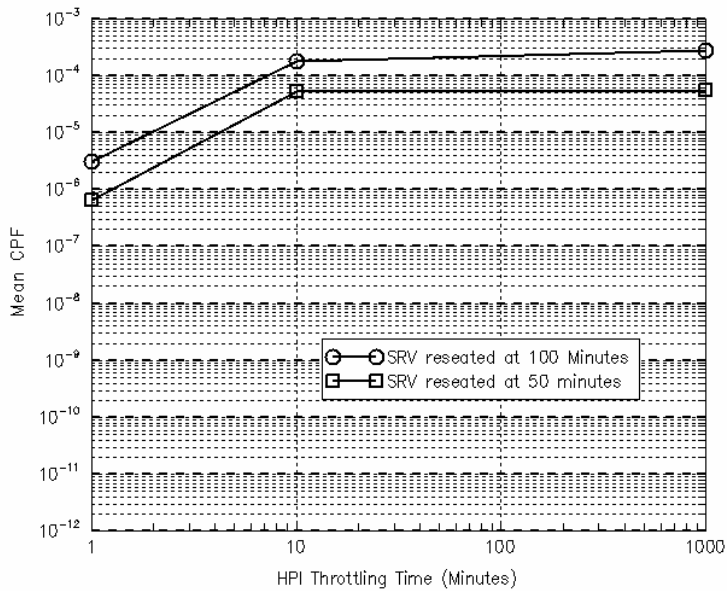


Figure 8-25 CPFs of varying pressurizer SRV reclosure times and HPI throttling times (low decay heat)

8.3 Parameter Ranking

Section 8.2 discussed the sensitivity of the various parameters in terms of T_{sen} and CPF. These results were used to establish the importance ranking of the parameters. Figures 8.26 to 8.29 compare the sensitivity studies performed for the key influencing parameters for four different LOCA break sizes for Oconee-1, in terms of T_{sen} and CPF. Figures 8.30 to 8.33 is a similar comparison for the same four break sizes for Beaver Valley. The table on the right of each figure ranks the parameter importance based on T_{sen} . Figures 8.26 to 8.33 show that the trends of T_{sen} and CPF are not always consistent for a given break size. The figures, however, show that in general there is consistency of the T_{sen} and CPF trends for a given parameter at different break sizes.

Some observations are discussed. First, trends of T_{sen} and CPF show coherence for breaks $> \sim 4$ inch. Some incoherence occurs for smaller sized LOCAs $< \sim 4$ inch. For small LOCA scenarios, the pressure effect might not be negligible and, in general, the outcome is more sensitive to other parameters such as break location. The use of T_{sen} assumes that the pressure effect is of second order importance. Second, T_{sen} is calculated based on the averaged T_{dc} for a long period of time (10,000 seconds). T_{sen} may not provide sufficient resolution to reflect the differences among small LOCAs, including the effects of dT_{dc}/dt .

Both $T_{dc}(t)$ and $dT_{dc}(t)/dt$ impact the determination of CPF. Figure 8-34 plots the minimum T_{dc} against CPF for all the Oconee-1 sensitivity studies. Scenarios with the lowest T_{dc} usually have larger CPFs, however, this is not always true. Figures 8.35 and 8.36 plot the lowest $dT_{dc}(t)/dt$ against CPF, where $dT_{dc}(t)/dt$ is averaged over 5 minute and 10 minute time intervals, beginning after T_{dc} falls below 422K (300F). The two figures show that, in general, a more rapid T_{dc} decrease is worse, but the relationship is not strong. The timing of variation in T_{dc} and dT_{dc}/dt is another important factor.

Figure 8-37 shows that Oconee-1, Beaver Valley, and Palisades have similar, but not identical, trends when comparing the effect of break size on CPF. Palisades has a maximum CPF at a break size about 4 inch; Beaver Valley tends to have its maximum CPF for breaks larger than 8 inch; Oconee-1 has its maximum CPF for breaks between 4 inch and 8 inch.

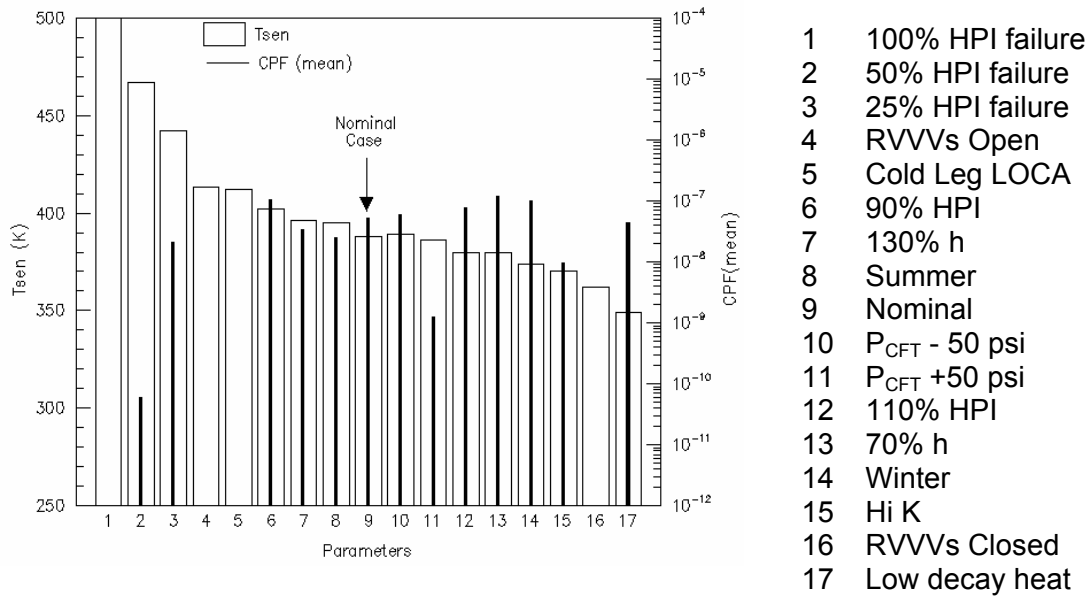


Figure 8-26 T_{sen} and mean CPF of the key influencing parameters for Oconee-1 2.8-inch LOCA

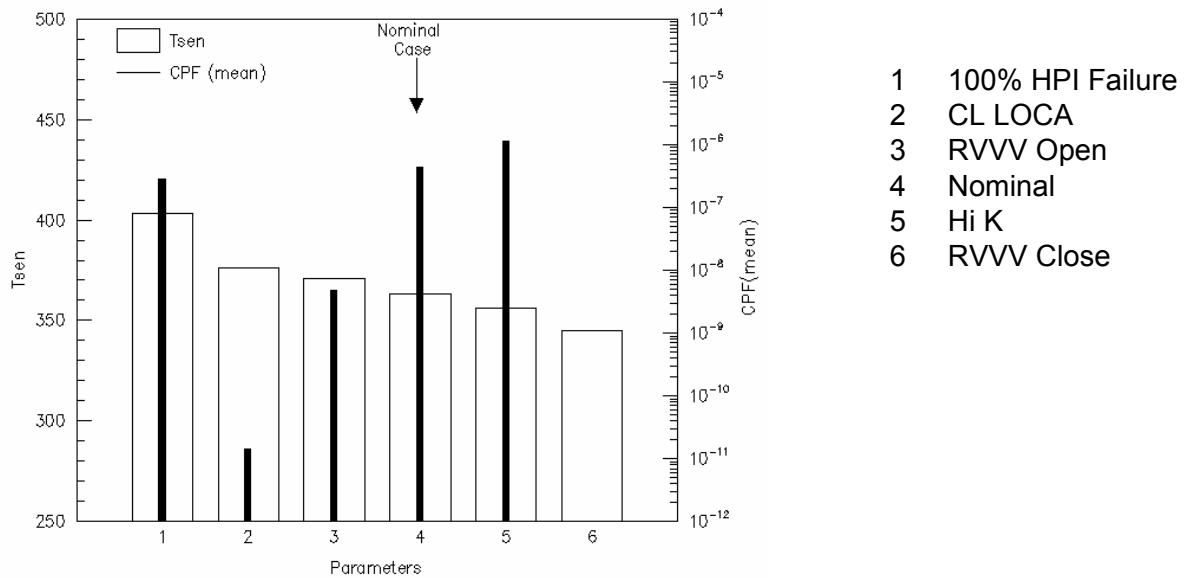


Figure 8-27 T_{sen} and CPF of the key influencing parameters for Oconee-1 4-inch LOCA

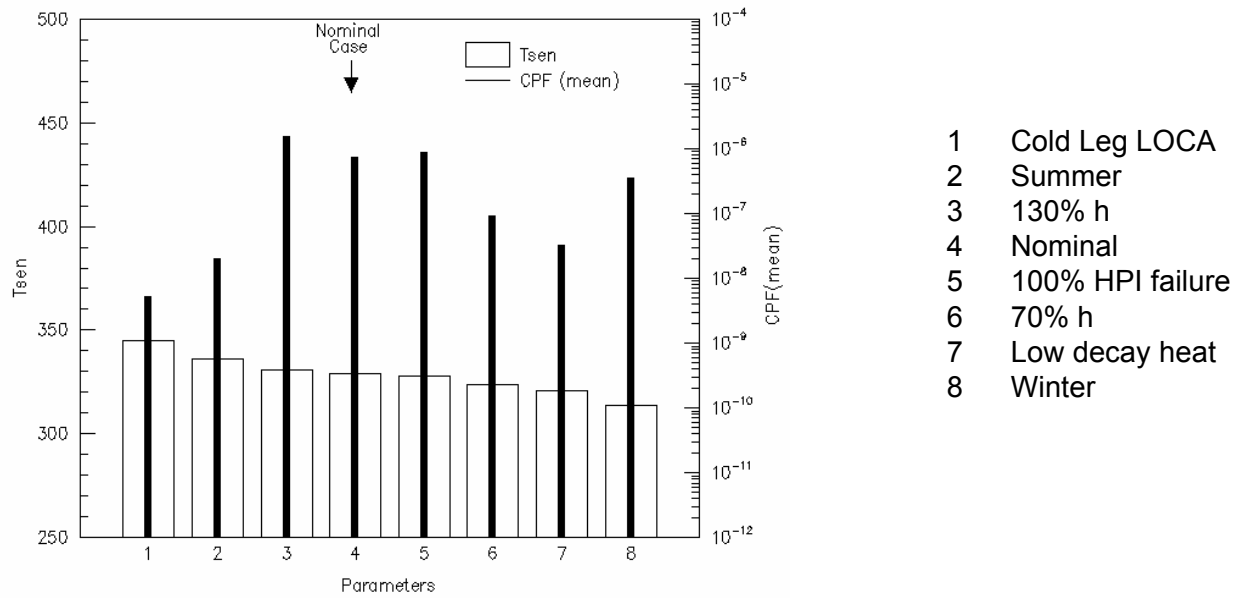


Figure 8-28 T_{sen} and CPF of key influencing parameters for Oconee-1 5.7-inch LOCA

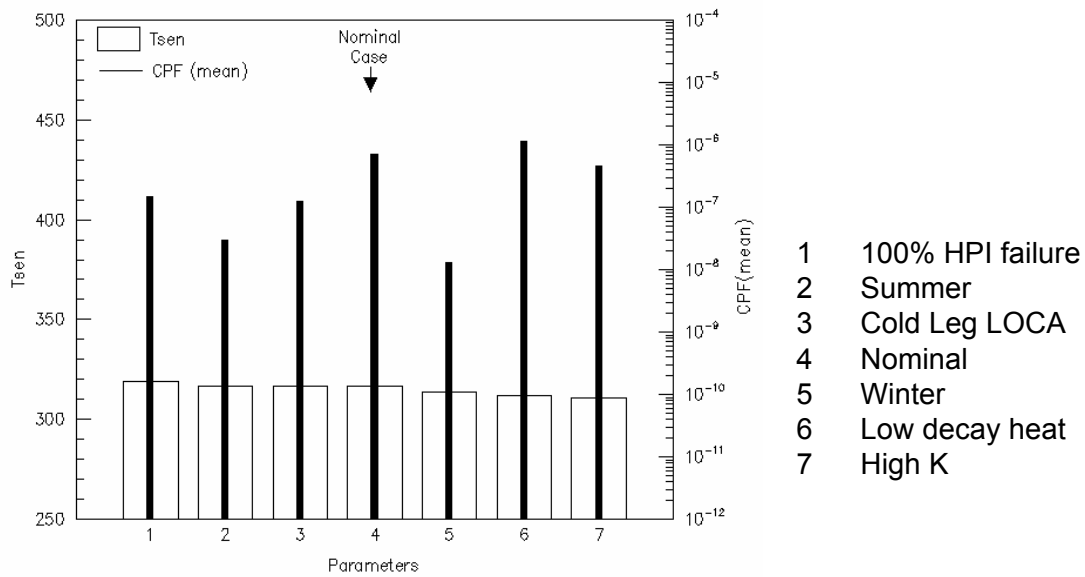
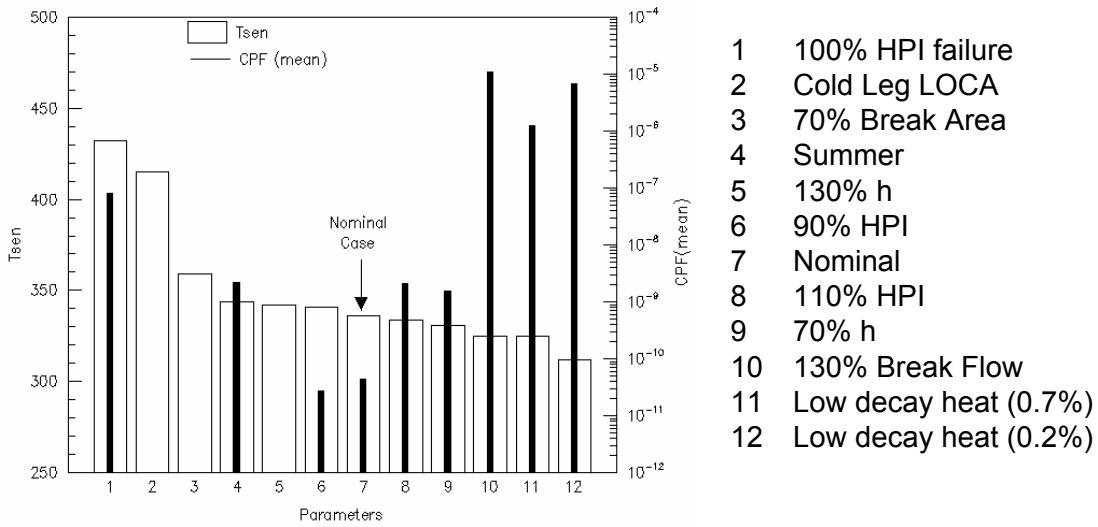
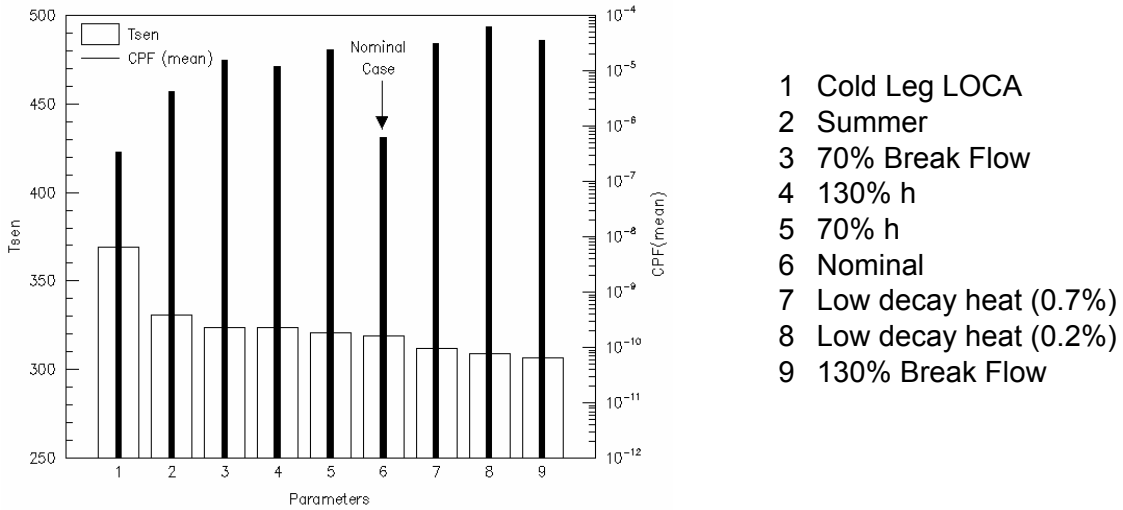


Figure 8-29 T_{sen} and CPF for key influencing parameters for Oconee-1 8-inch LOCA



- 1 100% HPI failure
- 2 Cold Leg LOCA
- 3 70% Break Area
- 4 Summer
- 5 130% h
- 6 90% HPI
- 7 Nominal
- 8 110% HPI
- 9 70% h
- 10 130% Break Flow
- 11 Low decay heat (0.7%)
- 12 Low decay heat (0.2%)

Figure 8-30 T_{sen} and CPF of influencing parameters for Beaver Valley 2.8-inch LOCA



- 1 Cold Leg LOCA
- 2 Summer
- 3 70% Break Flow
- 4 130% h
- 5 70% h
- 6 Nominal
- 7 Low decay heat (0.7%)
- 8 Low decay heat (0.2%)
- 9 130% Break Flow

Figure 8-31 T_{sen} and CPF for influencing parameters for Beaver Valley 4-inch LOCA

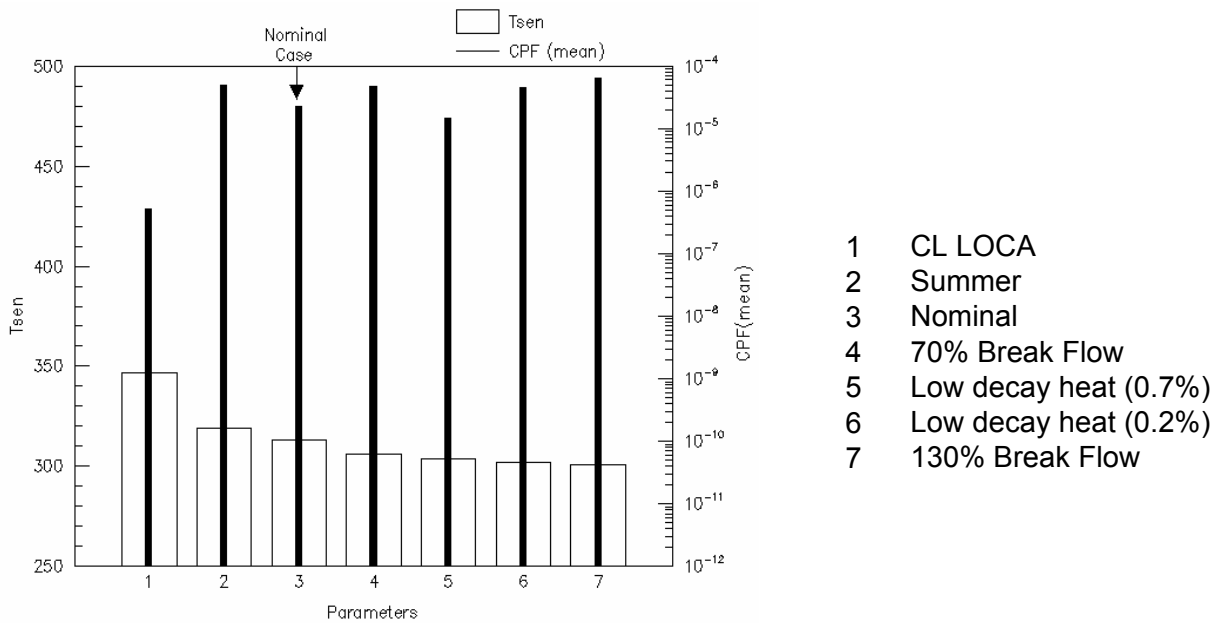


Figure 8-32 T_{sen} and CPF for influencing parameters for Beaver Valley 5.7-inch LOCA

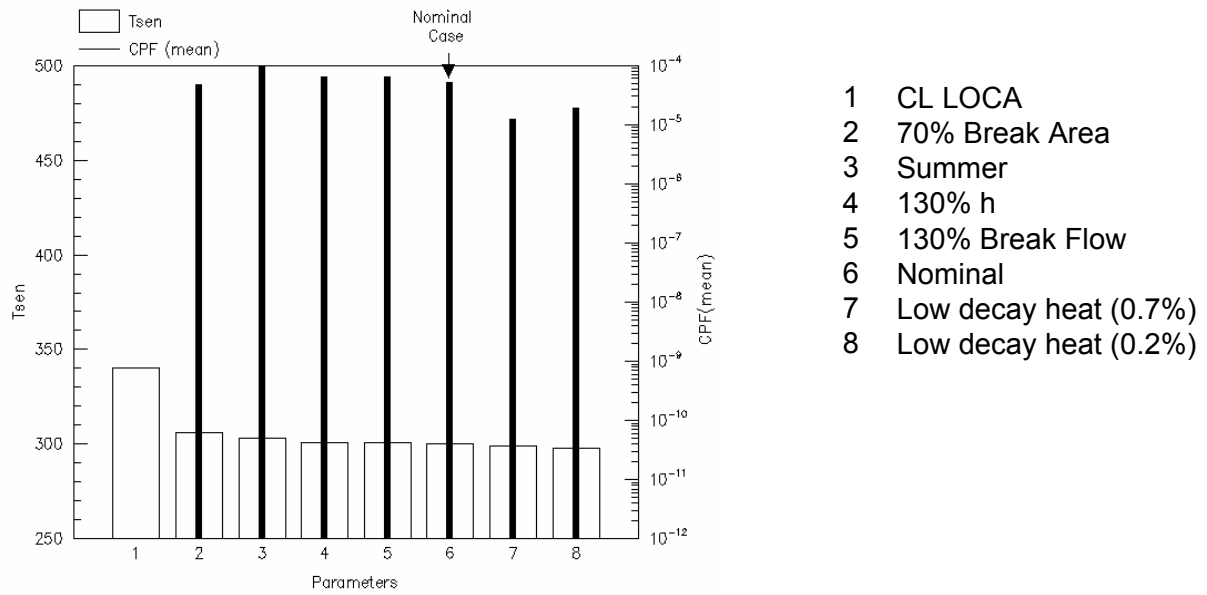


Figure 8-33 T_{sen} and CPF for the key influencing parameters for Beaver Valley 8-inch LOCA

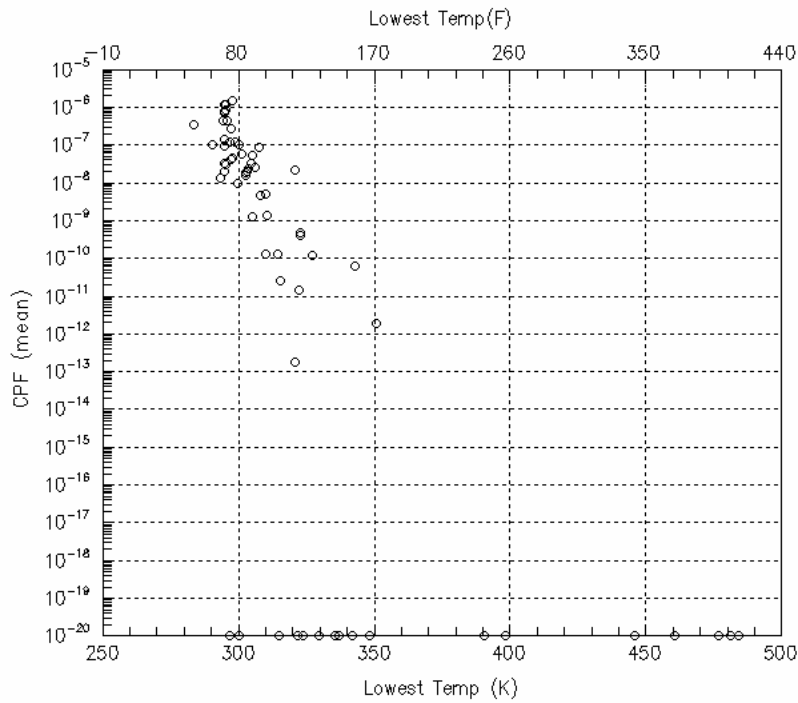


Figure 8-34 Lowest T_{dc} versus CPF for the Oconee sensitivity studies

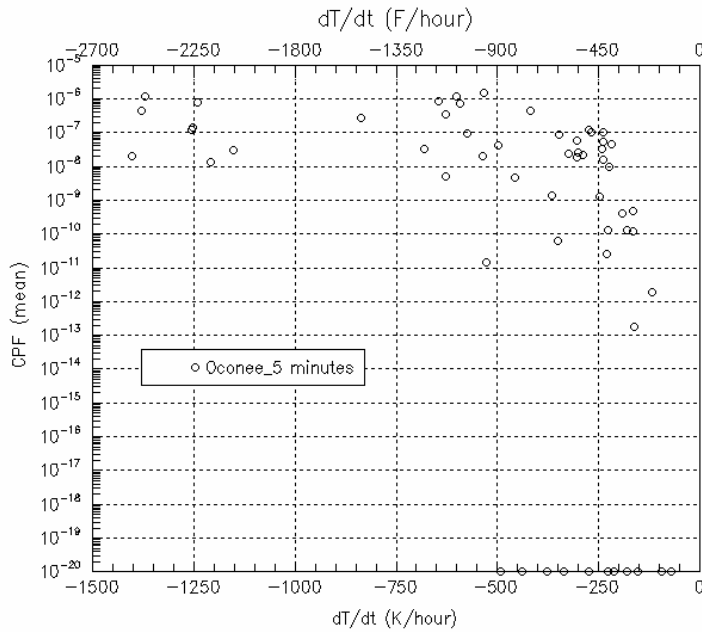


Figure 8-35 Lowest dT_{dc}/dt versus CPF for the Oconee sensitivity studies. The data are calculated when T_{dc} is less than 422K (300F) and the calculating time interval is five minutes.

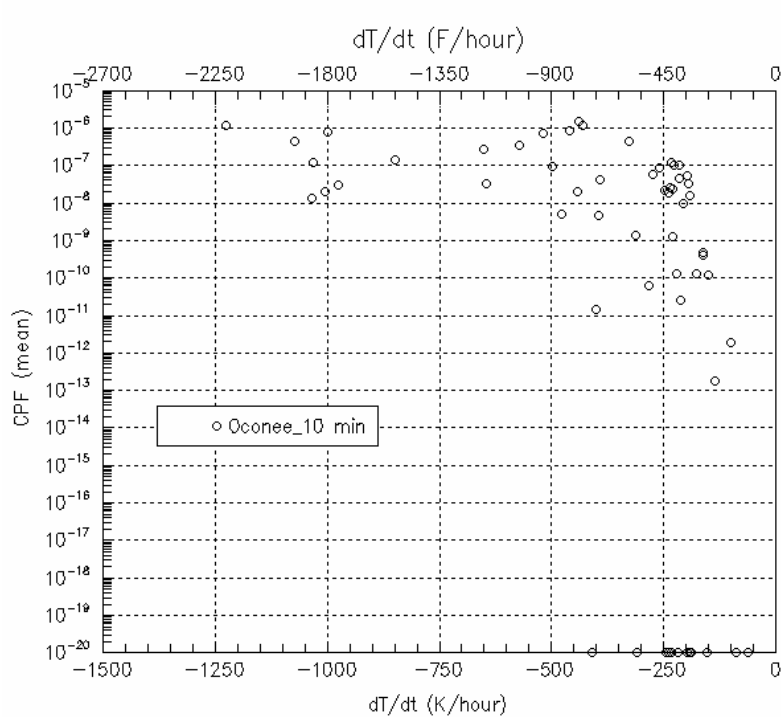


Figure 8-36 Lowest dT_{dc}/dt versus CPF Oconee sensitivity studies. The data are calculated when T_{dc} is less than 422K (300F) and the calculating time interval is ten minutes.

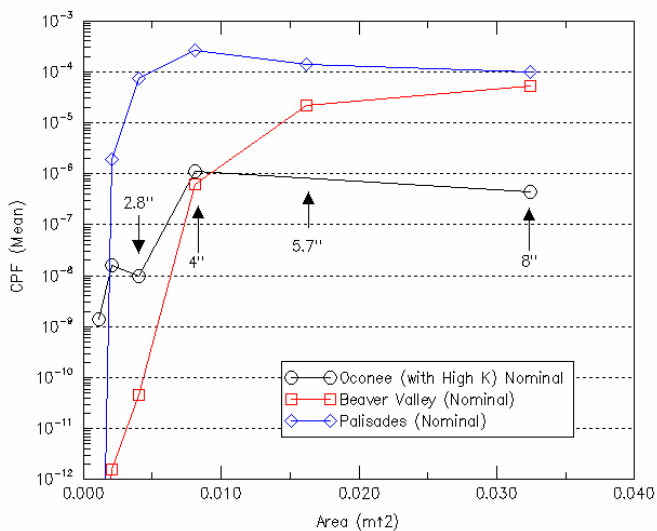


Figure 8-37 CPF versus LOCA size for Oconee, Beaver Valley, and Palisades

9. SUMMARY AND CONCLUSIONS

This report describes the thermal hydraulic uncertainty analysis and process used as input to determining overall uncertainty for PTS risk. The uncertainty analysis was performed for the Oconee, Beaver Valley, and Palisades plants. A top-down approach was used to identify the key factors affecting thermal stress and pressure stress applied to RPV wall. Sensitivity analyses were performed to rank these factors and to identify the uncertainty representative scenarios.

The analysis was coordinated with PRA model development to specify and identify the “scenario bins” which were PTS risk significant for further detailed uncertainty analysis. Each plant’s PTS PRA model contained more than ten thousand PTS risk scenarios. These scenarios were grouped (or binned) into a number of categories (or “Bins”) based on their TH similarities to PTS challenge. Example bins were small LOCA, medium LOCA, large LOCA, SRV stuck open, SG overfeed, and MSLB. A few scenarios, typically between 3 and 5, from each Bin were identified to represent its uncertainty. The probabilities of these representative scenarios were calculated along with their time histories of temperature, pressure, and heat transfer coefficient in the downcomer region (i.e., T_{dc} , P_{dc} , and h_{dc}) were transferred to the PFM group for calculating the final PTS risk.

Identification of the uncertainty representative scenarios considered factors beyond those which have been considered in the PRA model. Thus, each representative scenario can be specified with great detail for RELAP5 calculation. The following summarizes the TH uncertainty analysis.

STEP 1: Construct PTS Event Classification Matrix

Thermal stress and *pressure stress* are the two stressors that cause RPV failure. The main factors affecting thermal stress at high-level are:

- **Heat capacities** of the RCS
- **Heat sources** to RCS including core decay heat and heat generated from the RCP pumps. In some situations, the steam generators are heat sources to the RCS.
- **Heat sinks** to RCS such as loss of enthalpy from or gaining “negative” enthalpy to the RCS. Examples are primary system breach (e.g., LOCA, open PZR valves), steam generators, and HPI.
- **RCS energy distribution:** This is affected by the type of flow in RCS which can be forced circulation, natural circulation, or stagnated flow. Forced circulation causes the RCS to be well mixed resulting in less PTS risk. RCP state a deterministic factor for having a forced circulation.
- **RPV internal fluid/steam energy distribution:** could cause short term temperature instability within the downcomer. Examples are plume effects and steam condensation (caused for example by opening of the reactor vessel vent valves).

- **Rate of heat transfer from RPV structure to downcomer fluid:** the heat transfer coefficient (i.e., h_{dc}) was an important factor affecting the rate of enthalpy exchange between RPV wall and downcomer fluid.

The main factors affecting the pressure stress were:

- **Change in RCS coolant inventory** (e.g., loss of RCS inventory due to breach)
- **Change in net energy lost by RCS**
- **Steam condensation in RCS**
- **HPI filling the RCS until it is water solid with pressure determined by the pressurizer SRV**

PFM studies provided useful information to screen the PTS risk-significant scenarios including:

- T_{dc} lower than 300°F in order to fail RPV wall due to temperature dependent characteristics of materials properties
- PTS risk was more sensitive to change in T_{dc} than change in P_{dc} except for stuck open pressurizer SRV reclosure cases
- P_{dc} effect was significant when scenarios involving RCS repressurization

A wide range of events were screened to identify the event categories which were PTS risk significant. It was concluded that only three event categories, individually or combined, could significantly reduce T_{dc} to have PTS risk. These three event categories were primary system breach, secondary system breach, and secondary system overfed. A PTS event classification matrix was developed based on above conclusion to facilitate the analysis.

The primary system state was divided into three regions: integral, breach with forced circulation in RCS, and breach with natural or stagnated flow in RCS. The boundary between the latter two regions was determined by whether RCS lost subcooling margin. When subcooling margin is lost, the RCPs are tripped by operators. The RCS subcooling margin depends on whether HPI flow is sufficient to compensate for breach flow, and thus for the pressurizer to maintain pressure control. Sensitivity studies showed that HPI flow can maintain RCS subcooling for break sizes up to about 1.5 inches.

The other means of classification was the secondary system state, which was divided into four categories based on types of event (i.e., breach and overfed).

The PTS event classification matrix facilitated uncertainty analysis from two perspectives: firstly, through well defined event classification the number of uncertainty parameters needed to be considered was reduced; and secondly, the matrix provided a framework for preliminary event screening based on event frequencies.

STEP 2: Prioritize analysis effort

The main purpose of this step was to identify the high PTS-risk event categories in order to concentrate the analysis effort. An iterative process between the PRA, PFM, and TH work groups was required in this step.

In the PTS event classification matrix, the event category of primary system having greater than 1.5 inches breach and secondary system remaining integral contributed about 95% of the frequency of PTS-risk scenarios. The PFM group found that this event category had the most significant conditional PTS challenge. Thus, the TH uncertainty analysis effort was focused on this event class.

For finer analysis, the primary system breach was divided into scenarios of LOCA and PZR valve stuck open. The LOCA scenarios were further sub-classified into three groups based on the break size: 1.5 ~ 4 inches, 4 ~ 8 inches, and larger than 8 inches.

STEP 3: Assess sensitivity of individual parameter on thermal stress

This step was measured the sensitivity of each key factor on T_{dc} in order to assess the combined sensitivity of multiple factors.

A measurement system needed to be developed for measuring the sensitivity. From the TH perspective, thermal stress was dependent on the $T_{dc}(t)$ and $dT_{dc}(t)/dt$. Since there were no known rules specifying how these two parameters affecting thermal stress, for simplicity, a sensitivity indicator, T_{sen} , was defined as the average $T_{dc}(t)$ over the first 10,000 seconds of a given transient.

The *one-factor-at-a-time* method was used to calculate an individual parameter's sensitivity. This was done typically by applying the parameter's lower bound, nominal, and upper bound values separately while maintaining other parameters at their nominal values or state to calculate T_{sen} . The parameter's sensitivity was determined by the differences of the values of T_{sen} .

STEP 4: Assess the parameters' combined effect on thermal stress

This step was based on the sensitivity results obtained in Step 3 to assess the combined effect of multiple parameters on thermal stress.

A linear additive method was used for aggregating multiple parameters' effects on thermal stress. This was based on the fact that the heat capacitance of the RCS downcomer remained nearly constant. Thus, the fluid temperature in downcomer was dependent on the net heat/energy change in this region. Since each parameter's effect can be seen as depositing or extracting energy into or from the downcomer, the linear additive method was a reasonable approach.

Validation on the assumption was performed, and results indicate that the linear additive was appropriate for this implementation. The validation was performed by comparing the predicted values of T_{sen} with those calculated by RELAP5 for a 7.18 cm (2.828 in) surge line break. Five samples were selected for this comparison that cover a variation of about 111 K (200°F) in T_{sen} . The trend of the predicted T_{sen} s was consistent with the trend from RELAP5 calculation, indicating that linear addition of sensitivity parameters was a reasonable assumption.

STEP 5: Identify the uncertainty representative scenarios

This step identified a few TH scenarios to represent the uncertainty of an event category.

The results generated in Step 4 (i.e., T_{sen} and probability values for a specific scenario) were first plotted as a probabilistic density function (PDF) diagram, which was then converted to a cumulative density function (CDF). The uncertainty representative scenarios were identified by the following sub-steps:

- (a) specify the number of scenarios to represent the uncertainty of the event category;
- (b) identify the corresponding percentiles of these representative scenarios in the CDF diagram;
- (c) calculate the conditional probability of each uncertainty representative scenario (identified in step b). The conditional probability was calculated based on the proportional percentage represented by the representative scenario; The event frequency of a representative scenario is the product of its conditional probability and its event frequency assigned by PRA group;
- (d) identify the T_{sen} s based on the percentiles of the representative scenarios (identified in step b) from the CDF diagram;
- (e) the uncertainty representative scenarios can be identified by selecting the scenarios having the similar T_{sen} s from the list of scenarios identified in STEP 4. RELAP5 calculations were performed to calculate the time histories of T_{dc} , P_{dc} , and h_{dc} of these scenarios. The time histories of these three parameters along with their event frequencies (i.e., calculated in sub-step c) were transferred to PFM group for the final PTS risk calculation.

The importance of parameters can be ranked based on the sensitivity assessment results calculated in STEP 3. Higher ΔT_{sen} indicates lower TWCP since less thermal stress is imposed on the RPV wall. For example, failure of HPI at a 2.8-inch LOCA increases T_{sen} more than 100°K, which is expected to reduce thermal stress dramatically consequently reducing the PTS risk. The importance ranking of the key parameters is inversely corresponding to their ranking in ΔT_{sen} .

It is important to note that ΔT_{sen} only represents effect of thermal stress and not pressure stress. Pressure stress was specifically considered in the scenarios involving RCS repressurization.

Both $T_{dc}(t)$ and $dT_{dc}(t)/dt$ impact the determination of CPF. In general, a more rapid T_{dc} decrease is worse, but the relationship is not strong. The timing of variation in T_{dc} and dT_{dc}/dt is another important factor. Scenarios with the lowest T_{dc} usually have larger CPFs, however, this is not always true. Trends of T_{sen} and CPF show coherence for breaks $> \sim 4$ inch. Some incoherence occurs for smaller sized LOCAs $< \sim 4$ inch. In small LOCA scenarios, the pressure effect might not be negligible and, in general, the outcome is more sensitive to other parameters such as break location. The use of T_{sen} assumes that the pressure effect is of second order importance. Second, T_{sen} is calculated based on the averaged T_{dc} for a long period of time (10,000 seconds).

An important conclusion is, that short of running FAVOR, there is no simple way to accurately predict the CPF of a scenario based on examining the thermal hydraulic input.

10. REFERENCES

Almenas K., M. di Marzo, Z. Wang, and Y.Y. Hsu "The Phenomenology of a Small Break LOCA in a Complex Thermal Hydraulic Loop", Nuclear Engineering and Design, Vol. 110, pp. 107-116, 1988

Arcieri, W. C., R. M. Beaton, T. M. Lee and D. Bessette, "RELAP5 Thermal Hydraulic Analysis to Support PTS Evaluations for the Oconee-1 Nuclear Power Plant," Washington D.C., U.S. Nuclear Regulatory Commission, NUREG/CR-6858, September 2004

Bass, B. R., C. E. Pugh, J. Sievers and H. Schulz (1999), "International Comparative Assessment Study of Pressurized Thermal Shock in Reactor Pressure Vessels," Washington, D.C., U.S. Nuclear Regulatory Commission, NUREG/CR-6651, 1999

Bessette, D., "Thermal Hydraulic Evaluations of Pressurized Thermal Shock," NUREG-1809, U.S. Nuclear Regulatory Commission, October, 2004

Boyack, B. E., I. Catton, R. B. Duffey, P. Griffith, K. R. Katsma, G. S. Lellouche, S. Levy, U. S. Rohatgi, G. E. Wilson, W. Wulff and N. Zuber, "Quantifying Reactor Safety Margins, Part 1: An Overview of the Code Scaling, Applicability, and Uncertainty Evaluation Methodology," Nuclear Engineering and Design **119**: 1-15, 1990

Boyd, C. F. and T. Dickson, "Impact of the Heat Transfer Coefficient on Pressurized Thermal Shock," U.S. Nuclear Regulatory Commission, NUREG-1667, 1999

Burns, T. J., R. D. Cheverton, G. F. Flanagan, J. D. White, D. G. Ball, L. B. Lamonica and R. Olson, "Preliminary Development of an Integrated Approach to the Evaluation of Pressurized Thermal Shock as Applied to the Oconee Unit 1 Nuclear Power Plant," Washington D.C., U.S. Nuclear Regulatory Commission, NUREG/CR-3770, 1986

Cullen, A. C. and H. C. Frey, "Probabilistic Techniques in Exposure Assessment," New York, Plenum Press, 1999

Determan, J. C. and C. E. Hendrix, "Development of a SCDAP/RELAP5/MOD3 Model of Oconee 1 for Use With The Nuclear Plant Analyzer," Idaho National Engineering Laboratory, EGG-EAST-9793, 1991

Dickson, T. L., R. D. Cheverton, J. W. Bryson and B. R. Bass, "Pressurized Thermal Shock Probabilistic Fracture Mechanics Sensitivity Analysis for Yankee Rowe Reactor Pressure Vessel," Washington D.C., U.S. Nuclear Regulatory Commission, NUREG/CR-5782, August 1993

Frey, H. C. and S. R. Patil, "Identification and Review of Sensitivity Analysis Methods," Risk Analysis **22** (3): 553-578, 2002

Hanson, D. J., O. R. Meyer, H. S. Blackman, W. R. Nelson and B. P. Hallbert, "Evaluation of Operational Safety at Babcock and Wilcox Plants, Volumes 1 and 2," Washington D.C., U.S. Nuclear Regulatory Commission, NUREG/CR-4966, 1987

Henry, R. E. and H. K. Fauske, "The Two-Phase Critical Flow of One Convective Mixtures in Nozzles, Orifices and Steam Tubes," Journal of Heat Transfer **93**: 724-737, 1971

Ikonen, K., "Shallow Crack Effect on Brittle Fracture of Vessel During Pressurized Thermal Shock," Finnish Centre for Radiation and Nuclear Safety, Helsinki, STUK-YTO-TR-98; DE97616026, 1985

Mahaffy, J. H., "A Stability Enhancing Two-Step Method for Fluid Flow Calculations," Journal of Computational Physics, **40**: 329-341, 1981

Palmrose, D., "Demonstration of Pressurized Thermal Shock Thermal-Hydraulic Analysis with Uncertainty," Washington D.C., U.S. Nuclear Regulatory Commission, NUREG/CR-5452, March 1999

Pugh, C. E. and B. R. Bass, "Review of Large-Scale Fracture Experiments Relevant to Pressure Vessel Integrity Under Pressurized Thermal Shock Conditions," Washington D.C., U.S. Nuclear Regulatory Commission, NUREG/CR-6699, January 2001

Queral, C., J. Mulas and C. G. de la Rúa, "Analysis of the RELAP5/MOD3.2.2 β Critical Flow Models and Assessment Against Critical Flow Data from the Marviken Tests," Washington, D.C., U.S. Nuclear Regulatory Commission. NUREG/IA-0186, July 2000

Quick, K. S., "Oconee Unit 1 Pressurized Water Reactor RELAP5/MOD3 Input Model," Washington, D.C., U.S. Nuclear Regulatory Commission, DOE Contract No. DE-AC07-76IDO1570, August 1994

Ransom, V. H. and D. L. Hicks, "Hyperbolic Two-Pressure Models for Two-Phase Flows," Journal of Computational Physics **53**: 124-151, 1984

Ransom, V. H. and J. A. Trap, "The RELAP5 Choked Flow Model and Application to a Large Scale Flow Test," ANS/ASME/NRC International Topical Meeting, Saratoga Springs, NY, 1980

Riemke, R. and G.B. Johnsen, "The Recirculation flow Anomaly," Washington DC, Idaho National Engineering Laboratory, EGG-EAST-9365, January 1994

Rosdahl, O. and D. Caraher, "Assessment of RELAP5/MOD2 Against Critical Flow Data From Marviken," Washington DC, U.S. Nuclear Regulatory Commission, NUREG/IA-0007, September 1986

Rosenthal, J. (2001), "Status of Thermal Hydraulic PTS Calculations," Internal Memorandum, U.S. Nuclear Regulatory Commission, August 20, 2001

Selby, D. L., D. G. Ball, R. D. Cheverton, G. F. Flanagan and P. N. Austin, "Pressurized Thermal Shock Evaluation of the H. B. Robinson Unit 2 Nuclear Power Plant," Washington DC, U.S. Nuclear Regulatory Commission. NUREG/CR-4183, September 1985

Selby, D. L., D. G. Ball, R. D. Cheverton, G. F. Flanagan, W. T. Hensley, J. D. White, P. A. Austin, D. Bozarth, L. B. Lamonica, A. McBride, J. H. Jo, P. Gherson, K. Iyer, H. P. Nourbakhsh, T. G. Theofanous, P. Humphreys, L. D. Phillips, D. Embrey and L. S. Abbott, "Pressurized Thermal Shock Evaluation of the Calvert Cliffs Unit 1 Nuclear Power Plant," Washington D.C. NUREG/CR-4022, October 9, 1984

Theofanous, T. G. and H. Yan, "Unified Interpretation of One-Fifth to Full-Scale Thermal Mixing Experiments Related to Pressurized Thermal Shock," Washington D.C., U.S. Nuclear Regulatory Commission, NUREG/CR-5677, 1991

Wang, Z. and K. Almenas, "A Methodology Quantifying the Range of Applicability of Scaling Laws," Nuclear Science & Engineering **102** (1): 101-113, 1989

Wang Z., K. Almenas, M. di Marzo, Y.Y. Hsu and C. Unal, "Impact of Rapid Condensation of Large Vapor Spaces on Natural Circulation in Integral Systems," Nuclear Engineering and Design, Vol. 133, pp 285-300, 1992

Weisman, J. and A. Tentner (1978). "Models for Estimation of Critical Flow in Two-Phase Systems." Proceedings of Nuclear Energy **2**: 183-197.

Appendix A. Uncertainty Characteristics and Classification

This Appendix discusses thermal hydraulic-based uncertainty characteristics and classifications, based on mass and energy, to classify PTS relevant phenomena. Section A.1 classifies uncertainty according to three modes of uncertainty propagation: damped, proportional, and augmented. The important PTS risk factor, RCS flow state, is classified based on the modes of uncertainty propagation. The RCS flow states include forced circulation, natural circulation, and flow stagnation. Section A.2 classifies RCS flow state based on the change of coolant inventory and energy inside RCS. Section A.3 discusses flow state at different percentages of RCS inventory loss for a LOCA scenario

A.1 Characteristics of Uncertainty Propagation

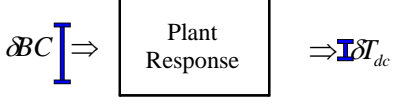
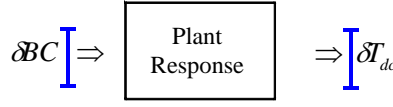
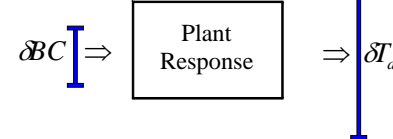
This section discusses the uncertainty ranges of T_{dc} caused by the uncertainty of different parameters. Three types of the T_{dc} uncertainty behaviors are classified: damped, proportional, and augmented (Table A-1).

The most prevalent, (in terms of number of PRA determined scenarios and their probability) is the damped mode. This is also the consequence of the dominant nature of \dot{Q}_{SG} . Basically, as long as the secondary side remains intact and natural or forced circulation is maintained, the thermal hydraulic conditions of the primary side will be determined by the conditions in the steam generators. Perturbations occurring in the primary side will then have little effect. For example, even large variations (on the order of factors of 2 or more) in the decay heat will, for this category of transients, produce minor variations in T_{dc} .

The proportional transformation mode is associated primarily with malfunctions on the secondary side. The energy removed by the steam generators, \dot{Q}_{SG} , is by far the dominant heat sink, and the uncertainty in its magnitude is transformed proportionally into uncertainties of T_{dc} . Another condition for which uncertainty is transmitted proportionally concerns the temperature difference between the fluid temperature at steam generator exit and the downcomer when HPI is operating, and RCPs are shut off. This difference is determined by the relative HPI and loop circulation flows. The uncertainties in these parameters therefore are reflected proportionally in the uncertainty of the temperature difference between T_{SG-out} and T_{dc} .

Finally, there is the category of transients for which the uncertainties can be augmented. Phenomena that can cause this transformation mode are a two-phase fluid state in the primary and a possibility that flow stagnation can occur. The 'augmentation' is introduced by the uncertainty associated with flow stagnation, which, in turn, depends on the sizable uncertainties associated with the evaluation of two-phase choked flow. Chapters A.1.1 to A.1.3 discuss the damped, proportional, and augmented uncertainty transmissions.

Table A.1 Classification of uncertainties according to their impact

Transformation type	Conditions and Parameters
<p><u>DAMPED</u></p> 	<ul style="list-style-type: none"> When SGs remain intact, and natural or forced circulation is maintained <p>$\Rightarrow \dot{Q}_{dec}, \dot{W} \& T_f$ of MFW, AFW, HPI flow & temp., SB LOCA flow</p>
<p><u>PROPORTIONAL</u></p> 	<ul style="list-style-type: none"> When P_{sec} is NOT controlled \Rightarrow e.g., TBV flow area, and valves open timing and time lapse When RCPs are OFF, and $\dot{Q}_{SG} \cong 0$ \Rightarrow HPI flow rate and temp.
<p><u>AUGMENTED</u></p> 	<ul style="list-style-type: none"> When primary side flow stagnation occurs \Rightarrow Break flow rate, HPI flow rate and temp.

A.2 Damped Uncertainty

The feed-bleed transient is well suited to illustrate the response of the T_{dc} parameter for conditions when the primary system is liquid solid and the source/sink terms are reasonably well known. System pressure for this type of transient remains fixed at the PORV setpoint pressure [for Oconee 170 bar (2460 psia)]. At such a high pressure, HPI flow is relatively low and is not able to remove the decay energy during the first ~6000 sec. The energy balance of the primary system is thus determined by two sources \dot{Q}_{dec} and \dot{Q}_{RCP} (when the RCPs are running) and by two sinks \dot{Q}_{SG} and HPI.

For this type of transient, it is the energy source side of the balance equation that can vary over a wider range and is thus subject to a larger uncertainty. An illustration of this is shown in Figure A.1, which depicts four possible time transients of the total energy source. The uppermost curve is \dot{Q}_{dec} plus \dot{Q}_{RCP} , where the decay heat curve is for infinite full power operation. The second curve includes \dot{Q}_{RCP} as before, but it is assumed low decay heat, with a brief return to power following a period of shutdown (hot zero power (HZP)). As shown, the difference in decay power generation is substantial. For the lower two curves it is assumed that the RCPs have been tripped, thus the heat source consists of \dot{Q}_{dec} alone. As Figure A.1 illustrates, the magnitude of the source varies significantly and for times longer than 1 hour, the difference between the limiting values can approach a factor of six. T_{dc} is determined by energy balance, thus it is appropriate to enquire what effect this large variation has on the downcomer temperature.

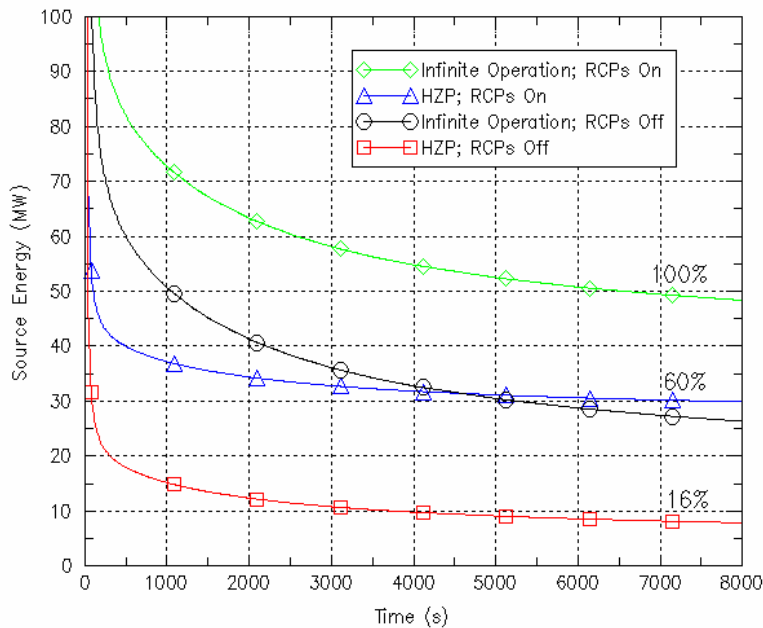


Figure A-1 Range of variation of energy source (decay heat + RCPs)

In contrast to some other safety related parameters (e.g. the fuel temperature), for PTS studies the direction of a conservative \dot{Q}_{dec} is reversed. Low \dot{Q}_{dec} , with other conditions being comparable, leads to lower temperatures and thus more severe PTS conditions. The magnitude of this influence was evaluated using RELAP5 for four nearly identical transients, which differ only in the magnitude of the time-dependent total energy source. The results, as reflected in T_{dc} , are shown in Figure A.2 for the case where RCPs are operating, and in Figure A.3 for the RCPs tripped condition. In Figure A.2, the temperature scale is significantly expanded. The two curves in Figure A.2, differences of up to 40% in the energy source term can hardly be distinguished. Similarly, for the natural circulation transients depicted in Figure A.3, where the energy source term differs by more than a factor of three, the resulting temperature difference is essentially zero.

The meaning of *damped uncertainty* is thus illustrated. The source of the damping effect is the large steam generator heat transfer area. From the steam generator point of view, the sources and sinks on the primary side could vary by almost an order of magnitude before the steam generator to primary temperature difference would increase noticeably. This implies that as long as the steam generator condition functions as a controlled heat sink, the secondary side determines the fluid conditions on the primary side. For such transients, thermal hydraulic uncertainties do not influence the PTS relevant parameters and thus do not matter.

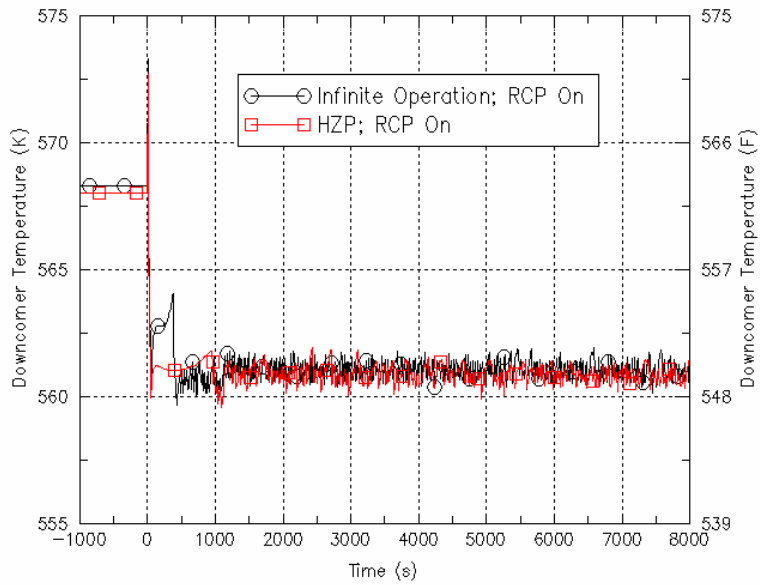


Figure A-2 $T_{dc}(t)$ comparing high power with hot zero power decay heat (RCPs on)

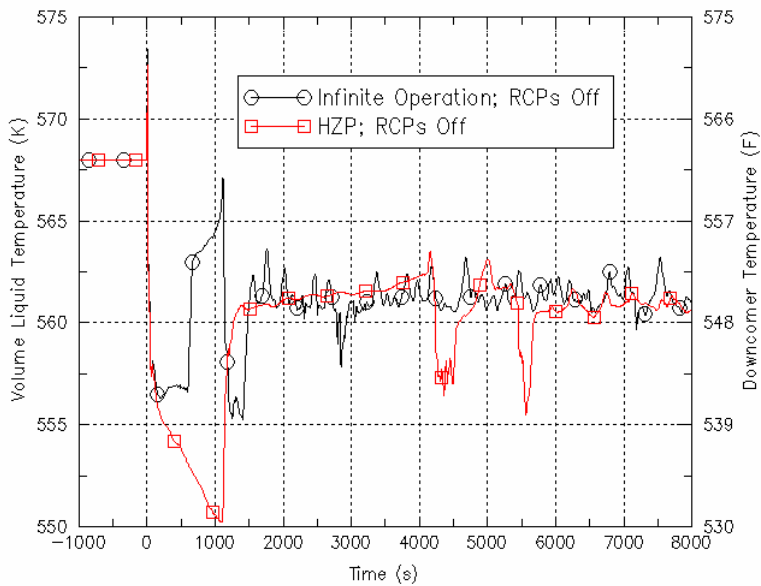


Figure A-3 $T_{dc}(t)$ comparing high power with hot zero power decay heat (RCPs off)

A.3 Proportional Uncertainty

The term *proportional* means, of a similar order of magnitude. That is, the uncertainty range of an independent variable (e.g. an imposed boundary condition like the flow area of a TBV) has an impact on the PTS-relevant dependent variables that is of a similar order of magnitude. While not a precise definition it is, nevertheless, useful. We illustrate by evaluating the effect on T_{dc} of two TBV stuck open scenarios; one valve in each steam generator compared to two valves in each steam generator.

Table A.2 classifies uncertainties for different possible conditions. For this type of transient, \dot{Q}_{SG} is not controlled since an uncontrolled heat sink has been introduced. The dominant boundary conditions contributing to the uncertainty are: A_{SG} , the “break” flow area from the steam generators; and \dot{Q}_{dec} , and the computed rate of mass and energy flow in the physical model uncertainty column. Assuming the same \dot{Q}_{dec} applies to both transients and that the break flow model exerts an equivalent influence, the changes in the boundary conditions thus are reduced to a change in the flow area. For two TBVs stuck open, the total break flow in the secondary side is 0.0622 m² (0.204 ft²). The second transient, with one TBV stuck open, has half the break area (0.0311 m²). The factor of two on break area is large relative other uncertainties in boundary conditions, and thus represents a severe test of the proportionality concept.

For the transient in which a single TBV fails, the intact steam generator becomes an energy source, while the lone sink is the on TBV. Figure A.4 shows that the pressures of both steam generators (upper curve in the figure) closely track each other. This is an additional illustration of the exceptionally large heat transfer area available. As shown in Figure A.5, the downcomer temperatures in both cases closely follow the steam generator secondary side temperature. The fluid temperature difference in the downcomer caused by the change in steam generator outflow area is ~30K, and this difference remains remarkably constant for the time period from 2000 s to 8000 s. The presented case study thus shows that a change of ~0.031 m² in the break area produces a change of ~30K in T_{dc} .

The illustrative example establishes a proportionality relationship between the outflow area in a steam generator and the temperature in the downcomer, however, the units of the parameters in question are so different that the reasons for this are not immediately apparent. A qualitative explanation can be gained by again considering Figure A.4. A change in the outflow area of the steam generator increases the energy loss term of the steam generator vapor region, and since the energy source terms and the heat capacities for both cases are equivalent, this produces a proportional decrease in pressure. The steam generators are at saturated conditions, thus the pressure change translates into a change in steam generator temperature. In Figure A.6 it is shown that the absolute value of the ΔT can be estimated along the saturation line. As shown, the inferred temperature change is ~30K. Since the primary system temperature closely follows the secondary temperature and since for this transient HPI is not actuated, this is close to the fluid temperature change in the downcomer.

Table A.2 Classification of PTS relevant transients based on propagation of uncertainties

Category (Dominant Energy Sinks)	Propagation of Uncertainty	Circulation Mode	Dominant Factor Contributing to Uncertainty	
			Boundary Condition	Physical Model
Feed and bleed \dot{Q}_{SG} controlled HPI-PORV	T_{dc} damped controlled P controlled	Forced	P_{sec}, T_{sec}	
SG cooldown \dot{Q}_{SG} controlled	T_{sg-dc} damped controlled P controlled ΔT_{sg-dc} proportional	Forced or Natural	P_{sec}, T_{sec} \dot{W}_{HPI}, T_{HPI}	\dot{W}_{circ}
Secondary transient \dot{Q}_{SG} uncontrolled 1. SG depressurized 2. SG overcooled	T_{dc} proportional P proportional ΔT_{sg-dc} proportional	Forced or Natural	1) $A_{SG-flow}, \dot{Q}_{dec}$ 2) $\dot{W}_{fw}, T_{fw}, \dot{Q}_{dec}$ \dot{W}_{HPI}, T_{HPI}	$\dot{W}_{brk}, \dot{Q}_{brk}$ \dot{W}_{circ}
LOCA \dot{Q}_{SG} not available $\dot{Q}_{brk} > \dot{Q}_{dec}, HPI$	T_{dc} augmented proportional P proportional	Natural or Flow Stagnation	$A_{brk}, \dot{Q}_{dec}, \dot{W}_{HPI}, T_{HPI}, A_{RVVV}$	$\dot{W}_{brk}, \dot{Q}_{brk}, \dot{W}_{RVVV}$

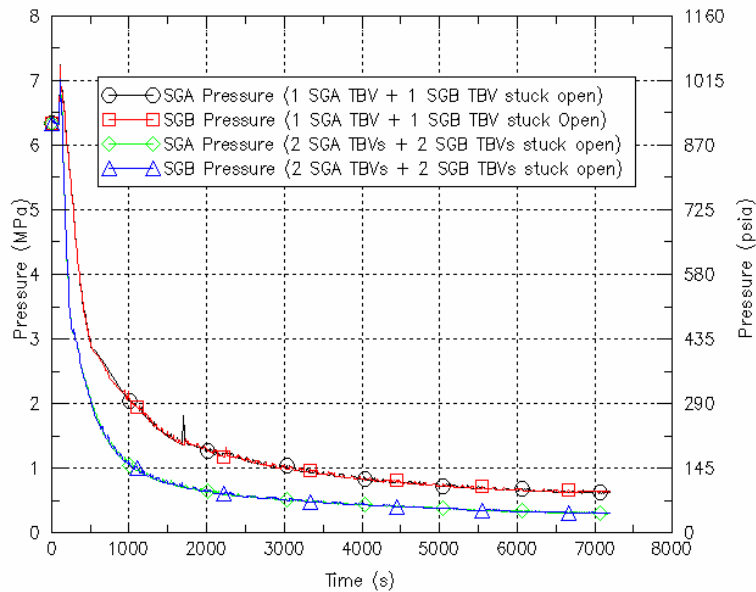


Figure A-4 Steam generator secondary side pressures for two and one TBVs stuck open per steam generator

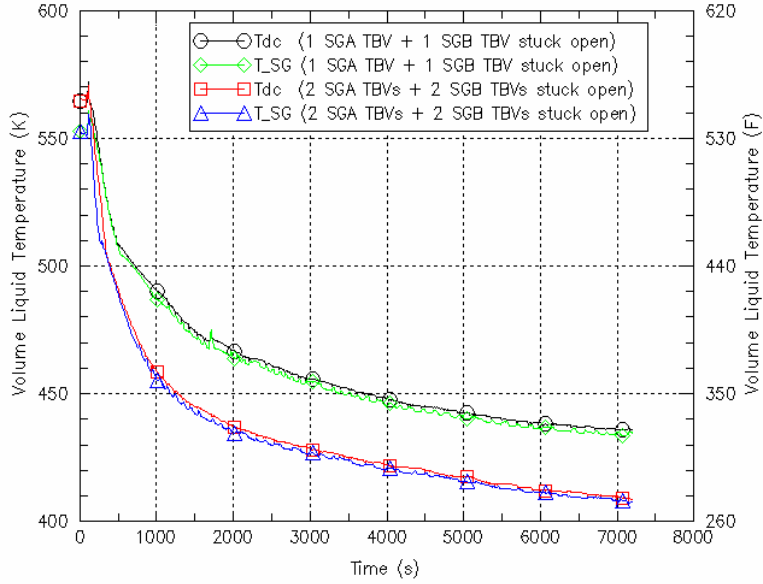


Figure A-5 Seam generator secondary side tube exit and RCS downcomer temperatures for two and one TBV(s) stuck open per steam generator

(downcomer temperature closely follows the steam generator secondary side temperature)

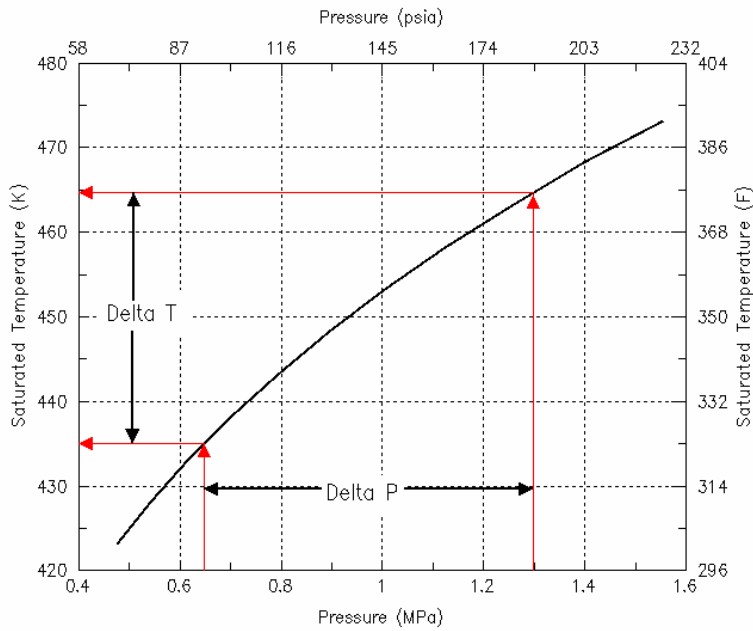


Figure A-6 Estimated ΔT by reflecting ΔP through saturation line

A.4 Augmented Uncertainty

Thermal hydraulic uncertainty analysis is considerably more complicated for transients in which regions within the primary become two-phase for significant time segments. The state of the fluid for such transients can deviate from thermal equilibrium, and the thermal hydraulic results then depend on the correct evaluation of energy/mass transfer rates. The volume-averaged approach employed by codes such as RELAP5 or TRAC then becomes a contributor to the uncertainty of the analytical results. An additional factor contributing significantly to the uncertainty is that, for a range of conditions, a change in the system wide flow pattern can be initiated by the loss of the steam generator heat sink. This leads to termination of loop circulation flow, or flow stagnation. This section illustrates *augmented uncertainty*.

Figure A.7 shows the computed downcomer temperatures for two small break LOCAs that are identical in all aspects except for the size of the break. For the upper T_{dc} trace the break is 1.54-inch, and for the lower trace it is 1.71-inch. The absolute difference in the break size is thus ~23%, whereas the downcomer fluid temperature difference at 5000 s is ~100K (compare to 100% change in break area and 30K in T_{dc} in the previous example). Clearly in this case, qualitatively different phenomena drive the transformation of a boundary condition difference into a divergence of the analytical results. The phenomenon in question is flow stagnation that occurs for the larger break and not for the smaller. Note that the difference in the break flows could very well be smaller and still produce this effect. No effort was made here to find the 'smallest' area difference, because the values chosen for the illustrative example already have a smaller difference than the uncertainty band imposed on this parameter by the boundary condition and model uncertainties.

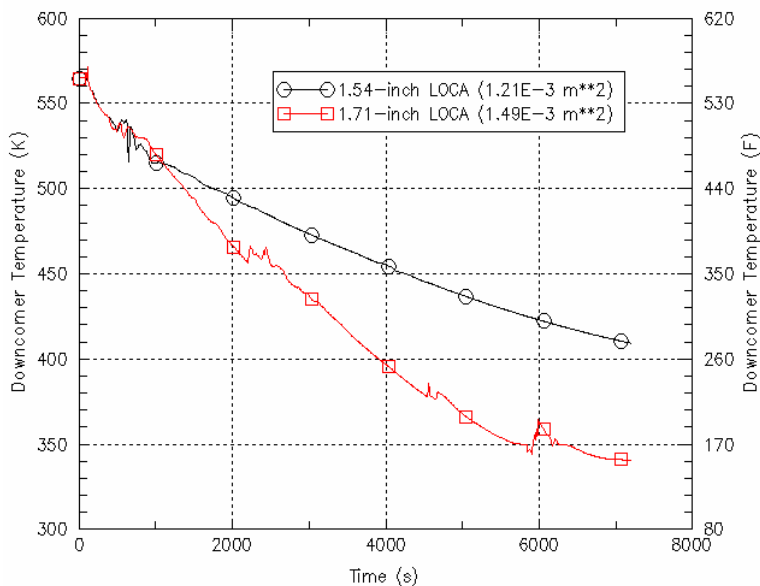


Figure A-7 T_{dc} for 1.71-inch and 1.54-inch surge line breaks
(no other system/component failures and no operator actions)

Table A.2 is a summary of the uncertainty categories and their dependence on boundary and analytical uncertainties. The second column lists the possible modes for the propagation of uncertainties of the PTS relevant parameters. Note that besides the two main parameters T_{dc} and P , it also includes ΔT_{sg-dc} , the difference in temperature between the secondary side of the steam generator and the fluid entering the downcomer. The distinction is useful because for some transients T_{sg} , can be determined by steam generator conditions, however, if the RCPs are off and HPI is on, the temperature of the fluid entering the downcomer is influenced by HPI flow and natural circulation or flow stagnation flows. The third and fourth columns list the operative circulation mode of the RCS and the dominant energy sinks.

Essential information for further analysis is provided in the split fourth column, which lists the parameters that affect the uncertainties of T_{dc} and P . They are divided into boundary condition and physical model uncertainties. The boundary condition uncertainty includes decay heat (\dot{Q}_{dec}), the HPI temperature (T_{HPI}), and the feed water flow rate (\dot{W}_{fw}). Note that some parameters, e.g. the HPI flow rate (\dot{W}_{HPI}) are not completely independent of the computed fluid state in the primary system and thus, to a degree, are also subject to physical model uncertainty. The classification follows what is judged to be the dominant characteristic.

On the physical model uncertainty side is the computed natural circulation flow (\dot{W}_{circ}). The circulation rate with RCPs running is not included, because it is so large in comparison to shutdown condition sinks/sources, that any uncertainty in its absolute value does not influence the PTS relevant parameters. Significant modeling uncertainties can be associated with the calculated mass (\dot{W}_{brk}) and energy outflow rates (\dot{Q}_{brk}) through breaks or stuck open valves. For conditions where flow stagnation occurs, internal circulation through the RVVVs becomes possible. Therefore the vent valve area (A_{RVVV}) is included in the boundary condition uncertainty column; and the computed flow through the valves (\dot{W}_{RVVV}) is included in the physical model column.

A.5 Classification of RCS Circulation Modes

The RCS circulation mode is an important factor for transients that exhibit augmented T_{dc} uncertainty. Except for limited times during overcooling transients, the primary system loops become saturated only during LOCAs. Loss of subcooling has a significant effect on the response of the plant and on the magnitude of the uncertainties associated with the evaluation of this response. The uncertainty band becomes considerably wider since,

- 1) Uncertainties of the boundary conditions are larger for two-phase conditions, since the boundary condition having the largest impact on transient response is the break flow. The influencing factors include the size, location, nature of the break opening, and the condition of the fluid near the break. All of these parameters are subject to sizable variability or uncertainty.
- 2) A break in the primary system introduces a heat sink. If this sink is larger than \dot{Q}_{dec} , the uncontrolled depressurization of the primary system becomes essentially independent of the steam generators. The primary system can then become decoupled from the steam generators, which means that circulation flow ceases, which changes the energy balance in the cold leg-downcomer region. This places the evolution of T_{dc} on a qualitatively different path, in effect, a bifurcation of T_{dc} occurs.

- 3) The modeling of two-phase flow regimes and the associated empirical correlations determining mass/energy transfer rates have larger uncertainties than for single-phase flows.
- 4) At stagnation conditions the physical driving forces for natural circulation become very small; this emphasizes the effect of numerical oscillations. Numerical oscillations, especially oscillations in parallel flow channels, can introduce unphysical mixing.

An example of an augmented T_{dc} transient was presented in Figure A.7. The boundary condition of break size for the two transients in the figure fall within the uncertainty range of break flow modeling, so the two categories are, in a sense, interchangeable. As shown, the difference in T_{dc} values between a transient that does not experience flow stagnation and one that does increases with time, therefore the uncertainty range associated with T_{dc} increases as well. Note, that such an augmentation of the uncertainty applies for all transients that approach conditions at which flow stagnation could occur. In the example shown, it applies not just for the trace for which flow stagnation exists, but also for the transient for which such a condition was not calculated. As long as boundary condition and physical model uncertainties encompass a range, which could lead to flow stagnation, uncertainties may be augmented. A key issue in the analysis of two-phase transients is, therefore, the evaluation of conditions for which flow-stagnation is possible.

The main criterion for classifying small break LOCA transients is the relative magnitude of the mass/energy loss rate through the break in comparison to the mass/energy source terms. That is the case because a necessary precondition for flow stagnation is a break of sufficient size so that mass/energy is depleted at a rate so that:

- 1) Mass cannot be replaced by HPI flow.
- 2) Energy removal rate through the break and HPI exceed the decay heat source.

These criteria lead to a four-fold grouping of two-phase transients shown in Table A.3. The classification is based on the relative magnitude of the energy/mass removal terms compared to the HPI flow rate and the decay heat. The net energy flow rate in the table is given by $\dot{Q}_{brk} - \dot{Q}_{HPI}$, (the break energy flow minus the enthalpy added by the HPI stream), and the corresponding mass flow rates are \dot{W}_{brk} and \dot{W}_{HPI} . Starting with the smallest break size, the four categories are:

- 1) If the break is sufficiently small so that both the mass and energy flows are smaller than the corresponding sources, then no long-term two-phase conditions will be present. Even if a short-term void in the primary system occurs during the initial depressurization phase, the inventory will recover and pressurizer control can be maintained.
- 2) If the break is sufficiently large that gradual depletion of inventory will occur, but the energy lost through the break is less than the decay energy input, then flow stagnation is possible, but it will be intermittent. For OTSG plants the thermal hydraulic response for such LOCAs is quite complex and is characterized by several distinct flow states. Periods of flow stagnation are possible, however, they will last for relatively brief time periods (compared to time constant of the vessel wall). As long as $(\dot{Q}_{brk} - \dot{Q}_{HPI}) < \dot{Q}_{dec}$, the energy of the primary system increases when flow is interrupted and system pressure rises. As pressure increases, the temperature difference $T_{sat} - T_{dc}$ increases as well and

the system moves further from an equilibrium condition. A thermal hydraulic system cannot depart from equilibrium indefinitely. In some locations (e.g. upper downcomer and at higher inventory losses, also in the cold leg region) steam is in close proximity to cooler water. With increasing pressure, the probability of a rapid condensation event increases as well. These events generate local pressure differences that induce large flows and mixing of the liquid inventory. This leads to more evenly distributed temperatures, thus, from the PTS perspective, these events are beneficial. A variety of condensation events have been observed in several test facilities, and they are described in a number of references [Wang, 1992; Bankoff, 1980].

- 3) A potentially serious state from the PTS standpoint is if the energy removed by break flow is slightly larger than decay heat, and HPI injection is less than break mass flow. For this set of conditions, inventory and pressure decrease gradually. When RCS pressure falls below secondary pressure, natural circulation is terminated and the steam generator heat sink is lost. This condition might persist for a relatively long time. If so, cold HPI liquid reduces the fluid temperature in the downcomer, while system pressure remains relatively high.
- 4) Finally, for the last category break flows are sufficiently large so that both pressure and system fluid temperatures, including T_{dc} , decrease rapidly. The answer to the question whether the combination of the P and T_{dc} parameters lead to conditions that are PTS relevant, depends on the outcome of PFM analysis.

Table A.3 Classification of two-phase transients

Transient Category	Break Energy/Mass Flow Rate		Energy/Mass Sources	Flow Stagnation Probability
1	$\frac{\dot{Q}_{brk} - \dot{Q}_{HPI}}{\dot{W}_{brk}}$	< <	\dot{Q}_{dec} \dot{W}_{HPI}	No flow stagnation
2	$\frac{\dot{Q}_{brk} - \dot{Q}_{HPI}}{\dot{W}_{brk}}$	< >	\dot{Q}_{dec} \dot{W}_{HPI}	Flow stagnation possible, but brief
3	$\frac{\dot{Q}_{brk} - \dot{Q}_{HPI}}{\dot{W}_{brk}}$	~ >	\dot{Q}_{dec} \dot{W}_{HPI}	Flow stagnation possible and could be prolonged
4	$\frac{\dot{Q}_{brk} - \dot{Q}_{HPI}}{\dot{W}_{brk}}$	>> >>	\dot{Q}_{dec} \dot{W}_{HPI}	Flow stagnation with rapid decrease of P

In PTS studies conducted in the past, two-phase transients were classified using an informal three fold scheme, which considered breaks to be either 'very small', 'PTS relevant' or 'large'. The following justification was employed:

- 1) Very small breaks were eliminated because for such breaks, control of pressure is maintained and thus can be kept above the pressure of the secondary system (1).

- 2) LOCAs caused by breaks that depressurize relatively rapidly (> 2-inch) were eliminated because of low final pressures (category 4).
- 3) The intermediate small break LOCA, for which the pressure remains sufficiently high and T_{dc} decreases, were considered to be 'PTS relevant'. In most past studies a ~2-inch ($\sim 0.002 \text{ m}^2$) [Fletcher, 1984; Palmrose, 1999] was taken as representative and most analytical effort was devoted to these transients.

As far as can be ascertained, no clear quantitative criteria were proposed to define the bounding values of the T_{dc} and P variables for this classification scheme. This study differs from the previous ones in that the boundary condition and model uncertainties are considered in evaluating the range of break sizes for which flow stagnation can occur. This broadens the range of breaks that could lead to stagnation.

A.6 Characteristics of Inventory Based Two-Phase Flow States in OTSG PWRs

If HPI flow is less than break flow, a decrease in primary system inventory occurs, and liquid levels form in the vessel, hot legs, and the tube side of the steam generators. As levels drop, geometric discontinuities are encountered. This leads to changes in local and system wide flow regimes. Vapor first appears in the vessel upper head and the tops of the hot legs. The upper head is a dead end volume fed directly by rising vapor from the core. With increasing loss of inventory the primary system will pass through the following sequential flow regimes:

8% to 15% Inventory Loss

The vessel upper plenum-upper head region above the hot leg entrance represents ~8 % of the primary system inventory. Vapor fills the upper vessel the vertical riser section of the hot legs. Saturated liquid will flash as it travels up the riser section of the hot leg due to loss of gravity head. The bubbly flow is accelerated up the riser due to the lower density of the two-phase mixture. As long as condensation surfaces are available in the steam generator, phase separation may not occur and continuous liquid natural circulation flow is maintained.

The behavior described can be altered by the presence of incondensable. Flow blockages created by the accumulation of noncondensable behave quite differently from those created by the accumulation of vapor. Vapor flow blockages can be removed by changes in system pressure and/or changes of local temperature. On the other hand, once noncondensable segregates, it can be removed only by inertia driven flow. In the candy cane geometry, this requires fluid velocities, which generate distributed flow regimes.

15% to 30% Inventory Loss

Sufficient vapor is available to fill the upper vessel and the top of the hot legs. Now flow blockage of the hot legs can occur. Resulting flow stagnation can be long term if $\dot{Q}_{decay} < \dot{Q}_{break}$ otherwise system pressure rises after the flow stagnates, and vapor is compressed leading to condensation, and the period of stagnation is relatively short. For these conditions a dynamic flow regime develops. The event sequence producing periodic phases of flow stagnation followed by periods of flow surges has the following physical interpretation:

- 1) Subcooled water from the downcomer enters the core.
- 2) This causes a decrease in boiling rate.
- 3) System pressure falls and saturated water in the hot leg flashes filling the candy canes and shutting off flow to both steam generators, thus losing the steam generator heat sink.
- 4) Natural circulation flow stops.
- 5) Boiling in the core increases.
- 6) The vapor region in the upper vessel expands and displaces hot water downwards.
- 7) Hot water and steam flows from the upper plenum through the RVVVs into the upper region of the downcomer and into the cold legs.
- 8) Simultaneously, increasing pressure reduces the vapor volume in the candy cane.
- 9) The steam entering the upper downcomer and cold legs encounters subcooled water; this can generate a 'condensation implosion' event.
- 10) The local condensation rate can increase dramatically, the local pressure decreases suddenly, and the generated pressure difference draws colder water to the vessel, which reduces or stops boiling in the core.
- 11) The cycle is repeated

This flow regime has been documented by Wang, et al. [Wang, 1989] and is the IRM (Interruption-Resumption Mode).

30% to 45% Inventory Loss

How the system responds to a larger net inventory loss depends on the location at which feed water is introduced (sprays or regular feedwater introduction) into the secondary system. By the time inventory loss approaches ~25%, the primary liquid level in the OTSG has dropped to the elevation of the liquid level in the secondary. System response will first be described for the low feed water introduction point.

Low Elevation Feedwater

When inventory loss has progressed to the point that the vessel liquid level approaches the hot leg entrance, the system wide flow regime is altered. The upper third of the primary system is now filled entirely with steam. Energy transport is determined by the availability of a condensing surface in the steam generator. The primary liquid level in the OTSG is at the same level as in the vessel. System response then depends upon the secondary liquid level. If secondary level is higher than primary, BCM occurs. If secondary side level is lower than primary side, the steam generator heat sink is lost and flow stagnates.

The physical reason for this response is shown schematically in Figure A.8. If the relative inventory levels are such that the collapsed liquid level inside the tubes is higher than the liquid on the secondary system (left side illustration of Figure A.8), no condensation surface is available and heat transfer to the steam generator is terminated. However, if inventory loss proceeds further, so that the liquid level in the tubes falls below the secondary system level (right side illustration of Figure A.8), energy transfer to the steam generator is resumed. For these conditions, flow stagnates for the time that is required for the loss of sufficient primary system inventory, so that a condensing surface is exposed.

High Elevation Feedwater

If feedwater is introduced through the spray nozzles located at the top of the tube bundle on the secondary side, flow interruption due to unequal secondary and primary system liquid levels will not occur. The steam on the primary system of an OTSG will be condensed in the upper regions of the OTSG reached by the feedwater spray. The transition to BCM will occur at higher primary system inventory levels and will be more gradual.

If a condensing surface is available after the upper part of the primary system is voided, energy/mass transfer occurs by BCM. In this mode, boiling in the core generates steam, which flows to the OTSG and returns to the vessel as liquid condensate. Because of the high latent heat of water, the rate of condensate flow in the cold leg is low, however, the energy transfer capability of this mode is high, therefore the system pressure will decrease rapidly towards levels set by the saturation temperature of the condensing surface.

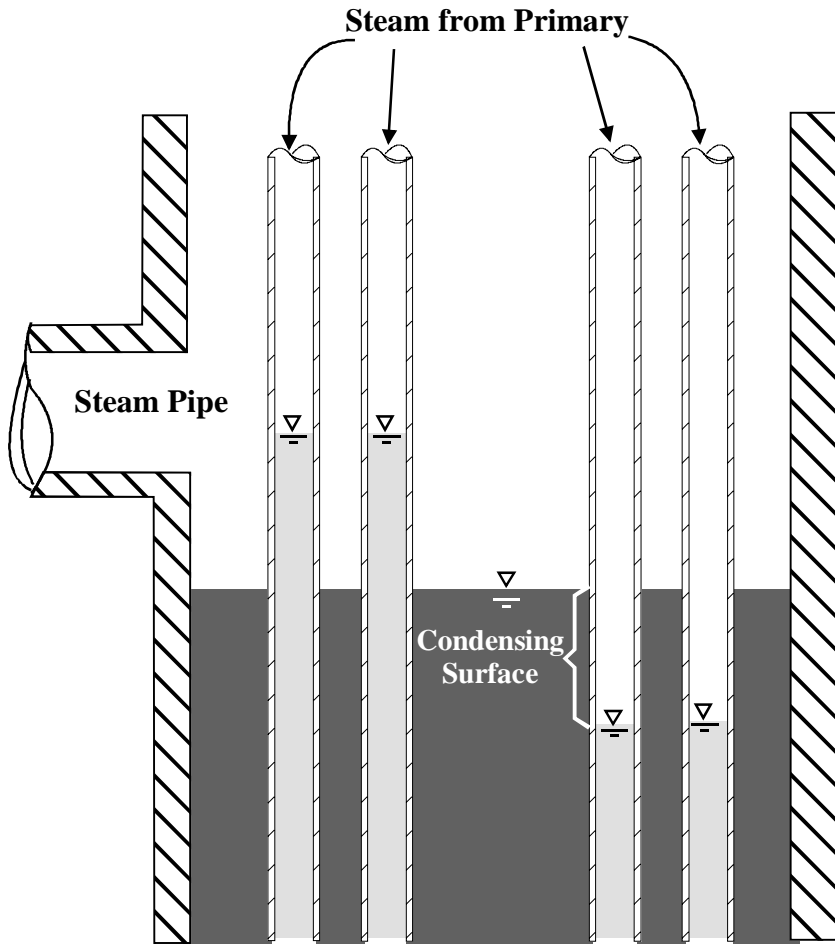


Figure A-8 Level dependent steam generator condensation surface

Appendix B. Effect of Convective Heat Transfer on Vessel Wall Temperature

The impact of $h(t)$ on the evaluation of temperature gradients within the vessel wall was considered in several previous studies, most recently by Boyd and Dickson [Boyd, 1999]. The studies concluded that heat transfer from the vessel wall is determined primarily by internal conductive resistance (conduction limited). The impact of $h_{dc}(t)$, as well as the computational uncertainties that are associated with $h(t)$, is therefore limited. This section considers the range and variation of $h_{dc}(t)$, and its dependence on the bulk properties of the fluid, primarily on $T_{dc}(t)$.

The evaluation of the convective resistance at a vertical wall is a classical energy transport problem that is treated in all basic heat transfer texts. Depending on how fluid convection is generated, two distinct convective modes are recognized:

- 1) Forced convection. The fluid velocity field along the wall is imposed externally. The empirical correlations employed to obtain the Nusselt (Nu) number are based on the Reynolds (Re) and Prandtl (Pr) numbers.
- 2) Free convection. The velocity field is generated by the temperature difference between the wall surface and the bulk fluid. The correlations used to obtain the Nu number depend on the Grashof (Gr) and Pr numbers (Ra).

For some flow conditions, the distinction is not clear cut, and mixed convection conditions between natural and forced circulation are possible. Such conditions can occur during PTS-relevant transients when the circulation rate decreases significantly. Additional phenomena which can complicate the evaluation of $h_{dc}(t)$ include entrance effects, the length dimension used to characterize the flow field (can be different for the Re and Gr numbers), characteristics of the flow field for time varying conditions, and others. The evaluation of an adequate $h_{dc}(t)$ can thus be fairly complicated; this is also reflected in the associated uncertainties. However, as noted, the major resistance to energy transfer into the thick vessel walls is the internal thermal diffusivity. Therefore, second order effects which influence $h_{dc}(t)$ can be disregarded. For PTS computations, it is sufficient to consider the generic variation of $h_{dc}(t)$ over the parameter's range of interest.

The dependence of $h_{dc}(t)$ on the bulk fluid temperature is shown schematically in Figure B.1. The solid line shows a generic variation of $T_{dc}(t)$ during a transient, while the dotted lines are the potential family of $h_{dc}(t)$ curves. As illustrated, a transient, which results in a cooldown of the downcomer region, will also lead to lower $h_{dc}(t)$ values. Even if the fluid velocity does not change (RCPs on), $h_{dc}(t)$ decreases because of temperature dependent changes of viscosity and the Pr number. Over the temperature range of interest to PTS transients, this decrease can be up to 50%.

If the RCPs are tripped, as they normally are, the velocity of the fluid in the downcomer drops sharply and the decrease in the magnitude of $h_{dc}(t)$ is considerably greater, and natural circulation determines fluid velocity. This can be the natural circulation flow of the primary system, or during "flow stagnation," in-vessel natural circulation generated by the temperature differences from decay heat and ECC injection, as well as heat transfer from structures to fluid. Lower values of fluid velocity are correlated with a faster $T_{dc}(t)$ decrease rate.

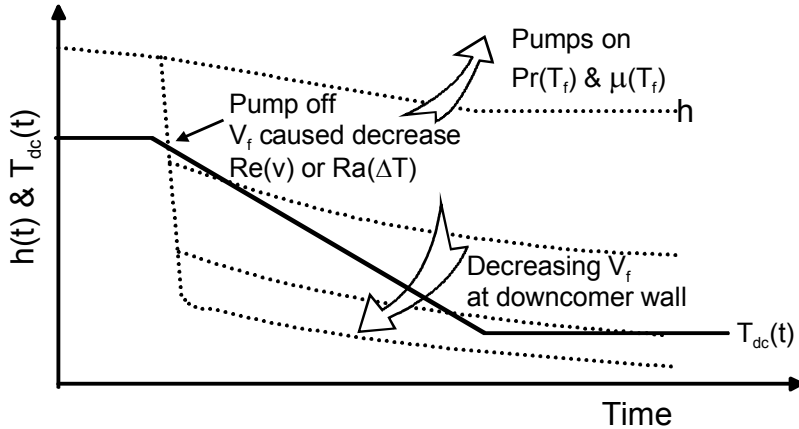


Figure B-1 Generic relationship between $T_{dc}(t)$ and $h_{dc}(t)$

Quantitative examples of $h_{dc}(t)$ dependence on $T_{dc}(t)$ and the local fluid velocity are evaluated using the correlations and algorithms employed in RELAP5. The code uses the classical Dittus-Boelter relationship for forced circulation flows and the Gr number dependent Churchill-Chu relationship for conditions where the predominant fluid motion is generated by internal natural circulation (RELAP5 manual, Vol. 4). The upper limit of forced circulation $h_{dc}(t)$ values occurs when the RCPs are operating. Coolant flows as well as velocities are then high ($\sim 18,000$ kg/s total flow, ~ 7 m/s fluid velocity in the downcomer). This leads to large Re numbers (on the order of $\sim 28,000,000$) and to very large $h_{dc}(t)$ values (on the order of $\sim 25,000$ W/m² K, or ~ 4400 BTU/hr ft² F). For such $h_{dc}(t)$ magnitudes, the surface resistance becomes completely negligible.

Of more practical interest are the 'forced' $h_{dc}(t)$ values when the RCPs are tripped and system flow is by natural circulation. That is not a contradiction in terms, since from the vessel wall point of view, what counts is whether the fluid in front of it is moved by an external driving force, or whether it has to be generated by a local buoyancy. Circulations that are driven by density differences in the core region and the steam generator's are as much 'external' to the vessel wall as circulation imposed by RCPs. They differ only in the magnitude of the fluid velocity.

The range of $h_{dc}(t)$ values generated by external natural circulation is shown in Figure B.2. Two bounding traces are presented as a function of fluid temperature. The upper trace corresponds to a circulation rate of ~ 440 kg/s, which represents natural circulation flow corresponding to $\sim 1\%$ decay heat. The lower trace shows a lower limit of ~ 110 kg/s that would apply when the decay energy is quite low. As shown, the range is from ~ 1500 to ~ 400 W/m²-K (270 to 70 BTU/hr-ft²-F).

The bottom trace shown in Figure B.2 is a lower limit in two respects. It is limited by the rate of external natural circulation and by the internal circulation generated by a fluid to surface temperature difference. The switchover in the correlations from the local 'forced' to the internal 'natural' circulation occurs when

$$Gr > Re^2$$

An example of Nu number dependence on $T_{dc}(t)$ for flow conditions at which the switchover occurs is shown in Figure B.3. For this example, $Gr > Re^2$ when the local fluid velocity is ~ 0.12 m/s and the wall surface to $T_{dc}(t)$ temperature difference is $\sim 3K$. The figure shows that both correlations exhibit quite similar trends with respect to the local fluid temperature.

The switchover conditions illustrated in Figure B.3 implies that for the duration of most transients, RELAP5 will choose the 'forced' circulation option. At a relatively low flow velocity of 0.12 m/s, a surface to bulk temperature difference of $\delta T_s > 3K$ is required before the Gr-Ra number relationship is chosen. Since the thick vessel wall is conduction limited, the fluid to surface δT_{wall} generally be low (on the order of several degrees); $h(t)$ is then determined by a Re number correlation and is proportional to $V_f^{0.8}$, where V_f is the bulk fluid velocity and, as illustrated in Figure B.2, it depends also on fluid temperature.

To complete a quantitative overview of the $h(t)$ range, Fig B.4 shows the variation of $h(t)$ determined using the Churchill-Chu correlation employed in RELAP5. Note that in this case the driving force is the 'internal' temperature difference between the fluid and the wall surface and is thus independent of external circulation. It applies therefore also for the case of flow stagnation. As shown in Figure B.4, when the surface-to-fluid temperature difference drops down to $\sim 0.5K$, the magnitude of $h(t)$ is on the order of ~ 600 W/m² K. Based on the results presented in Figs B.2 and B.4, this value can be taken as a lower bound for $h(t)$.

The effect of the entire possible range of $h_{dc}(t)$ values is shown in Fig B.5, which presents RELAP5 computed temperature distributions within the vessel wall 400 sec after a step temperature change of 100 K. The high ($\sim 27,000$ W/m² K) and low (~ 600 W/m² K) limiting values of $h_{dc}(t)$ are employed. Comparisons of the external and internal thermal resistances to the centerline of the vessel wall yields Bi numbers of 2 and 70 for the two cases. This confirms the conclusion reached by Boyd and Dickson (Boyd, 99) that energy transfer from the vessel wall is conduction limited over the entire possible range of $h_{dc}(t)$ values. The evaluation of temperature gradients within the wall then depends principally on the fluid temperature $T_{dc}(t)$, and the uncertainties associated with the evaluation of $h_{dc}(t)$ have a small influence. As long as the $h_{dc}(t)$ value supplied to PFM computations is of the right order of magnitude, the effect of its uncertainty can be disregarded.

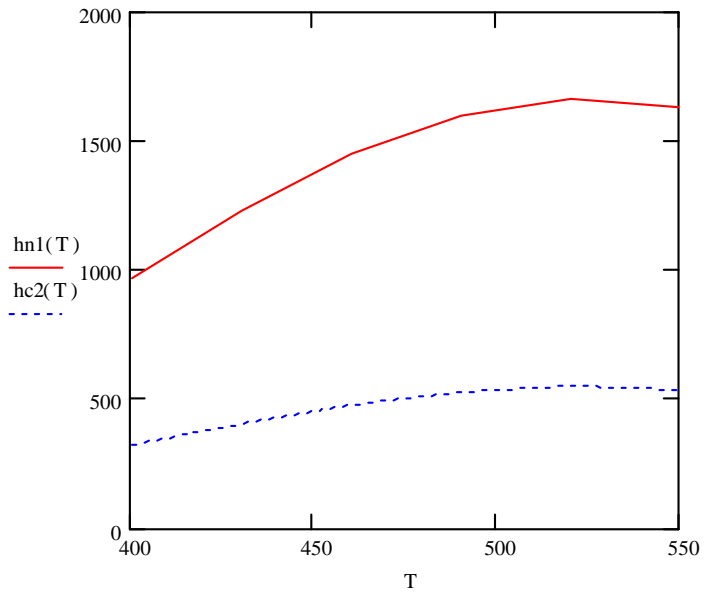


Figure B-2 Range of $h_{dc}(t)$ for external natural circulation conditions

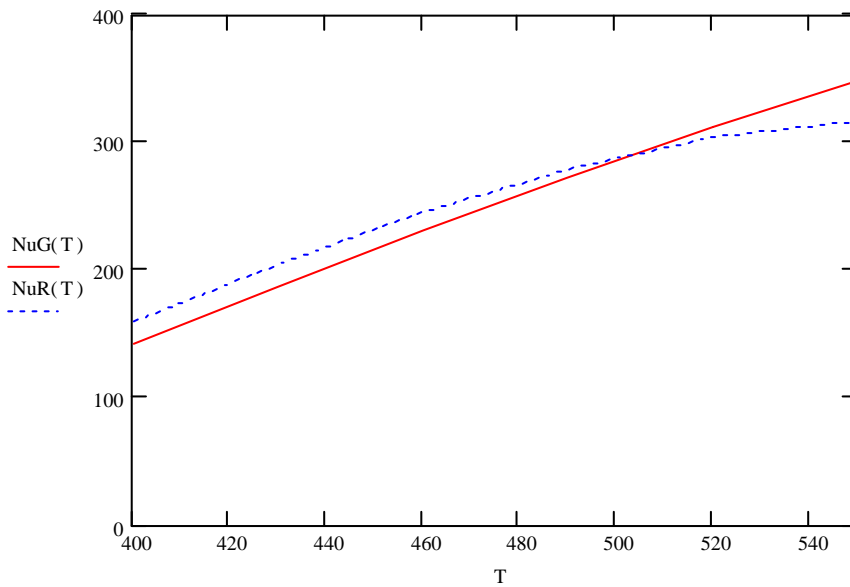


Figure B-3 Nu number dependence on $T_{dc}(t)$ for the forced and natural circulation correlations,
 NuG(T) is calculated from Churchill-Chu
 NuR(T) is calculated from Dittus-Boelter

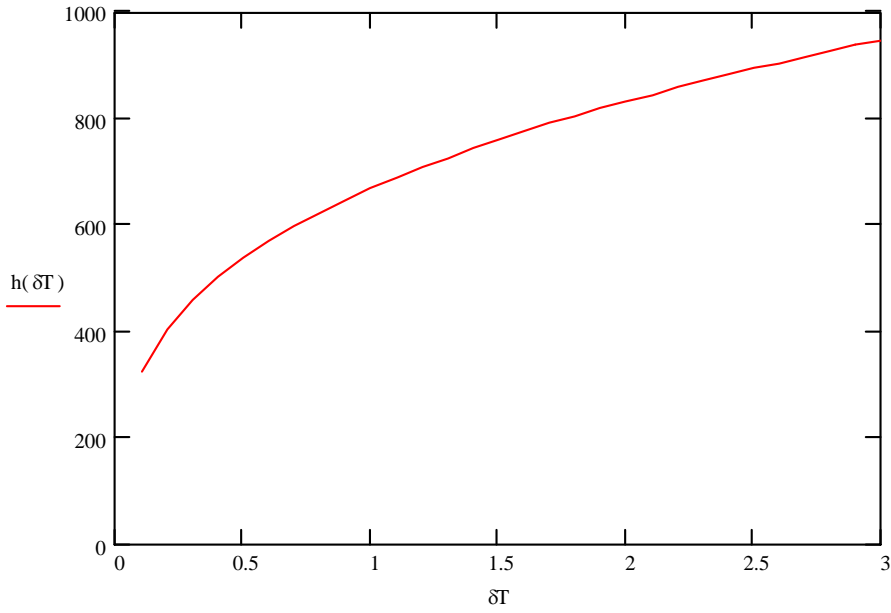


Figure B-4 $h(\delta T)$ determined from local buoyancy circulation fluid-to-surface δT

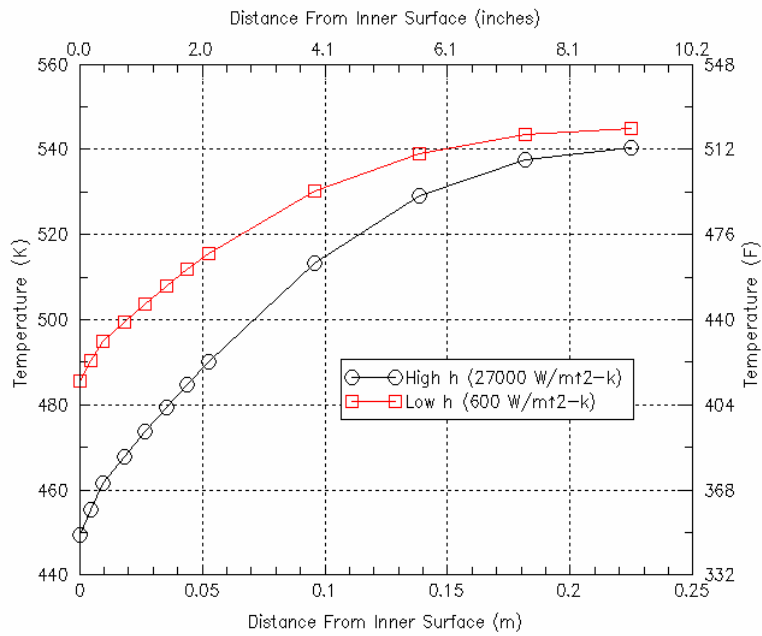


Figure B-5 Temperature distribution in vessel wall

Appendix C. Steam Generator Heat Transfer

This study has noted repeatedly that, for shutdown conditions, the steam generators are greatly over designed. As long as the steam generators are available (feedwater), the primary system temperature will closely follow that of the secondary. This appendix presents a quantitative analysis that verifies this conclusion.

RELAP5 models secondary-to-primary heat transfer by representing the steam generator tube walls as a distinct solid region. The thermal time constant of the thin tube wall is quite short (~2 s to 4 s). Compared to other relevant time constants, such as the vessel wall, this time can be disregarded. The steam generator tube wall is, therefore, effectively always at thermal equilibrium. The energy transfer rate across this wall can then be represented by:

$$\dot{Q}_{SG}(t) = \sum_{n=1}^N h_{eff,n}(t) A_n [T_{prim,n}(t) - T_{sec,n}(t)] \quad C.1$$

where,

N is the total number of segments used in the analysis

$h_{eff,n}$ is the effective heat transfer coefficient for segment n , obtained from:

$$\frac{1}{h_{eff,n}} = \frac{1}{h_{prim,n}} + \frac{\Delta x_{tb}}{k_{tb}} + \frac{1}{h_{sec,n}} \quad C.2$$

where,

Δx_{tb} tube thickness

k_{tb} conductivity

$h_{prim,i}$ heat transfer coefficient on primary side in sequence i

$h_{sec,i}$ heat transfer coefficient on secondary side in sequence i

RELAP5 employs complex algorithms to compute h on the primary and secondary side. These algorithms choose the flow regime at time t (dependent on fluid state, velocity etc). Then, based on the flow regime, they choose an empirical correlation that can depend on a variety of variables. Finally, for cases where transitions occur, they can apply time averages. Note that this process is explicit, that is, the h applied for time interval t is based on the conditions determined for time interval $t-\delta t$. Unsurprisingly, such a complex process is burdened with many uncertainties. These include uncertainty in the choice of the flow regime, uncertainty in the appropriateness of the empirical correlation, uncertainty in the code-determined variables employed in the correlation, and finally, uncertainties imposed by the finite difference nature of the code and the explicitness of the computation. The clarification and quantification of these uncertainties is a formidable task.

Fortunately, because of the large, “over-designed” heat transfer surface area available in the steam generators, the impact of these uncertainties on the temperature of the primary system liquid exiting from the steam generators is small. The reason for this is illustrated by the following expression:

$$T_{pr, o}(t) = T_{sec} - \delta T \quad C.3$$

where,

$T_{pr, o}(t)$ is the temperature of the primary system liquid exiting from the steam generator
 δT is the temperature difference between the primary and secondary.

If the secondary side conditions are controlled, then all of the uncertainties associated with the evaluation of heat transfer between primary and secondary are reflected in the value of δT . If δT is small in relation to T_{sec} , then the impact of the associated uncertainties will be small as well. This is illustrated quantitatively in Figures C.1 to C.3

Of the three heat transfer resistances shown in Equation C.2 that determine the effective heat transfer coefficient h_{eff} , the largest is the forced convection resistance inside the tubes. It depends strongly on the fluid velocity. The dependence of h_{eff} on liquid velocity is significant, as shown in Figure C.1. Nominal velocities with RCPs operating are ~ 5 m/s; for natural circulation conditions, this drops down to ~ 0.1 to 0.2 m/s. The small difference between the two upper traces is caused by the possible variation of the heat transfer resistance on the secondary side. On the secondary side, boiling will take place and RELAP5 uses the Chen correlation for nucleate boiling, or the modified Unal-Lahey correlation for bubbly flow (the most prevalent mode). The range extends over values of h from $\sim 5,000$ to $30,000$ W/m²-K. The impact of this broad range on h_{eff} is small because the external resistance usually represents a small fraction of the total resistance. For completeness a third h_{eff} trace is included for the case where film boiling occurs at the external surface. Under shutdown conditions, the heat fluxes are not sufficiently large for film boiling, so this trace represents an outside bounding value.

As noted, uncertainties associated with the employed correlations or the computation method will also be reflected in the evaluated magnitude of δT . However, for PTS analysis it is the absolute temperature of the fluid that is of interest. An example of how this parameter changes for the case where secondary temperature is maintained at 560 K and h_{eff} varies over its possible range is shown in Figure C.3.

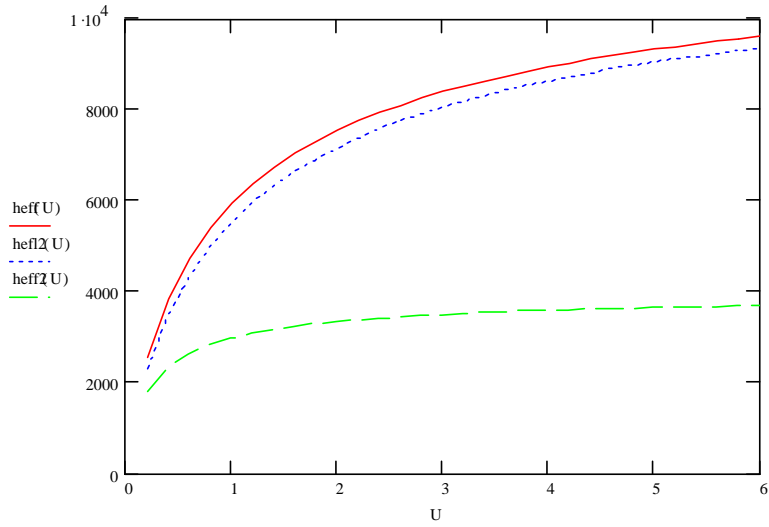


Figure C-1 h_{eff} as a function of liquid flow velocities in tubes

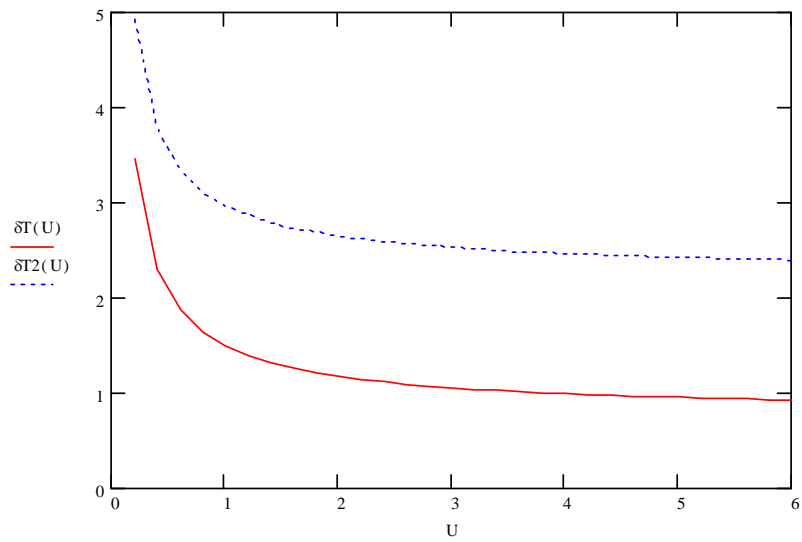


Figure C-2 Temperature difference across steam generator tubes vs. tube side liquid velocity

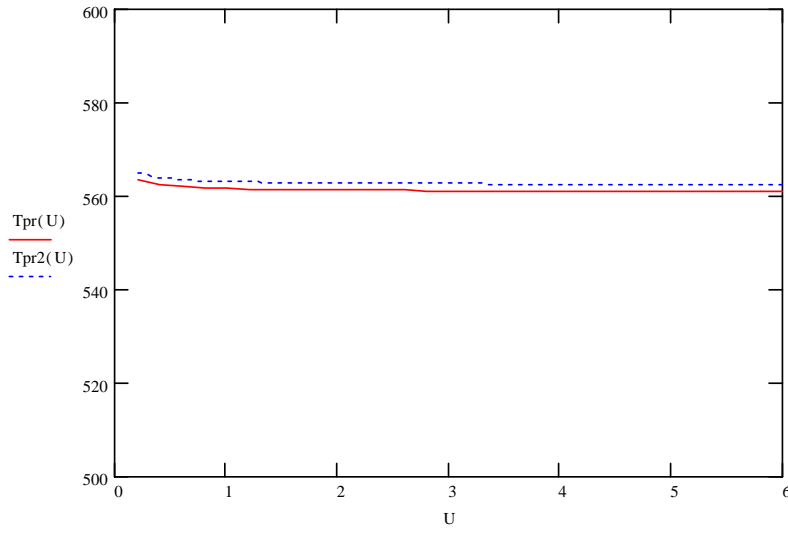


Figure C-3 Primary side temperature exiting steam generator as function of h

Appendix D. Program to Calculate Temperature Distributions

The C++ computer program written for calculating the linear multiple factor combine impact is included. The "Main.cpp" is the main program. The "TFactor.cpp" and "TFactor.h" define a class for calculation.

```
/////////////////////////////////////////////////////////////////
// Main.cpp : Defines the entry point for the console application.
// Author: Y.H. Chang 10/14/2001
// Use linear relationship to calculate expected average downcomer temperature
// for Oconee thermal-hydraulic uncertainty study
/////////////////////////////////////////////////////////////////
#include "stdafx.h"
#include "TFactor.h"
#include <iostream>
#include <vector>
#define ref 285.4243
typedef vector<TFactor> Clsf;
using namespace std;
int main(int argc, char* argv[])
{
    int ii, count;
    Clsf Isf0, Isf1, Isf2, Isf3, Isf4, Isf5, Isf6, Isf7, Isf8, Isf[42];
    Clsf::iterator itr0, itr1, itr2, itr3, itr4, itr5, itr6, itr7, itr8, itr;
    TFactor *factor_ptr;
    string t_name, str;
    double t_prob;
    double t_temp;
    bool not_found;
    //input data ("description", temp, probability)
    //Season
    factor_ptr = new TFactor("Winter", 264.8161, 0.25);
    Isf0.push_back(*factor_ptr);
    factor_ptr = new TFactor("Nom", ref, 0.50);
    Isf0.push_back(*factor_ptr);
    factor_ptr = new TFactor("Summer", 290.0, 0.25);
    Isf0.push_back(*factor_ptr);
    //p(CFT)
    // factor_ptr = new TFactor("p(CFT)+=50psi", 234.3168, 0.1);
    // Isf1.push_back(*factor_ptr);
    factor_ptr = new TFactor("", ref, 1.0);
    Isf1.push_back(*factor_ptr);
    // factor_ptr = new TFactor("p(CFT)-=50psi", 237.5232, 0.1);
    // Isf1.push_back(*factor_ptr);
    //m(HPI)
    factor_ptr = new TFactor("110%m(HPI)", 258.0331, 0.1);
    Isf2.push_back(*factor_ptr);
    factor_ptr = new TFactor("", ref, 0.8);
    Isf2.push_back(*factor_ptr);
    factor_ptr = new TFactor("90%m(HPI)", 291.304, 0.1);
```

```

lsf2.push_back(*factor_ptr);
//Model Uncertainty
factor_ptr = new TFactor("130%A", 269.8725, 0.25);
lsf3.push_back(*factor_ptr);
factor_ptr = new TFactor("", ref, 0.5);
lsf3.push_back(*factor_ptr);
factor_ptr = new TFactor("70%A", 300.9761, 0.25);
lsf3.push_back(*factor_ptr);
//VV state
factor_ptr = new TFactor("VVClose", ref - 50.0, 0.25);
lsf4.push_back(*factor_ptr);
factor_ptr = new TFactor("", ref, 0.5);
lsf4.push_back(*factor_ptr);
factor_ptr = new TFactor("VVOpen", ref + 50.0, 0.25);
lsf4.push_back(*factor_ptr);
//Heat transfer rate
factor_ptr = new TFactor("130%HTR", 294.3794, 0.1);
lsf5.push_back(*factor_ptr);
factor_ptr = new TFactor("", ref, 0.8);
lsf5.push_back(*factor_ptr);
factor_ptr = new TFactor("70%HTR", 268.5074, 0.1);
lsf5.push_back(*factor_ptr);
//Loop flow resistance
// factor_ptr = new TFactor("200%Resis", 234.2071, 0.10);
// lsf6.push_back(*factor_ptr);
factor_ptr = new TFactor("", ref, 1.0);
lsf6.push_back(*factor_ptr);
//HZP
factor_ptr = new TFactor("HZP", 256.5954, 0.02);
lsf7.push_back(*factor_ptr);
factor_ptr = new TFactor("", ref, 0.98);
lsf7.push_back(*factor_ptr);
//ColdLeg
factor_ptr = new TFactor("CL", 393.069, 0.5);
lsf8.push_back(*factor_ptr);
factor_ptr = new TFactor("", ref, 0.5);
lsf8.push_back(*factor_ptr);
//
ofstream fout1("all.txt", ios::out);
for(itr0 = lsf0.begin(); itr0 != lsf0.end(); itr0++){
    for(itr1 = lsf1.begin(); itr1 != lsf1.end(); itr1++){
        for(itr2 = lsf2.begin(); itr2 != lsf2.end(); itr2++){
            for(itr3 = lsf3.begin(); itr3 != lsf3.end(); itr3++){
                for(itr4 = lsf4.begin(); itr4 != lsf4.end(); itr4++){
                    for(itr5 = lsf5.begin(); itr5 != lsf5.end(); itr5++){
                        for(itr6 = lsf6.begin(); itr6 != lsf6.end(); itr6++){
                            for(itr7 = lsf7.begin(); itr7 != lsf7.end(); itr7++){
                                for(itr8 = lsf8.begin(); itr8 != lsf8.end(); itr8++){
                                    str = itr0->getName();
                                    t_name = str;
                                    if(str.length() > 0){

```

```

        t_name += ';';
    }
    str = itr1->getName();
    if(str.length() > 0){
        t_name += str;
        t_name += ';';
    }
    str = itr2->getName();
    if(str.length() > 0){
        t_name += str;
        t_name += ';';
    }
    str = itr3->getName();
    if(str.length() > 0){
        t_name += str;
        t_name += ';';
    }
    str = itr4->getName();
    if(str.length() > 0){
        t_name += str;
        t_name += ';';
    }
    str = itr5->getName();
    if(str.length() > 0){
        t_name += str;
        t_name += ';';
    }
    str = itr6->getName();
    if(str.length() > 0){
        t_name += str;
        t_name += ';';
    }
    str = itr7->getName();
    if(str.length() > 0){
        t_name += str;
        t_name += ';';
    }
    str = itr8->getName();
    if(str.length() > 0){
        t_name += str;
        t_name += ';';
    }
    t_prob = itr0->getProbability() * itr1->getProbability() * itr2->getProbability() *
        itr3->getProbability() * itr4->getProbability() * itr5->getProbability() *
        itr6->getProbability() * itr7->getProbability() * itr8->getProbability();
    t_temp = itr0->getTemp() + itr1->getTemp() + itr2->getTemp() + itr3->getTemp()
+
        itr4->getTemp() + itr5->getTemp() + itr6->getTemp() + itr7->getTemp()
        + itr8->getTemp() - 8.0 * ref;
    //write to the all.txt file
    fout1 << t_temp << '\t' << t_prob << '\t' << t_name << '\n';

```



```

}
TFactor::TFactor(string c_name, double c_temp, double c_prob){
    Name = c_name;
    Temp = c_temp;
    Probability = c_prob;
}
TFactor::~TFactor()
{
}
string TFactor::getName() const {return Name;}
double TFactor::getTemp() const {return Temp;}
double TFactor::getProbability() const {return Probability;}
void TFactor::output(){
    cout << Name << '\t' << Temp << '\t' << Probability << '\n';
}
void TFactor::setName(string c_name){Name = c_name;}
void TFactor::setTemp(double c_temp){Temp = c_temp;}
void TFactor::setProbability(double c_probability){Probability = c_probability;}

```

```

////////////////////////////////////
// TFactor.cpp: implementation of the TFactor class.
//
////////////////////////////////////

```

```

#include "stdafx.h"
#include "TFactor.h"
TFactor::TFactor()
{
}
TFactor::TFactor(string c_name, double c_temp, double c_prob){
    Name = c_name;
    Temp = c_temp;
    Probability = c_prob;
}
TFactor::~TFactor()
{
}
string TFactor::getName() const {return Name;}
double TFactor::getTemp() const {return Temp;}
double TFactor::getProbability() const {return Probability;}
void TFactor::output(){
    cout << Name << '\t' << Temp << '\t' << Probability << '\n';
}
void TFactor::setName(string c_name){Name = c_name;}

```

```
void TFactor::setTemp(double c_temp){Temp = c_temp;}  
void TFactor::setProbability(double c_probability){Probability = c_probability;}
```

Appendix E. Sensitivity Assessment of Parameters

Tables E.1 and E.2 list the scenarios that were the subject of the sensitivity study. Table E.3 shows calculated results by FAVOR of the scenarios listed in Tables E.1 and E.2.

Table E.1 RELAP5 sensitivity calculations for surge line LOCA

Break Size	1.5"	2"	2.828"	4"	5.656"	8"
Nominal	NRC S64	NRC S65	NRC S66	NRC S67	NRC S68	NRC S69
Winter*	UMCP S1		UMCP S20		UMCP S45	UMCP S52
Summer*			UMCP S21		UMCP S46	UMCP S53
P _{CFT} +50 psi			UMCP S22			
P _{CFT} - 50 psi			UMCP S23			
110% HPI RCP on	UMCP S3		UMCP S24			
110% HPI RCP off	UMCP S63					
90% HPI	UMCP S4		UMCP S25			
HPI Failed and Recovered ~7000s			UMCP S26			UMCP S54
HPI Failed and Recovered ~1000s			UMCP S27			
HPI Failed and Recovered ~2000s			UMCP S28			
100% HPI Failed			UMCP S29	UMCP S41	UMCP S48	UMCP S55
25% HPI Failed	UMCP S7	UMCP S11	UMCP S30			
50% HPI Failed	UMCP S8	UMCP S12	UMCP S31			
HZP	UMCP S9		UMCP/NRC U32		NRC S49	UMCP S56
RVVV Closed			UMCP S33	UMCP S42		
RVVV 2/6 Open			UMCP S34			
RVVV 4/6 Open			UMCP S35			
RVVV 6/6 Open			UMCP S36	UMCP(S43)		
High CL Reverse Flow Resistance	UMCP S10	NRC S13	NRC/UMCP U(S37)	NRC(S44)		UMCP S57
130% h		NRC S14	UMCP S38		UMCP S50	
70% h		NRC S15	UMCP S39		UMCP S51	
200% Loop Flow Resistance		NRC S16				
200% Bypass Area		NRC S17				
No Bypass		NRC S18				
No heat structure		NRC S19				

*Winter: T_{HPI} = 4C (40F) T_{CFT} = 21C (70F) T_{LPI} = 4C (40F);
 Summer: T_{HPI} = 29C (85F) T_{CFT} = 38C (100F) T_{LPI} = 29C (85F);
 Spring/fall: T_{HPI} = 21C (70F) T_{CFT} = 27C (80F) T_{LPI} = 21C (70F)

Table E.2 RELAP5 sensitivity studies for cold leg LOCAs

Break Size	2"	2.828"	4"	5.656"	8"
Cold Leg LOCA	NRC(S58)	UMCP(S59)	NRC(S60)	NRC(S61)	UMCP(S62)

Table E.3 Summary of PFM Analysis of RELAP5 Sensitivity Calculations for Oconee-1
(evaluated at 60 EFPY)

Sequence	T _{min} F	T _{last} F	P _{min} psi	P _{last} psi	CPI ⁽¹⁾	CPF ⁽²⁾
S1	98	106	501	586	2.20 E-8	1.27 E-10
S3	412	412	841	942		
S4	118	118	521	622	4.91E-10	1.83 E-13
S7	167	171	434	434	0	0
S8	398	411	531	532	0	0
S9	343	343	619	807	0	0
S10	99	102	595	619	5.23 E-8	1.39 E-9
S11	172	172	240	240	3.70 E-9	1.90 E-12
S12	407	407	383	386		
S13	85	85	240	255	3.66 E-7	1.55 E-8
S14	129	129	248	276	3.18 E-8	1.19 E-10
S15	106	106	238	262	2.28 E-8	1.27 E-10
S16	121	122	249	261	5.19 E-8	4.80 E-10
S17	123	123	247	261	0	0
S18	107	125	234	255	0	0
S19	76	78	243	276	2.64 E-6	4.53 E-8
S20	63	63	195	213	3.11 E-6	9.77 E-8
S21	91	91	195	213	1.06 E-6	2.50 E-8
S22	89	89	190	211	2.14 E-6	1.24 E-9
S23	82	82	190	213	1.86 E-6	5.93 E-8
S24	94	94	185	212	2.86 E-6	8.45 E-8
S25	81	81	192	213	2.79 E-6	1.03 E-7
S26	257	257	243	249	0	0
S27	85	85	192	213	9.32 E-7	1.82 E-8
S28	87	87	192	212	1.06 E-6	2.30 E-8
S29	369	388	207	216		
S30	118	118	184	211	1.09 E-6	2.09 E-8
S31	158	158	206	206	3.13 E-8	6.09 E-11
S32	75	76	187	214	2.13 E-6	4.29 E-8
S33	81	82	174	214	0	0
S34	134	137	199	213	0	0
S35	144	146	198	213	0	0
S36	147	147	202	213	0	0
S37	80	80	181	212	4.99 E-7	9.57 E-9
S38	88	88	194	210	1.42 E-6	3.33 E-8
S39	78	78	190	213	3.97 E-6	1.18 E-7
S41	76	76	142	171	9.89 E-6	2.79 E-7
S42	74	74	154	187	0	0

Sequence	T _{mim} F	T _{last} F	P _{min} psi	P _{last} psi	CPI ⁽¹⁾	CPF ⁽²⁾
S43	95	95	170	190	5.28 E-7	4.71 E-9
S44	72	72	178	187	2.95 E-5	1.13 E-6
S45	51	51	122	141	2.07 E-5	3.54 E-7
S46	86	86	125	142	1.21 E-6	2.02 E-8
S48	71	72	114	143	1.96 E-5	8.56 E-7
S49	71	71	129	143	1.89 E-6	3.29 E-8
S50	76	76	117	145	3.23 E-5	1.52 E-6
S51	71	71	125	143	3.40 E-6	9.15 E-8
S52	68	69	67	84	1.80 E-6	1.31 E-8
S53	72	72	73	84	9.29 E-6	2.92 E-8
S54	71	71	68	84	1.28 E-6	2.03 E-8
S55	71	71	54	69	7.51 E-6	1.46 E-7
S56	71	71	63	84	2.94 E-5	1.12 E-6
S57	70	70	62	84	3.16 E-5	4.47 E-7
S58	243	243	306	314	0	0
S59	155	155	190	213	0	0
S60	120	121	158	189	2.29 E-8	1.41E-11
S61	90	117	109	132	3.69 E-7	5.16 E-9
S62	74	76	67	83	1.07 E-5	1.23 E-7
S63	108	108	690	846	5.49 E-9	2.48 E-11
S64	119	120	589	620	0	0
S65	121	124	256	274	5.65 E-8	4.09 E-10
S66	89	89	197	212	1.70 E-6	5.18 E-8
S67	73	73	162	189	1.27 E-5	4.43 E-7
S68	71	74	124	143	2.19 E-5	7.41 E-7
S69	71	71	69	84	2.56 E-5	7.72 E-7

CPI is conditional probability of crack initiation

CPF is conditional probability of vessel failure (penetration to 90% considered as failure)

PFM analysis was performed for 183550 simulated vessels where each simulated vessel had an average of 7937 postulated flaws. This analysis took approximately 11 days on a 1.7 GHz Pentium 4. The results for each transient were reasonably well converged.

Appendix F. Description Thermal Hydraulic Runs for Oconee-1

This appendix lists the Oconee-1 scenarios calculated using RELAP5 (Table F.1), and places them in the PTS event classification matrix (Table F.2). The University of Maryland RELAP5 calculations listed in Tables 6.2 to 6.4 as well as specific runs for studying certain phenomenon are not included.

Table F.1 Scenario descriptions of RELAP5 calculations for Oconee-1 (Arcieri, 2001)

#	Type	Primary Side Failure	Secondary Side Failure	Operator Action	LDH	Hi K	PRA
1	LOCA	1 inch surge line break	None	None	No	No	
2	LOCA	1.414 inch surge line break	None	None	No	No	
3	LOCA	2 inch surge line break	None	None	No	No	x
4	LOCA	2.828 inch surge line break	None	None	No	No	x
5	LOCA	4 inch surge line break	None	None	No	No	x
6	LOCA	1.414 inch cold leg break	None	None	No	No	
7	LOCA	2 inch cold leg break	None	None	No	No	
8	LOCA	1 inch surge line break	1 stuck open SRV in SG-A	None	No	No	x
9	LOCA	1 inch surge line break	2 stuck open SRVs in SG-A	None	No	No	
10	LOCA	1.414 inch surge line break	2 stuck open SRVs in SG-A	None	No	No	
11	LOCA	1 inch surge line break	1 stuck open SRV in SG-A	HPI stopped when subcooling exceeds 100F	No	No	
12	LOCA	1 inch surge line break	1 stuck open SRV in SG-A	HPI throttled to maintain 50F subcooling margin	No	No	x
13	LOCA	1 inch surge line break	2 stuck open SRVs in SG-A	HPI stopped when subcooling >100F	No	No	
14	LOCA	1.414 inch surge line break	None	Trip RCPs at 5F subcooling.	No	No	
15	LOCA	1 inch SL break with HPI Failure	None	15 minutes opens all TBVs to lower RCS pressure and allow CFT and LPI injection.	No	No	x
16	LOCA	1 inch surge line break	None	None	Yes	No	
17	LOCA	1 inch surge line break	1 stuck open SRV in SG-A	None	Yes	No	
18		None	SG level control failure, overfill.	EFW stopped at level 96% operating range.	No	No	
19		None	SG level failure, overfill. EFW on	Throttle EFW, maintaining flooded steam generators without flooding the steam lines.	No	No	
20		None	One stuck open TBV in SG-A	Throttles HPI to maintain 220 inch in prsr	No	No	
21		None	None	None	No	No	
22		Stuck Open PORV	None	None	No	No	
23		None	SG level control failure, overfill. EFW on	Trip MFW and turbine driven EFW. Motor driven EFW on	No	No	

#	Type	Primary Side Failure	Secondary Side Failure	Operator Action	LDH	Hi K	PRA
24		None	SG level control failure, overflow. MFW on	Trip MFW when water enters the steam lines.	No	No	
25	MSLB	None	MSLB with trip of turbine driven EFW	None	No	No	
26	MSLB	None	MSLB without trip of turbine driven EFW	None	No	No	
27	MSLB	None	MSLB without trip of turbine driven EFW	throttles HPI to maintain 50F subcooling margin.	No	No	x
28	MSLB	None	1 stuck open SRV in SG –A	None	No	No	x
29	MSLB	None	1 stuck open SRV in SG-A and 2 nd stuck open SRV in SG-B	None	No	No	x
30	MSLB	None	1 stuck open SRV in SG-A	None	Yes	No	x
31	MSLB	None	1 stuck open SRV in SG-A and 2 nd stuck open SRV in SG-B	None	Yes	No	x
32	Overflowed	None	SG level control failure overflow. MFW on	Trip MFW when water enters steam lines. Throttle HPI 50F subcooling and 120" przr level	No	No	
33	MSLB	None	One stuck open TBV in SG-A recloses at 10 min	None	No	No	
34	SRV	Stuck open pressurizer SRV Valve	None	None	No	No	x
35	MSLB	None	1 stuck open SRV in SG-A	Throttle HPI to maintain 50F subcooling or 120 inch level in przr, whichever controlling.	No	No	
36	MSLB	None	1 stuck open SRV in SG-A and 1 stuck open SRV in SG-B	Throttle HPI to maintain 50F subcooling or 120 inch level in przr, whichever controlling.	No	No	x
37	MSLB	None	1 stuck open safety valve in SG-A	Throttle HPI to maintain 50F subcooling or 120 inch level in przr, whichever controlling	Yes	No	x
38	MSLB	None	1 stuck open SRV in SG-A and 1 stuck open SRV in SG-B	Throttle HPI to maintain 50F subcooling or 120 inch level in przr, whichever controlling.	Yes	No	x
39	SGTR	None	SGTR with stuck open SRV in SG-A	None.	No	No	
40	SGTR	None	SGTR	Pressurizer sprays to depressurize.	No	No	
41	SRV	Stuck open pressurizer SRV recloses at 6000s	None	None	No	No	x
42	SRV	Stuck open pressurizer SRV recloses at 6000s	None	None	Yes	No	x
43	SRV	Stuck open PORV recloses at 400 s	None	None	No	No	
44	LOCA	1 inch SL break with HPI Failure		15 minutes open all TBVs to depressurize the RCS to CFT. When CFTs 50%, HPI recovered. TBVs remain open	No	No	x
45		None	Loss of MFW and EFW. 30 min after, start HPI and open PORV, EFW is restored. Normal EFW level control	Feed and bleed by HPI and opening PORV at RCS pressure > 2275 psia. Trip one RCP in each loop. If 0.5 subcooling margin reached, remaining two RCPs tripped. Close PORV and throttle HPI to maintain 100F subcooling.	No	No	
46		None	Loss of MFW and EFW. 30 min after, start HPI and open PORV, EFW restored. Normal EFW level control	Feed and bleed by HPI and opening PORV at RCS pressure > 2275 psia. Trip one RCP in each loop. If 0.5F subcooling margin reached, remaining two RCPs tripped. Then close PORV but fail to throttle HPI.	No	No	

#	Type	Primary Side Failure	Secondary Side Failure	Operator Action	LDH	Hi K	PRA
47		None	Loss of MFW and EFW. At 30 min starts HPI and open the PORV, EFW restored, level control fails SGs overfilled	Feed and bleed by HPI and opening PORV at RCS pressure > 2275 psia. Trip one RCP in each loop. If 5F subcooling margin reached, remaining two RCPs tripped	No	No	
48		None	Loss of MFW and EFW. Start HPI and open PORV, At 30 min EFW restored. Normal EFW level control	Feed and bleed by HPI and opening the PORV at RCS pressure > 2275 psia. Trip one RCP in each loop. At 5F subcooling margin, remaining two RCP tripped. Close PORV and throttle HPI to maintain 100F subcooling.	No	No	
49		None	Loss of MFW and EFW.	Open TBVs to depressurize SGs below condensate booster pumps. Booster pumps uncontrolled SGs overfilled. Booster pump then stopped. Throttle HPI to maintain 100F subcooling and przr level 100'. Throttle TBVs to maintain SGs 500 psi	No	No	
50	LOFW, overfeed	None	Loss of MFW and EFW.	Operator opens all TBV to depressurize the secondary side to below the condensate booster pump shutoff head so that these pumps feed the steam generators. Booster pumps are assumed to be uncontrolled so that the steam generators are filled to the top. Booster pump flow is then assumed to be terminated. Operator throttles HPI to maintain ~ 55 K (100° F) subcooling and a pressurizer level of 254 cm (100 in) or more. The TBVs are kept fully opened due to operator error.	No	No	
51	LOFW	None	Loss of MFW and EFW.	Open TBV to depressurize SGs below condensate booster pumps. Booster pumps uncontrolled fill SGs to the top. Booster pump then stopped. Throttle HPI to maintain 100F subcooling and przr level 100'. Throttle TBVs to maintain SGs 500 psi	Yes	No	
52	LOCA	5.656 inch SL break	None	None	No	No	x
53	LOCA	8 inch SL break	None	None	No	No	x
54	LOCA	2 inch SL break	None	None	No	Yes	x
55	LOCA	2.828 inch SL break	None	None	No	Yes	x
56	SRV	Stuck open pressurizer SRV	None	None	No	Yes	x
57	MSLB	None	2 stuck open SRVs in SG-A	Isolate EFW to SG-A	No	No	
58	LOCA	4 inch SL break	None	None	No	Yes	
59	MSLB	None	2 stuck open SRVs in SG-A	Throttle HPI to maintain 50F subcooling and przr level 120 inch, whichever limiting. Stop EFW to SG-A 15 min	No	No	
60	MSLB	None	2 stuck open SRVs SG-A	Throttles HPI to maintain 50F subcooling and przr level 120 inch, whichever limiting. Stop EFW to SG-A 15 min	Yes	No	
61	MSLB	None	MSLB trip MFW and turbine driven EFW	Stop motor driven EFW flow to the broken SG 10 min	No	No	

#	Type	Primary Side Failure	Secondary Side Failure	Operator Action	LDH	Hi K	PRA
62	MSLB	None	MSLB trip MFW and turbine driven EFW. RCP trip from containment isolation	None	No	No	
63	LOCA-S	2 inch SL break. CFT 294K (70F). Nominal T 300K (80F)	None	None	No	No	x
64	LOCA-S	2 inch SL break. CFT 310K (100F). Nominal T 300K (80F)	None	None	No	No	x
65	LOCA-S	2 inch SL break. HPI 278K (40F). Nominal T 294K (70F)	None	None	No	No	x
66	LOCA-S	2 inch SL break. HPI 300K (80F). Nominal T 294K (70F)	None	None	No	No	x
67	LOCA	2 inch SL break. 130% h	None	None	No	No	x
68	LOCA	2 inch SL break. 70% h	None	None	No	No	x
69	LOCA	2 inch SL break. 200% loop flow resistance	None	None	No	No	x
70	LOCA	2 inch SL break	None	None	Yes	No	x
71	LOCA	2 inch SL break. Reduced vent valve opening delta-P by 0.5	None	None	No	No	x
72	LOCA	2 inch SL break. RVVVs closed	None	None	No	No	x
73	LOCA	5.656-inch SL break	None	None	Yes	No	x
74	LOCA	1 inch SL break with HPI Failure	None	At 15 min open all TBVs to lower RCS pressure to CFT and LPI injection.	Yes	No	x
75	LOCA	1 inch SL break with HPI Failure	None	At 15 min open all TBVs to lower RCS pressure to CFT. CFTs 50% HPI recovered. TBVs remain open for duration of transient	Yes	No	x
76	LOCA	1.5 inch SL break	None	None	No	No	x
77		None	One stuck open TBV in SG-A, recloses at 20 min	Throttles HPI to maintain 220 inch level in przr	No	No	
78	LOCA	2 inch SL break. No heat structures.	None	None	No	No	
79	LOCA	2 inch SL break. No heat structures. RVVVs closed	None	None	No	No	
80	LOCA	2 inch SL break. RVVVs closed	None	None	No	No	
81	LOCA	2 inch SL break with HPI Failure	None	At 15 min open all TBVs to lower RCS pressure for CFT and LPI injection.	No	No	x
82	LOCA	1 inch surge line break with HPI Failure	None	At 15 min open all TBVs to lower RCS pressure for CFT and LPI injection. When CFTs 50% HPI recovered. At 3000s throttle HPI to 5F subcooling and 100" przr level.	No	No	x
83	SRV	Stuck open pressurizer SRV recloses at 6000s	None	After valve recloses, throttle HPI 1 min after 5F subcooling and 100" przr level reached	No	No	x
84	SRV	Stuck open pressurizer SRV recloses at 6000s	None	After valve recloses, throttle HPI 10 min after 5F subcooling and 100" przr level reached	No	No	x
85	SRV	Stuck open pressurizer SRV recloses at 3000s	None	After valve recloses, throttle HPI 1 min after 5F subcooling and 100" przr level reached	No	No	x
86	SRV	Stuck open pressurizer SRV recloses at 3000s	None	After valve recloses, throttle HPI 10 min after 5F subcooling and 100" przr level reached	No	No	x

#	Type	Primary Side Failure	Secondary Side Failure	Operator Action	LDH	Hi K	PRA
87	SRV	Stuck Open Pressurizer SRV and HPI Failure	None	15 min open all TBVs to lower RCS pressure and allow CFT and LPI injection. When CFTs 50%, HPI recovered. HPI throttled 20 min after 5F subcooling and 100" przr level reached	No	No	x
88	SRV	Stuck Open Pressurizer SRV and HPI Failure	None	15 minutes open all TBVs to lower primary pressure and allow CFT and LPI injection. When CFTs 50% HPI recovered. SRV closed 5 mins after HPI recovered. HPI throttled 1 min after 5F subcooling and 100" przr level reached	No	No	x
89		None	Loss of MFW and EFW.	Open all TBVs to depressurize SGs below condensate booster pumps feed SGs. Booster pumps uncontrolled overflow SGs (240 inch startup level). Control booster pump flow to maintain SG 30 inch startup level due to RCP on. Throttle HPI to maintain 100F subcooling and przr level 100". TBVs kept fully opened.	No	No	x
90	MSLB	None	2 stuck open SG-A safety valves	Throttle HPI 20 min after 5F subcooling and 100" przr level reached	No	No	x
91	SGTR	None	SGTR with stuck open SRV in SG-B, recloses 10 min after initiation.	RCP trip 1 min after initiation. Throttle HPI 10 min after 5F subcooling and 100" przr level reached	No	No	x
92	SRV	Stuck open pressurizer SRV recloses at 6000s	None	After valve recloses, throttle HPI at 1 min after 5F subcooling and 100" przr level reached	Yes	No	x
93	SRV	Stuck open pressurizer SRV recloses at 6000s	None	After valve recloses, throttle HPI 10 min after 5F subcooling and 100" przr level reached	Yes	No	x
94	SRV	Stuck open pressurizer SRV recloses at 3000s	None	After valve recloses, throttle HPI 1 min after 5F subcooling and 100" przr level reached	Yes	No	x
95	SRV	Stuck open pressurizer SRV recloses at 3000s	None	After valve recloses, throttle HPI 10 min after 5F subcooling and 100" przr level reached	Yes	No	x
96	SRV	Stuck Open Pressurizer SRV and HPI Failure	None	At 15 minutes, open all TBVs to lower RCS pressure and allow CFT and LPI injection. CFTs 50% discharged, HPI recovered. HPI throttled 20 min after 5F subcooling and 100" przr level reached	Yes	No	x
97	MSLB	Stuck Open Pressurizer SRV and HPI Failure	None	At 15 minutes open all TBVs to lower RCS pressure to allow CFT and LPI. When CFTs 50% discharged, HPI recovered. SRV closed 5 min after HPI recovered. HPI throttled 1 min after 5°F subcooling or 100" przr level reached	Yes	No	x
98	MSLB	None	Loss of MFW and EFW.	Open all TBVs to depressurize the SGs below condensate booster pump shutoff head. Booster pumps initially uncontrolled SGs overfilled (240 inches startup level). Booster pump flow to maintain SG level at 30" startup level for RCPs on. Throttle HPI to maintain 100F subcooling and przr level 100". TBVs are kept fully open.	Yes	No	x
99	MSLB	None	MSLB with trip of turbine driven EFW by MSLB Circuitry.	HPI throttled 20 min after 5F subcooling and 100" przr level reached).	No	No	x
100	MSLB	None	MSLB with trip of turbine driven EFW	Throttle HPI 20 min after 5F subcooling and 100" przr level reached	Yes	No	x

#	Type	Primary Side Failure	Secondary Side Failure	Operator Action	LDH	Hi K	PRA
101	MSLB	None	MSLB with trip of turbine driven EFW	None	Yes	No	x
102	MSLB	None	2 stuck open safety valves in SG-A	Operator throttles HPI 20 minutes after 2.77 K (5°F) subcooling or 254 cm (100 in) pressurizer level is reached (throttling criteria is 2.77 K (5°F) subcooling and 100" pressurizer level).	Yes	No	x
103	SGTR	None	SGTR with stuck open SRV in SG-B recloses @ 10 min	RCP trip @ 1 min. Throttle HPI 10 minutes after 5F subcooling and 100 inch przr level	Yes	No	x
104	LOCA	3.59 cm (1.414 in) SL break	None	None	Yes	No	x
106	LOCA	7.18 cm (2.828 in) SL break	None	None	Yes	No	x
107	LOCA	2.54 cm (1 inch) SL break	2 stuck open safety valves in SG-A	HPI terminated when subcooling margin exceeds 100F)	No	Yes	
108	SRV	Stuck open pressurizer SRV	None	None	No	Yes	x
109	SV	Stuck open pressurizer SRV recloses at 6000s	None	None	No	Yes	x
110	LOCA	5.08 cm (2 inch) surge line break with HPI Failure	None	At 15 min open both TBVs to lower primary system pressure and allow CFT and LPI injection.	No	Yes	x
111	LOCA	2.54 cm (1 in) surge line break with HPI Failure	None	At 15 min open all TBVs to lower primary pressure and allow CFT and LPI injection. When the CFTs are 50% HPI recovered. At 3000s, throttle HPI to 5F subcooling and 100" przr level.	No	Yes	x
112	SRV	Stuck open pressurizer SRV recloses at 6000.	None	After valve recloses, throttle HPI 1 min after 5F subcooling or 100" pressurizer level	No	Yes	x
113	SRV	Stuck open pressurizer SRV recloses at 6000s.	None	After valve recloses, throttle HPI 10 min after 5F subcooling or 100" pressurizer level reached	No	Yes	x
114		Stuck open pressurizer SRV recloses at 3000s.	None	After valve recloses, throttle HPI 1 min after 5F subcooling or 100" pressurizer level reached	No	Yes	x
115		Stuck open pressurizer SRV recloses at 3000s	None	After valve recloses, throttle HPI 10 minutes after 5F subcooling and 100" pressurizer level reached	No	Yes	x
116	SRV	Stuck Open Pressurizer SRV and HPI Failure	None	At 15 minutes, open all TBVs to lower RCS pressure and allow CFT and LPI injection. When CFTs 50% HPI recovered. HPI throttled 20 min after 5F subcooling and 100" pressurizer level reached	No	Yes	x
117	SRV	Stuck Open Pressurizer SRV and HPI Failure	None	At 15 minutes, open all TBV to lower RCS pressure and allow CFT and LPI injection. When CFTs 50% discharged, HPI recovered. SRV closed 5 min after HPI recovered. HPI throttled 1 min after 5F subcooling and 100" pressurizer level reached	No	Yes	x
118	LOCA	5.08 cm (2 inch) surge line break	None	None	Yes	Yes	x
119	LOCA	1 in surge line break with HPI Failure	None	At 15 minutes, open all TBVs to lower RCS pressure and allow CFT and LPI injection.	Yes	Yes	x
120	LOCA	1 in surge line break with HPI Failure	None	At 15 minutes, open all TBVs to depressurize the RCS. When the CFTs are 50 percent discharged, HPI recovered. TBVs remain open	Yes	Yes	x

#	Type	Primary Side Failure	Secondary Side Failure	Operator Action	LDH	Hi K	PRA
121	SRV	Stuck open pressurizer SRV recloses at 6000s	None	Throttle HPI 1 min after 5F subcooling and 100" pressurizer level reached	Yes	Yes	X
122	SRV	Stuck open pressurizer SRV recloses at 6000s	None	Throttle HPI 10 min after 5F subcooling and 100" prizr level reached	Yes	Yes	x
123	SRV	Stuck open pressurizer SRV recloses at 3000s.	None	Throttle HPI 1 minute after 5F subcooling and 100" przr level reached	Yes	Yes	x
124	SRV	Stuck open pressurizer SRV recloses at 3000s.	None	Throttle HPI 10 min after 5F subcooling and 100" przr level reached	Yes	Yes	x
125	SRV	Stuck Open Pressurizer SRV and HPI Failure	None	At 15 min open all TBVs to lower RCS pressure and allow CFT and LPI injection. When CFTs 50%, HPI recovered. HPI throttled 20 min after 5F subcooling and 100" przr level reached	Yes	Yes	x
126	Hi K	Stuck Open Pressurizer SRV and HPI Failure	None	At 15 min open all TBVs to lower RCS pressure and allow CFT and LPI injection. When CFTs 50%, HPI recovered. SRV closed 5 min after HPI recovered. HPI throttled 1 min after 5F subcooling and 100" przr level reached	Yes	Yes	x
127	SGTR-HiK	None	SGTR with stuck open SRV in SG-B, reclosed @ 10 min	Trip RCPs 1 min after initiation. Throttle HPI 10 min after 5F subcooling and 100" przr level reached.	Yes	Yes	x
128	LOCA	7.18 cm (2.828 in) SL break	None	None	Yes	Yes	x
129	LOCA	10.16 cm (4 inch) CL break	None	None	No	No	
130	LOCA	14.37 cm (5.656 in) CL break	None	None	No	No	
131	LOCA	10.16 cm (4 inch) SL break	None	None	Yes	No	x
132	LOCA	20.32 cm (8 inch) SL break	None	None	Yes	No	x
133	LOCA	10.16 cm (4 inch) SL break	None	None	Yes	Yes	x
134	LOCA	20.32 cm (8 inch) SL break	None	None	Yes	Yes	x
135	LOCA	8.53 cm (3.36 in) SL break (70% 4-inch break). RVVVs closed	None	None		No	
136	LOCA	4.34 cm (1.71 in) SL break (130% 1.5-inch break). Winter (HPI, LPI = 277K (40F) CFT = 294K (70F)).	None	None	No	No	
137	SRV	Stuck open SRV (area reduced 30%). Summer (HPI, LPI 302K (85F) CFT 310K (100F)). RVVVs closed	None	None	No	No	
138	SRV	Stuck open SRV. Summer (HPI, LPI temp = 302K (85F) CFT temp = 310K (100F)).	None	None	No	No	
139	SRV	Partially stuck open SRV (1.5-inch). 130% h	None	None	No	No	
140	SRV	Stuck open SRV reclosed at 3000s. HPI not throttled.	None	None	No	No	
141	LOCA	3.22-inch SL break (130% 2.828-inch break	None	None	No	Yes	x
142	LOCA	2.37-inch SL break (70% 2.828-inch break	None	None	No	Yes	x

#	Type	Primary Side Failure	Secondary Side Failure	Operator Action	LDH	Hi K	PRA
143	LOCA	2.828-inch CL break.	None	None	No	Yes	X
144	LOCA	3.36 inch SL break (70% 4-inch break). RVVVs closed	None	None	No	Yes	x
145	LOCA	1.71 inch SL break (130% 1.5-inch break). Winter (HPI, LPI = 277K (40F) CFT = 294K (70F).	None	None	No	Yes	x
146	LOCA- HiK	Stuck open SRV (valve flow area reduced by 30 percent). Summer (HPI, LPI = 302K (85F) CFT = 310K (100F). RVVVs closed	None	None	No	Yes	x
147	Hi K	Stuck open SRV. Summer (HPI, LPI = 302K (85F) CFT = 310K (100F).	None	None	No	Yes	x
148	Hi K	Partially stuck open SRV (1.5-inch). 130% h	None	None	No	Yes	x
149	Hi K	Stuck open SRV reclosed at 3000s. HPI not throttled	None	None	No	Yes	x

Table F.2 Placement of the Oconee-1 scenarios calculated by RELAP5 in the PTS classification matrix

Primary Secondary	Intact	Small Break < ~1.5"	Medium Break > ~1.5"
Neither SG break nor SG overfeed	A1B1 21(Rx trip)	A2B1_1 1 (1" surge line) 16 (#1 + HZP) 22 (pressurizer PORV SO, 1.1") 2 (1.4" surge line) 14 (#2 + RCP trip) 104 (#2 + HZP) 6 (1.4" CL) 43 (pressurizer PORV SO, valve reclosed @ 400 s) 46 (F&B + loss /recovery of FW)	76 (1.5" surge line) 136 (1.5", Break flow +30%, RCPs trip) 145 (#136 + Hi CL Rev. K) 3 (2" surge line) 105 (#3 + HZP) 54 (#3, Hi CL Rev. K) 63 (#3, t(CFT) = 70 F) 64 (#3, t(CFT) = 100 F) 65 (#3, t(HPI) = 40 F) 66 (#3, t(HPI) = 80 F) 67 (#3, 130% h after RCPs trip) 68 (#3, 70% h after RCPs trip) 69 (#3, 200% flow resistance) 70 (#3, HZP) 118 (#70 + Hi CL Rev. K) 71 (#3, 200% bypass flow) 72 (#3, zero bypass flow) 78 (#3, No heat structure) 79 (#3, No heat structure + RVVVs closed) 80 (#3, RVVVs closed) 7 (2" CL){0} 4 (2.828" surge line) 55 (#4 + Hi CL Rev. K) 106 (#4 + HZP) 128 (#106 + Hi CL Rev. K) 141 (#4 with 130% Break flow + Hi CL Rev. K) 142 (#4 with 70% Break flow + Hi CL Rev. K) 5 (4" surge line) 58 (#5, Hi CL Rev. K) 129 (4" cold leg) 143 (#129 + Hi CL Rev. K) 135 (#4, 70% break flow, RVVV Closed) 144 (#135 + Hi CL Rev. K) 131 (#4 + HZP) 133 (#131 + Hi CL Rev. K) 34 (pressurizer-SRV, 2.54") 56 (#34 + Hi. Rev. K) 137 (#34, 70% break flow, Summer, RVVVs Closed) 146 (#137 + Hi CL Rev. K) 138 (#34 + summer) 147 (#138 + Hi CL Rev. K) 139 (pressurizer SRV Stuck open area = 1.5", 130% h, RCPs trip) 148 (#139 + Hi CL Rev. K) 108 (same as 56) 41 (pressurizer-SRVs reclose at 100 minutes) 109 (#41 + Hi CL Rev. K) 42 (#41 + HZP) 140 (pressurizer-SRVs reclose at 50 minutes) 149 (#140 + Hi CL Rev. K) 52 (5.656" surge line) 73 (#52 + HZP) 130 (5.656" Cold Leg) 53 (8" surge line) 132 (#53 + HZP) 134 (#132 + Hi CL Rev. K)

		<p>A2B1_2 <u>40</u> (SGTR) <u>45</u> (F&B < 2000 s) <u>48</u> (F&B, pressurizer PORV reclosed @ 2000 s)</p>	<p>A3B1_2 <u>83</u> (pressurizer SRV stuck open, reclosed at 100 min, HPI throttled 1 min after 5F subcooling and 100" pressurizer level) <u>112</u> (#83 + Hi CL Rev. K) <u>92</u> (#83 + HZP) <u>121</u> (#92 + Hi CL Rev. K) <u>84</u> (pressurizer SRV stuck open and reclosed at 100 min, HPI throttled 10 min after 5F subcooling and 100" pressurizer level) <u>113</u> (#84 + Hi CL Rev. K) <u>93</u> (#84 + HZP) <u>122</u> (#93 + Hi CL Rev. K) <u>85</u> (pressurizer SRV stuck open and reclosed at 50 min, HPI throttled 1 min after 5F subcooling and 100" pressurizer level) <u>114</u> (#85 + Hi CL Rev. K) <u>94</u> (#85 + HZP) <u>123</u> (#94 + Hi CL Rev. K) <u>86</u> (pressurizer SRV stuck open and reclosed at 50 min, HPI throttled 10 min after 5F subcooling and 100" pressurizer level) <u>115</u> (#86 + Hi CL Rev. K) <u>95</u> (#86 + HZP) <u>124</u> (#95 + Hi CL Rev. K)</p>
		A2B1_3	A3B1_3
		A2B1_4	A3B1_4
One SG Break	A1B2_1*	<p>A2B2_1 <u>8</u> (1" surge line + SG-A 1SV) <u>17</u> (#8 + HZP) <u>9</u> (1" surge line, SG-A 2SVs) <u>10</u> (1.4" surge line, SG-A 2SVs) <u>28</u> (F&B, 1 SG SV SO) <u>30</u> (#28 + HZP) <u>39</u> (SGTR + SG-B 1SV) <u>57</u> (2 SVs, SG-A EFW isolated)</p>	A3B2_1
	<p>A1B2_2 <u>20</u> (1TBV) <u>33</u> (1TBV, $t_{dpt_ctrl} = 10$ min) <u>35</u> (1SV) <u>37</u> (#35 + HZP) <u>27</u> (MSLB) <u>101</u> (#27 + HZP)</p>	<p>A2B2_2 <u>11</u> (1" surge line, 1SV, HPI_{trip}) <u>12</u> (1" surge line, 1SV) <u>13</u> (1" surge line, SG-A 2SVs, HPI trip when subcooling > 100F) <u>107</u> (#13 + Hi CL Rev. K) <u>59</u> (2 SVs, HPI_{throttled}, SG-A EFW stopped at 15 min) <u>60</u> (#59 + HZP) <u>90</u> (SG-A 2 SVs SO, HPI throttled @ 20 min after permitted) <u>102</u> (#90 + HZP) <u>91</u> (SG-A TR+ 1SG-B SV SO and reclosed @ 10 min after initiation + RCP tripped @ 1 min + HPI throttled @ 10 min after permitted) <u>103</u> (#91 + HZP) <u>127</u> (#103 + Hi CL Rev. K) <u>99</u> (MSLB + HPI throttled 20 min after permitted) <u>100</u> (#99 + HZP)</p>	A3B2_2
	<p>A1B2_3 <u>61</u> (MSLB, TD EFW & MFW stopped. MD EFW to bad SG tripped at 10 min) <u>62</u> (MSLB, TD EFW & MFW tripped, RCPs tripped at 1 min)</p>	A2B2_3	A3B2_3
	A1B2_4	A2B2_4	A3B2_4

Two SG Break	A1B3_1*	A2B3_1 29 (2SVs) 31 (#29 + HZP)	A3B3_1
	A1B3_2 36 (2SVs) 38 (#36 + HZP)	A2B3_2	A3B3_2
	A1B3_3	A2B3_3 15 (1" + 4 TBVs fully open) 74 (#15 + HZP) 119 (#74 + Hi CL Rev. K) 77 (1 TBV SO and reclosed @ 20 min, HPI is stopped @ ~15 min)	A3B3_3 81 (2" surge line, 4 TBVs opened @ 15 min) 110 (#81 + Hi CL Rev. K)
	A1B3_4	A2B3_4 44 (1" + 4 TBVs Opened @ 15 min, HPI recovered when CFTs are 50% discharged) 75 (#44 + HZP) 120 (#75 + Hi CL Rev. K) 82 (1" + 4 TBVs Opened @ 15 min, HPI recovered when CFTs are 50% discharged, HPI throttled @ 50 min) 111 (#82 + Hi CL Rev. K)	A3B3_4 87 (pressurizer SRV SO, HPI fail, 4 TBVs opened @ 15 min, HPI was recovered when CFT are 50% discharged; HPI was throttled @ 20 min after available) 116 (#87 + Hi CL Rev. K) 96 (#87 + HZP) 125 (#96 + Hi CL Rev. K) 88 (pressurizer SRV SO, HPI fail, 4 TBVs opened @ 15 min, HPI was recovered when CFT are 50% discharged; SRV reclosed 5 min after HPI was recovered, HPI throttled 1 min after available). 117 (#88 + Hi CL Rev. K) 97 (#88 + HZP) 126 (#97 + Hi CL Rev. K)
SG(s) Overfeed	A1B4_1*	A2B4_1 47 (F&B, loss/recover FW, EFW OF)	A3B4_1
	A1B4_2	A2B4_2	A3B4_2
	A1B4_3 18 (EFW, 96%) 19 (EFW, level maintained at 100%) 23 (EFW) 24 (MFW OF, MFW tripped when water enters MSL) 32 (MFW OF, MFW tripped when water enters MSL, same as #24)	A2B4_3	A3B4_3
	A1B4_4	A2B4_4	A3B4_4
SG(s) Break + SG(s) Overfeed	A1B5_1*	A2B5_1 25 (MSLB, 32.6", AFW _{motor} + MFW overfeed broken SGs, intact SG level 50%) 26 (MSLB, 32.6", AFW _{motor} + AFW _{tb} , MFW overfeed broken SGs, intact SG level 50%)	A3B5_1
	A1B5_2 89 (F&B, + 4 TBVs are opened and HPI is throttled after RCS pressure reaches 2275 psi) 98 (#89 + HZP)	A2B5_2 49 (4 TBVs throttled to maintain SG P at 3.45 MPa + SG overfeed to 100% then stop FW) 50 (4TBVs + SG overfeed to 100% then stop FW) 51 (#49 + HZP) {0}	A3B5_2
	A1B5_3	A2B5_3	A3B5_3

NUREG/CR-6899

BIBLIOGRAPHIC DATA SHEET

(See instructions on the reverse)

2. TITLE AND SUBTITLE

Thermal-Hydraulic Uncertainty Analysis in Pressurized Thermal Shock Risk Assessment Methodology and Implementation on Oconee-1, Beaver Valley, and Palisades Nuclear Power Plants

3. DATE REPORT PUBLISHED

MONTH

YEAR

4. FIN OR GRANT NUMBER

K6007

5. AUTHOR(S)

Y.H. J. Chang, A. Mosleh, K. Almenas, D. Bessette

6. TYPE OF REPORT

Technical

7. PERIOD COVERED (Inclusive Dates)

8/1998-8/2004

8. PERFORMING ORGANIZATION - NAME AND ADDRESS (If NRC, provide Division, Office or Region, U.S. Nuclear Regulatory Commission, and mailing address; if contractor, provide name and mailing address.)

Center for Risk and Reliability, University of Maryland, College Park, MD 20742

9. SPONSORING ORGANIZATION - NAME AND ADDRESS (If NRC, type "Same as above"; if contractor, provide NRC Division, Office or Region, U.S. Nuclear Regulatory Commission, and mailing address.)

U.S. Nuclear Regulatory Commission, Office of Nuclear Regulatory Research, Division of Systems Analysis and Regulatory Effectiveness, Washington, DC 20555-0001

10. SUPPLEMENTARY NOTES

D. Bessette, Project Manager

11. ABSTRACT (200 words or less)

A method was developed to evaluate thermal hydraulic uncertainty for the analysis of pressurized thermal shock. This was part of a joint program with probabilistic risk assessment (PRA) and probabilistic fracture mechanics (PFM). The objective was to perform a comprehensive, best-estimate analysis of PTS, with uncertainty quantification for three representative pressurized water reactors, Oconee-1, Beaver Valley-1, and Palisades. A top-down approach was used that has some similarities to the Code Scaling, Applicability, and uncertainty (CSAU) method. The thermal hydraulic analysis was based on the application of the RELAP5/MOD3 code. The uncertainty method developed addressed both boundary conditions and physical models in the RELAP5 code. The method utilized the nominal range sensitivity analysis (NRSA) method to determine the relative affects of the various key influencing parameters that contributed to uncertainty.

12. KEY WORDS/DESCRIPTORS (List words or phrases that will assist researchers in locating the report.)

pressurized thermal shock, uncertainty, Oconee-1, Beaver Valley, Palisades, RELAP5, thermal-hydraulic, reactor vessel

13. AVAILABILITY STATEMENT

unlimited

14. SECURITY CLASSIFICATION

(This Page)

unclassified

(This Report)

unclassified

15. NUMBER OF PAGES

175

16. PRICE